A STUDY OF BEAM MASERS AND ALTERNATE GRADIENT FOCUSING OF NEUTRAL PARTICLES

by

D. KAKATI, M.Sc.

Being a thesis
presented to the University of Keele
for the Degree of Doctor of Philosophy

- - - - - -

Department of Physics
University of Keele,
Keele,
Staffordshire.

November, 1968.

BEST COPY AVAILABLE.

VARIABLE PRINT QUALITY

ARTICLE FROM "PHYSICS LETTERS, 5 JUNE 1967, VOL.24A, NO.12, P.678" NOT SCANNED AT REQUEST THE OF UNIVERSITY

QUOTE

"GOD DOES NOT CARE FOR OUR MATHEMATICAL DIFFICULTIES. HE INTEGRATES EMPIRICALLY."

EINSTEIN[a]

MISQUOTE

"ANY DEVICE YOU CAN THINK OF CAN BE BUILT, UNLESS IT ACTUALLY VIOLATES THE LAWS OF CONSERVATION OF ENERGY OR MOMENTUM"

CLOGSTON[b]

To

MY FATHER

ACKNOWLEDGEMENTS

The author wishes to express his gratitude to,

Professor D.J.E. Ingram for the use of his laboratory and research facilities.

Dr. D.C. Laine for his constructive criticism and dynamic guidance all through this work.

The members of the Maser Group at Keele for useful discussions.

Mr. F. Rowerth and his technical staff for their assistance in constructional work.

The staff of the Library for their help in copying etc.

Mrs. B. Haywood for the typing of the thesis.

Miss Joan Cox, Miss Ruth Parker, Miss Elizabeth Button, Miss Margaret Lane for helping in various ways in completing the thesis.

The University of Keele for the provision of a research grant.

My parents for their inspiration and for financing my studies abroad.

And last, but not least, all my good friends, who introduced me to the vagaries of the British way of life.

ABSTRACT

An ammonia beam maser is constructed and its basic characteristics established. An attempt is made to put the theory of state selection and focusing of molecules in a maser in a generalized form so as to include the case of lower state focusing as well as the higher state focusing used in masers. Alternate-Gradient (AG) focusing is presented as a practical method for lower state focusing. A theory of alternate gradient focusing of uncharged particles is developed with particular reference to a molecular beam of ammonia. It is shown that the method can be used to focus molecules in any particular energy state preferentially. An AG focusing system is constructed and its basic characteristics established.

Some coherence phenomena in a molecular system are investigated both in the case of a bulk gas (in absence of state selection) as also in the case of a state selected beam. In the latter case both upper state selection by using an octapole focuser and lower state selection using an AG focuser have been used. The generality of these coherence phenomena has been established for a two level quantum mechanical system.

Some possible applications of an AG system, particularly in the area of aerothermo-chemistry are considered..

CONTENTS

		Page
ACKNOWLEDGEMENTS		
ABSTRACT		
CHAPTER I	INTRODUCTION	
1.1	Historical	1
1.2	Special features of Radio-frequency Physics	3
1.3	Scheme of Presentation	6
CHAPTER II	INTERACTION OF RADIATION WITH MATTER: THE MASER PRINCIPLE	
2.1	Introduction	8
2.2.	Spectroscopy of Atoms, Molecules and Nuclei	9
2.3	Stimulated Emission and Absorption	13
2.4	The Maser Principle	17
2.5	The Maser Medium	19
CHAPTER III	MECHANICS OF THE AMMONIA MOLECULE	
3.1	Introduction	21
3.2	Rotational Spectrum	22
3.3.	Vibration: The Inversion States of Ammonia	25
3.4	Inversion and Symmetry	30
3.5	Fine Structure	30
3.6	Hyperfine Structure	32
3.7	The Ammonia Molecule in a Static Electric Field	36
3.8	Population Distribution	38

CHAPTER IV	GENERALIZED THEORY OF STATE SELECTION	
4.1	Introduction	39
4.2	Static Focusing Conditions	39
4.3	Upper State Selection: Multipole Focusers	44
4.4	Ring and Spiral Focuser	47
4.5	Non Uniform Focuser	50
4.6	Other Types of Focuser	51
4.7	The High Field Situation	51
4.8	Velocity Distribution in a Focused Beam	52
CHAPTER V	THE AMMONIA BEAM MASER	
5.1	Introduction	56
5.2	Basic Features	57
5.3	Effuser, Resonator and State Selector	58
	(a) The Effuser	58
	(b) The Resonator	61
	(c) The State Selector	65
5.4a	Power Output	65
5.4b	Sensitivity	72
5.4c	Noise	78
5.4d	Stability and Linewidth	81
5.5	Experimental Apparatus	
5.5a	General	85
5.5b	Vacuum Assembly and Ammonia System	87
5.5c	Cavity Stabilization	91

CHAPTER V (continued)

5.5d	Microwave System	91
5.5e	Superheterodyne Detection	93
5.5f	General Electronics	95
5.6	Operation and Basic Characteristics	98

CHAPTER VI	ALTERNATE GRADIENT FOCUSSING OF A MOLECULAR BEAM	
6.1	Introduction	101
6.2	Optical Analogue	103
6.3	Neutral Particle Analogue	104
6.4	AG Focusing of a Molecular Beam with Dipolar Multiplets	105
6.5	Adiabatic Conditions	118
6.6	Velocity Effects	119
6.7	Design Considerations	121
6.8	Experimental	123
6.9	Operation and basic characteristics	124

CHAPTER VII	COHERENCE PHENOMENA AND RELAXATION PROCESSES IN A MOLECULAR SYSTEM	
7.1	Introduction	128
7.2	The NMR Analogue	129
7.3	The Optical Analogue	129
7.4a	Theoretical Approach	130
7.4b	A Direct Approach	130
7.4c	The Mixed Energy State Model	133

CHAPTER VII (continued)

7.4d	The Correlation Model of Dicke	136
7.5	Experimental	142
7.6	Results and Comments	143
	(a) State selected beam of lower state molecules of NH_3 J = K = 3 inversion state using AG focusing	143
	(b) State selected beam of upper state molecules of NH_3 J = K = 3 inversion state using an Octapole focuser	143
	(c) Superradiative transition in bulk gas	144
	(d) Measurement of Relaxation Times	145
	(e) Pre-Ringing of Molecular Resonance	146
	(f) Line Width Measurements	146

CHAPTER VIII	Further Comments on Transient Phenomena, Dielectric Relaxation, Chemical Kinetics and AG-System	147
8.1	Introduction	147
8.2	State of the Art in Nuclear Physics	149
8.3	State of the Art and Some Current Problems in Chemistry	149
8.4	State of the Art in Dielectric Relaxation Processes and Molecular Behaviour	152
8.5	AG System	152
8.6	A Conceptual Experiment	153
	(a) An Experimental Arrangement	153
	(b) Possibility of Obtaining Non-Boltzmann Distribution without Electric or Magnetic Focusing.	154

CHAPTER VIII (continued)

8.7 Further Application of the AG System 155

APPENDIX I

Alternate Gradient Focusing of a Molecular Beam of Ammonia,

Kakati, D., Laine, D.C., Physics Letters, 1967.

REFERENCES

List of Diagrams.

CHAPTER I

INTRODUCTION

1.1 Historical:

Until recently radio-frequency physics was mainly concerned with the absorption of micro- and radio frequency-waves by transitions of atoms and molecules from lower energy states to higher energy states. It is also possible to formulate the reverse concept: to use atoms and molecules not for absorption but for emission of electromagnetic radiation. The solution of this problem resulted in the development of new methods for generation and amplification of electromagnetic radiation.

Radio-frequency physics is based on the phenomenon of resonant interaction of electromagnetic radiation with matter in the radio frequency and microwave regions. Historically, studies of interactions between radiation and matter began nearly half a century ago. Einstein and Ehrenfest showed theoretically that a change in orientation of atomic dipole moments in a magnetic field should be accompanied by radiation or absorption of electromagnetic waves. This is now familiar as the phenomenon of magnetic resonance.

The first experimental investigation of the microwave spectra of gases was carried out by Cleeton and Williams in 1934. The spectrometer used by them to observe microwave absorption in ammonia vapour was however far removed from contemporary microwave spectrometers.

In 1937 Rabi developed the theory of magnetic resonance for particles with a magnetic moment and applied the theory to the experimental determination of nuclear magnetic moments, using atomic and molecular beams.

These were the fundamental steps which led to the development of radio-frequency and microwave spectroscopy. In these developments three distinct streams may be noticed:

1. Following Rabi's method of atomic and molecular beams, vigorous investigations were conducted to verify and refine the Dirac theory of the electron. This resulted in two major discoveries in 1947: (a) establishment of the shift of S levels of hydrogenlike atoms (called the Lamb shift) by Lamb and Retherford, and (b) correction of the magnetic moment of the electron - both by radio-frequency spectroscopic methods. Both these effects were later accounted for by considering the interaction of the electron with the zero-point fluctuations of the electromagnetic and electron-positron fields.

2. Barring the isolated efforts of Cleeton and Williams (1934) who observed microwave absorption in ammonia, development of gaseous radio-frequency spectroscopy was held up by the absence of the necessary equipment till the second world war. The development of radar for the war made this equipment available and was followed by a rapid development of this branch of radio-frequency spectroscopy.

3. The third branch of radio-frequency spectroscopy is concerned with the absorption of radiation by solids: electron paramagnetic resonance (E P R) and nuclear magnetic resonance (N M R).

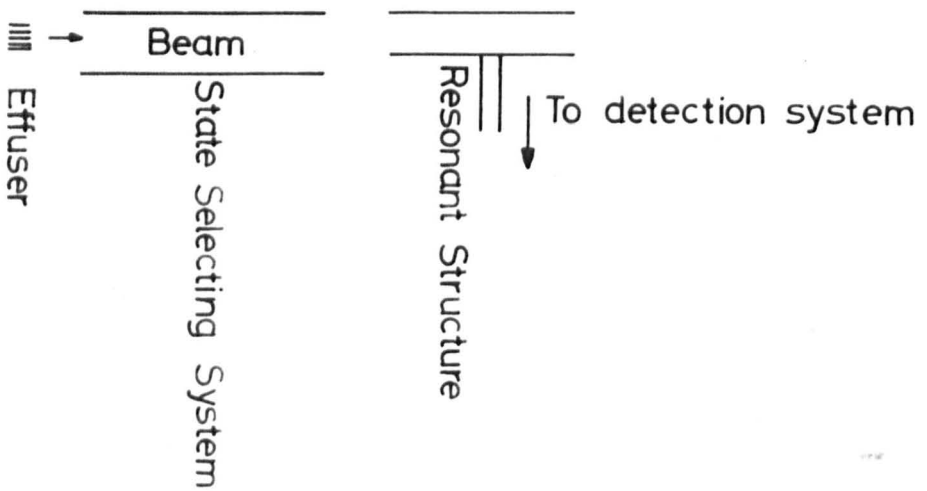

Fig. 1.1.1. Schematic of a Beam Maser.
(3)

Until the early nineteen fifties, gaseous radio-frequency spectroscopy was mostly limited to observation of absorption spectra of molecules, the reason being that the intensity of "incoherent" spontaneous emission is very low and induced emission is usually more than compensated by absorption. However the "maser" (Microwave or Molecular Amplification by Stimulated Emission of Radiation) has recently made it possible to observe induced emission in "pure" form. The maser was developed simultaneously by Gordon, Zeiger and Townes in U.S.A. (1954) and by Basov and Prokhorov in U.S.S.R. In its essentials a beam maser consists of an effuser which produces a molecular beam that is passed through a state-selector. The state selector separates and focuses the excited molecules into a resonant cavity wherein they emit coherently (Fig. 1.1.1)

The third branch of RF spectroscopy mentioned above similarly led to the development of solid state masers. This area is beyond the scope of this thesis and will not be discussed here.

From the foregoing, it would appear that the basic problem in Quantum Electronics, to use contemporary terminology, is to utilise absorption and emission spectroscopy in the microwave and radio-frequency region either for studies of atoms and molecules or for development of new methods of generation and amplification of electromagnetic radiation.

1.2 Special Features of Radio-frequency Physics:

Radio-frequency spectroscopy has a number of features which distinguish it from optical spectroscopy:

(i) In the radio-frequency range, the difference between energy levels of quantum mechanical systems usually satisfies the condition

$$| E_1 - E_2 | << kT$$

(ii) A large electromagnetic field intensity in the radio-frequency range can be easily obtained.

(iii) The wavelength of the emitted radiation may be much larger than the distance between the neighbouring radiating objects.

The first characteristic leads to the fact that in thermodynamic equilibrium, the occupation (or molecular populations) of levels E_1 and E_2 is almost the same, the role of induced emission is therefore most important.

The second characteristic leads to the appearance of saturation effects which have been used to explain the operation of a maser.

The third characteristic leads to the fact that the molecules of a radiating gas cannot be considered as emitting spontaneous radiation independently of each other. A molecular source of microwaves similar but different in principle to the maser is made feasible by this fact, namely a "super-radiant" gas in which the gaseous system emits coherent spontaneous radiation with an intensity proportional to the square of the number of molecules. This was realized by Dicke and Romer (1955) shortly after the first maser was operated in 1954. In their experiment the super-radiant state was created by subjecting the gas, initially in an incoherent state, to a radiation pulse after which the gas emits radiation

coherently and spontaneously. Theoretically however, to obtain maximum super-radiance it is necessary to start either (i) with a system in which all the molecules are in the upper energy level, or (ii) all the molecules are in the lower energy level. Such a situation can be realised by using an appropriate type of state selector.

The problem of obtaining a state selected beam of molecules in which nearly all the molecules are in an upper energy state is now almost trivial as evident from the simplicity of the focusing schemes used in the ammonia maser. The situation becomes complicated in the case of lower state molecules. However the problem of lower state as well as upper state focusing arises naturally in the study of molecular beams. As a matter of fact, from a spectroscopic point of view, there is no reason why the maser problem should not be formulated in the reverse way.

In a two level system (e.g. the inversion states of ammonia) the upper and lower energy levels normally behave differently in an applied electric field in that the upper energy level increases and the lower one decreases in energy with increasing field. A different situation arises in the case of linear molecules with small rotational constants (e.g. Na Cl) in high fields. Unlike the ammonia molecule for which the energy of a particular state increases or decreases monotonically, the Stark energy of these molecules undergo a sign reversal of its slope at certain value of the applied field strength, and the upper energy level decreases in energy as the field is further increased. In principle this simply means that one needs to construct a configuration with reverse characteristics from the state selectors used in the ammonia maser. In practice the problem

turns out to be rather elusive as it is not only desirable to separate the molecules but also to impart a stable periodic motion to them which results in focusing. The present work is devoted mainly to the investigation of the possibility of developing a system to satisfy these requirements. More generally, it may be worthwhile to investigate a system which can be made sensitive to any particular quantum state. An answer seems to lie in the alternate-gradient focusing system discussed in this thesis. The principle of alternate-gradient focusing (A-G focusing) has hitherto been applied to space focusing of charged particles. It is shown in the present work that the principle can indeed be applied to neutral particles with an electric or magnetic moment. Such a system is shown to have other properties of physical interest.

1.3 Scheme of Presentation:

The themes delineated above are elaborated in subsequent chapters. The basic concepts are introduced in Chapter II and the different types of radiation interaction which lead to different characteristic spectra are briefly mentioned. The salient features of the theory of induced emission are then presented and the maser principle is introduced as a logical development to indicate the advantage of removing from a system either the lower state molecules or the upper state ones.

In the experimental investigation of the problems raised, ammonia has been used as the active medium. An understanding of the mechanics of the ammonia molecule thus becomes essential. This topic has therefore been considered in some detail in Chapter III. This is followed by a

discussion of the principles involved in state selection and focusing of molecules in Chapter IV. A general approach is made so as to incorporate the principle of both upper and lower state focusing. Upper state selection of ammonia in a multipole focuser is given some prominence in order to bring out various aspects of focusing which are quite general.

In Chapter V, the ammonia beam maser is discussed. The experimental set-up is described and basic characteristics established. Basically the same set up is used for testing the A.G. focusing schemes. A theory of A.G. focusing of neutral particles is developed in Chapter VI and some characteristics established. The chapter which then follows is devoted to an investigation of coherence phenomena in a molecular system. The theoretical background is presented and some results are given which are obtained using multipole and A.G. focusing of a beam as well as with a volume of gas in thermal equilibrium. The generality of the phenomenon of super-radiance for a two level quantum mechanical is established and is followed by some concluding comments in the final chapter.

CHAPTER II

INTERACTION OF RADIATION WITH MATTER:

THE MASER PRINCIPLE

2.1. Introduction:

Ions, atoms and molecules can exist in arrangements with considerable variations in their energy. The internal energy of such a system is quantized, that is, they can exist only in certain discrete energy states. For the sake of brevity, all such systems will be referred to as "molecules" except where confusion is likely. A molecule consists of an assembly of electrons and atomic nuclei. The energy of such an assembly can change only if the electrons or nucleons change their motion or orientation or both, corresponding to one permitted energy state to yield another permitted energy or quantum state of the system. For an isolated molecule to alter its internal energy state the energy difference between the two states involved must either be absorbed from an electromagnetic field or be emitted in order to conserve energy and momentum. The process is therefore one of absorption or emission of radiation according as the final state is higher or lower in energy.

The radiation field is also quantized in energy so that it can exchange only a discrete amount of energy in the form of a photon (quantum of energy)with the interacting molecule. If the two states have energies W_2 and W_1 ($W_2 > W_1$), then the frequency of the radiation

involved in an upward transition $1 \rightarrow 2$ (absorption) or a downward transition $2 \rightarrow 1$ (emission) between the two states is given by

$$h\nu = W_2 - W_1 \qquad (2.1.1)$$

where h is Planck's constant. The observed emission or absorption line is however not monochromatic, the most fundamental source of broadening being the uncertainty relation $\Delta W \, \Delta t \simeq \hbar$.

2.2 Spectroscopy of Atoms, Molecules and Nuclei:

It follows from preceding paragraphs that there must be a change with time in some features of the charge distribution of the particle in order that there be a fluctuation of the electro-magnetic field. Thus for a radiative transition to occur, there must be either a change of the overall electronic charge of the system, or the spatial charge or in the state of the moment. The interaction may be with either the electric or the magnetic component of the radiation field, depending upon whether the change of molecular energy is primarily electric or magnetic in character. Each radiative transition can therefore be associated with an oscillating electric or magnetic moment, usually dipolar, but may be of higher order (for example quadrupolar etc.). The transitions have characteristic frequencies depending upon the type of interaction involved. A brief review of the various types of spectra follows.

The angular momentum of a quantum mechanical system is of the order of $\hbar$. The moment of inertia however has different order of

magnitudes for various cases. For example, the moment of inertia of a molecule is given by $I \simeq Mr^2$, where M is the mass of an atom and r is the interatomic distance. The rotational energy of a molecule is therefore

$$W_{rot} \simeq \frac{\hbar^2}{Mr^2} \tag{2.2.1}$$

where $\hbar = h/2\pi$, h being Planck's constant.

The vibrational and the electronic energy of a molecule can be expressed respectively as

$$W_{vib} \simeq \frac{\hbar^2}{\sqrt{mM}\, r^2} \tag{2.2.2}$$

and

$$W_{el} \simeq \frac{\hbar^2}{mr^2} \tag{2.2.3}$$

where m is the mass of the electron, e the electronic charge and $r \simeq a_o = \hbar^2/me^2$. The movement of the charge inside a nucleus leads to the radiation of γ-rays and the nuclear excitation energy may be written as

$$W_N \simeq \frac{\hbar^2}{M_p R^2} \tag{2.2.4}$$

where R is the nuclear radius, M_p is the proton mass.

Inserting the values $\hbar = 10^{-27}$ erg. sec., $r = 10^{-8}$ cm.

$R = 10^{-13}$cm, $M = 10^{-22}$gm, $m = 10^{-27}$gm, the following typical transition frequencies are obtained.

(i) $W_{rot}/h \simeq 10^{11}$ Hz, $\lambda_{rot} \simeq 2$ mm

(ii) $W_{vib}/h \simeq 3 \times 10^{13}$ Hz, $\lambda_{vib} \simeq 60$ μm

(iii) $W_{el}/h \simeq 10^{16}$ Hz, $\lambda_{el} \simeq 200$ nm

(iv) $W_N/h \simeq 10^{21}$ Hz, $\lambda_N \simeq 0.02$ Å

The actual transition frequencies may be two orders of magnitude higher or lower than indicated.

The electronic energy of an atom may be expanded in the form

$$W \simeq \frac{\hbar^2}{mr^2}\left[1 + 0\left(\frac{R^2}{r^2}\right) + 0\left(\frac{R^4}{r^4}\right) + \ldots\right]$$

where r is the distance of an electron from the centre of the nucleus. The first term in the above equation represents the dipolar interaction already noted. The second term represents the quadrupole hyperfine structure which is not zero when the nuclear spin $I > 1$. Inserting the values for different quantities as above, the energy of the quadrupole hyperfine structure is obtained as

$$W_Q/h \simeq \left(\frac{\hbar}{mr^2}\right)\left(\frac{R^2}{r^2}\right) \simeq 10^6 \text{ Hz} \qquad (2.2.5)$$

(W_Q is usually written as eqQ, where $Q \simeq R^2$, $q \simeq e/r^3$).

In principle, higher order interactions should occur for atoms with nuclei of larger spin, but they are usually too small to be detected.

As remarked before, the interaction may also be magnetic. The magnetic moment of an electron is of the order of one Bohr magneton, $\mu_B = 0.927 \times 10^{-20}$ cgs, and that of a nucleus is of the order of the nuclear magneton $\mu_N = 5.05 \times 10^{-24}$ cgs. The frequency of the atomic fine structure, being due to the magnetic dipole interaction between electrons is therefore ($r^{-3} \simeq 10^{26}$ cm^{-3}):

$$W_{ee}/h \simeq \mu_B^2 / r^3 h \simeq 10^{13} \text{ Hz} \qquad (2.2.6)$$

The magnetic dipole interaction between electron and nucleus gives the hyperfine structure (for $I > \frac{1}{2}$) of frequency

$$W_{eN}/h \simeq \mu_B \mu_N / r^3 h \simeq 5 \times 10^9 \text{ Hz} \qquad (2.2.7)$$

The magnetic dipole interaction between nuclei in a molecule gives the magnetic hyperfine structure

$$W_{NN}/h \simeq \mu_N^2 / r^3 h \simeq 2 \times 10^4 \text{ Hz} \qquad (2.2.8)$$

where $r \simeq 10^{-8}$cm is the distance between nuclei. So far molecules, atoms and nuclei have been considered without an externally applied field. Under the action of an external magnetic field of several thousand oersted,

the nuclear magnetic moment has the energy corresponding to the transition frequency of about 10 MH_z. This is the nuclear magnetic resonance effect expressed by

$$W_{NMR} \simeq \mu_N H \qquad (2.2.9)$$

where H is the external magnetic field.

If the magnetic moment pertains to an atom or an ion, the effect is called electron paramagnetic resonance expressed by

$$W_{EPR} \simeq \mu_B H \qquad (2.2.10)$$

The frequency of EPR transitions is found in the microwave range in a magnetic field of the order of 10^4 oersteds.

2.3 Stimulated Emission and Absorption :

There are two distinct types of transitions which involve energy levels plus photons: "spontaneous transitions" and "induced transitions". The spontaneous transitions are always "spontaneous emissions" due to the zero-point fluctuation of the electromagnetic field and consist of the spontaneous falling of a molecule from a higher energy state to a lower one, with thbe emission of a photon given by Eq. 2.1.1. This photon may have any polarization σ and any frequency in the range ν to $\nu + \Delta\nu$. In addition, if the molecule in the higher energy state is irradiated with an electromagnetic field whose frequency ν is approximately equal to $(W_2 - W_1)/h$, the incident radiation may induce a transition of

the molecule from state 2 to state 1, with the emission of a photon. This is known as "stimulated emission". If the induced transition is upward in energy, the process is one of absorption.

The concept of stimulated emission was introduced by Einstein in 1917 in order to be able to describe adequately the interaction of radiation and matter. The Einstein description [1,2] is based on thermodynamic and phenomenological considerations. A complete and rigorous theory has been given by Dirac based on quantum electrodynamics. Both stimulated and spontaneous emission are naturally accounted for in Dirac's theory as a consequence of quantizing the radiation field. The spontaneous emission acts as a damping term in the theory and leads to an explanation of the natural line width of spectral lines. A detailed account of this theory is given in reference 10.

A one-photon absorption process is schematically represented in Fig. 2.3.1. The initial state of an atom with two energy levels is in this case the ground state 1 and a radiation field is incident on the atom with $n_{\ell\sigma}$ quanta of frequency ω_ℓ ($\omega_\ell = 2\pi \nu_\ell$), where ℓ and σ specify the direction and polarization of the quanta respectively. If one quantum is absorbed, the atom will jump to an excited state 2.

The atom and the radiation field consitute a single system. Since only those transitions in which energy is conserved will occur, the initial energy W_i of the system must be equal to the final energy W_f. Therefore

$$W_2 - W_1 = h\omega_\ell \qquad (2.3.1.)$$

Fig. 2.3.1. Schematic Representation of a One Photon absorption by an atom

Fig. 2.3.2. Schematic Representation of a One Photon emission by an atom in excited state.

A one-photon emission by an atom in an initially excited state is shown schematically in Fig. 2.3.2. The matrix element of the interaction hamiltonian between the two states for the absorption and stimulated emission processes are respectively given by [10].

$$\left| \langle f \mid H_1 \mid i \rangle \right|^2_{abs.} = \frac{n_{\ell\sigma} \hbar\omega_\ell}{2V} \left| \bar{e}_{\ell\sigma} \cdot \bar{\mu}_{12} \right|^2 = \text{constant} \times n_{\ell\sigma} \qquad (2.3.2)$$

$$\left| \langle f \mid H_1 \mid i \rangle \right|^2_{emis.} = \frac{(n_{\ell\sigma}+1)\hbar\omega_\ell}{2V} \left| \bar{e}_{\ell\sigma} \cdot \bar{\mu}_{12} \right|^2 = \text{constant} \times (n_{\ell\sigma}+1) \qquad (2.3.3)$$

where H_1 is the energy of interaction between the atom and the radiation field, $|i\rangle$ is the initial state function, $|f\rangle$ the final state function, V the volume of the cavity containing the atoms and the radiation field, $\bar{e}_{\ell\sigma}$ the photon polarization vector, and $\bar{\mu}_{12}$ the dipole matrix element between the two states of the atom. The matrix element of the interaction hamiltonian for the emission process consists of two parts. The term containing $n_{\ell\sigma}$ arises due to the interaction of the atom and the radiation field, and therefore represents stimulated emission. This term is identical with the matrix element for absorption and can be calculated without quantizing the radiation field as indeed is done classically. The term containing 1 in Eq. 2.3.3. arises due to the zero point energy of the radiation field which is $\frac{1}{2}\hbar\omega_\ell$ rather than zero. The consequence of this is that when $n_{\ell\sigma} = 0$, that is in the absence of any radiation field, there

still may be emissive transitions between the initial and final states of the system. This represents spontaneous emission.

The total transitional probabilities are obtained after multiplying the interaction matrix elements given above by the radiation density and suitably averaging. In cgs units these appear as the familiar Einstein coefficients

$$A = \frac{64\pi^4 \nu_\ell^3}{3hc^3} \left| \bar{\mu}_{12} \right|^2 \qquad (2.3.4)$$

for spontaneous emission and

$$B = \frac{8\pi^3}{3h^2} \left| \bar{\mu}_{12} \right|^2 \qquad (2.3.5)$$

for absorption and stimulated emission probabilities which are identical.

An important observation to make here is that the stimulated emission is in phase with the incident radiation and is therefore coherent. Remembering that in thermal equilibrium, the emission (stimulated and spontaneous) and absorption must be balanced, from Eq. 2.3.4 - 5, using Boltzmann's distribution one directly obtains Planck's law of radiation

$$U(\nu) = \frac{8\pi h\nu^3}{c^3} \quad \frac{1}{\exp(\frac{h\nu}{kT})-1} \qquad (2.3.6)$$

and

$$A/B\ U(\nu) = \exp \frac{h\nu}{kT} - 1 \qquad (2.3.7)$$

The relative importance of stimulated and spontaneous emission in various parts of the spectrum due to a thermal radiation field may now be obtained from Eq. 2.3.7 as follows.

$\frac{h\nu}{kT} \sim 5 \times 10^{-3}$ at 1 cm. (30 GH_z or 10,000 μm)

0.5 at 100 μm (3000 GH_z or 0.1 mm)

50 at 1 μm (300,000 GH_z or 1,000 nm)

at normal room temperatures. Thus at microwave frequencies spontaneous emission will be negligible and in the far infrared it will be small compared to the thermally induced emission. At optical frequencies however the spontaneous emission is considerably greater than stimulated emission due to thermal radiation.

2.4 The Maser Principle :

The comparative importance of induced and spontaneous emission for various frequencies has been shown in the preceding section. Since the probability of spontaneous emission is very small in the microwave and radiofrequency range, the molecules in an excited state radiate only very weak microwaves. For example at

$$\nu_\ell = 3 \times 10^{10} \text{ Hz}, \quad |\mu| = 10^{-18} \text{cgs-esu}, \quad \text{Eq. (2.3.4)}$$

gives $A = 3.2 \times 10^{-7}$ sec^{-1}, and the life time of the excited state is 3×10^{6} sec.

However, since the probability of stimulated emission is frequency independent as shown by Eq. (2.3.5.), there is the possibility of obtaining appreciable emission at low frequencies, if some excess population of the excited state is realized.

When the system of molecules is placed in a radiation field which is stronger than the thermal radiation of Eq. (2.3.6), a fraction of the incident power is absorbed by the molecules. The radiation density of a monochromatic incident power flow P through unit area is U = P/c. Thus for the two state system having populations N_2, N_1 with energies W_2, W_1 where $W_2 > W_1$ and $N_1 + N_2 = N$, the power of induced absorption is $N_1 h\nu BP/c$ while that of induced emission is $N_2 h\nu BP/c$. The net absorption of power in a unit length of path is

$$P_{abs} = (N_1 - N_2)\, h\nu BP/c = (N_1 - N_2)\, \frac{8\pi^3 \nu}{3ch} \left| \bar{\mu} \right|^2 P \qquad (2.4.1)$$

From the normal Boltzmann's distribution, the excess population taking part in the process is

$$N_1 - N_2 \simeq \frac{N}{2} \frac{h\nu}{kT} \qquad (2.4.2)$$

and therefore

$$P_{abs} \simeq \frac{4\pi^3 N \nu^2}{3ckT} \left| \bar{\mu} \right|^2 P \qquad (2.4.3)$$

When $N_2 > N_1$, Eq. (2.4.1) shows negative absorption, that is net emission of power. This is the principle of maser action.

The observed net absorption of power by molecules in thermal equilibrium given by the difference of induced emission and absorption

actually taking place is only a fraction which is $h\nu/kT$ times the true induced emission or absorption. Therefore in the frequency range where $h\nu << kT$, if molecules in either state W_1 or W_2 are removed, emission or absorption will be observed with $kT/h\nu$ times greater intensity. Thus for example at normal temperatures and at a wavelength of 1.25 cm (24 GH_z), $N_1 - N_2$ is only N/500. This means that from a spectroscopic point of view only one in 500 active molecules can in effect contribute towards the observable absorption, the remaining "absorptions" are paired off by "induced emission". If in some way the populations are altered to non-thermal values, the observed signal might in principle be increased by a factor up to 250.

2.5 The Maser Medium :

In order to be able to use a molecular beam in non-thermal equilibrium condition as indicated in the preceding section, it would appear that the primary requirement is to be able to select and focus the molecules according to their energy states. Under favourable conditions this can be done by magnetic or electrostatic state selection. The problem of deciding the usefulness of a given molecular transition for maser action can therefore be divided into two parts : (a) the determination of the fraction f of the molecules at the source in the quantum states of interest (Chapter III, Section 3.8); (b) determination of whether it is possible to obtain a population difference (between the two levels concerned) in excess of the thermal equilibrium values with a state selecting structure. The subject of state selection is considered in detail in Chapter IV. To obtain maser oscillation (Chapter V) the number of the higher state

TABLE I

(To face page 20)

Population and focusing constants for possible maser molecules.

Molecule	Quantum state	Population density (percent)	Focusing force constant C in Farad meters^2
NH_3	J = 3 K = 3 M = 2	6	5.6×10^{-37}
	J = 2 K = 1 M = 1	4	3.9×10^{-37}
	J = 1 K = 1 M = 1	2.8	5.7×10^{-37}
	J = 1 K = 0 M = 1	2	$-.09 \times 10^{-37}$
	J = 3 K = 2 M = 2	4.2	2.64×10^{-37}
	J = 4 K = 3 M = 3		4.6×10^{-37}
HCN	J = 1 M = 0	1	6.9×10^{-37}
	J = 0 M = 0	.7	-11.3×10^{-37}
	J = 1 M = 1	1	-3.5×10^{-37}
$L_1{}^7Br^{79}$	J = 1 M = 0	.4	6.7×10^{-36}
	J = 0 M = 0	.3	-11×10^{-36}
	J = 1 M = 1	.4	-3.4×10^{-36}
$L_1{}^7H$	J = 1 M = 0	1.3	6.5×10^{-37}
	J = 0 M = 0	.93	-11×10^{-37}
	J = 1 M = 1	1.3	-3.2×10^{-37}

The population densities for NH_3 represent the percentage of molecules in a given J and K state. In the case of HCN the population in each M state was assumed to be approximately the same.

molecules $N = N_2 - N_1$ entering the resonant structure must be sufficiently in excess of the thermal equilibrium value in order that the power radiated by induced emission can be made greater than the power losses in the resonant structure and the detecting system. This number depends upon the fraction f mentioned above and the focusing efficiency. The latter in turn depends upon the focusing force constant defined by a relation of the form

$$f_r = C E \frac{dE}{dr} \qquad (2.5.1)$$

where f_r is the focusing force upon a molecule in an inhomogeneous electric field E (Chapter IV). For comparison the values of f and C for some molecular transitions are listed in Table I [10a].

It is apparent from Table I that the J = K = 3 inversion transition of ammonia at the frequency $\nu = 23870$ MH_z is the most convenient for maser action. This transition of ammonia has therefore been popularly used in beam maser work by various authors as also in the present investigations. In the following chapter some aspects of the ammonia molecule are considered from the point of view of maser action.

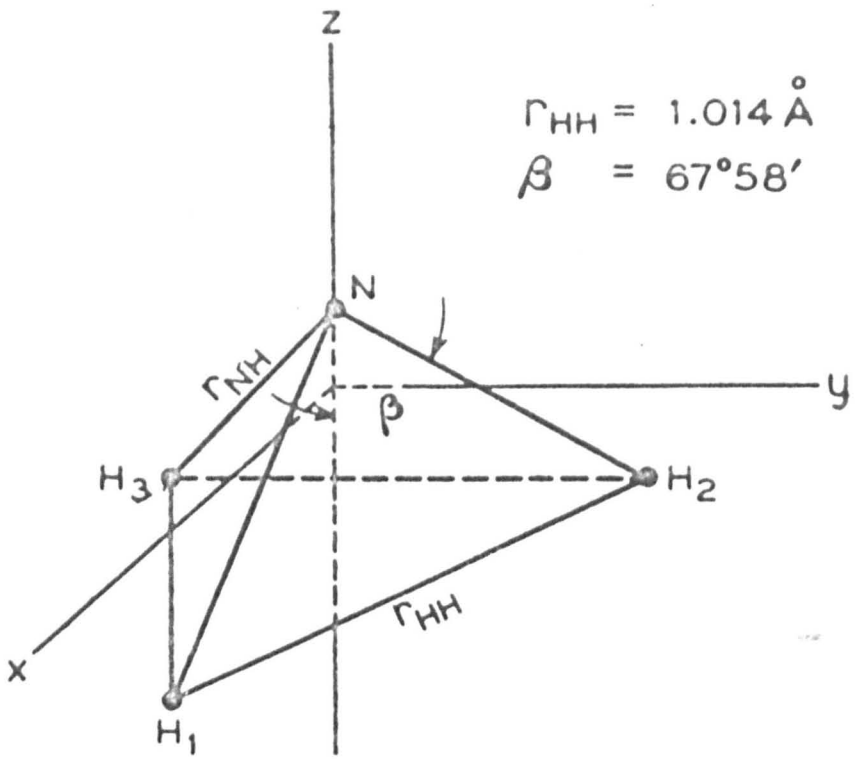

Geometrical structure of the ammonia molecule.

Fig. 3.1.1a. (21)

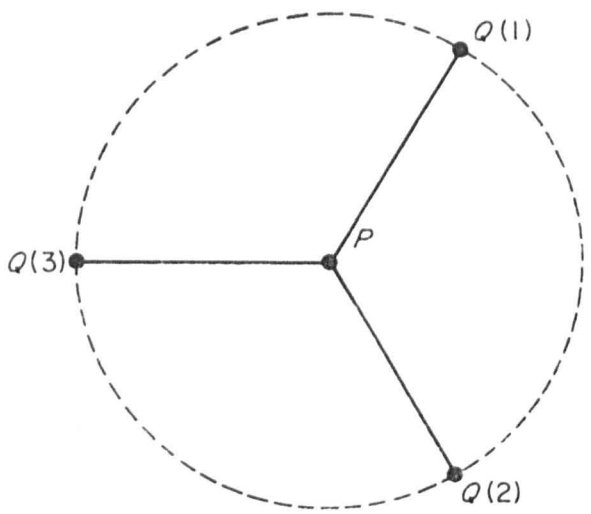

Diagram of a symmetric top PQ_3 viewed along the figure axis

Fig. 3.1.1b. (21)

CHAPTER III

MECHANICS OF THE AMMONIA MOLECULE.

3.1. Introduction :

From the microwave spectroscopist's point of view, interest in the ammonia molecule (NH_3) lies in the fact that it is one of the best understood molecules and has provided a large number of easily observable lines on which to try experimental techniques as well as theory. Evidence presented by its infrared and Raman spectra has shown that it has the general dynamical properties of a vibrating, symmetrical top, and the general shape of a pyramid or tetrahedron. In the Chemist's picture of the molecule, the nitrogen atom which has the configuration $1s^2\ 2s^2\ 2p^3$, is covalently bound to the three hydrogen atoms ($1s^1$) so that each hydrogen completes its K-shell and the nitrogen completes its octet giving it a neon like structure. The pyramidal structure arises from the tervalent valency state of the nitrogen atom in which the three p-electrons are oriented in three mutually perpendicular directions [3, 7, 11, 12].

Fig. 3.1.1a gives a schematic representation of this configuration. The three H-atoms lie at the vertices of the equilateral triangular base, and the N-atom at the apex of the tetrahedron. The bond angle is only $106^\circ\ 47'$ which is less than the tetrahedral angle $109^\circ\ 28'$ because there is a slightly greater repulsion between the non-bonding electrons and the hydrogen bonding electrons than the mutual repulsion between the hydrogen bonding electron pairs which are therefore pushed closer together [12]. The

distance between the H-atoms is 1.014 Å, and the angle θ is 67° 58'.

The total energy W of the molecule can be expressed as

$$W = W_T + W_V + W_R + W_I \qquad (3.1.1)$$

Where W_T, W_V, W_R, represent respectively the translational, vibrational, and rotational energies and W_I represents the energy of interaction between the vibrational and rotational motions. In the context of the present discussion, W_T and W_I can be ignored, and the dynamical features of the molecule may, in first order, be discussed in terms of W_R and W_V only, i.e.

$$W = W_R + W_V \qquad (3.1.2)$$

3.2 Rotational Spectrum:

The rotational energy levels of a symmetric top molecule can be obtained in a simple way by considering it as a rigid rotor and treating the problem semi-classically [7,11].

The total angular momentum $\bar{J}$ of the top is fixed in space and the rotational energy is given by

$$W_R = \frac{J_x^2}{2I_x} + \frac{J_y^2}{2I_y} + \frac{J_z^2}{2I_z} \qquad (3.2.1)$$

where x, y, z are Cartesian co-ordinates along the principal axes. The z-axis of the principal axis system is customarily taken along the axis of greatest symmetry of the molecule. For ammonia this axis contains the nitrogen atom and the centre of mass of the triangular base. It is

obvious that this axis has got threefold symmetry. If the molecule is rotated through an angle of $2\pi/3$ radians, the ellipsoid of inertia remains unchanged, that is to say that the momental ellipsoid is a rotational ellipsoid. It is therefore assumed that $I_x = I_y = I_B$. Then, since

$$J^2 = J_x^2 + J_y^2 + J_z^2 \tag{3.2.2}$$

therefore

$$W_R = \frac{J^2}{2I_B} + J_z^2 \left(\frac{1}{2I_c} - \frac{1}{2I_B} \right) \tag{3.2.3}$$

where $I_z = I_c$. J^2 and J_z are quantized and are given by

$$J^2 = J\,(J + 1)h^2, \quad J_z^2 = K^2 h^2 \tag{3.2.4}$$

where J and K are integers and $K = J, J - 1, \ldots . -J$. Hence Eq. 3.2.3. becomes

$$W_R = \frac{h^2}{2I_B} J\,(J + 1) + \frac{h^2}{2} \left(\frac{1}{I_c} - \frac{1}{I_B} \right) K^2 \tag{3.2.5}$$

which gives the quantized rotational energies of the molecule. Defining the rotational constants as

$$B = \frac{h^2}{2I_B}, \qquad C = \frac{h^2}{2I_c} \tag{3.2.6}$$

the familiar expression

$$W/h = BJ\,(J + 1) + (C - B)K^2 \tag{3.2.7}$$

is obtained.

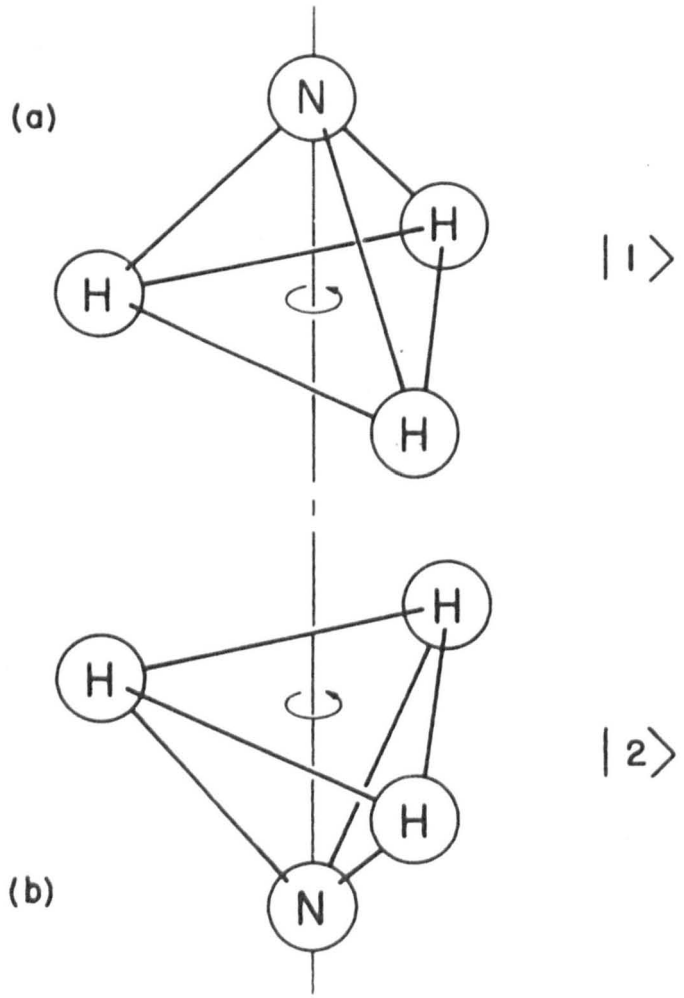

Two equivalent geometric arrangements of the ammonia molecule.

Fig. 3.2.1. (24)

The general motion of the molecule is shown in Fig. 3.2.1. K is the projection of J on the figure axis (symmetry axis) of the molecule and is a constant of the motion. The molecule spins about its figure axis with energy given by the quantum number $|K| \leq J$. For $|K| = J$, this is the only rotational motion to be observed. However when $|K| \neq J$, in addition to the spinning, the molecule executes a precession about the total angular momentum J. Further, J is also space-quantized and orientates itself relative to an arbitrary axis in space such that its projection on this axis is given by $Mh/2\pi$ where $M = 0, \pm 1, \pm 2, \ldots, \pm J$. J, K, M are the total angular momentum, rotational angular momentum, and the magnetic quantum number respectively.

It may be noted that W_R depends on K^2. Therefore all levels for which $|K| \neq 0$, are doubly degenerate, and a given value of J is associated with a series of only (J + 1) levels. For each value of K, there is an infinite series of levels with different values of J. Although for each K series the exact energies for corresponding J levels are different, the separation between equivalent J-levels are constant, so that only one series spectrum will be observed, with the selection rules

$$\Delta K = 0, \quad \Delta J = 0, \pm 1, \quad \text{for } K \neq 0$$
$$\Delta K = 0, \quad \Delta J = \pm 1 \quad \text{for } K = 0 \qquad (3.2.8)$$

The rotational spectrum of a symmetric top should therefore be governed by the frequency relation

$$\nu = \frac{\hbar^2}{I_B} (J + 1) = 2B (J + 1) \qquad (3.2.9)$$

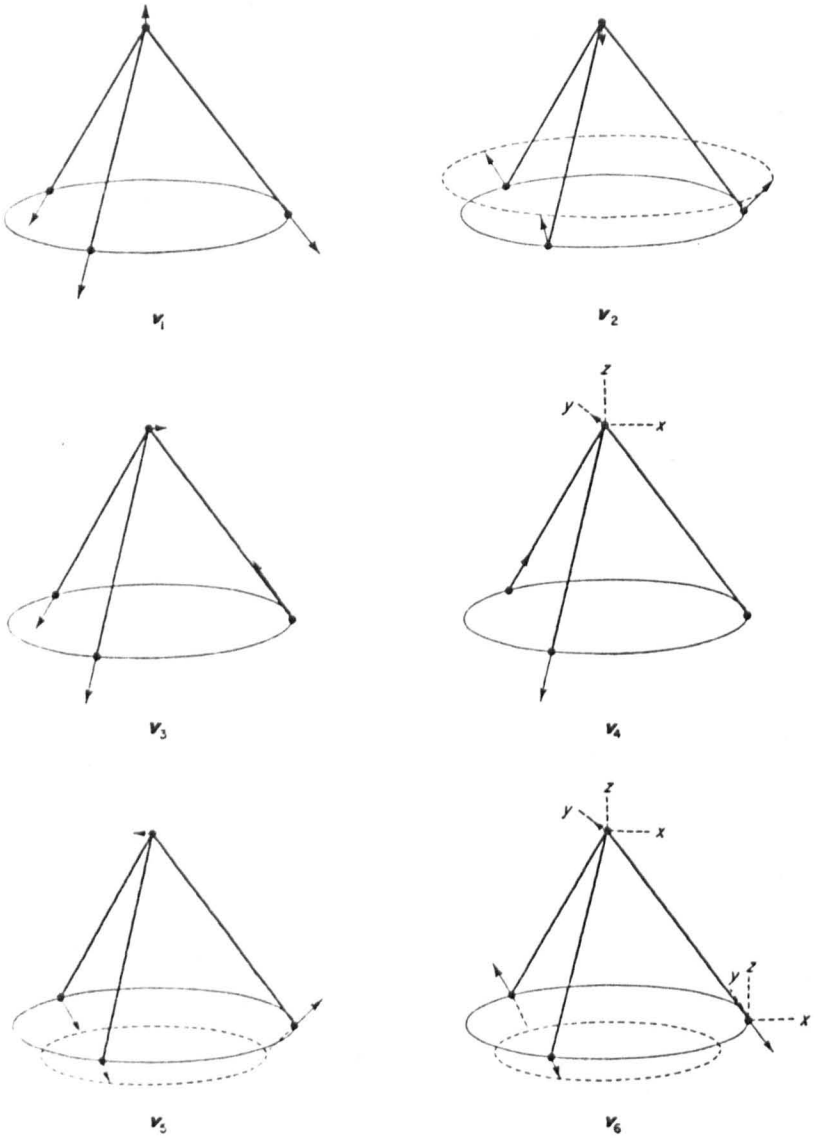

Fig 3.3.1 Vibrational modes of the Ammonia Molecule.

for $J \rightarrow (J + 1)$, all lines with different K values being coincident. However this is not the precise case.

The ammonia molecule is not quite rigid and it distorts centifrugally. If centifrugal distortion is taken into account, the energy may be expressed as

$$W/h = BJ\,(J + 1) + (C - B)K^2 - D_J\,J^2\,(J + 1)^2 - D_{JK}\,J\,(J + 1)K^2 - D_K\,K^4 \qquad (3.2.10)$$

where the term in D_J refers to stretching along the figure axis, that in D_K to stretching at right-angles to that axis, while the term in D_{JK} represents an interaction between the two. For ammonia B = 298,000 MHz, D_J = 19 MHz, and D_{JK} = -28 MHz.

With the selection rules $\Delta J = \pm 1$, $\Delta K = 0$, the frequencies of allowed transitions are

$$\nu = 2\,(B - D_{JK}\,K^2)\,(J + 1) - 4\,D_J\,(J + 1)^3 \qquad (3.2.11)$$

for $J \rightarrow (J + 1)$. The transition is split into (K + 1) lines and the rotational spectrum of ammonia in the far infrared region is no longer degenerate for different values of K.

3.3. Vibration: The Inversion States of Ammonia.

The ammonia molecule has six normal modes of vibration. Two of these, V_1 and V_2 involve the nitrogen atom oscillating along the principal axis of the system (Fig. 3.3.1). The other four modes, V_3, V_4,

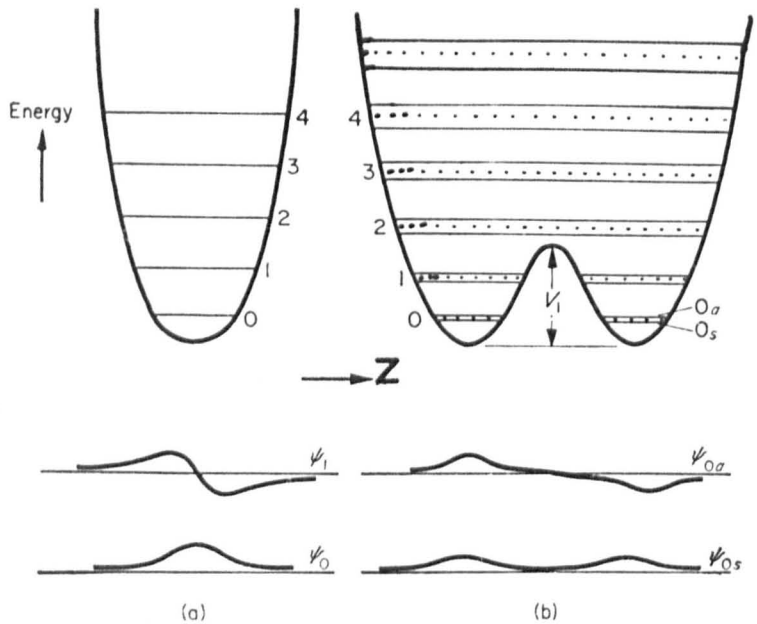

v = 0

Diagrammatic representation of energy levels and potential energy function (upper) and lowest two wave functions (lower) for (*a*) a simple harmonic oscillator, and (*b*) an oscillator with a hindering potential

3·3·2a,b(26)

V_5, V_6 are degenerate in pairs and have a considerably greater frequency (1627 cm^{-1}, 3414 cm^{-1}), than V_2 which vibrates at about 950 cm^{-1}, whereas V_1 is more energetic (~ 3335 cm^{-1}).

The rotational structure of the ground vibrational state (V = 0) has been discussed in the preceding section. Similarly, each vibrationally excited state has got a rotational structure. It has been shown that the vibrational energy levels are split into pairs because there exist two equivalent positions for the nitrogen atom[15, 16]. This gives rise to a doubling in the far infrared spectrum which has been observed by Wright and Randall[17]. To explain this structure necessitates an energy difference between the two lowest levels which falls in the microwave range. Absorption in the microwave range (~ 0.8 cm^{-1}) was first observed by Cleeton and Williams in 1934[18].

It has been stated above that the ammonia molecule has a pyramidal structure. If the N-atom is moved through the H-3 plane to an equivalent position on the other side, an inverted configuration is obtained. The potential energy as a function of the distance z of the N-atom from the H-3 plane is depicted in Fig. 3.3.2b showing two identical potential minima. Classically, the N-atom in the lower vibrational states will not have enough energy to move from one side to the other of the central potential hill.

Fig. 3.3.2a shows the potential energy diagram of a simple harmonic oscillator, with its equally spaced energy levels, also the form of the eigenfunctions ψ_o and ψ_1 for the first two levels. If a potential barrier is raised at the centre of the well (Fig. 3.3.2b), then the spacing

of the energy levels and the shape of the wave functions change and a series of split levels results. The broken horizontal lines represent the energy levels one would obtain if one had two independent minima not connected by a potential hill. The transitions between the components of the split levels are called "inversion transitions", because classically they correspond to the molecule inverting or "turning inside out" about a plane through the centre of mass. Such a motion is forbidden classically and is explained in terms of the wave mechanical tunnel effect.

Following reference 7, let the wave function for the ground state of simple harmonic oscillation with the N-atom on the left side of the H-3 plane be U_L and that for N to the right be U_R. It may readily be seen that there will be finite overlap between the wave functions of the two potential wells. This overlap can take place in two ways, consistent with the symmetry of the whole system, to give the eigenfunctions ψ_{os} and ψ_{oa} (Fig. 3.3.2B) as

$$\psi_{os} = 1/\sqrt{2}.\ (U_L + U_R)$$

$$\psi_{oa} = 1/\sqrt{2}\ \ (U_L - U_R) \qquad (3.3.1)$$

These eigenfunctions are respectively symmetric and antisymmetric to reflection at the origin. The symmetric function (ψ_{os}) corresponds to the lower one of the pair of levels.

If N is definitely on the left at time t = 0,

$$\psi = U_L = 1/2^{\frac{1}{2}}\ (\psi_o + \psi_1) \qquad (3.3.2)$$

or, with the time variation included,

$$\psi = 1/2^{\frac{1}{2}} (\psi_{os} + \psi_{oa} \exp 2\pi i\nu t) \exp (2\pi i W_o t/h) \qquad (3.3.3)$$

where $h\nu$ is the energy separation of the two inversion states and W_o the energy of the lower state corresponding to ψ_{os}. After time $t = 1/2\nu$ the wave function becomes

$$\psi = 2^{-\frac{1}{2}} (\psi_{os} - \psi_{oa}) \exp (2\pi i W_o t/h)$$

$$= U_R \exp (2\pi i W_o t/h) \qquad (3.3.4)$$

which corresponds to N being on the right side. The eigenfunctions tell us that in the two limiting cases, the nitrogen is either on the left or the right of the H-3 plane with equal probability. For intermediate cases, the eigenfunction has components on both sides of the forbidden zone.

The "doublet splitting" and therefore the probability for the "tunnelling" is found to be very sensitive to the height of the potential barrier, but its exact shape is not critical. Dennison and Uhlenbeck[16] were able to assume a simple shape in their theoretical model in 1932. Vuylsteke[3] has obtained a reasonable solution by using a square well approximation.

An approximate solution of the Schroedinger equation for the wavefunction of Eq. 3.3.3 in the forbidden zone $-a \leq z \leq +a$, can be written as

$$\psi = \exp \left\{ - h^{-1} \int_{-a}^{z} \left[2m' (V_z - W) \right]^{\frac{1}{2}} dz \right\} \qquad (3.3.5)$$

where m' is the reduced mass of the molecule, V_z is the potential energy

of the barrier at z, and W is the vibrational energy. Eq.3.3.5 gives a measure of the penetration of the wave function into the barrier and shows that the small component of the wave function in the forbidden zone decreases exponentially from the values of the boundary where the nitrogen strikes. The average time the nitrogen takes to go from one side to the other i.e. to penetrate the barrier is given by $1/2\Delta E$ if ΔE is the energy difference in cm^{-1} of the two sublevels for a given vibrational state[11]. For ammonia in the ground state, this quantity is $\sim 2 \times 10^{-11}$ sec. corresponding to $\Delta E = 0.8\ cm^{-1}$. The molecule may be visualized as rapidly vibrating with the nitrogen in the potential well on one side of the H-3 plane, at the frequency V_2 (= 950 cm^{-1}) which lie in the infrared and then begin oscillating on the other side after penetrating the barrier at the much slower rate of 0.8 cm^{-1} in the microwave region for the ground state[16,19].

The transmitted amplitude of the wave function is

$$\psi_{z=a} = \exp.\left[-2h^{-1} \int_o^a \left[2m\ (V_z - W)\right]^{\frac{1}{2}} dz \right]$$

$$= A^{-2} \qquad (3.3.6)$$

It is readily seen that the total transmitted amplitude after time t is $V_2 t\ A^{-2}$ and the inversion frequency is $\nu = V_2 \pi^{-1} A^{-2}$. For ammonia in the ground state A^2 is about $e^6 (\approx 400)$. This explains why the inversion frequency is very sensitive to the barrier height. If the barrier becomes infinitely high, the splitting becomes zero. By the same consideration, the splitting increases for higher levels as the top of the barrier is approached. Far above the top, the energy levels still show the effect by being grouped into pairs, but this pairing becomes less obvious for the higher levels.

3.4 Inversion and Symmetry :

The wave equation for a rotating molecule may be written as

$$H_{op}\,\psi = W\psi \qquad (3.4.1)$$

where H_{op} is the Hamiltonian operator which remains unchanged when the co-ordinate system is inverted about the origin. If the coordinate change $(x, y, z) \rightarrow (-x, -y, -z)$ is made in Eq. 3.4.1, then the new wave function ψ must be a solution of Eq. 3.4.1 for the same energy W. For a non-degenerate level $\psi = C\psi$, where C is a constant. If now another transformation $(x, y, z) \rightarrow (-x, -y, -z)$ is made, $\psi = C\psi = C^2\psi$.

Since the second transformation is just a reversal of the first transformation, ψ must be the same as ψ and thus $C^2 = 1$ or $C = \pm 1$. If $C = +1$, ψ is not altered by inversion about the origin, and is said to be symmetric with respect to this operation. If $C = -1$, ψ merely changes its sign on inversion, and is said to be antisymmetric. The inversion levels can therefore be designated as an even (+) and an odd (-) level. The selection rule

$$+ \leftrightarrow - \qquad + \not\leftrightarrow + \qquad - \not\leftrightarrow - \qquad (3.4.2)$$

is readily established.

3.5 Fine Structure :

The rotational-vibrational interaction of the ammonia molecule shows up as a doublet structure characteristic of inversion changes superposed on the pure rotational spectrum. In addition, the fact that the molecule is rotating causes the pure inversion spectrum to be split into a very large number of lines, each line corresponding to a given

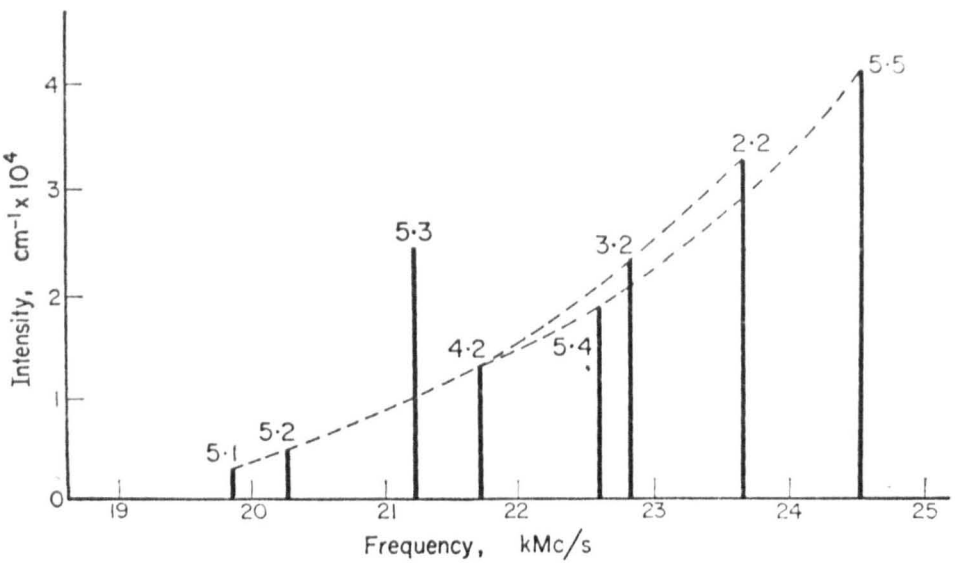

Relative intensities at room temperature of various rotational components of the ammonia inversion spectrum. Two series of lines are shown—one for $J = 5$ with K ranging from 1 to 5, and one for $K = 2$ with J ranging from 2 to 5

Fig. 3. 5.1. (31)

rotational state.

The rotational frequencies of ammonia are considerably higher (far infrared) than the inversion frequencies of the ground state (microwave), so that no resonance interactions occur. However, the centrifugal forces due to rotation changes the effective potential in which the molecule moves. If the molecule is rotating about the symmetry axis, centrifugal forces will tend to push the H-atoms outwards to give a rather flattened pyramid. Such a pyramid will have lower potential barrier to inversion than will that for the non-rotating molecule, and consequently a higher inversion frequency. Similarly rotation about an axis perpendicular to the symmetry axis will lower the inversion frequency. This is precisely what is observed and is illustrated in Fig. 3.5.1.

The above considerations lead to the following form of the inversion frequency :

$$\nu = \nu_o - a\left[J(J+1) - K^2\right] + bK^2 + \text{higher powers of J and K.}$$

Attempts at numerical solutions of the modified wave equation for the non-rigid rotor have produced limited agreement with observation[20,21]. Among recent theoretical works, Swalen and Ibers[22] have obtained a somewhat better solution for a harmonic oscillator potential well with a Gaussian barrier and Bagdanskis and Bulanin[23] have given a generalized treatment for possible inversion states of ammonia in the condensed phase.

A large number of observed lines have been fitted by Costain[24] to a formula given by

$$\nu = \nu_o \exp. \left| aJ(J+1) + bK^2 + CJ^2 (J+1)^2 + dJ (J+1)K^2 + eK^4 \right| \text{ MHz} \qquad (3.5.2)$$

This fits all lines with $J \leq 16$ ranging from 16798.3 MHz ($J = 9$, $K = 5$) to 39,941.54 MHz ($J = 16$, $K = 16$) to within 1.3 MHz, with the following values for the constants :-

$$\begin{aligned} \nu_o &= 23785.88 \text{ MHz} \\ a &= -6.36996 \times 10^{-3} \\ b &= +8.88986 \times 10^{-3} \\ c &= +8.6922 \times 10^{-7} \\ d &= -1.7845 \times 10^{-6} \\ e &= +5.3075 \times 10^{-7} \end{aligned}$$

3.6 Hyperfine Structure :

The inversion spectrum of ammonia shows hyperfine structure on account of the electric quadrupole coupling of the N^{14} ($I_N = 1$) nuclear spin to the rotational motion and other smaller interactions. The hyperfine structure of the $J = K = 3$ line was first observed by Good[19] in 1946 and was examined in great detail both theoretically and experimentally by Gunther-Mohr et al[25, 26] in 1954 using a spectrometer with 100 KHz resolution. Using a beam maser with 7 KHz resolution Gordon[27] in 1955 found additional structures in the inversion spectrum. In view of further resolution (350 Hz, a factor of 20 improvement on Gordon) afforded by a double cavity Ramsey type maser, these measurements have been recently repeated by Kukolich (1967).[28, 29].

The various hyperfine interactions are described in terms of the following additional quantum numbers besides J and K which specify the rotational state of the ammonia molecule in zero applied electric field :

I_N : spin of the nitrogen nucleus.

I_i (i = 1,2,3) : spin of the ith hydrogen nucleus.

$I = I_1 + I_2 + I_3$

$F_1 = J + I_N$, $F = F_1 + I$

M_F : projection of F on some axis in space.

(i) The interaction between the nuclear quadrupole moment Q of the nitrogen and the gradient of the electric field $q = \partial^2 V/\partial^2 z$ due to the other molecular charges is given by

$$\alpha_1 = -eq\,Q \left[1 - \frac{3K^2}{J(J+1)}\right] \Omega_1 (J, I_N) \qquad (3.6.1)$$

where $$\Omega_1 (J, I_N) = \frac{3(I_N.J)^2 + \frac{3}{2}(I_N.J) - I_N(I_N + 1)\, J\,(J + 1)}{(2J - 1)\,(2J + 3)\,2\,I_N\,(2\,I_N - 1)} \qquad (3.6.2)$$

$$eq\,Q = -4084.2\,(1 + 10^{-4}J(J + 1) + 10^{-4}\,K^2) \pm 0.3\ \text{KHz} \qquad (3.6.3)^{25}$$

Other important interactions in the hyperfine structure are :

(ii) Interaction between the magnetic moment of the nitrogen nucleus and magnetic fields produced by molecular rotation, discovered by R.S. Hendersen in 1948 :

$$\alpha_2 = \left[a + \frac{(b-a)K^2}{J(J + 1)}\right] (I_N.\, J) \qquad (3.6.4)$$

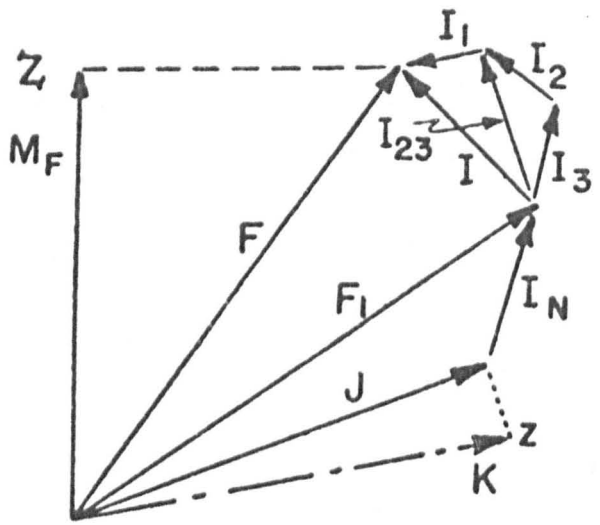

$N^{14}H_3$ molecular coupling scheme referred to laboratory axis. Z is the fixed direction in the laboratory, z is the axis coinciding with the molecular symmetry axis, and K is the projection of J on the molecular symmetry axis.

Fig. 3.6.1. (34)

where the coupling constant a is proportional to the transverse magnetic field at the nitrogen nucleus, b is proportional to the axial field and given by [25]

$$a = 6.1 \pm 0.2\ KH_z, \qquad b = 6.5 \pm 0.2\ KH_z .$$

(iii) Hydrogen magnetic interaction with molecular rotation:

$$\alpha_3 = \left[A + \frac{CK^2}{J(J+1)} + {}_{K1}(-1)^{J+v} B \right] (I.J) \qquad (3.6.5)$$

where A, B, C are functions of the magnetic field strengths at the position of the hydrogen nuclei.

(iv) Hydrogen-nitrogen spin-spin interaction

$$\alpha_4 = g_H\, g_N\, \mu_o^2\, r_{NH}^{-3} \sum_{i=1,2,3} \left[(I_i.I_N) - 3\,(I_i.r_{iN})\,(I_N.r_{iN}) \right] \qquad (3.6.6)$$

(v). Hydrogen-hydrogen spin-spin interaction, which is present for the J = K = 3 state, was introduced by Gordon[27]:

$$\alpha_5 = (g_H\, \mu_o)^2\, r_{HH}^{-3} \sum_{i<j} \left[I_i.I_j - 3\,(I_i.r_{ij})\,(I_j.r_{ij}) \right] \qquad (3.6.7)$$

where the subscripts i, j refer to the ith or jth hydrogen atom. The molecular coupling scheme[26] is shown in Fig. 3.6.1. Since magnetic interactions are much smaller than the nitrogen quadrupole coupling

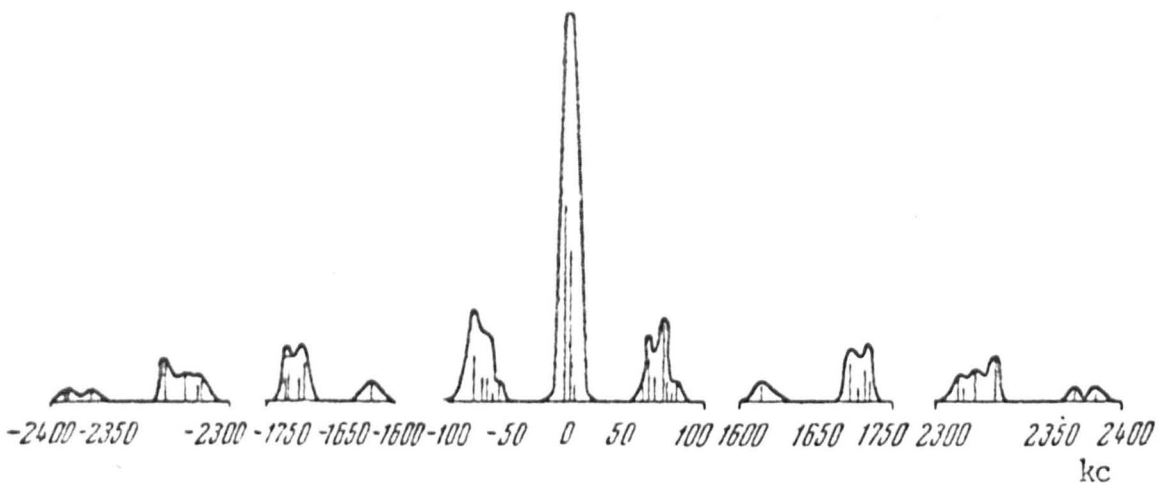

Structure of the spectral line J = 3, K = 3 of $N^{14}H_3$.

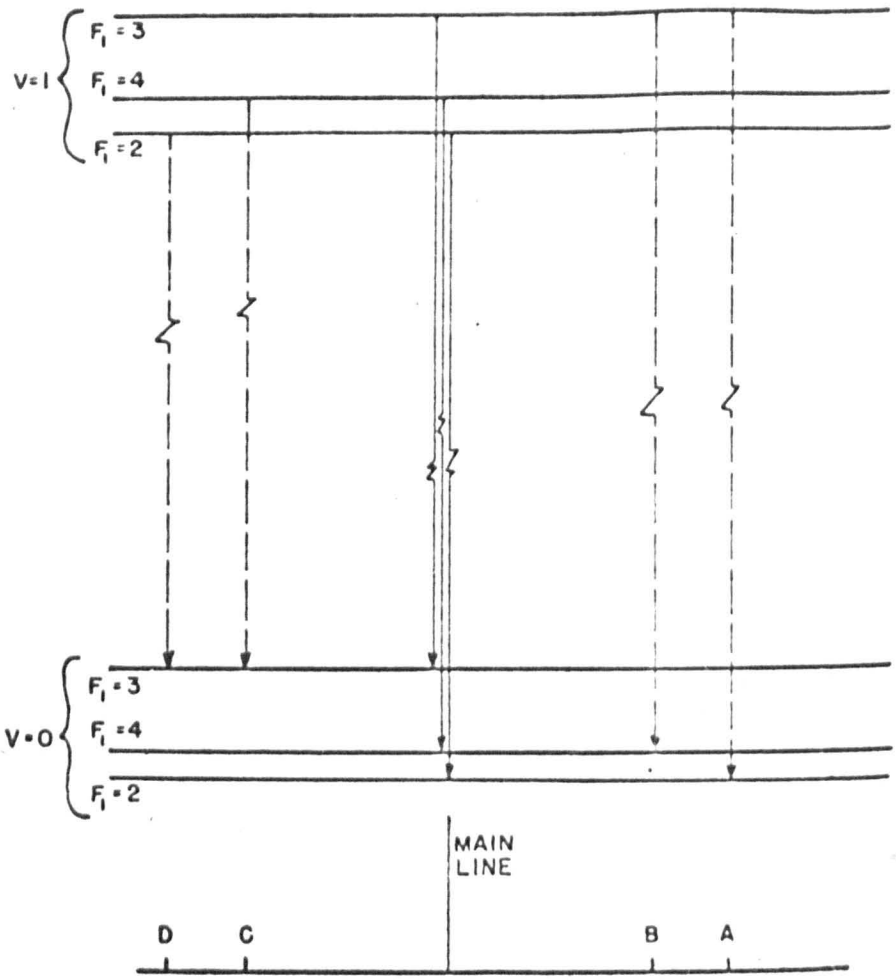

Hyperfine sublevels of $N^{14}H_3$ 3–3 inversion lines (top) and the corresponding frequency spectrum (bottom) in which "*B*", "*C*" and "*A*", "*D*" are inner and outer quadrupole statellites respectively. $F_1 = J + I_N$, where J is the angular momentum due to molecular rotation, and I_N the nitrogen nuclear spin.

Fig. 3.6.3. (35)

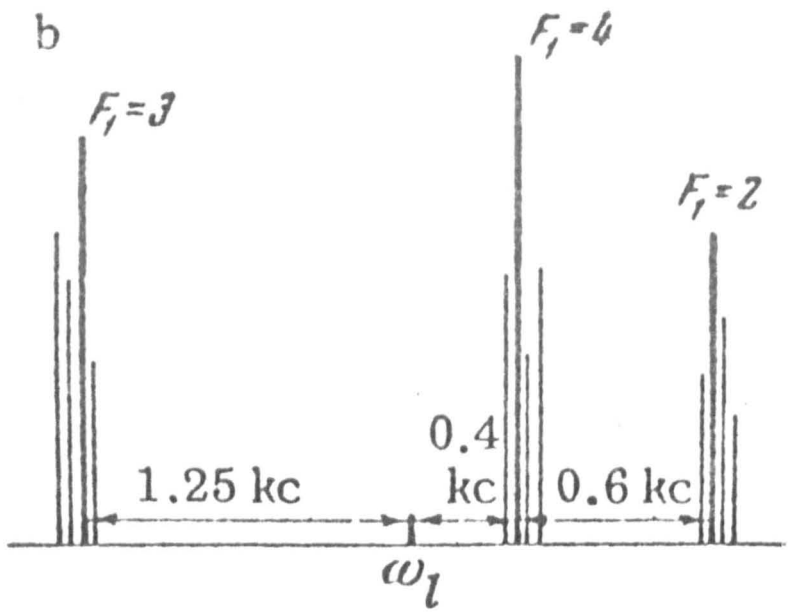

Fig. 3.6.4 Structure of the F_1 components of the ammonia inversion line $J=K=3$, $\Delta F_1 = \Delta F = 0$. (35)

energy, the nitrogen spin I_N is first coupled to J to give F . The protons can then be numbered according to their positions relative to the chosen molecular axes and coupled together to give I, which is in turn coupled to F to give the total angular momentum of the molecule F.

It has been shown from symmetry arguments that the hydrogen-hydrogen spin spin interaction α_5 does not affect the hyperfine structure unless K is a multiple of 3.[27] The hyperfine structure of the J = K = 3 line is shown in Fig. 3.6.2. The main line consists of the transitions $\Delta F_1 = \Delta F = 0$. The nominal frequency of this transition is 23,870 MH_z and is popularly used in molecular beam work. The quadrupole interaction is the dominant energy term for $N^{14}H_3$ spectra and produces splitting of a few MH_z. Since $I_N = 1$ in this case, the transitions $\Delta F_1 = \pm 1$ result in a pair of quadrupole satellites on each side of the main line. These transitions are schematically represented in Fig. 3.6.3. The quadrupole satellites are further split by magnetic interactions of magnitude 10 to 50 KH_z. The transitions $\Delta F_1 = 0$, $\Delta F = \pm 1$ produce magnetic satellites on each side of the main line separated from the main line by about 65 KH_z. Each satellite is composed of 9 individual contributing components. The main line ($\Delta F_1 = \Delta F = 0$) consists of three components, one for each value of F_1 ($F_1 = 2, 3, 4$), and separated by less than 2 KH_z. Each F_1 component is made up of 4 unresolved contributing components (Fig. 3.6.4). Using a maser with an auxiliary stimulating field, Shimoda and Wang[30] measured some of the weak lower frequency components of the quadrupole satellites. Kukolich[28, 29]

has recently made a very detailed examination of the J, K 1-1, 2-2, 3-3, 3-2 lines of N^{14} H_3 and 1-1, 2-2, 3-3 lines of N^{15} H_3. In view of the extremely high resolution (350 Hz) of his apparatus, he found it necessary to take account of all the spin-spin and spin-rotational terms off diagonal in F_1.

The 3-2 line of N^{14} H_3 (ν = 22,834 MH_z) has the interesting feature in that the factor $\left|J(J+1) - 3K^2\right|$ vanishes and so the only non-zero interactions are the nitrogen magnetic interaction α_2 and the hydrogen magnetic interaction α_3. In view of the frequency pulling effect due to the presence of hyperfine structure the 3-2 transition is therefore more suitable than the 3-3 transition for beam maser frequency standards.

3.7 The Ammonia Molecule in a Static Electric Field :

The ammonia molecule does not exhibit a first order Stark effect normally characteristic of symmetric tops, because of its inversion. Classically it resembles a rapidly reversing dipole and has no average dipole moment in any direction in zero field. In a strong electric field (> 1000 volts/cm), the inversion is quenched and a net dipole moment appears. Neglecting hyperfine effects, the energies of the inversion states are given by

$$W = W_o \pm \left[\left(\frac{h\nu_o}{2} \right)^2 + \left(\mu_o E \frac{M_J K}{J(J+1)} \right)^2 \right]^{\frac{1}{2}} \qquad (3.7.1)$$

or,
$$W = W_o \pm \left| A^2 + \mu^2 E^2 \right|^{\frac{1}{2}} \qquad (3.7.2)$$

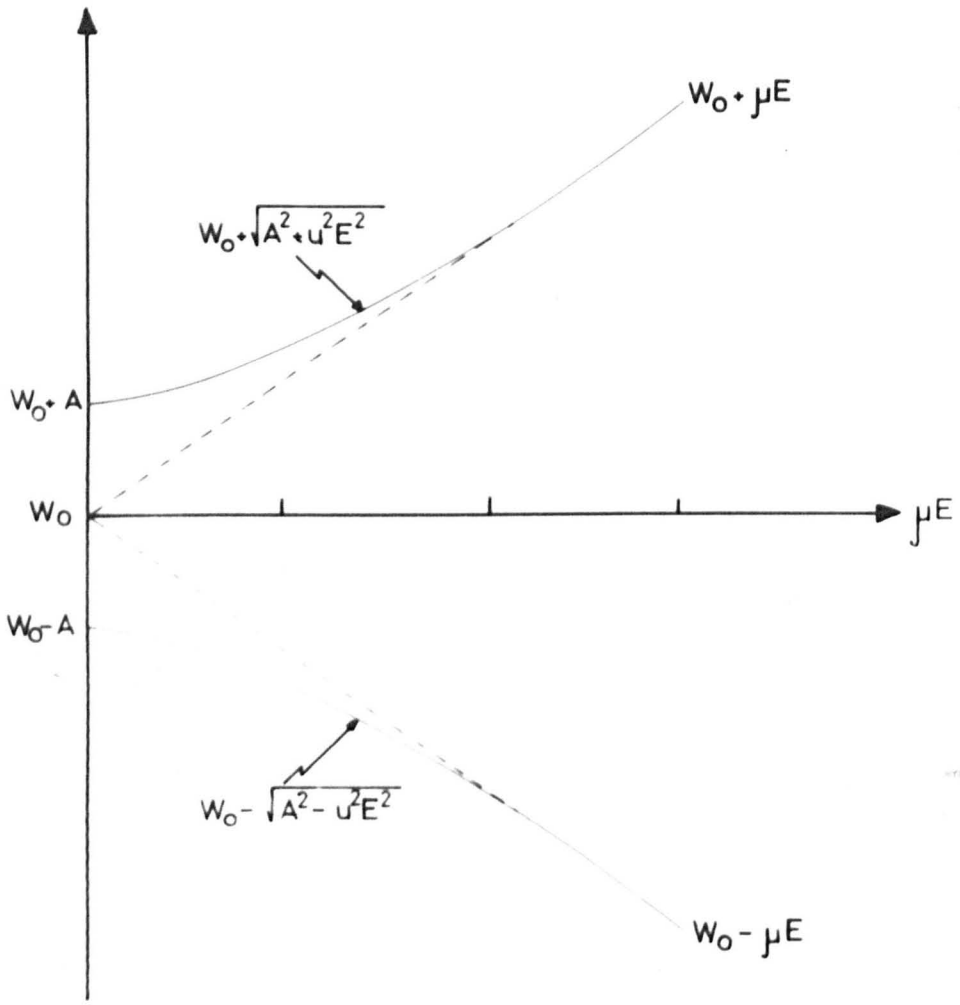

Fig 3.7.1 Energy levels of the ammonia molecule in an electric field.

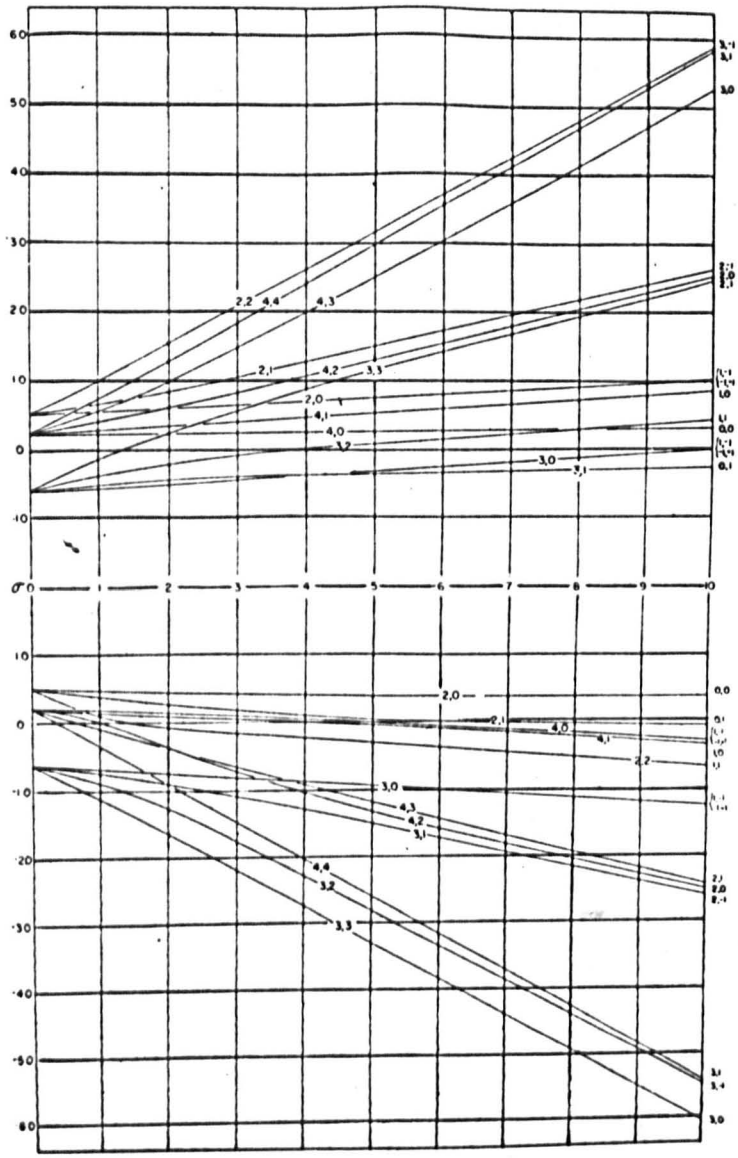

Energy levels in units e^2qQ for the ammonia inversion line $J=K=3$ as a function of the parameter

$$\sigma = \mu^2 E^2/[\Delta(J, K)e^2qQ].$$

The numbers at the right-hand edge denote M_J, M_i. The numbers in the figure give F, M_F for each line.

Fig. 3.7.2 (37)

for all field strengths. Here W_o is the average energy of the two states, ν_o the inversion frequency in zero field, μ_o the permanent dipole moment the molecule would have in absence of inversion, E the electric field strength, and M_J is the projection of J on the direction of the field. $\mu = \mu_o M_J K/J(J + 1)$ can be taken as the "effective" dipole moment for simplicity. In the equations above the upper sign refers to the upper inversion state and the lower sign to the lower state. The general nature of the effect of an external field on the energy states of the molecule is shown in fig. 3.7.1, while fig. 3.7.2 shows in detail the energy levels of $J = K = 3$ inversion line in an electric field. It is to be noted that the $M_J = 0$ states will not be affected by the field but $M_J = 0$ states will have different energies - the upper inversion states increasing in energy with increasing field and lower states decreasing in energy with increasing field. It follows that in an inhomogeneous field there will be a force on the molecule given by

$$f = - \text{grad } W = \mp \left[\frac{\mu^2 E \text{ grad } E}{(h\nu/2)^2 + \mu^2 E^2} \right]^{\frac{1}{2}} \qquad (3.7.3)$$

Thus molecules in the upper inversion state will experience a force in the direction of minimum electric field while molecules in the lower state will experience a force in the opposite direction. This is the basis of various techniques used to obtain a state selected beam of molecules (which have an electric dipole moment) in a maser type of system.

3.8 Population Distribution :

At thermal equilibrium the fraction of molecules in any particular inversion state of ammonia is given by

$$f = f_v \times f_r \times f_s \qquad (3.8.1)$$

where f_v and f_r are the fractions of molecules in the particular vibrational and rotational state respectively, f_s is the degeneracy due to spin and K degeneracy. For lower rotational states, f_r is approximately given by

$$f_r = \frac{(2J + 1)}{4I^2 + 4I + 1} \left| \frac{B^2 Ch^3}{\pi (KT)^3} \right|^{\frac{1}{2}} \qquad (3.8.2)$$

where I is the spin of a hydrogen nucleus.

f_s is given by

$$f_s = \begin{cases} 2\,(4I^2 + 4I + 3) & \text{for } K = 3n \neq 0 \\ 2\,(4I^2 + 4I) & K \neq 3n \\ (4I^2 + 4I + 3) & K = 0 \end{cases} \qquad (3.8.3)$$

The J = K = 3 ground vibrational state is the most populated level at room temperature, having 6% of the total number of molecules. Using the equation $N_2 = N_1 \exp(-h\nu/KT)$ for thermal distribution in the two levels, the ratio of populations in the upper and lower inversion states for J = K = 3 is given by

$$N_u/N_\ell = 250/251 \qquad (3.8.4)$$

CHAPTER IV.

GENERALIZED THEORY OF STATE SELECTION.

4.1. Introduction :

In order to realise resonance interaction of radiation with molecules in a desired energy state, the molecules have to be state selected by some means. The problem of state selection is often allied with that of space focusing. The possibility of focusing neutral particles by an electric or magnetic field will be discussed in general in the following sections. Although the electric case will be assumed, the discussions are valid for the magnetic case as well. It may also be noted that the term "focusing" is not used here in the strictly optical sense. That is, molecules starting at the entrance of the focusing system as considered here with the same position but different velocities and directions do not converge to one point at the end of the system.

4.2 Static Focusing Conditions :

The problem here is whether a slightly divergent beam of particles injected into a "lens" has the possibility of being reconverged and whether the lens can discriminate between different energy states. For a force field to keep a particle in stable equilibrium two conditions must be met:
(i) The applied force $\bar{F}$ must vanish, so that there is a point where the particle will experience no accelerative force i.e. $\bar{F} = 0$.
(ii) The force field near by must be restorative, that is, it should

tend to restore the particle to the point where $\bar{F} = 0$. In a coordinate system in which the gradient $\nabla\bar{F}$ is diagonal this condition can be stated as $\nabla.\bar{F}$ is equal to a negative quantity, where $\nabla.F$ is the divergence of the force field and is in this case given by the trace of the gradient

$$\nabla\bar{F} = \frac{\partial Fx}{\partial x} + \frac{\partial Fy}{\partial y} + \frac{\partial Fz}{\partial z} \qquad (4.2.1)$$

In practice a molecular beam is injected into an array of electrodes. The trajectory of the particle along the beam axis is called the axial trajectory. The differential motion of neighbouring particles is obtained by assuming that they experience the same force field as the axial particle and in addition a first order correction force. If $\Delta.\bar{F}$ is negative, it is possible that the particles in the neighbourhood will oscillate in bound motion about the axial trajectory. The crossing points on the axis can therefore be defined as the focal points. In the preceding discussion it has been implicitly assumed that the force constants do not vary along the particle path. Therefore the focusing criterion established does not include the effect of time variation of these parameters and simply require that $\nabla.\bar{F}$ be negative. For the sake of definition this case may be referred to as "static focusing". When the above criteria do not hold, focusing may still be possible under certain conditions. To distinguish such a situation from the one above the term "dynamic focusing" may be used. A method of dynamic focusing will be dealt with in detail in Chapter VI.

The sign of $\nabla.\bar{F}$ depends upon the type of molecular interaction with the applied field. In the usual situation the force field is derived

from a scalar potential function, and the potential energy of the molecule varies as the second or first power of the applied field. A second order interaction with field can be generally expressed as

$$W = -\tfrac{1}{2}\alpha_m |\bar{E}|^2 \qquad (4.2.2)$$

where W is the potential energy, $|\bar{E}|$ the magnitude of the applied electric field, and α_m a constant which is called the polarizability of the molecule. The value and sign of α_m depends on the particular quantum state of the molecule. It will be noticed that when α_m is negative, Eq. 4.2.1. corresponds to the case of ammonia in the upper inversion state.

Assuming that the field $\bar{E}$ acts in a source-free region and that $\bar{E}$ is the negative gradient of some scalar potential ϕ the following relations are satisfied,

$$\nabla.\bar{E} = 0 \quad \text{and} \quad \bar{E} = -\nabla\phi \qquad (4.2.3)$$

The force upon the particle is given by

$$\bar{F} = -\nabla W \qquad (4.2.4)$$

Using the equations given above, in a principal coordinate system

$$\nabla.\bar{F} = \alpha_m \sum_{p=1}^{3} \left(\frac{\partial^2\phi}{\partial x_p^2}\right)^2 \qquad (4.2.5)$$

where x_1, x_2, x_3 are the three principal coordinates. It follows that the sign of the divergence of forces for a second-order interaction is

determined by the sign of the polarizability α_m alone. For a first-order interaction of the type

$$W = - \mu_m |\bar{E}| \tag{4.2.6}$$

the corresponding relation is

$$\nabla.\bar{F} = \frac{\mu_m}{|\bar{E}|^3} \sum_{p,=q=1}^{3} \left(\frac{\partial\phi}{\partial\chi_p}\right)^2 \left(\frac{\partial^2\phi}{\partial\chi_q^2}\right)^2 \tag{4.2.7}$$

In this case the sign of $\nabla.\bar{F}$ is determined by the sign of μ_m which may be called the "effective moment". The case of first-order interaction will not be discussed further.

The sign of α_m indicates whether the molecular state gains or loses energy in an applied field. For a given sign of α_m, that is for molecules in a given quantum state, focusing or defocusing will depend upon the functional dependence of the electric field on the displacement from the axis of the system. In a general way it can be stated that a focusing system will exert a force on the molecules of the following form :

$$F = \bar{+} kr^n \tag{4.2.8}$$

where r is the distance from the origin of an appropriate co-ordinate system to the molecule.

Here the minus and plus sign applies to molecules in the upper (negative α_m) and lower energy state (positive α_m) respectively. Here n is a constant determined by the focuser configuration, and the sign of α_m is taken into account explicitly. The following special cases arise :

(i) n>1 : This is the case of the multipole focusers frequently used

in beam masers, n increasing with the number of poles. Such a system focuses molecules in states that increase in energy with increasing field, and defocuses molecules in states which decrease in energy with increasing field. This will be discussed in some detail in the following section.

(ii) $0<n<1$: This condition is met if the focuser is composed of a cylindrical cavity excited by a radio-frequency source[33a]. Such a focuser will discriminate between quantum states in the same way as in case (i). The frequency of the cavity should be much lower than the resonance frequency of the molecules and the cavity should operate in such a mode that the field configuration will provide the necessary space gradient for the focusing action.

(iii) $n<0$: In contrast to (i) and (ii), in this case the field has a maximum value at the centre and diminishes with increasing radius. Such a system will act as a lower state focuser for ammonia. The obvious configuration which achieves this is a co-axial line with voltage applied between the centre conductor and the outer conductor. This is however not a true focuser in as much as the motion of the molecules in such a system is not periodic and stable. Conceivably this limitation may be circumvented by cutting away the centre conductor at regular intervals.

Historically the earliest deflection experiments were done by Stern and Gerlach in 1924 using magnetic fields to deflect atomic beams. The first experiment by the molecular beam electric-resonance method using electric focusing field was that of H.K. Hughes (1947)[33b]

with CsF. Paul et al [34, 35] have used multipole magnetic fields for focusing atomic beams. Various types of electric and magnetic focusing techniques have been generally treated by Ramsey[36].

In subsequent sections certain types of upper state separator and focusers are discussed with particular reference to the ammonia molecule. The octapole focuser which has been used extensively in the present investigation will be discussed in some detail to highlight various aspects of focusing.

4.3 Upper State Selection : Multipole Focusers :

It was seen in Section 3.7 that ammonia molecules in different inversion states have different Stark energies, and that the force on a molecule in an inhomogeneous electric field is such that the upper inversion state molecules experience a force towards a region of lower field while lower state molecules experience a force towards a region of higher field. If a beam of ammonia molecules in thermal equilibrium passes through a system in which the magnitude of the electric field increases with increasing distance from the axis, then the upper state molecules will be directed towards the axis and the lower state molecules away from it. The kind of configuration envisaged can be obtained by having a multipole focuser consisting of an even number of alternately charged parallel rods located symmetrically about the beam axis. Such focusers have been used in ammonia masers by Gordon et al and others[37-44]. Theoretical analyses have been given by Shimoda[42], Vonbun[45], Hirono[46], Shimizu[47].

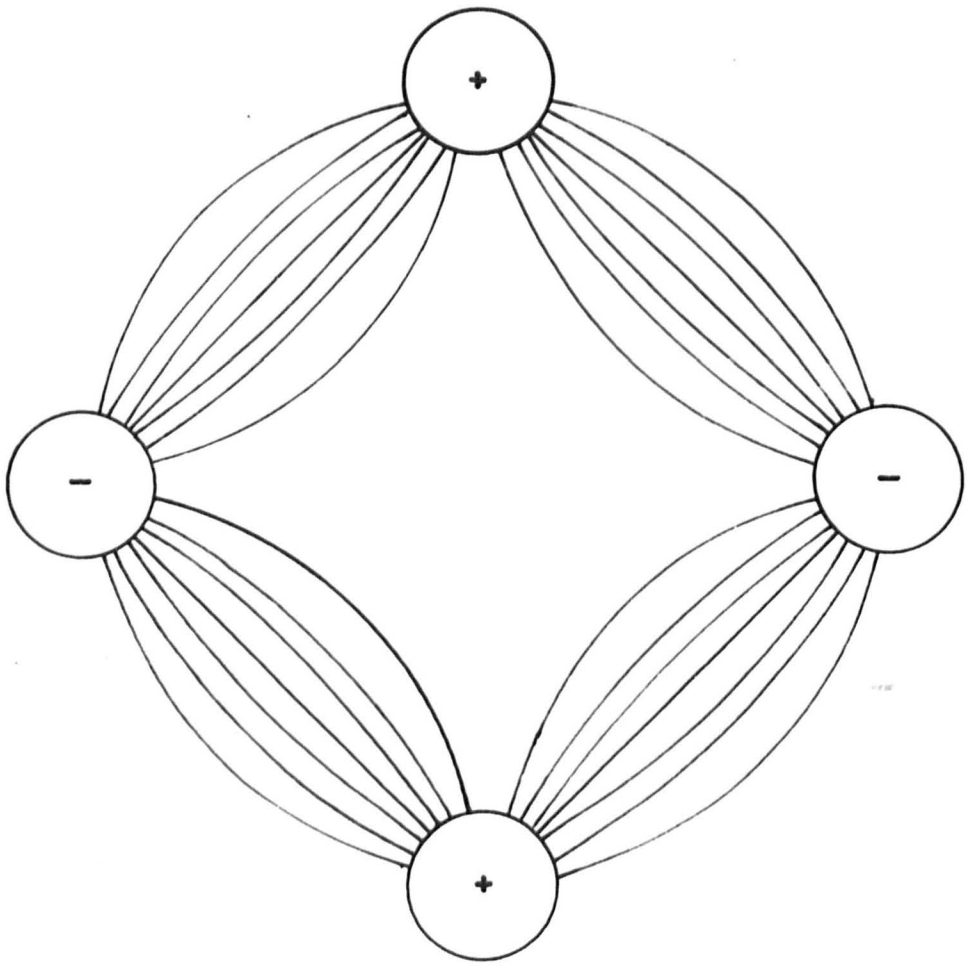

Fig 4.3.1. Field configuration of an Electric Quadrupole

The action of a multipole focuser can be immediately visualized by drawing the lines of force on a transverse plane as in Fig. 4.3.1 The electrostatic potential in a 2n-pole focuser with appropriate electrodes can be expressed by

$$\phi = \frac{V}{2R^n} \text{ Re } (x + iy)^n \qquad (4.3.1)$$

where V is the potential difference between neighbouring electrodes and R the distance of the electrode surface from the axis. The field at a distance r from origin is

$$E_r = \frac{nr^{n-1}}{2R^n} V \qquad (4.3.2)$$

The maximum field is at the inner surface of the electrodes (R = r) and is given by

$$E_m = E_R = \frac{n}{2R} V \qquad (4.3.3)$$

In practice fairly thick electrodes of circular cross section are used and Eq. 4.3.1-3 are satisfied to a good approximation.

Assuming that μE_r is smaller than $h\nu/2$, from Eq. 3.7.1 the energy of a molecule is given by

$$W = W_o \pm \left[h\nu/2 + \frac{\mu^2 E_r^2}{h\nu} \right] = W_o \pm \frac{h\nu}{2} \pm U(r) \qquad (4.3.4)$$

where ν is the inversion frequency in zero field. The radial focusing

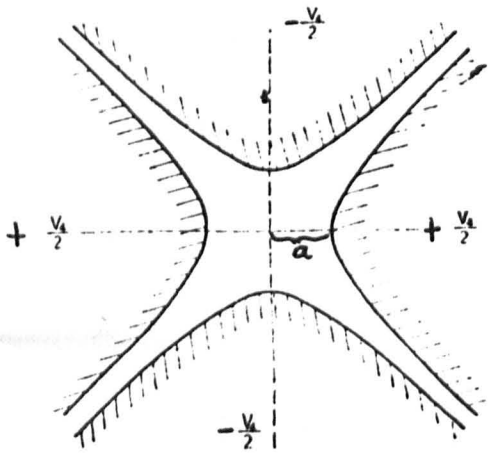

The cross section of the four-pole (harmonic) focuser.

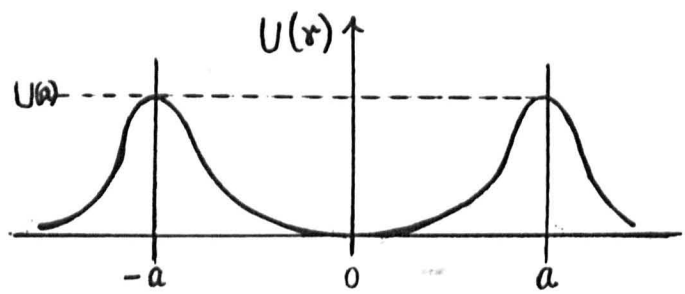

Upper state potential well.

Fig. 4.3.2 (46)

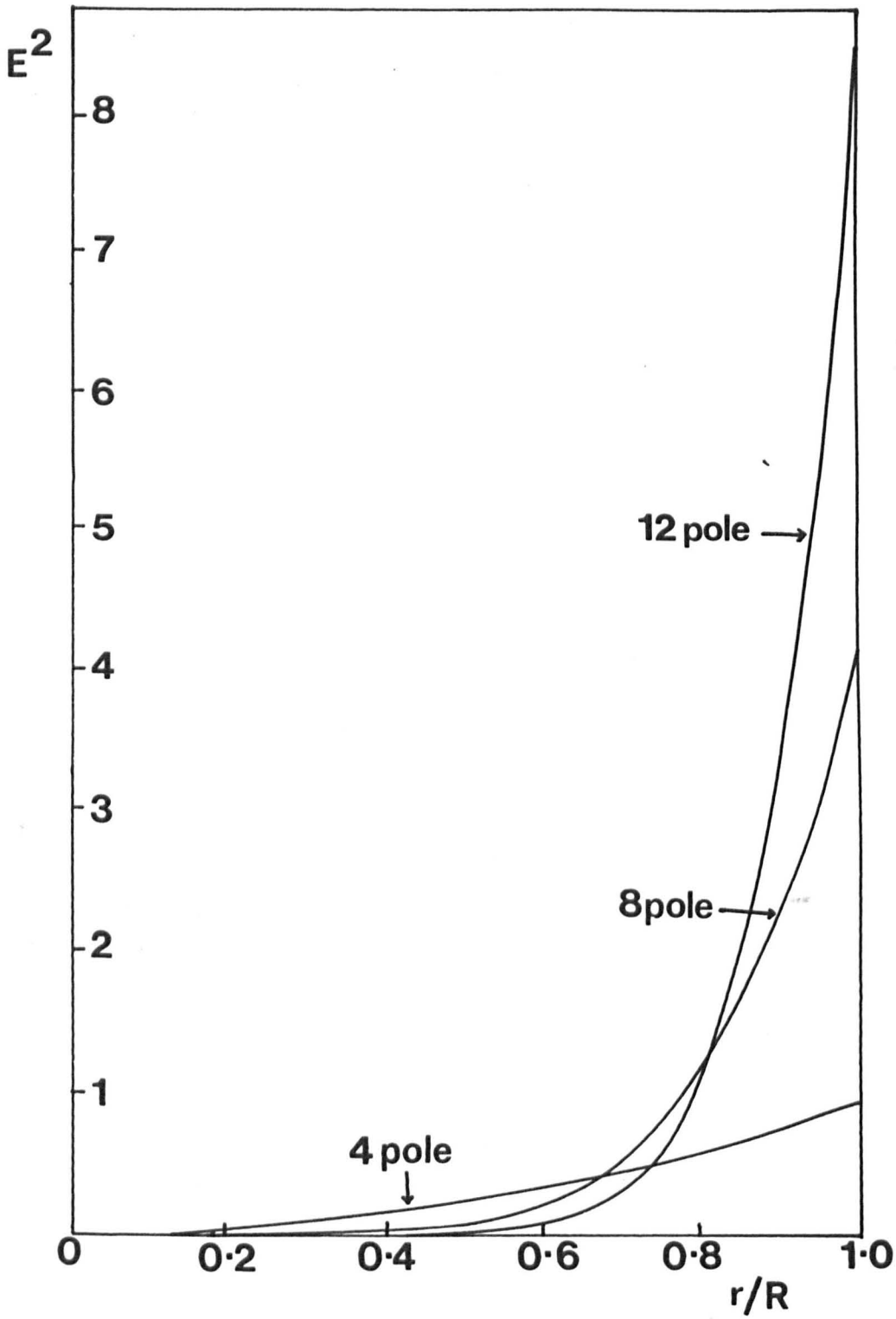

Fig. 4.3.3. DISTRIBUTION OF FIELD (E) IN MULTI POLE FOCUSERS. (46).

force on a molecule is

$$f_r = -\frac{\partial W}{\partial r} = \mp \frac{\partial U(r)}{\partial r} = \mp \frac{2\mu^2}{h\nu} E_r \frac{\partial E_r}{\partial r} \qquad (4.3.5)$$

where the upper sign corresponds to upper state molecules. A potential well is created for the upper state molecules as shown in Fig. 4.3.2. An infinitely long focuser will confine in upper states all those molecules for which the radial kinetic energy is smaller than the maximum Stark energy. The radial velocity for the focused molecules is therefore given by

$$v_r < v_c \equiv \left[\frac{2}{mh\nu}\right]^{\frac{1}{2}} \mu E_R \qquad (4.3.6)$$

In practice this condition is only partly true since the focuser length is limited and the axial velocity v_z is quite large. Upper state molecules satisfying above conditions execute a periodic motion in the potential well.

A comparative understanding of the properties of focusers with different numbers of rods can be obtained from Fig. 4.3.3. It is seen that with an increased number of rods, the additional contribution to the field magnitude and gradient is most effective in the peripheral region near the rods. What is gained in field strength is lost in focusing strength near the axis in a 4-pole focuser over a 12-pole focuser, the gradient of E being steeper in the latter. The 8-pole focuser is a good compromise between the two types of multipole structures. Some typical molecular trajectories for NH_3 have been calculated by

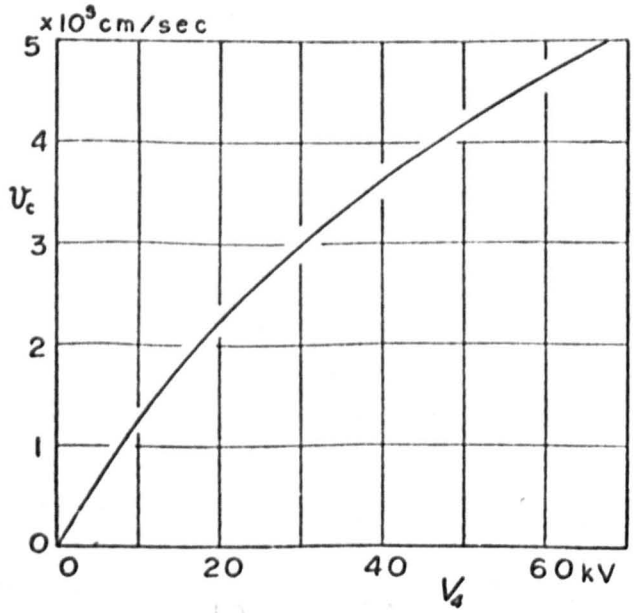

Critical radial velocity of ammonia for $J=K=3$, $\langle M^2\rangle=7$, and $R=0.5$cm.

Vonbun[45]. It is shown that the position, velocity and angle at the entrance to the focuser have considerable action upon separation; the nearer the periphery the stronger the focusing. Further slower molecules are more strongly focused. It is also shown that in addition to state separation and focusing action some degree of velocity selection takes place. Under optimum operating conditions the effect of Maxwellian velocity distribution and the velocity selection is such that almost all the molecules delivering power to the cavity in a maser fall within a narrow velocity range.

The focusing length or skip-distance[46] of a 8-pole focuser is $2.43\ (R/v_c)\ v_z$ where v_z is the axial velocity of the molecules. The axial velocity of molecules to be focused should approximately satisfy the condition

$$v_z < \frac{1}{1.21} \frac{\ell}{R} v_c \qquad (4.3.7)$$

where ℓ is the focuser length. Following Shimoda[42] the maximum radial velocity v_c for the 3,3 line of ammonia has been calculated for the weighted average of M^2 and is shown in Fig. 4.3.4 where the abscissa is the octapole focuser voltage for R = 0.5 cm.

4.4 Ring and Spiral Focuser :

Becker[48,49], Basov et al[50,51] and Krupnov[52] have used ring and spiral type of focusers for upper state selection of ammonia molecules. In a ring separator the beam passes through a series of equally spaced identical rings which are alternately charged positively and negatively. The field produced is inhomogeneous and increases from the axis to the

periphery in the same way as the field in the 2n-pole focuser. Fig.4.4.1 shows a ring focuser schematically. It is easy to see that the optimum ratio ξ_{opt} of the ring radius R_o to the distance Z_o between rings ought to be of the order of unity :

$$\xi_{opt} = (R_o/Z_o)_{opt} \simeq 1 \qquad (4.4.1)$$

As distinct from the field of a multipole focuser, the field of a ring type system is on the average parallel to the axis. The length over which the molecules interact with the field is less than the apparent length of the system. The double spiral is a variant of the ring focuser with a similar field cofiguration produced by two parallel spiral wires charged positively and negatively.

The field in a ring system[53] is given by

$$E = \frac{V_o}{I_o\left(\frac{2\pi R}{L}\right)} \quad \frac{\sin\frac{\pi}{2}\left(1 - \frac{2\delta}{L}\right)}{\frac{\pi}{2}\left(1 - \frac{2\delta}{L}\right)} \frac{2\pi}{L} \; Y \qquad (4.4.2)$$

$$\text{where} \quad Y^2 = I_o^2\left(\frac{2\pi r}{L}\right)\cos^2\frac{2\pi z}{L} + \left(I_o^1\right)^2\left(\frac{2\pi r}{L}\right)\sin^2\frac{2\pi z}{L} \qquad (4.4.3)$$

$$\text{and} \quad I_o(x) = 1 + \frac{x^2}{4} - \frac{x^4}{2^4(2!)^2} + \qquad (4.4.4)$$

$$\simeq 1 + \frac{x^2}{4} \quad \text{if x is small}$$

$I_o(x)$ is a modified Bessel function of the first kind of zero order, L is the period of the ring system, R the radius and δ the thickness

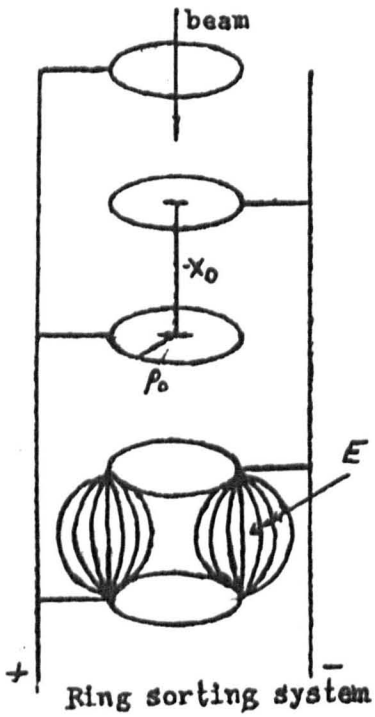

Ring sorting system

Fig. 4.4.1 (48)

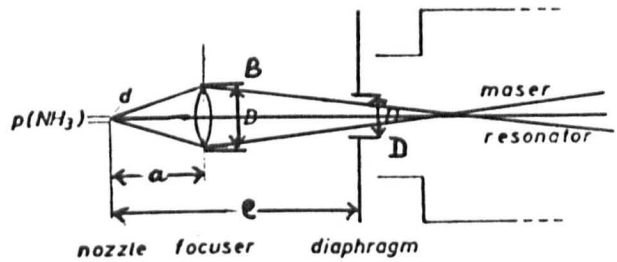

Basic arrangement. The focuser is represented by a lens. varied during maser oscillation.

$$N = \frac{\pi}{4} I_0 \frac{D^2}{e^2} \left| \frac{1}{\left(1 - \frac{a(e-a)}{ef}\right)^2} - \frac{1}{\left(1 + \frac{a(e-a)}{ef}\right)^2} \right|$$

Fig. 4.4.2 (49)

of a ring. With $\delta = 0$, for the paraxial case ($r = 0$) the field is

$$E = \frac{4V_o}{L}\left[1 + \frac{\pi R}{L}^2\right]^{-1} \cos\frac{2\pi z}{L} \qquad (4.4.5)$$

Inserting the values R = 0.25 cm, L = 0.5 cm and V_o = 30,000 volts in Eq. (4.4.5) on the axis the field is seen to vary from 0 to 60,000 volt/cm. Thus an important advantage of the ring type separators over other types is its ability to separate the axial molecules more efficiently.

Becker[49] has shown that the diameter y_o of the beam of upper state molecules is given by

$$y = \frac{eB}{a}\left[1 - \frac{a(e-a)}{ef}\right] \qquad (4.4.6)$$

where e is the distance between the source nozzle of diameter d and the diaphragm of diameter D at the entrance to the resonator, a is the distance between the nozzle and the centre of the separator (internal diameter B), f is the focal length of the lens equivalent (Fig. 4.4.2) of the focuser given by the aperture ratio

$$B/f = bmU \qquad (4.4.7)$$

where U is the potential difference between the rings (or spiral wires), m the number of rings (or windings of a single wire) and b is a constant, being 0.87×10^{-6} per volt for ring- and 1.03×10^{-6} per volt for spiral-focusers. Eqs (4.4.6-7) show that the aperture ratio is independent of the focuser diameter. Consequently there is no need to use rings of large diameters. This has made it possible to construct focusers of much

smaller dimensions, with better focusing and efficiency than achieved with multipole focusers. One basic advantage of ring type systems is the freedom to vary the shape and area of the beam cross section.

Mednikov and Parygin[54] have shown that a ring or helical system may be four times as effective as a quadrupole system due to a more complete utilization of molecules with different values of the quantum number M and greater maximum voltage. Krupnov[55] however finds that the performance should be nearly the same.

4.5 Non uniform Focusers :

To achieve maximum beam transmission it is not necessary to have uniform beam cross section. The shape of the beam is primarily determined by an upper limit on the allowed rate of variation. The focusing conditions are fulfilled as long as the beam diameter r changes sufficiently slowly, the criterion for which is

$$\frac{1}{2\pi} \frac{dT}{dt} \lesssim 1 \qquad (4.5.1)$$

that is the period T of the molecular trajectory should change slowly. The condition that $\frac{dT}{dt}$ = constant leads to the equation

$$R^2 = At + B \qquad (4.5.2)$$

which is the equation of a parabolic envelope. Such focusers have been constructed by Helmer[56,57] and found superior to the uniform multipole type. It is shown that a tapered quadrupole focuser captures a larger solid angle than a straight one. The practical consequence of this is that the load on the evacuating system is significantly reduced.

It is suggested that the quadrupole parabolic focuser performs best with a long cavity because of better defocusing of the lower state molecules which travel close to the axis.

A very interesting variant of the ring separator and the parabolic separator is the parabolic ring separator. This opens up entirely new possibilities in the field since it is found that by a proper design and excitation the molecules may be slowed down[53].

4.6 Other Types of Focusers :

Many interesting variants of the focusing systems mentioned so far are discussed in the literature. Some examples are (i) Design of a system for maser at sub-millimeter range with a disc resonator as proposed by Prokhorov, (ii) an annular system to be used with a higher mode resonator in order to increase the power of a maser[52]. (iii) grid type separators consisting of two sets of parallel rods as used by Becker[58] and Shimoda[59], also presently investigated by Smart[60]. This type which produces a flat beam is particularly suited for use with Fabry-Perot resonators.

In dealing with the problem of focusing the question of lower state as well as upper state focusing naturally arises. The coaxial type lower state selector mentioned in Section 4.2 has been discussed by Helmer[56,57,61]. An entirely new approach to this problem will be discussed in Chapter VI.

4.7 The High Field Situation :

At high field strength in any of the systems described here a complicated situation may arise in that the molecular constants change.

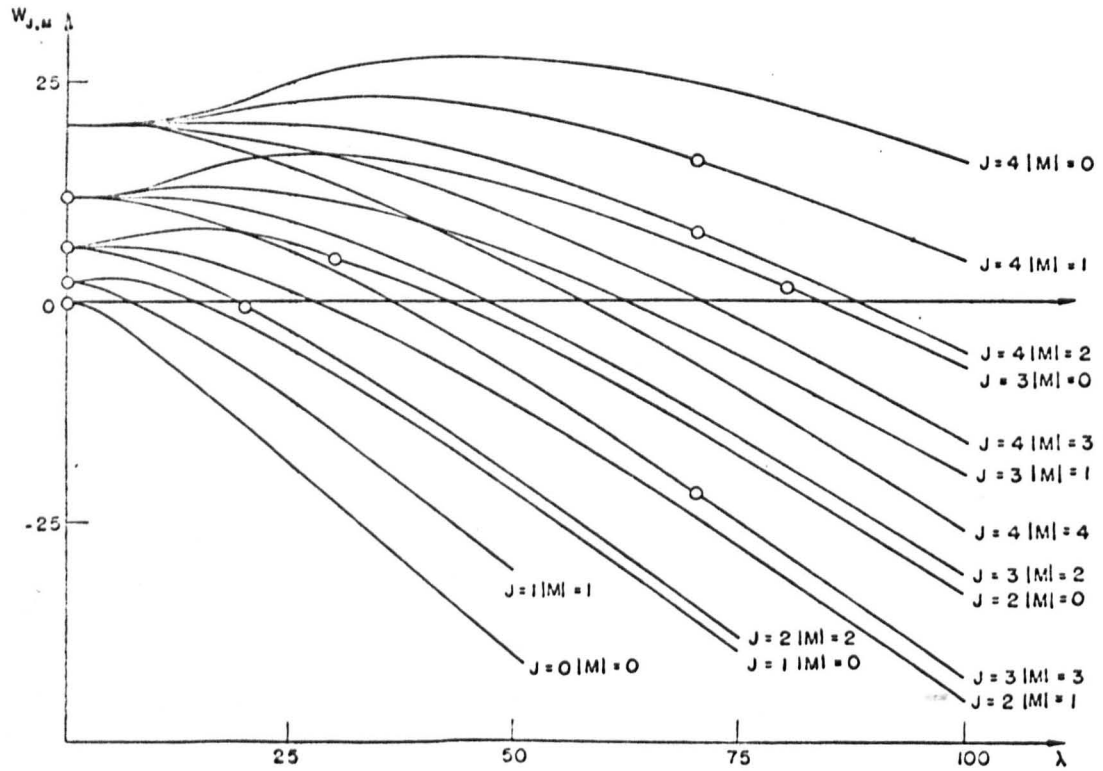

High-field Stark effect in rigid linear rotors.

Fig. 4.7.1 (52)

In ammonia, the Stark energy undergoes a transition from second order to first order for field strengths above 30,000 volts/cm. This may easily happen at the small end of a non-uniform focuser. In the high field region $W \propto |E|$. This is already implied in Eq. 4.4.7 for ring separators. Such a situation also arises in the focusing of linear molecules which have rotational constants above 30 GH_z. Molecules with small rotational constants undergo a sign reversal in the slope of the Stark energy. Peter and Strandberg[62,63] have calculated the Stark energy of sodium chloride ($B = 6.54$ GH_z) for various field strengths. Their result is shown in Fig. 4.7.1, where the abscissa represents the reduced Stark energy W/hB and the ordinate represents the reduced field $\lambda = \mu E/hB$. The curves are applicable to all diatomic molecules with electric dipole moments. It can be seen that for each quantum state there is a critical field for which the force on the molecule vanishes. Below these critical fields, the forces on the corresponding quantum states act in the direction of the beam axis; above these fields, the forces act away from the beam axis. The problem of state selecting and focusing can be appreciated if these curves are compared with those for ammonia (Fig. 3.7.2). Peter, Venkates, Strandberg[63] proposed a lattice structure of charged rods for state selection of NaCl molecules, which however was not found to be very effective. Here again a new approach to the situation is needed.

4.8 Velocity Distribution in a Focused Beam :

Velocity distribution in a molecular beam is not the same as in bulk gas. State selection brings in further complications since the beam is no longer in thermal equilibrium. The beam is formed of molecules

which effuse into a high vacuum through one or more small holes. The most probable velocity is no longer α, but $(3/2)^{\frac{1}{2}}\ \alpha$ and the R.M.S. velocity is $2^{\frac{1}{2}}\alpha$ rather than $(3/2)^{\frac{1}{2}}\alpha$ where $\alpha = (2kT/m)^{\frac{1}{2}}$ 36. Assuming a Maxwell-Boltzmann distribution to be a sufficiently realistic description, the number of molecules with velocity components v_x, v_y, v_z is

$$N\ (v_x,\ v_y,\ v_z)\ dv_x\ dv_y\ dv_z\ = \frac{2N}{\alpha^3 \pi^{3/2}} \exp\left(-\frac{v^2}{\alpha^2}\right) dv_x\ dv_y\ dv_z \tag{4.8.1}$$

For simplicity the case of a multipole focuser only is discussed below. The forces exerted in such a focuser have cylindrical symmetry and therefore one can conveniently use cylindrical co-ordinates :

$$v_r^{\,2} = v_x^{\,2} + v_y^{\,2}$$

$$N\ (v_r,\ v_z)\ dv_r\ dv_z\ = \frac{4Nv_r}{\alpha^3 \pi^{\frac{1}{2}}} \exp\left(-\frac{v^2}{\alpha^2}\right) dv_r\ dv_z \tag{4.8.2}$$

The total beam flux flowing out from the source is

$$n_o\ = \int_0^{\alpha}\int_0^{\alpha} A_o\ N v_z\ dv_r\ dv_z = A_o\ \frac{N\alpha}{\pi^{\frac{1}{2}}} \tag{4.8.3}$$

where A_o is the cross-sectional area of the beam at the source. The critical radial velocity v_c for focusing is defined in Section 4.3 such that $v_r \leq v_c$ (see Eq. 4.3.6). The flux of focused molecules in a particular energy state E_i with a statistical fraction $f_{JK} = N_{JK}/N$ is

then given by

$$n_{JK} = f_{JK} \int_0^{\alpha} \int_0^{v_c} AN\,(v_r, v_z)\, v_z\, dv_r\, dv_z \qquad (4.8.4)$$

where A is the cross-section of the beam at the entrance of the cavity. When the beam cross-section at the source is the same as at the cavity entrance i.e. $A = A_o$, then

$$n_{JK} \simeq f_{JK}\, n_o\, \frac{v_c^2}{\alpha^2} = f_{JK}\, n_o\, \frac{W}{kT} \qquad (4.8.5)$$

where the Stark energy W is as defined in Eq. 3.7.1. It has been tacitly assumed above that the focuser is very long. However for molecules with large velocity in z-direction, state-separation is not very effective when the focuser has a finite length ℓ. From Eq. 4.3.7 a simple focusing criterion for v_z for an octapole focuser is obtained as

$$v_{zc} \equiv v_z < \frac{1}{1.21}\, \frac{\ell}{R}\, v_c \qquad (4.8.6)$$

The integration in Eq. 4.8.4 should therefore be over $v_z = o$ to v_{zc}. The number of effective molecules entering the cavity is then readily obtained as

$$n_{JK} = f_{JK}\, n_o\, \frac{W}{kT} \left[1 - \exp\left[- \left(\frac{\ell}{1.21R} \right)^2 \frac{W}{kT} \right] \right] \qquad (4.8.7)$$

Letting $A = A_o$, and $(\ell/1.21R)(W/kT) << 1$, the beam flux is

$$n_{JK} \simeq f_{JK}\, n_o \left(\frac{\ell}{1.21R}\right)^2 \left(\frac{W}{kT}\right)^2 \qquad (4.8.8)$$

or using the approximation of Eq. 4.3.4

$$n_{JK} \simeq f_{JK}\, n_o \left(\frac{\ell}{1.21R}\right)^2 \frac{(\mu E)^4}{(kTh\nu)^2} \qquad (4.8.9)$$

The maximum value of the beam flux depends upon geometrical details and background pressure, but generally will be of the order 10^{17} molecules per second. Any deviation from Eq. 4.8.9 will be in the factor (ℓ/1.21R) which is a measure of the focal length of the system.[42,59]

An estimation of the effective average velocity of the molecules in the beam which actually contribute to the maser action needs a detailed consideration of the geometrical parameters of the cavity and the focusing system. For reasonable designs of ammonia masers using a cylindrical cavity and a multipole focuser, Shimoda[42] has calculated the effective average velocity to be given by

$$\langle V \rangle \simeq \frac{\pi L + 2\ell}{4\pi R}\, v_c \qquad (4.8.10)$$

where L is the length of the cavity. Inserting numerical values for the various constants in the equations, for a 10 cm. long cavity and an octapole focuser with $\ell \simeq 10$ cm, $R \simeq 0.5$ cm then with an excitation voltage V = 30 KV it follows that for a molecule to be focused $v_c \simeq 10^4$ cm sec^{-1}, $v_{zc} < 1.6 \times 10^5$ cm sec^{-1}, $\langle V \rangle < 8 \times 10^4$ cm sec^{-1}.

CHAPTER V.

THE AMMONIA BEAM MASER

5.1 Introduction :

The ammonia beam maser was the first quantum electronic device to operate. The discovery of the maser followed the realization by physicists that the bound states of electrons in atoms and molecules can be employed to generate RF power utilizing the concept of stimulated emission to obtain power directly from the internal energy of molecules in contrast to devices which transform the kinetic or positional energy of a flow of charge to RF energy. The basic principle of maser action has been briefly mentioned in chapter II of this work. The first problem here is to create a condition of non-thermal equilibrium or to invert the population distribution of a molecular system. To be able to use such a system, the thermal relaxation time must be longer than the time required to change the relative population of the energy levels concerned. This can be achieved by various methods.[5,6] Historically population inversion and stimulated emission were first achieved by Bloch[64] and Purcell and Pound[65] in nuclear spin systems. These were, however, transient systems and far removed from the maser as such. Ideas about the possibilities of molecular amplification and oscillation were lurking around in the early fifties of this century. Some suggestions came in the wake of a search for a millimeter wave oscillator. Nethercot presented a paper on behalf of Townes with the suggestion of a molecular oscillator

at a symposium on sub-millimeter waves at Illinois. The feasibility of such a system was pointed out independently by Basov in his speech at the All-Union Conference on Radio Frequency Spectroscopy in 1952. The first serious consideration to a practical system in the published literature was given by Weber in 1953[66]. Basov and Prokhorov worked out the theory of a molecular oscillator.[39-41] In 1954 Gordon, Zeiger and Townes [37, 38] of Columbia published results of the first successful operation of a maser at 24 GHz using ammonia gas.

5.2 Basic Features :

In the ammonia maser a collimated molecular beam is formed by passing ammonia gas through an effuser into a high vacuum. The beam is then passed through a very strong inhomogeneous electrostatic field (~ 100,000 volts/cm) which creates a second order Stark effect and at the same time physically separates the molecules in various energy states. Each rotational level of the ammonia molecule is split by the so called "inversion" process (Chapter III). With an appropriate electrostatic field configuration, the molecules in the upper energy state are selected and focused along the axis of the beam while molecules in the lower state are deflected away. The J = K = 3 inversion transition at 23.870 GH_z has been popularly used in beam maser work since the pioneering work of Gordon et al. The state selected beam enters a resonant cavity where it produces either stimulated emission under the action of an external field or self-sustained oscillation when the flux, state selection and the cavity quality factor are sufficient, with a typical power output of about 10^{-11} watt. Doppler broadening of the line is drastically reduced

by observing the emission of radiation in a direction which is normal to the beam axis[67,68], and the linewidth is limited in practice by the time of flight through the cavity only. Gordon used this device as a high resolution spectrometer to observe the hyperfine structure of the ammonia molecule[27]. It can also be used as a very low noise amplifier[38]. In the case of an ideal maser amplifier having no cavity losses and having all the molecules in the upper state, the ultimate noise performance is limited only by the fundamental processes of zero-point energy which gives rise to spontaneous emission, and the uncertainty principle which gives rise to an uncertainty in phase[69-72]. The intrinsic maser noise temperature is only a few degrees absolute which is, however, masked by the much greater system noise temperature. Discussions of these aspects and comparative studies of low noise amplifiers are to be found in references 71-74. Use of the maser as an amplifier is however restricted because of its extremely narrow bandwidth. As an oscillator the ammonia maser is highly stable. The measured stability is a few parts in 10^{12} over a few minutes and $\sim 2 \times 10^{-11}$ over a few hours[75].

5.3 Effuser, Resonator and State Selector :

(a) The Effuser : The molecular effuser normally used in ammonia masers consists of a large number of parallel tubes of very small diameter which form, under conditions of molecular flow, a directed beam of ammonia molecules. The behaviour of molecular flow in tubes is discussed by Ramsey[36]. It is shown that the effusion from tubes is more directive than the cosine distribution obtained in effusion from thin holes. For molecular flow the condition to be satisfied is $\omega << \lambda$ where ω is the

is the slit width , and λ is the mean free path. In practice the requirement is much less stringent, and a source may be effective even when ω is slightly greater than λ. If ω is much larger, a turbulent gas jet is created instead of free molecular flow. With a well collimated molecular beam at low source pressures, the beam intensity on the axis is proportional to the source pressure i.e. pressure behind the effuser. The angle with respect to the axis for which the beam intensity has dropped to one half of its central value is about equal to the ratio of the diameter to the length of the tube. The total rate of effusion is proportional to this angle. As long as the general vacuum is not degraded the beam intensity will be limited mainly by collisions between the beams from individual tubes occurring in a short region of high beam intensity immediately in front of the effuser. An effuser of small over-all diamter (i.e. with a small number of tubes) therefore produces the greatest intensity. An approximate relation for the limiting intensity is given by

$$I \sim \left(\frac{t}{dD} \right)^{\frac{1}{2}} \qquad (5.3.1)$$

where t is the transparency of the effuser, d is the tube diamter and D is the over-all diameter. The geometrical details of a source for operation of a maser are not too critical, the requirement being that the source should produce a sufficiently directed and intense beam so as not to put too severe a demand on the vacuum system. The necessary peak beam intensity in an ammonia maser is of the order of 10^{19} molecules sec^{-1} $steradian^{-1}$. Giordmaine and Wang[76] find that an effuser of the kind described can yield a beam with peak intensity 20 times as high as that from a non-directional source. This peak intensity is not to be

confused with the critical number of molecules needed for oscillation to be defined in Section 5.4a.

Optimum beam collimation is obtained only with collision free molecular flow, condition for which is

$$\lambda >> L >> a \tag{5.3.2}$$

where λ is the mean free-path of the molecules over the length of the tube, L the tube length, and a is the tube radius. The tube is transparent under these conditions. The source used in the present work is 0.5 cm long, 0.33 cm in over-all diameter and consists of a honeycomb of fine parallel copper tubes of about 0.025 cm in diameter. These dimensions may be compared with the mean free-path of ammonia at 20°C given by $\lambda = 5 \times 10^{-3}$cm, 5×10^{-2}cm, 5×10^{-1}cm at pressure p = 1 torr, 0.1 torr and 0.01 torr respectively. Under normal operational conditions, the pressure behind the effuser is 1 torr or more and the source is opaque ($a \tilde{<} \lambda << L$). The half-width at half intensity of the beam, which is of the order of a/L for a transparent source is now given by[76]

$$\theta_{\frac{1}{2}} \simeq \frac{2^{3/4}\ 3^{\frac{1}{2}}\ \sigma}{1.78\ a^{\frac{1}{2}}\ c^{\frac{1}{2}}}\ (N)^{\frac{1}{2}} \tag{5.3.3}$$

where σ is the collision cross section of the molecules, c is the average molecular velocity and N is the flow rate per individual tube given by

$$N = \frac{2\pi}{3}\ \frac{n_o\ c\ a^3}{L} \tag{5.3.4}$$

where n_o is the molecular density behind the effuser. The beam shape

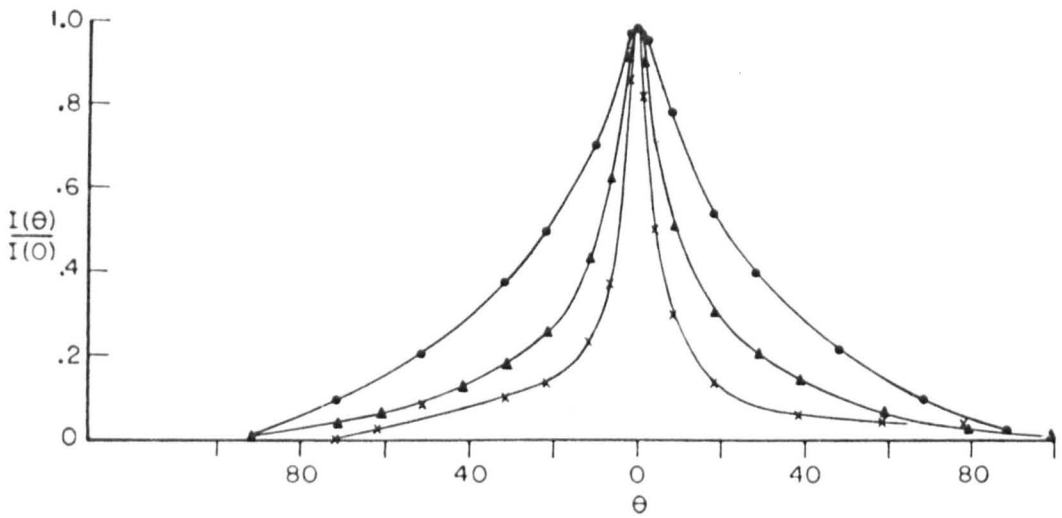

Some representative measurements of $I(\theta)/I(0)$ as a function of θ for various sources and source pressures, showing the characteristic dependence of beam shape on half-width.

Fig. 5.3.1. (61)

is given by the theoretical curves reproduced from Giordmaine and Wang in Fig. 5.3.1. The curves illustrate the beam shapes corresponding to half-widths at half-intensity of 5°, 10° and 20°. It would appear that a focuser will best utilize a beam with narrow half-width and therefore most effectively state separates at very low nozzle pressure.

A critical source length may be defined by the length at which the source becomes opaque. Increasing the source length beyond this point does not change the available collimation of the source. For a given peak intensity this is given by[76]

$$L_c \simeq \frac{2.5\, 2^{1/4}\, c\, a^2}{8\, \pi^{\frac{1}{2}}\, \sigma^2\, I(o)} \qquad (5.3.5)$$

where I(o) is the peak intensity per individual tube. Taking $I(o) \sim 10^{19}$ molecules per sec per steredian, calculation for ammonia using Eq. 5.3.5. shows that the critical length is of the order of 1×10^{-2} for tube radius 1 mm. and 1.5×10^{-4}cm. for tube radius 0.125 mm.

(b) The Resonator : The resonant structure normally used at microwave frequencies is some form of cavity resonator. They are of convenient size and highly efficient. Both cylindrical cavity and Fabry-Perot resonators have been used in ammonia masers. In the present work a cylindrical cavity has been used throughout. The resonant frequency of a cavity resonator is obtained by solving Maxwell's equations with the boundary conditions imposed by the reonator. A general theoretical analysis of this problem will be found in reference 77.

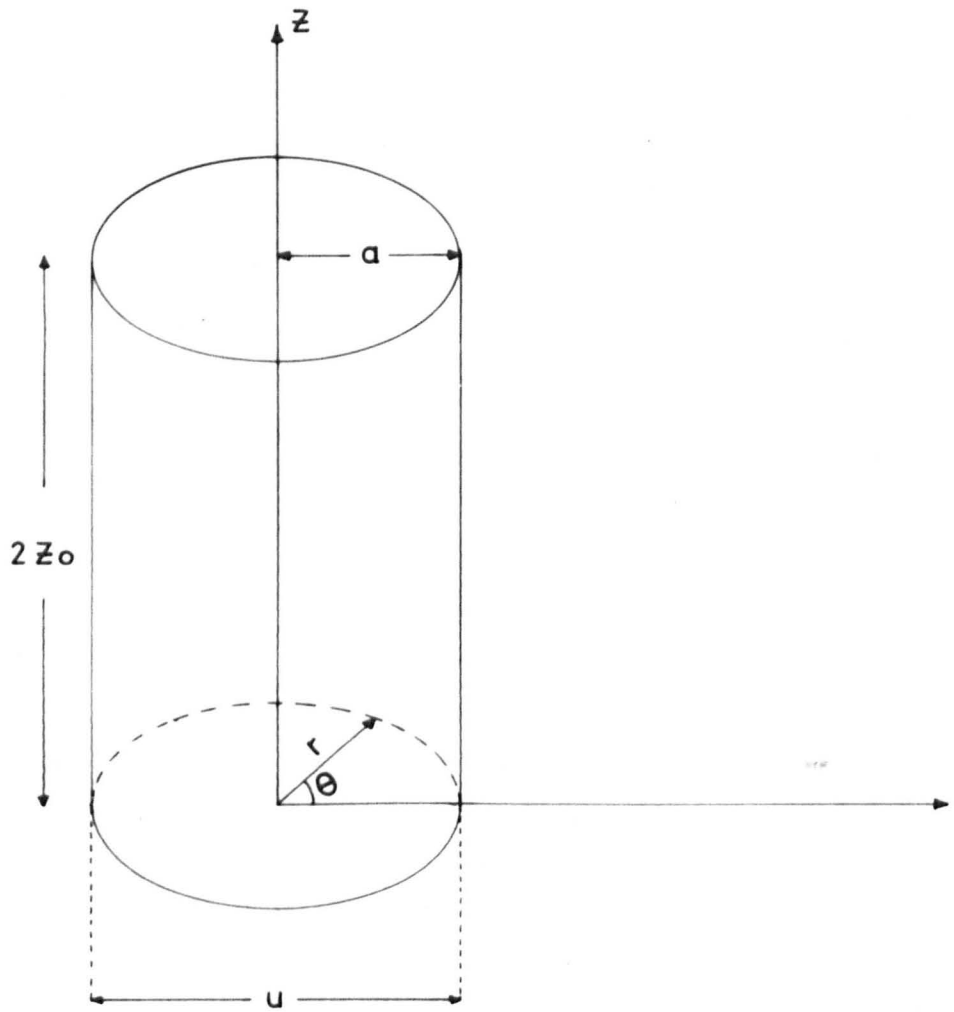

Fig 5.3.2 A circular cylindrical cavity illustrating the notations

The infinite number of resonant modes associated with a cylindrical cavity may be divided into two classes: (i) the TE or H modes in which the electric field is everywhere transverse to the axis of the cylinder, (ii) the TM or E modes in which the magnetic field is everywhere transverse to the axis of the cylinder. For either TM or TE mode, the resonant wavelength is given by[78]

$$\lambda_o = \frac{4}{\left[\left(\frac{\ell}{Z_o}\right)^2 + \left(\frac{2\ Umn}{\pi\ a}\right)^2 \right]^{\frac{1}{2}}} \qquad (5.3.6)$$

where a is the radius and 2 Z_o the length of the cavity (Fig. 5.3.2);

m = the number of half-period variation of E_r with respect to θ for TE modes (or H_r for TM modes).

n = the number of half-period variations of E_θ with respect to r for TE modes (or H_θ for TM modes)

ℓ = the number of half-period variations of E_r with respect to Z for TE modes (or H_r for TM modes).

U_{mn} = the nth root of $J'_m(x) = 0$ for the TE modes or of $J_m(x) = 0$ for the TM modes,

where J_m's are the mth order Bessel functions which determine the axial field[78,79]. The modes are designated by the subscripts m, n, ℓ, e.g. $TM_{mn\ell}$ (or $E_{mn\ell}$). No TE mode exists in which $\ell = 0$. The TM modes can however exist when $\ell = 0$. These modes have an electric field that is everywhere parallel to the axis. The field in this case ($\ell = 0$) does not vary in the Z-direction. Consequently the resonant frequency is

independent of the cavity length and determined solely by its diameter. The Q-factor for the TM-modes is given by[78]

$$Q_o \frac{\delta}{\lambda_o} = \frac{\left[U_{mn}^2 + p^2R^2\right]^{\frac{1}{2}}}{2\pi\,(1 + R)} \quad \text{for } \ell > 0 \tag{5.3.7}$$

and

$$Q_o \frac{\delta}{\lambda_o} = \frac{U_{mn}}{\pi\,(2 + R)} \quad \text{for } \ell > 0 \tag{5.3.8}$$

where $R = (a/Z_o)$, $p = (\ell\pi/2)$ and δ is the skin-depth of the wall material given by

$$\delta = \frac{1}{2\pi}\left[\frac{\lambda_o \psi}{30\mu}\right]^{\frac{1}{2}} \tag{5.3.9}$$

where ψ is the resistivity and μ the permeability of the material. From Eq. (5.3.6) resonant wavelengths are,

$$\text{for } TE_{01\ell} \text{ modes } \lambda_o = \frac{4}{\left[\left(\frac{1}{0.420a}\right)^2 + \left(\frac{\ell}{Z_o}\right)^2\right]^{\frac{1}{2}}} \tag{5.3.10}$$

$$\text{for } TM_{01\ell} \text{ modes } \lambda_o = \frac{4}{\left[\left(\frac{1}{0.653a}\right)^2 + \left(\frac{\ell}{Z_o}\right)^2\right]^{\frac{1}{2}}} \tag{5.3.11}$$

$$\text{for } TM_{010} \text{ mode } \lambda_o = 2.61a \tag{5.3.12}$$

At the ammonia inversion frequency $\nu = 23.87\ GH_z$, for the TM_{010} mode the cavity diameter obtained is $2a = 0.9614$ cm, and Q is obtained from Eq. 5.3.8 as (using $U_{01\ell} = 2.405$[79])

$$Q_o \frac{\delta}{\lambda_o} = \frac{0.383}{1+\frac{a}{2Z_o}} \qquad (5.3.13)$$

Using the values $\delta = 4.24 \times 10^{-5}$cm for copper at $\lambda = 1.25$ cm, for a 10 cm long cavity operating in TM_{010} mode, a theoretical value $Q_o = 10900$ is obtained.

The sensitivity of the maser depends on the cavity design through the Q-factor, but this alone does not give a measure of the relative performance of a cavity. It will be shown in the following section that the sensitivity depends also on the length (L) and cross section (A) of the cavity. Shimoda, Wang and Townes (SWT)[80] have defined a figure of merit M of the cavity resonator for producing induced transitions as

$$M = \frac{LQ_o}{A}\left(\frac{8}{\pi^2}\right)^{\ell}, \quad \ell = 0 \text{ or } 1 \qquad (5.3.14)$$

The factor $(8/\pi^2)^{\ell}$ takes into account the broadening of the resonance line due to the variation of the field along the Z-axis. The significance of Eq. 5.3.14 will be clear from Eq. 5.4b.11 appearing in the following section. For comparison some values of the parameters for a cylindrical cavity with L = 12 cm, $\lambda = 1.25$ cm are quoted below in Table I[80].

TABLE I.

Mode	Radius a in cm.	M	Q_o
TE_{111}	0.37	5.9	6 100
TM_{010}	0.48	7.7	10 800
TM_{011}	0.48	6.0	10 400
TE_{211}	0.61	2.9	8 100
TE_{011}	0.76	4.1	17 800

The figures quoted in Table I are for a uniform intensity of beam throughout the cross section of the cavity. For a sharp, narrow, axial beam the figures are more impressive than shown. It would appear from the table that TM_{010} mode of the cylindrical cavity is the most convenient one.

(c) The State Selector: Theoretical considerations of the multipole- and ring-type state-selector and focusers used in ammonia masers are already given in Chapter IV and will not be discussed here. Constructional details of the focusers used in present experiments are given in Section 5.5.

5.4a Power Output :

Ignoring the presence of hyperfine effects, the ammonia maser can be legitimately regarded as an ideal two level quantum mechanical

for the purpose of the following analysis. The stationary states of the molecules can be described by the state functions $\psi_1 \exp -i(W_1/\hbar)t$ and $\psi_2 \exp -i(W_2/\hbar)t$ which are solutions of the equations

$$H_o \psi_1 = W_1 \psi_1 , \quad H_o \psi_2 = W_2 \psi_2 \tag{5.4a.1}$$

where W_1, W_2 are the energies of the two states, H_o is the hamiltonian of the non-interacting system and $W_2 > W_1$. It is assumed that the molecules enter the cavity in which a radiation field $E(x,t) = E(x) \cos \omega t$ induces transitions between the two states. When the radiation field $E(x,t)$ acts on the system, it is no longer in a stationary state but in a superposition or mixed state which can be described by a linear combination of the stationary state functions as in Eq. 5.4a.2 below :

$$\psi(x,t) = a_1(x,t)\psi_1 + a_2(x,t)\psi_2 \tag{5.4a.2}$$

Assuming that initially all the molecules which enter the cavity at time $t = 0$ are in the upper state and therefore $|a_2| = 1$ and $|a_1| = 0$ at $t = 0$, the coefficients a_1 and a_2 are obtained as [5,80]

$$a_1(t) = - e^{\frac{1}{2} i\delta t} \frac{\lambda}{\left[\delta^2+\lambda^2\right]^{\frac{1}{2}}} \sin\left(\left[\delta^2+\lambda^2\right]^{\frac{1}{2}} \frac{t}{2}\right) \tag{5.4a.3}$$

$$a_2(t) = e^{\frac{1}{2} i\delta t} \left\{ - \frac{\delta}{(\delta^2+\lambda^2)^{\frac{1}{2}}} \sin\left[(\delta^2+\lambda^2)^{\frac{1}{2}} \frac{t}{2}\right] + i \cos\left[(\delta^2+\lambda^2)^{\frac{1}{2}} \frac{t}{2}\right] \right\} \tag{5.4a.4}$$

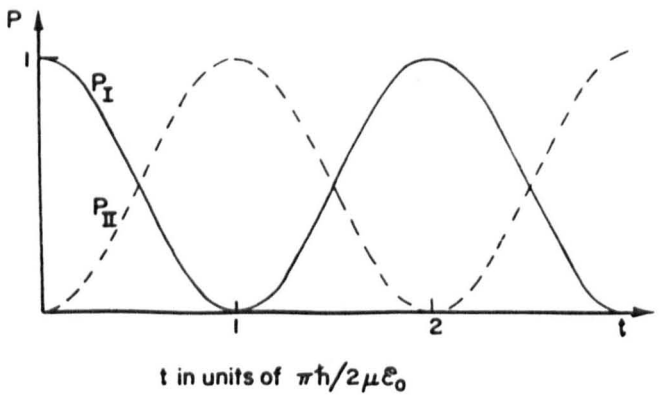

Probabilities for the two states of the ammonia molecule in a sinusoidal electric field.

Fig. 5.4.1. (67)

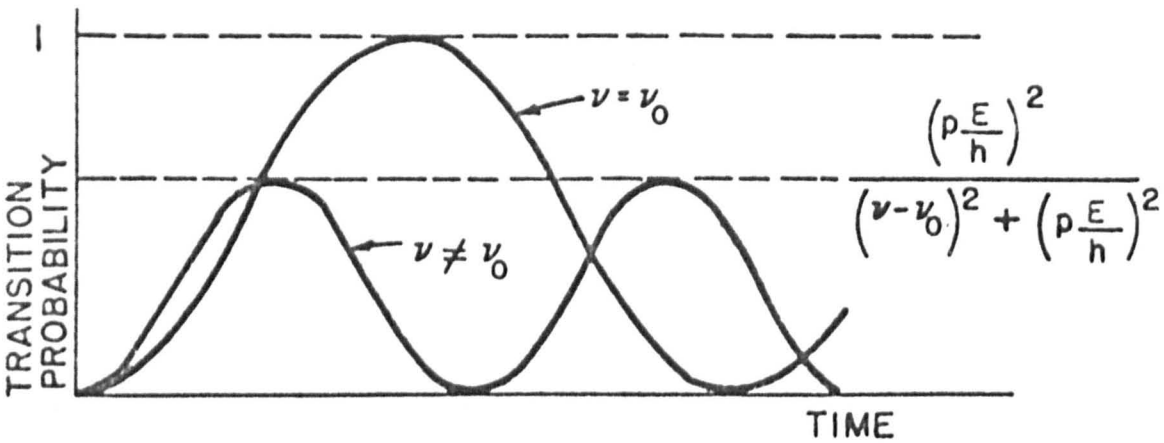

-Transition probabilities between energy states as a function of time for molecules initially in one of two microwave-coupled states when subjected to microwave radiation at or near the resonant frequency.

Fig. 5.4.2. (67)

where $\delta = \omega - \omega_o$, $\lambda = E\mu/h$, and $\omega_o = (W_2 - W_1)/\hbar$ is the resonant frequency of the molecule. Here μ is the dipole matrix element between the two states for the component of the dipole moment along the direction of E and is given by $\mu^2 = \frac{1}{3}|\mu|^2$ where μ is defined for ammonia in Chapter III, section 3.7.

The probability for transition very near resonance is given by, from Eq. 5.4a.3 as

$$P_{II-I} = |a_1|^2 = \frac{\lambda^2}{\delta^2+\lambda^2} \sin^2 \left[(\delta^2+\lambda^2)^{\frac{1}{2}} \frac{T}{2}\right] \qquad (5.4a.5)$$

where T is the time of interaction and is given by $T = L/v$ where L is the cavity length and v the molecular velocity. For transitions at resonance $\omega = \omega_o$ and the probability that the molecule is in the state 1 or 2 is given by

$$P_I = |a_1|^2 = \sin^2 \frac{\lambda t}{2} \qquad (5.4a.6)$$

and

$$P_{II} = |a_2|^2 = \cos^2 \frac{\lambda t}{2} \qquad (5.4a.7)$$

respectively and $|a_1|^2 + |a_2|^2 = 1$. So long as E is small and the system is on resonance, the probabilities are given by simple oscillating functions as in Eq. 5.4a.6-7 above. The time variation of the two probabilities is shown in Fig. 5.4.1. For comparison Eqs 5.4a.5 and 5.4a.6 are plotted together in Fig. 5.4.2. As shown there, the

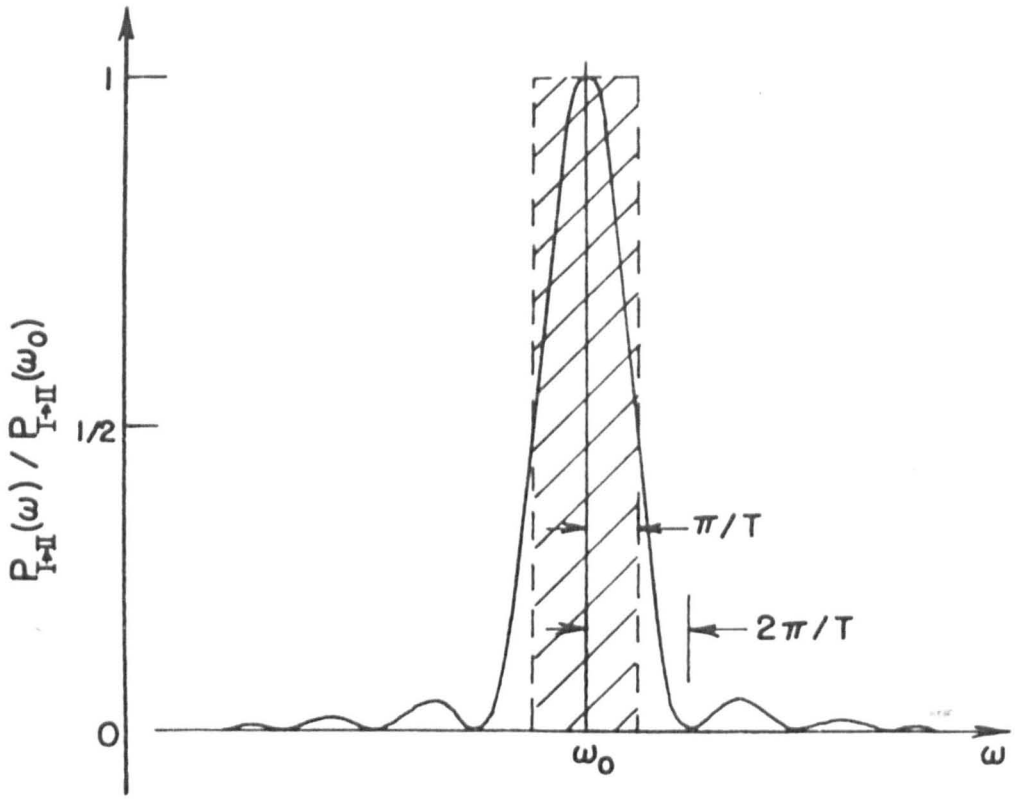

Transition probability for the ammonia molecule as a function of frequency.

Fig. 5.4.3. (68)

transition probability oscillates between zero and

$$\frac{\lambda^2}{\delta^2+\lambda^2} = \frac{(\mu E/\hbar)^2}{(\omega-\omega_o)^2+(\mu E/\hbar)^2} \qquad (5.4a.8)$$

At resonance, the molecules oscillate between the two states while somewhat off resonance, the probability that a molecule starting in one state will exactly get to the other state is never unity, that is, some molecules will in fact never get to the other state before the process is reversed. Alternatively the situation can be visualized in terms of a macroscopic polarization of the whole molecular ensemble which will be deferred to a later chapter.

In order to illustrate the sensitivity of the transition probability to the frequency of the inducing field, the probability P_{I-II} is plotted in Fig. 5.4.3. as a function of the frequency of the cavity field. It can be seen that the curve falls abruptly to zero for $\omega - \omega_o = 2\pi/T$ and never regains a significant size for large frequency deviations. As a matter of fact, as shown by the shaded rectangle, transitions occur predominantly within the range $\pm \pi/T$. Taking the time of flight of the ammonia molecules through the cavity to be 200 μsec for a 10 cm. long cavity and $\nu_o = 24{,}000$ MH_z ($\nu_o = \omega o/2\pi$), the probability for a transition falls to zero for a frequency deviation of $\frac{\omega - \omega_o}{\omega_o} = \frac{1}{\omega_o T}$ which is 2 parts in 10^7.

Assuming a uniform velocity as has been done in the foregoing discussions, and a uniform field distribution within the cross section A of the cavity given by the relation

$$W = \frac{E^2 AL}{8\pi} \tag{5.4a.9}$$

where W is the microwave energy stored in the cavity, the power emitted from the beam of N molecules is given by

$$\Delta P = N\hbar\omega_o |a_1(T)|^2$$

$$= N\hbar\omega_o \frac{(\lambda T/2)^2}{(\delta T/2)^2 + (\lambda T/2)^2} \sin^2 \left|(\delta T/2)^2 + (\lambda T/2)^2\right|^{\frac{1}{2}}$$

$$= N\hbar\omega_o \frac{\theta^2}{d^2 + \theta^2} \sin^2 (d^2 + \theta^2)^{\frac{1}{2}} \tag{5.4a.10}$$

where $d = \frac{\delta T}{2} = (\omega - \omega_o) \frac{L}{2v}$

$$\theta^2 = \frac{\lambda^2 T^2}{4} = \frac{\mu^2 E^2 L^2}{4\hbar^2 v^2}$$

$$= \frac{E^2 AL/8\pi}{\hbar^2 Av^2/2\pi\mu^2 L}$$

$$= W/W_c \tag{5.4a.11}$$

with

$$W = (E^2 AL/8\pi) \text{ and } W_c = (\hbar^2 Av^2/2\pi\mu^2 L) \tag{5.4a.12}$$

It would appear from Eq. 5.4a.10 above that the resonance begins to saturate significantly when $\theta \geq 1$, that is $W \geq W_c$. When the input power to the cavity is small enough to make saturation insignificant the emitted power is given by

$$\Delta P = N h \omega_o \theta^2 \frac{\sin^2 d}{d^2} \qquad (5.4a.13)$$

under the condition

$$d >> \theta << 1 \qquad (5.4a.14)$$

At resonance $\omega = \omega_o$ and $d = 0$, so that from Eq. 5.4a.10

$$\frac{\Delta P}{\theta^2} = N h \omega_o \frac{\sin^2 \theta}{\theta^2} \qquad (5.4a.15)$$

Since $\sin^2 \theta/\theta^2 \simeq 1$ for small values of θ and $\theta^2 = W/W_c$,

$$\frac{\Delta P}{\omega_o W} = \frac{N h}{W_c} \qquad (5.4a.16)$$

Remembering that at the threshold of oscillation the loss in the cavity ($= \omega W/Q$) is just balanced by the power delivered by the beam, it can be readily shown that the oscillation threshold N_{th} is given by

$$N_{th} = \frac{h \nu^2 A}{2\pi \mu^2 L Q} \qquad (5.4a.17)$$

where Q is the quality factor of the cavity. For the 3-3 inversion transition of ammonia, inserting the values

$$\mu^2 = \frac{1}{3} (1.5 \times 10^{-18})^2 \frac{7}{16}$$

$$A = 1 \text{ cm}^2, \quad L = 10 \text{ cm}$$

$$Q = 5000$$

the oscillation threshold is obtained as :

for $V = 5 \times 10^3$ cm sec^{-1} $N_{th} = 8.4 \times 10^{11}$ molecules sec^{-1}

4×10^4 " " 5.4×10^{13} " "

5×10^4 " " 8.4×10^{13} " "

6×10^4 " " 1.2×10^{14} " "

In the above calculations $\tilde{\mu}$ is computed from the equations

$$\tilde{\mu}^2 = \frac{1}{3}|\mu|^2, \qquad \mu = \frac{\mu_o MK}{J(J+1)} \tag{5.4a.18}$$

and the weighted average of M^2 given by $\langle M^2 \rangle = 7$ in this case is used.[42] The equation for the number of effective molecules flowing into the cavity is given in Chapter IV as

$$N = f(J,K)\, N_o \left\{\frac{2\ell}{\pi R}\right\}^2 \left(\frac{\mu E}{kTh\nu_o}\right)^4 2 \tag{5.4a.19}$$

where f(J,K) is the fractional population in the rotational state, N_o is the total number of molecules coming from the source in a unit time, ℓ is the length and R the radius of the focuser, and E is the maximum value of the electrostatic field inside the focuser. N_o is calculated for the source used in present experiments using equation 5.3.4. Assuming there to be 175 effective channels in the source, for a source pressure of 1 torr, N_o is found to be $\sim 4 \times 10^{18}$ molecules sec^{-1}. Using the values $f(J,K) = 6 \times 10^{-2}$, L = 8 cm, R = 0.5 cm and V = 30 KV for an octapole focuser Eq. 5.4a.19 gives $N \simeq 10^{14}$. Thus with a source pressure of about 2 torr, the flux obtained in the present set up is about three times as large as the minimum flux required for oscillation.

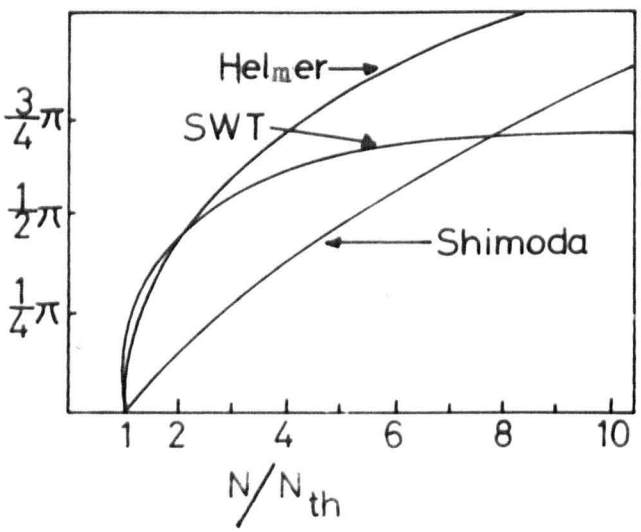

Fig. 5.4.4. Saturation Characteristics of a Maser.

If N molecules enter the cavity per unit time, Eq. 5.4a.15 can be written as

$$\frac{N}{N_{th}} = \frac{\theta^2}{\sin^2 \theta} \qquad (5.4a.20)$$

showing that the oscillation amplitude saturates when $\theta = \pi$. In this analysis it has been assumed that all the molecules have the same velocity. However, in order to allow for the velocity distribution and the change of effective average velocity this theory needs some modification. Shimoda[42] derived the saturation characteristics assuming an effective average velocity as defined by Eq. 4.8.10 in the preceding chapter. Oscillation characteristics assuming a velocity distribution have also been derived by Helmer. Fig. 5.4.4. shows the saturation characteristics according to these theories. Characteristics obtained in a practical maser may be quite different as most of the assumptions involved in the theory are only partially fulfilled. (See Fig. 5.6.4).

5.4b. Sensitivity :

The sensitivity of the ammonia maser can be estimated by comparing the change in power in the detection system in presence of emission by molecules in the cavity with the noise power of the microwave superheterodyne detection system (SHD). The latter is given by $FkT\Delta\nu$ where F is the overall noise figure of the detector and amplifier and $\Delta\nu$ its effective bandwidth. Here k and T have their usual meaning. Following Shimoda[44] it can be shown that the signal is detectable when

$$\frac{(\Delta P_o)^2}{16\, P_o} > FkT\Delta\nu \qquad (5.4b.1)$$

where P_o is the output power in the absence of the beam and ΔP_o is the change in power due to the presence of the beam. The numerical factor in earlier works[81-83] was taken to be 4. The modification is considered necessary in view of the fact that the noise figure F is defined for a heterodyne system.

The emission of power by molecules in the cavity can be represented by

$$\Delta\left(\frac{1}{Q_L}\right) = \left(\frac{1}{Q_m}\right) = \frac{\Delta P_m}{\omega_o W} \qquad (5.4b.2)$$

$$\text{Or} \qquad \Delta Q_L = -\frac{Q_L^2}{Q_m} \qquad (5.4b.3)$$

where W is the stored energy of the cavity, ΔP_m the power emitted by the molecules, Q_L is the loaded quality factor of the cavity and Q_m is the molecular Q defined by Eq. 5.4b.3. At optimum level of signal power $Q_L = Q_o/2$ and for a reflection cavity $Q_1 = Q_o$ where Q_o is the unloaded Q of the cavity and Q_1 is the Q of the coupling between the cavity and the waveguide. The minimum detectable absorption is then given by

$$\left|\frac{1}{Q_m}\right|_{min} = \frac{4}{Q_o}\left(\frac{FkT\Delta\nu}{P_i}\right)^{\frac{1}{2}} \qquad (5.4b.4)$$

where P_i is the input power.

The power emitted from the beam at resonance is from Eq. 5.4a.15.

$$\Delta P_m = Nh\omega_o \sin^2\theta \qquad (5.4b.5)$$

for the beam flux of N excited molecules per second.

The transition is therefore detectable when

$$\frac{1}{Q_m} = \frac{\Delta P_m}{\omega_o W} > \frac{4}{Q_o} \left[\frac{FkT\Delta\nu}{P_i}\right]^{\frac{1}{2}} \qquad (5.4b.6)$$

From the theory of the cavity, at resonance the stored energy in the cavity is given by

$$\omega_o W = \frac{4\, Q_L^{\,2}}{Q_1} P_i \qquad (5.4b.7)$$

Using the relationship of Eq. 5.4a.9, that is

$$W = \frac{3AL\, \hbar^2 \lambda^2}{8\pi\, \mu^2} \qquad (5.4b.8)$$

where $\bar{\mu}^2 = \frac{1}{3} |\mu|^2$. Combining Eqs. 5.4b.5-8 and using the relation $\theta = \lambda L/2V$,

$$N\pi\mu \frac{1}{\lambda} \sin^2 \left(\frac{\lambda L}{2v}\right) > \left| \frac{3ALFkT\Delta\nu}{\nu_o Q_o} \right|^{\frac{1}{2}} \qquad (5.4b.9)$$

The left hand term takes an optimum value when λ takes the optimum value given by

$$\lambda_{opt} = 2.33\ v/L \quad (\text{i.e. } \theta = 1.16) \qquad (5.4b.10)$$

The minimum detectable beam flux is then given by

$$N_{min} = \frac{1.52v}{\mu} \left| \frac{A}{Q_o \nu_o L} \right|^{\frac{1}{2}} \left| FkT\Delta\nu \right|^{\frac{1}{2}} \qquad (5.4b.11)$$

From Eq. 5.4b.8, using the values $\lambda_{opt} = 2.33\ v/L$, $v = 5 \times 10^{4}$ cm sec^{-1}, $L = 10$ cm, $A = 1$ cm^{2} and $\mu = 0.97 \times 10^{-18}$ cgs, the optimum energy in the cavity is found to be

$$W = 1.9 \times 10^{-10} \text{ ergs} \qquad (5.4b.12)$$

Using the values $Q_1 = Q_o = 2Q_L = 10^{4}$, the net power flow from the cavity under optimum conditions is therefore

$$P_o = \frac{2\pi\nu W}{Q_1} = 2.86 \times 10^{-10} \text{ watt} \qquad (5.4b.13)$$

This is to be compared with the value $P_o = 0.97 \times 10^{-10}$ watt given by SWT. The value calculated here is a factor of 3 larger as, following Shimoda[44], the average value of μ given by $\mu^2 = \frac{1}{3}|\mu_{12}|$ has been used. It follows from these estimates that the optimum sensitivity is attained with a very small flow of power. To calculate the sensitivity of the maser spectrometer, the values $F = 100$, $\Delta\nu = 10$ cps, $kT = 4 \times 10^{-14}$ can be used. Eq. 5.4b.11 then yields

$$N_{min} = 1 \times 10^{10} \text{ molecules sec}^{-1} \qquad (5.4b.14)$$

Since the number of molecules focused into the cavity is of the order of 10^{14} sec^{-1}, a signal to noise ratio of the order of 10^{4} can be expected for the ammonia maser operating on the $J = K = 3$ inversion transition.

To compare the sensitivity of a beam maser with that of a cavity absorption spectrometer, Beers[84] has deduced the following equations for the two cases respectively,

$$S_m = \frac{\pi N_m f \Omega \mu}{3(\Delta\nu)_m} \left| \frac{Q_m \nu}{2FkTBV_m} \right|^{\frac{1}{2}} \qquad (5.4b.15)$$

$$S_a = \frac{\pi N_a f h\nu\mu}{3kT} \left| \frac{Q_a V_a \nu}{2FkTB} \right|^{\frac{1}{2}} \qquad (5.4b.16)$$

where the subscripts m and a describe the maser and the absorption spectrometer respectively. Here Nf is the number of molecules in the particular quantum state concerned emitted by the effuser, Ω the efficiency of the maser focuser, $\Delta\nu$ is the half width of the line observed, B the noise band width, V the cavity volume, while the rest of the parameters have their usual meaning.

Assuming that the same detection system has been used in both cases, the relative sensitivity of the two systems is given by

$$S_m/S_a = \frac{N_m \Omega}{N_a(\Delta\nu)_m} \left| \frac{kT}{h\nu} \right| \left| \frac{Q_m}{Q_a V_a V_m} \right|^{\frac{1}{2}} \qquad (5.4b.17)$$

If the same cavity is used, $V_a = V_m = V$, $Q_a = Q_m = Q$

and

$$S_m/S_a = \frac{N_m \Omega}{N_a(\Delta\nu)_m} \left(\frac{kT}{h\nu} \right) \frac{1}{V} \qquad (5.4b.18)$$

For molecules having a second order Stark effect, $\Omega \propto 1/\nu$. In the situation in which the linear dimensions of the cavity are scaled in proportion the wavelength $\Delta\nu \propto \nu$, and $V \propto \nu^3$. Since the Doppler width is proportional to the frequency, in order to hold the contribution to

line width due to wall collisions at some constant fraction of the Doppler width N_a must be made proportional to frequency. Therefore, under these conditions the sensitivity of the maser relative to the absorption spectrometer is inversely proportional to frequency. It can be estimated that the two instruments would have sensitivity of the same order in the region of 1500 MH_z to 2000 MH_z. At lower frequencies the maser should have higher sensitivity, while the absorption spectrometer should be superior at higher frequencies. Thus, in applications where high resolution is not a requirement, the pressure and power level in an absorption spectrometer may be made very large so that its sensitivity can be superior to that of a maser. However, if it is operated to give the highest possible resolution, its sensitivity may or may not be superior to that of a maser, depending upon the frequency and other conditions.

In the preceding discussion the effect of the presence of spontaneous emission in the cavity has not been taken into account. Shimoda, Takahasi and Townes[69] have considered this problem from a phenomenological point of view. Townes[85] has shown that the sensitivity of a maser type spectrometer can be increased by some orders of magnitude by introducing the excited molecules directly into the cavity. This increases the apparent temperature of the waveguide system and at the same time effectively decreases the absorption in the waveguide. The latter process dominates and a net increase in sensitivity results. This approach is however not applicable to the ammonia maser techniques usually followed as in the present investigations.

In all analyses of sensitivity reported in the literature,

spontaneous emission in the cavity is either ignored or assumed to be incoherent. However, spontaneous emission in the cavity is not necessarily incoherent under all conditions. This aspect will be discussed in Chapter Vll.

5.4c. Noise :

It was commented in Section 5.2 that the maser can be used as a very low noise amplifier. The subject of noise in a beam maser has been discussed in detail by various authors.[69-72, 86-95] The "effective input noise temperature" T_n (ENT) has been defined by Gordon and White as the temperature of the input termination which results at frequency ν in output noise power per unit bandwidth double that which would occur if the same input termination were at absolute zero. In other words, it is the input power which will give an output power just equal to that which is present with zero input, i.e. which doubles the total output power. The ENT is related to the noise figure F of the amplifier with the same input by

$$T_n = (F - 1)\ 290^{\circ}K \qquad (5.4c.1)$$

Unlike microwave amplifiers and oscillators which employ electron beams, the maser operates with a beam of uncharged particles which interact with the electromagnetic field. The source of shot noise is therefore absent in the maser. Apart from the amplifying medium itself, there is a number of sources of thermal noise: the cavity walls, the input circuit (and the output circuit in transmission cavity type), and cavity losses from absorption due to background ammonia gas. Noise

created by electric and magnetic fields in the cavity due to electrical heaters and sensing elements and other stray fields including the earth's field, will tend to be cyclical according to the system, and should normally be distinguishable from random noise.

The beam flux may fluctuate because of mechanical vibrations, corona on the electrostatic focuser, fluctuations in the focuser voltage and source pressure, and finally, due to statistical fluctuation of the number of molecules. All except the last can be reduced to insignificant amounts by careful design. If the number of the upper state molecules focused into the cavity per second is n, then the fluctuation in time t is $(nt)^{\frac{1}{2}}$. Expressing the power generated by these molecules as P_o = Knhν where K is a constant, the average fluctuation in power is obtained as

$$\Delta P_o = Kh\nu\,(nt)^{\frac{1}{2}} \qquad (5.4c.2)$$

There are about 10^{12} molecules in the cavity at any time. The fluctuation in the output power due to statistical fluctuation of the beam flux will therefore be $\Delta P_o/P_o = 10^{-6}$ only, when time averaged over 1 second. Thus the beam shot effect is negligible. It is assumed here that there is no amplification or saturation. In an ideal maser having no cavity losses and having all the molecules in the upper state, there is still a noise output due to spontaneous emission. It is shown in Chapter II (Eq. 2.3.3) that the transition probability for downward transitions of a molecule in the upper state can be written as

$$P_{emis} = \text{constant} \times (n_{\ell o} + 1) \qquad (5.4c.3)$$

where $n_{\ell o}$ is the number of quanta in the radiation field, and the 1 which follows $n_{\ell o}$ represents the effect of spontaneous emission. Since mode density per unit frequency is $8\pi\nu^2/c^3$ and energy of a single quantum is $h\nu$, from Planck's law as given by Eq. 2.3.6, at thermal equilibrium

$$n_{\ell o} = \frac{1}{\exp \frac{h\nu}{kT} - 1} \qquad (5.4c.4)$$

The equivalent temperature for spontaneous emission is obtained by setting $n_{\ell o}$ equal to unity in Eq. 5.4c.4 above,[88] and is therefore

$$T_{eq} = \frac{h\nu}{k \ \ell n \ 2} = 6.54 \times 10^{-11} \nu \qquad (5.4c.5)$$

Thus, for the ammonia maser $T_{eq} = 1.5^{\circ}K$ which is the absolute minimum noise temperature. Since the maser gives information simultaneously of the number (n) of quanta and the phase (ϕ) of the wave, its performance must therefore be limited by an uncertainty relation between these two complementary quantities.[70,94] This uncertainty for the maser is given by

$$\Delta n \ \Delta\phi \simeq 1 \qquad (5.4c.6)$$

and indicates that the ideal maser is capable of giving the minimum fluctuation in the product $\Delta n \ \Delta\phi$ which is allowed by quantum mechanics.

The noise contribution of the beam can be estimated by defining the beam temperature as

$$T_b = - h\nu/k\ell n \ \frac{N_2}{N_1} \qquad (5.4c.7)$$

where N_2, N_1 are the populations in the upper and lower energy states respectively. T_b is negative and much smaller in absolute magnitude than $h\nu/k\ell n2$. The contribution to the ENT by background ammonia has been estimated by Gordon to be typically of the order of 4° K. In practice by far the greatest contribution comes from the thermal noise due to the cavity losses and the microwave circuit coupled to the cavity. Gordon[89] measured this to be about 80°K.

5.4d. Stability and Linewidth :

The absolute stability of the maser oscillation is defined by the relation

$$\delta_{abs} \equiv \left| \frac{\omega - \omega_o}{\omega_o} \right| \qquad (5.4d.1)$$

where ω_o is the molecular transition frequency and ω is the maser oscillation frequency. The dependence of the maser frequency on various parameters and conditions for steady-state oscillations have been discussed exhaustively in the literature.[96-111] The characteristics for non-uniform cavity fields have been studied by Tsaregradskii and others[112-115]. The basic parameters which enter into the maser frequency ω are

(i) the natural frequency ω_c of the cavity resonator,

(ii) the intensity of the molecular beam, and

(iii) the shape and width of the spectral line.

Shimoda, Wang and Townes[80] derived the following expression for the frequency

$$\frac{\omega - \omega_o}{\omega_o} = \frac{2Q_c(v/L)(1 - \cos 2\theta)}{\omega_o (1 - \sin 2\theta/2\theta)} \quad \frac{\omega_c - \omega_o}{\omega_o} \qquad (5.4d.2)$$

where Q_c is the Q of the cavity and $\theta = (\mu EL/2hv)$ as defined in Eq. 5.4a.11. For the saturated line, the line width is precisely given by

$$\Delta\omega = 2\pi\left|(0.8\ v^2/L^2) + E^2\left|\mu\right|^2/3h^2\right|^{\frac{1}{2}} \qquad (5.4d.3)$$

When the transition is observed below threshold at a low power level, the line width is determined practically by the time of interaction of the molecules with the cavity field and is given by[108]

$$\Delta\omega = 2\pi(v/L) \qquad (5.4d.4)$$

Under present experimental conditions L = 10 cm, $v = 5 \times 10^4$ cm sec^{-1}, and $\Delta\nu = \Delta\omega/2\pi = 5$ KH_z. When the maser oscillates at a power level P_o, however, the random frequency deviation takes a value which is approximated by

$$\delta\omega = 2kT(\Delta\omega)^2/P_o \qquad (5.4d.5)$$

This gives a theoretical limit to the accuracy of the frequency in the absence of any systematic frequency shift.

Using the value $\Delta\omega = 2\pi(v/L)$ and the Q of the line defined by

$$Q_\ell = \frac{\omega_o}{\Delta\omega} = \frac{\omega_o}{2\pi(v/L)} \qquad (5.4d.6)$$

the expression for frequency deviation becomes

$$\frac{\omega - \omega_o}{\omega_o} = \frac{Q_c}{Q_\ell}\,\frac{1}{\pi}\,\frac{1 - \cos 2\theta}{1 - \sin 2\theta/2\theta}\,\frac{\omega_c - \omega_o}{\omega_o} \qquad (5.4d.7)$$

When $\theta << 1$, $\frac{1 - \cos 2\theta}{1 - \sin 2\theta/2\theta} \rightarrow 3$ (5.4d.8)

and $$\frac{\omega - \omega_o}{\omega_o} = \frac{Q_c}{Q_\ell} \frac{\omega_c - \omega_o}{\omega_o} \quad (5.4d.9)$$

Since $Q_\ell \sim 10^7$ and $Q_c \sim 5 \times 10^3$, therefore $Q_c/Q_\ell \sim 5 \times 10^{-4}$. The output frequency of the maser is thus changed by very much less than the change in the resonant frequency. It is important to have the cavity well stabilised because the total spectral width of the oscillation is considerably smaller than $\Delta\omega$ as shown by Eq. 5.4d.5. For $\Delta\nu = 5$ KH_z and normal operating conditions $\delta\nu \sim 10^{-1} H_z$. This compares with the theoretical value of the absolute natural linewidth given by Troitskii[99] and Chikin[116] as $\delta\nu \sim 10^{-4} H_z$. The apparent discrepancy is due to the fact that Troitskii has used a value $P_o = 10^{-9}$ watt for power output. The ammonia maser has been used as a frequency standard and for this purpose it is necessary that the output frequency be both stable and resettable. Ignoring the frequency pulling effect due to the presence of hyperfine structure in the 3-3 line, to obtain maximum stability the cavity must be tuned precisely to the frequency of the spectral line. In practice it is difficult to determine the frequency of the loaded cavity with sufficient accuracy because of the distortion of the amplitude-phase characteristics of the cavity introduced by the waveguide connected to it. A more effective means of tuning the cavity is to use the dependence of the oscillation frequency on various parameters. It was mentioned earlier that the frequency shift depends upon the beam flux, so variations in source pressure and focuser voltage both may change the

frequency. Thaddeus and Krisher[117] have used the method of modulating the focuser voltage for sensitive detection. Modulation of the beam flux in this way can be used to tune the cavity. Alternatively, Zeeman modulation can be used to tune the cavity[118]. It has been shown by Basov et al[119] and Strakhovskii[120] et al, that the frequency and intensity of oscillation depend strongly on a constant electric or magnetic field applied across the beam of active molecules between the focuser and the resonator. Basov et al have found that the frequency can be changed by a few hundred H_z in this way, and that there exists only one frequency of the resonator at which electric or magnetic fields have the least effect on frequency. This phenomenon therefore suggests a new method of tuning. Such methods are generally undesirable for frequency standard work because of associated frequency pulling effects. Bonanomi et al[121] have shown that if two cavities are coupled together with the beam passing through one cavity only, then the curve of frequency against cavity temperature presents a plateau, thus reducing cavity pulling considerably. It is seen from Eq. 5.4d.6,9, that stability increases with narrowing of the line. It has been found that enormous imrovment in sensitivity and monochromaticity of the output can be achieved by pre-stimulating the molecules. This principle is used in the multicavity masers in which the state selected beam is passed through two or more cavities in series.[122-133].

The unbalanced travelling waves in the microwave cavity also affect the frequency.[80] To reduce this effect for a E_{010} cavity, the coupling hole is placed at the centre of the cavity. This is, however, only a compromise. De Prins[134] and Suburi et al[135] have found that by

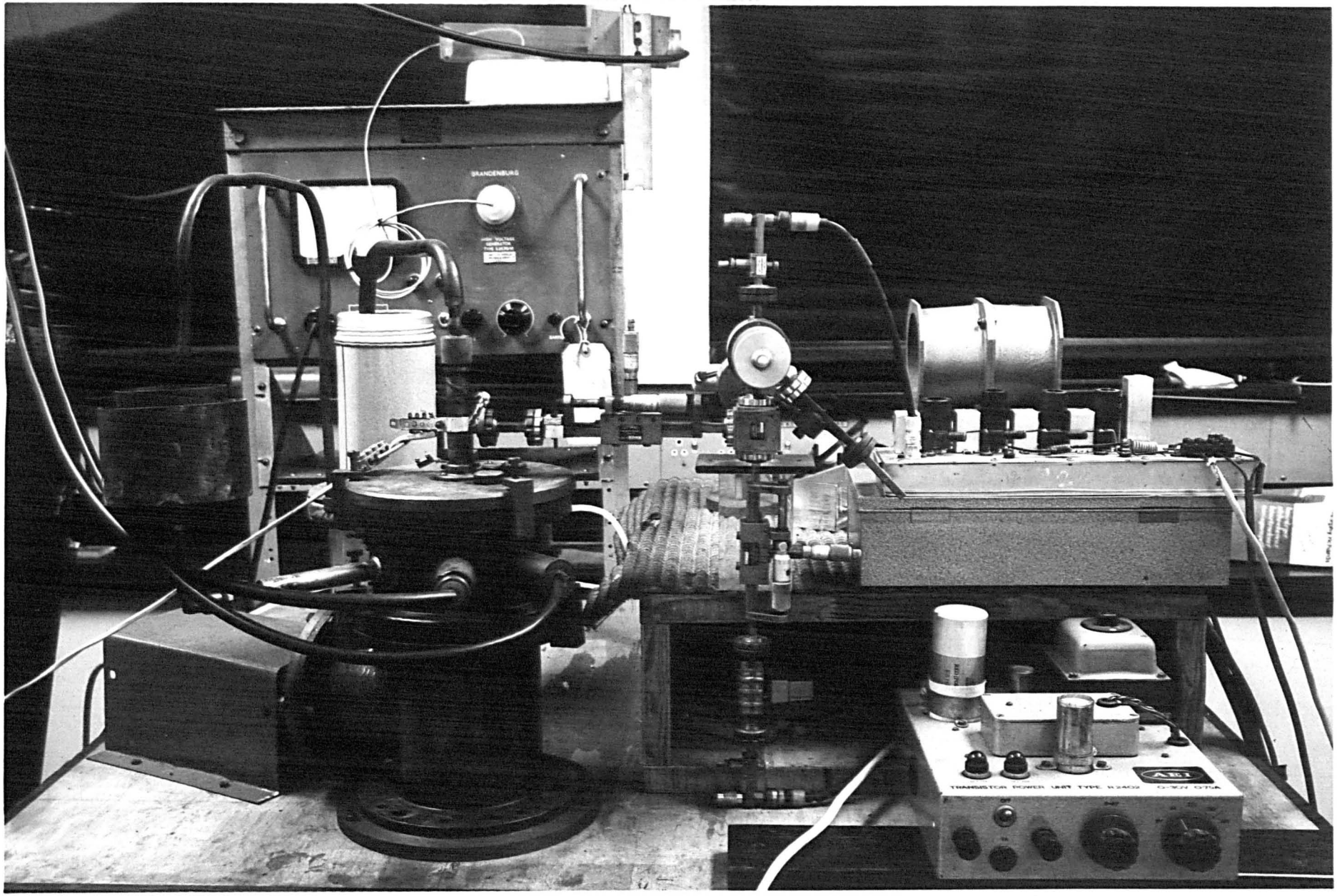

Fig. 5.5.1 General view of the maser system (85)

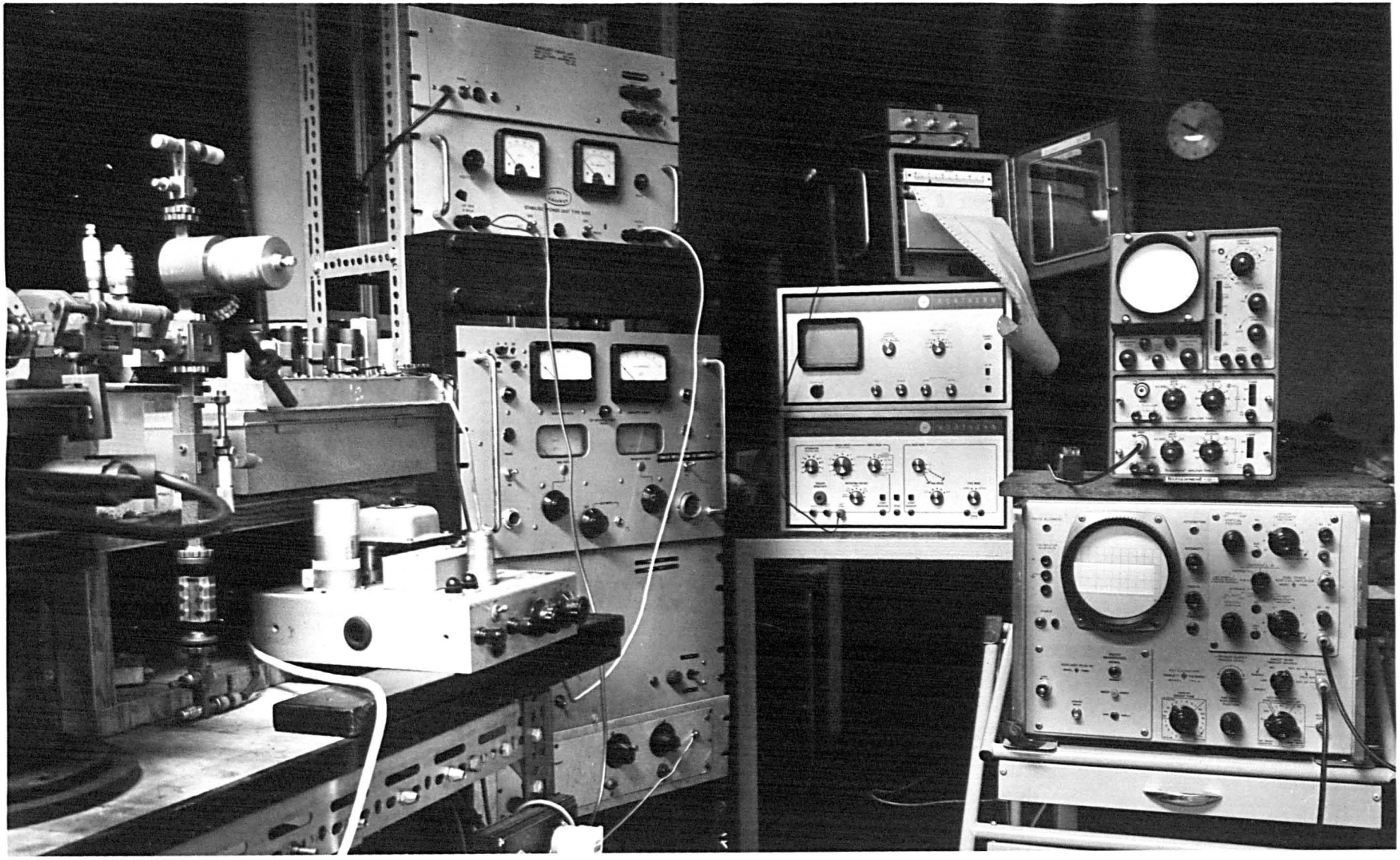

Fig. 5.5.2 A general view of the maser assembly and detection system. (85)

sending two opposing beams the effect can be considerably reduced and stability increased. A further improvement can be achieved by using two opposing beams with two resonators. Veselago[137] et al suggests that the effect of the travelling waves can be eliminated by varying the distance between the two resonators. With various improvements in techniques, including use of N^{14} H_3 3-2 lines and N^{15} H_3 3-3 line, the best stability obtained is of the order of 1×10^{-12}, and reproducibility is of the order of 2×10^{-10}. This is to be compared with the respective figures 2×10^{-14} and 5×10^{-13} of the atomic hydrogen maser.[138] It is suggested that by using slow molecules it may be possible to improve the stability of a maser by a factor of 10 - 100. Marchenko[141] et al has shown theoretically that highly improved stability and noise performance can be achieved by mutual synochronization of several intercoupled masers. Suchkin[142] has proposed a device called the moleculechron, based on this principle, and predicts that the stability can be increased by a factor of 10^{-k} where $k + 1$ is the number of masers coupled together.

5.5 Experimental Apparatus :

5.5a General :

A general view of the maser is shown in Fig. 5.5.1 and Fig. 5.5.2. The maser assembly consists of a molecular beam source, focuser and cavity resonator, which are mounted vertically on the top of a Dexion frame about 4 x 4 feet square and $3\frac{1}{2}$ feet from the ground. The microwave system and intermediate frequency amplifier are also mounted on the same frame. Most of the electrical apparatus is mounted on two 'post office' racks. The beam source is a hcneycomb made from klystron grid

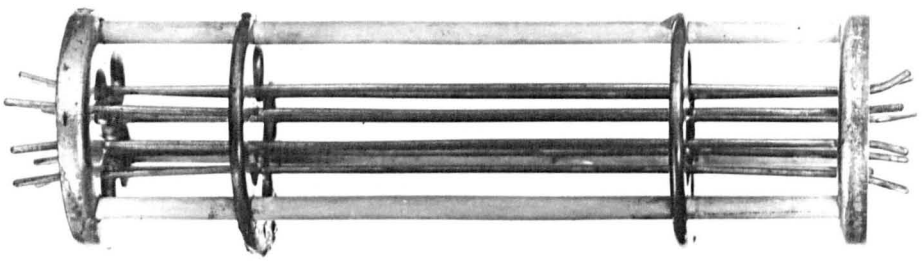

Fig. 5.5.3. Octapole Focuser Used (86)

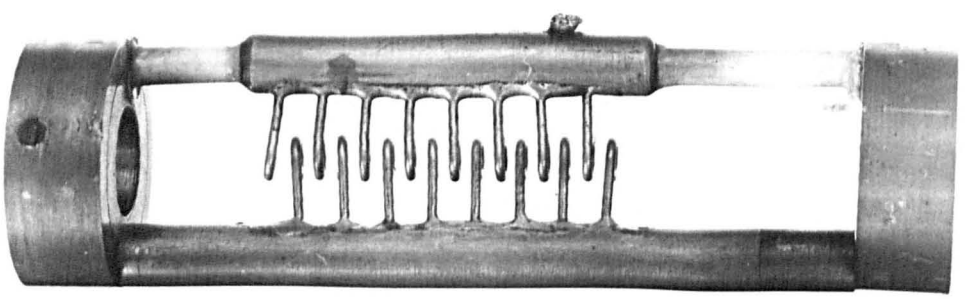

Fig. 5.5.4. Ring Focuser Used (86)

bar stock supplied by Varian Associates, 0.5 cm long, 0.33 cm in overall diameter and is formed by a number of fine parallel copper tubes of about 0.025 cm in diameter. These tubes are made by depositing copper on to aluminium wires, which are then cut to length and stacked to fill a copper tube used as a mount. After machining the honeycomb to the right length, the aluminium is dissolved away in a solution of potassium hydroxide.

Figs 5.53,4 show the octapole and ring type separators used. The octapole was made of eight silver plated 26 swg steel electrodes on a 1 cm diameter circle. Each set of alternate electrodes is connected to a pair of metal rings which are accurately spaced and insulated from one another by ceramic rods. The separator has a total length of 10 cm. When cleaned and outgassed, it supports up to 40 KV between the electrodes at about 10^{-5} torr in the vacuum chamber without electrical breakdown. This is found satisfactory because the maser is normally operated at 30 KV or less.

The ring separator is made of two sets of metal rings soldered into the grooves on two bass rods. Some of the dimensions of the ring separator are: total length 9 cm, focusing length 3.5 cm, ceramic spacers 1 cm each, 7 rings are used on one rod and 8 on the other. The internal diameter of the ring is 2.41 mm, made of 0.96 mm thick wires. Spacing between successive rings is 1.2 mm. A second ring separator with 3 + 4 rings each made of 2.2 mm thick wires and internal diameter 6.1 mm. The rings are in each case soldered to brass rods 4.5 cm long and 0.6 cm thick.

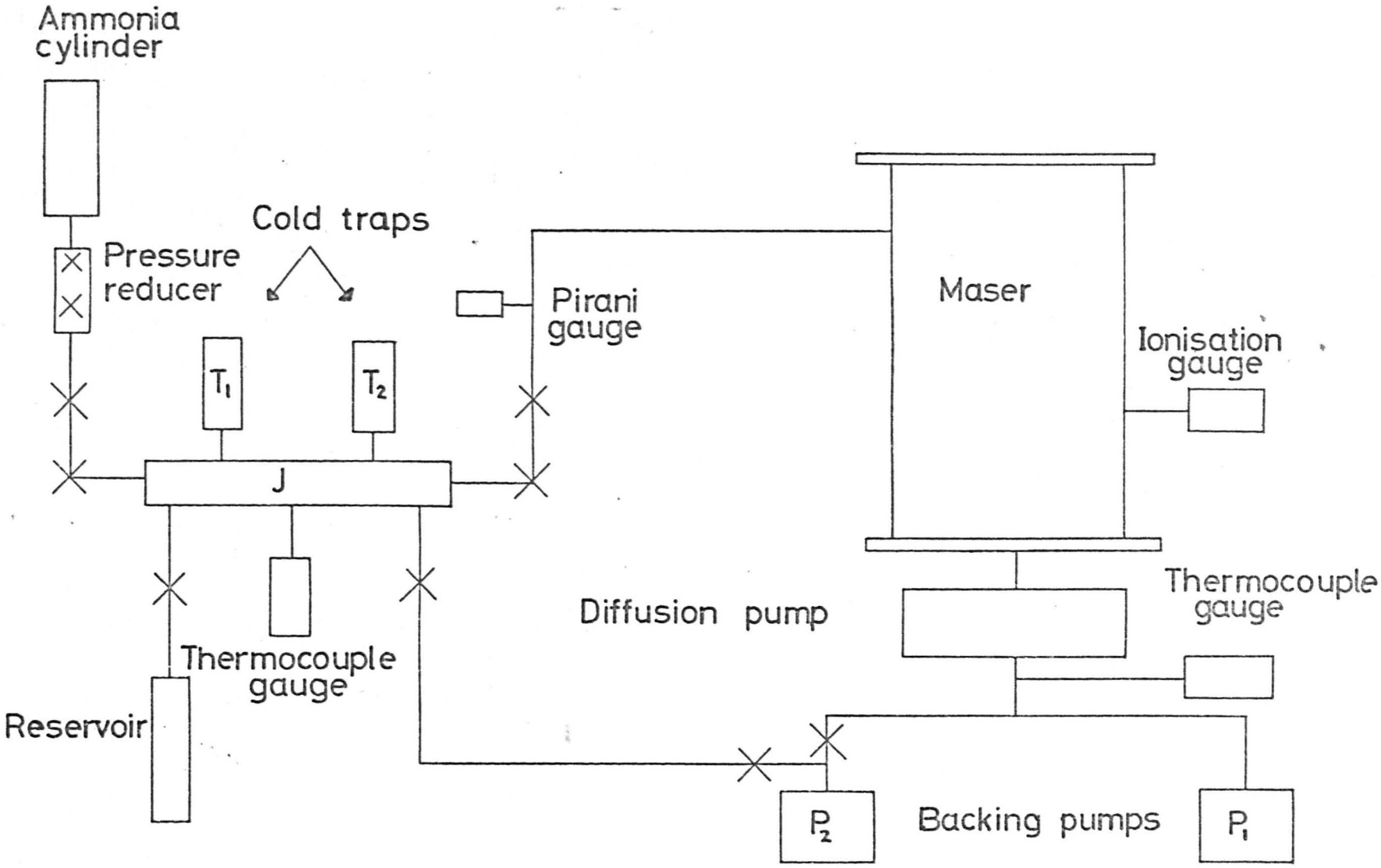

Fig. 5. 5. 5. Maser vacuum system and ammonia source

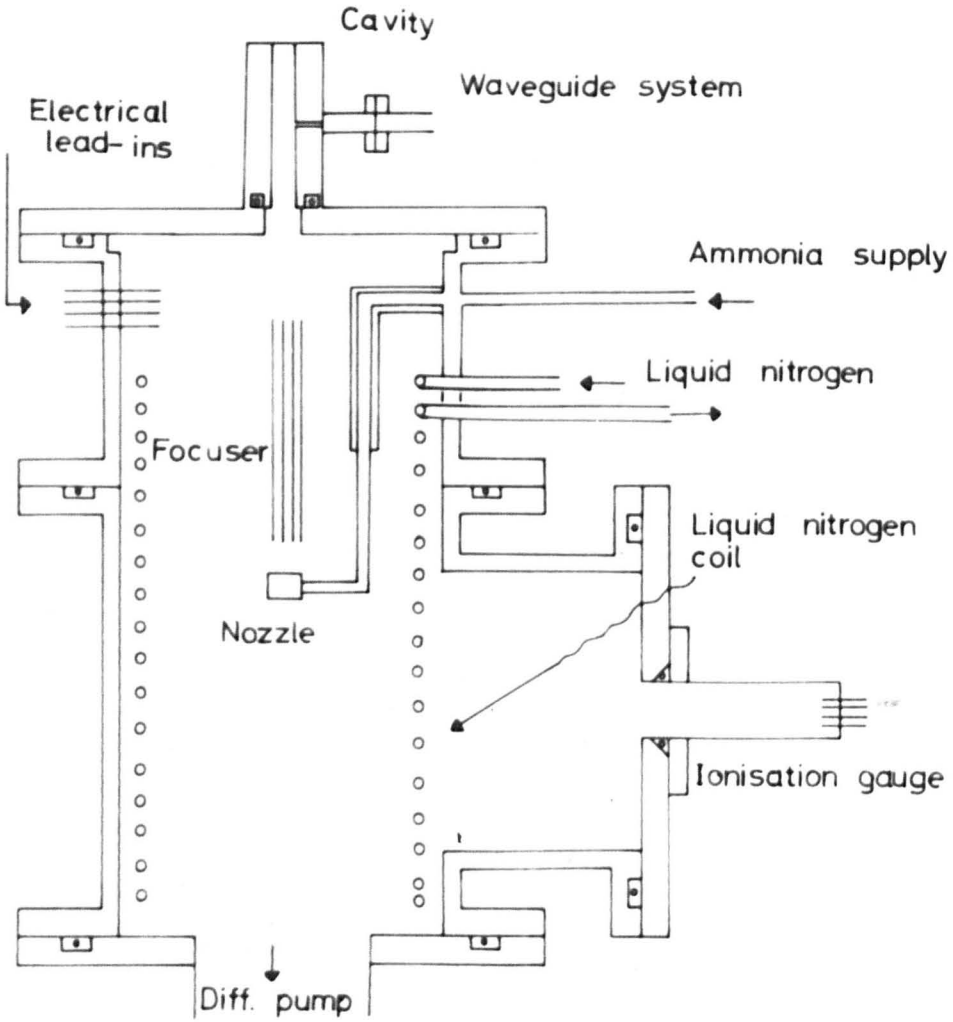

Fig. 5.5.6. Maser vacuum chamber

The microwave cavity oscillating in the TM_{010} mode is made from electroformed copper. This has a diameter 2a = 0.9614 cm. A change by unity in the third decimal place may change the resonance frequency by as much as 20 MH_z. Even providing for thermal control of the cavity dimensions, this must be made to a precision of $\pm \frac{1}{10}$ thou in diameter. Such precision is difficult to obtain by drilling and therefore the cavity is electroformed. The mandrel for this purpose is made of S-80 stainless steel and electroplated with copper. The electroform is then machined and removed from the mandrel by heating it in oil. The cavity is made slightly too small in diameter, so that the final tuning can be achieved by heating the cavity. The electroformed cavity would tune by about 0.5 MH_z for $1^{\circ}C$ change in temperature. To improve the effective quality factor, end caps are inserted at the two ends of the cavity and are adjusted for maximum Q. The cavity used is 10 cm long with a coupling hole of diameter $\sim \frac{1}{10}$ inch in the middle of the cavity. Helmer's[143] calculations show that from the point of view of linewidth the critical length of the cavity should be very small, e.g. less than 1 cm. It is shown, however, in Section 5.3 that a cavity of about 10 cm length has a good Q and good figure of merit. The loaded Q of the cavity made is about 5000, which compares favourably with the theoretical value of 10,800 for the unloaded Q.

5.5b Vacuum Assembly and Ammonia System :

Figs 5.5.5,6 show diagrammatically the maser vacuum system. Normal operation of the maser requires a background vacuum of $\sim 10^{-5}$ torr. The source produces a beam of $\sim 10^{18}$ molecules per second in the vacuum

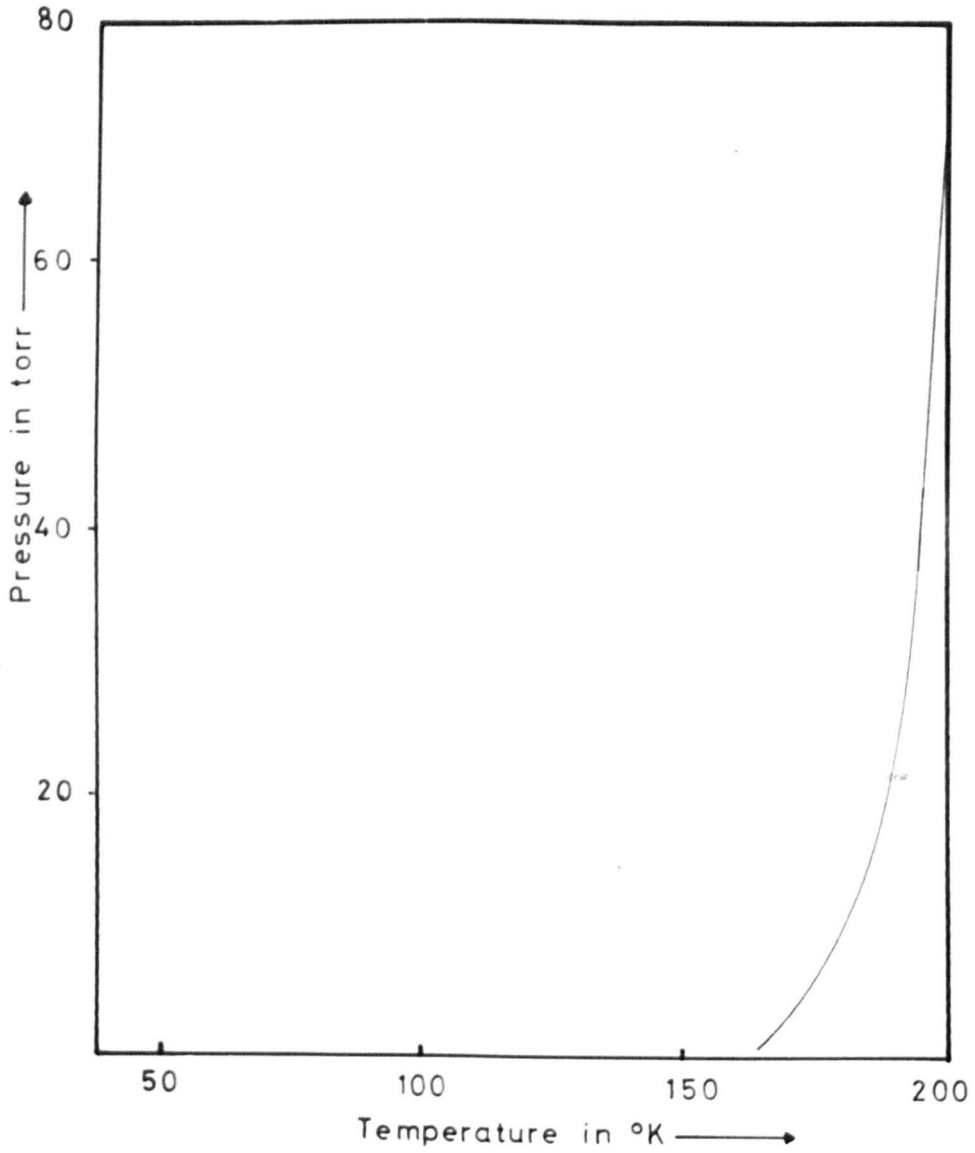

Fig. 5.5.7. Ammonia vapour pressure — temperature relation.

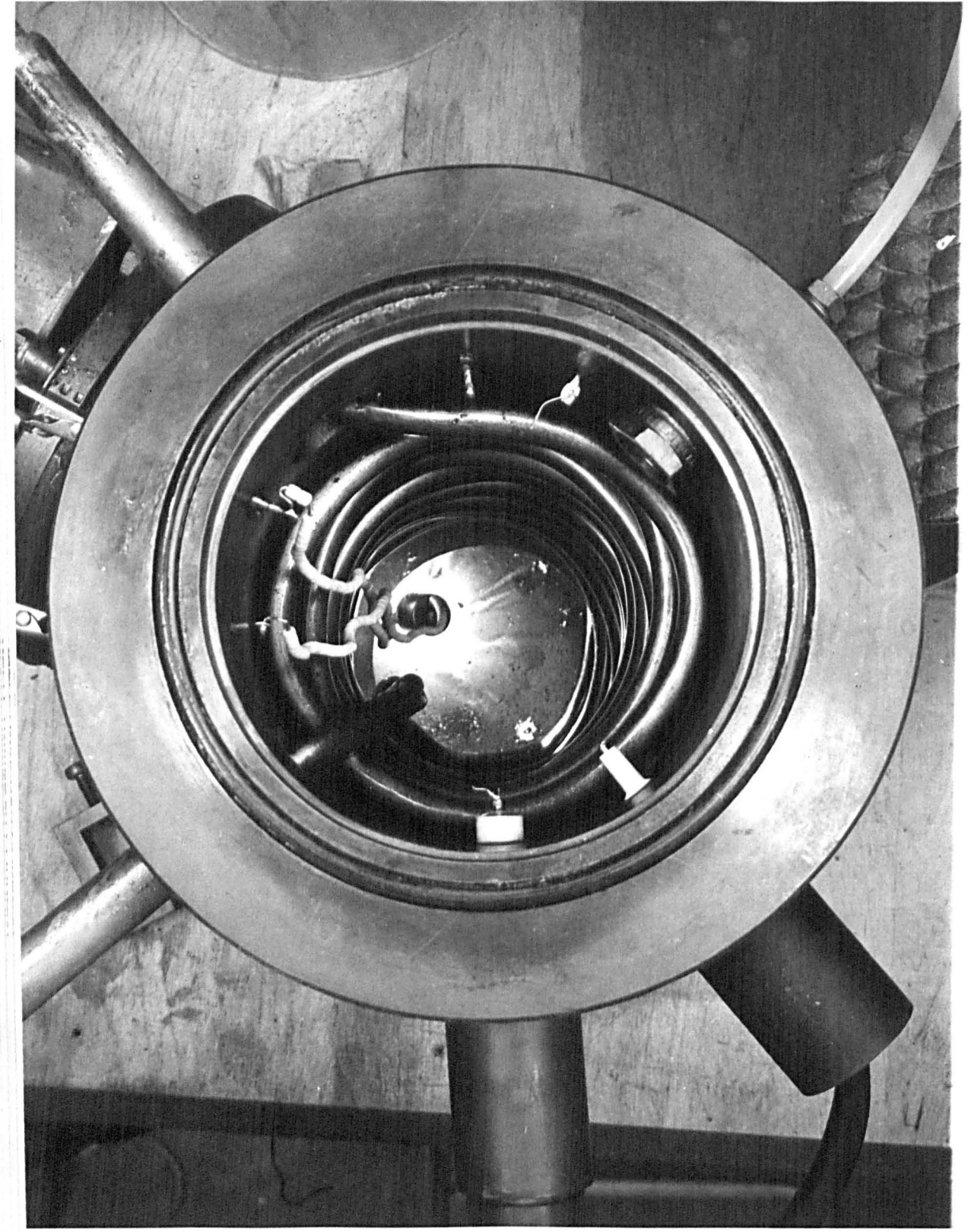

Fig. 5.5.8 Interior of the maser chamber showing the liquid nitrogen cooling coil

chamber, so that in order to maintain the required vacuum, the pumps must remove ~ 10^4 litres of gas per second. However, the required vacuum is obtained more easily by freezing the ammonia on a cold surface at liquid nitrogen temperature, since the vapour pressure of ammonia at this temperature is ~ 10^{-9} torr only. Fig. 5.57 shows the vapour pressure - temperature relation of ammonia. Liquid nitrogen cooling is provided by a copper coil concentric with the vacuum chamber (Fig. 5.5.8) The chamber itself is made of two brass sections sealed with rubber 'O' rings. The main cylinder has an internal diameter of 12 cm, and overall height of 26.5 cm. The top section of the cylinder is provided with

(i) four feed-throughs for various electrical connections inside such as a lamp for visual alignment of the system, and provision for producing a constant electric or magnetic field in front of the cavity.

(ii) two E.H.T. feed-throughs,

(iii) inlet and outlet for liquid nitrogen, and

(iv) inlet for ammonia.

The E.H.T. feed-throughs are long reach spark-plugs suitably machined and extended at the atmospheric end with an araldite casting. The other feed-throughs were made of glass sealed cover rods. All these connections and electrical lead-throughs are sealed with appropriate 'O' rings. The liquid nitrogen pipes are connected to the vacuum chamber by a length of cupro-nickel jacket doubling on the pipe. This provides a thermal break between the liquid nitrogen coil and the rest of the system, and prevents the freezing of the 'O' rings in the neighbourhood.

The cavity is connected to the top-plate through a collar and

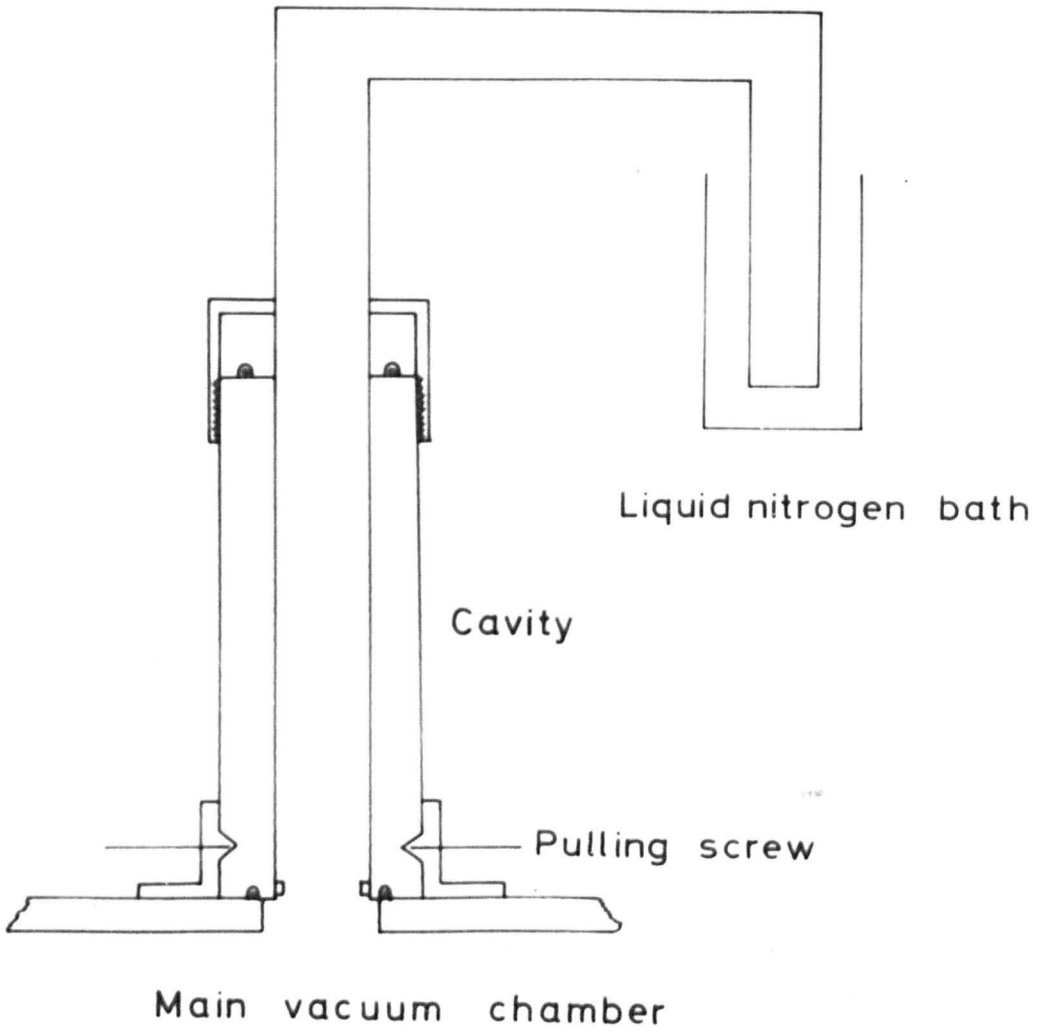

Fig. 5.5.9. Cavity connection at top - plate.

'O' ring and is placed outside the vacuum chamber. This is shown in Fig. 5.5.9. The screws working through the collar on the V-groove outside the cavity pull down the cavity and make the 'O' ring seal firm. Only the inner volume of the cavity is therefore evacuated. Although for temperature stabilisation of the cavity, it should ideally be wholly inside vacuum, this arrangement is found simple and convenient for the present work. Incidentally, it may be commented that such an arrangement would be ideal for spectroscopic work with different molecules, since the cavity can be changed very easily without disturbing the rest of the assembly. At first the top of the cavity was sealed with a mica foil and a cap was screwed on to the cavity. By adjusting the cap the cavity can be roughly tuned. However, this arrangement leads to accumulation of the spent molecules in the cavity. Therefore, in the final version, a small reservoir in the form of an inverted U-tube is connected to the cavity (Fig. 5.5.9) This reservoir is put in a liquid nitrogen bath and provides efficient pumping of the spent gas for about three hours under normal operational conditions. The 'K'-band waveguide attached to the cavity is soldered to it and sealed with a mica disc between the flanges and 'O' rings of a waveguide junction coupler.

The vacuum connecting pipes are made from copper pipe with 'Yorkshire' lead solder sealed junctions, and for isolating different sections 'Genevac' or 'Edwards' pressure actuated hand valves are used. The maser chamber is directly connected to the 4" diameter oil diffusion pump (Model Edwards 403 A), operated with Silicone 704 oil. This pump has a speed of 300 litres/sec, at a backing pressure of less than 0.5 torr.

The diffusion pump is connected by 1" diameter copper pipes and flexible couplings to two rotary pumps (1 litre/sec) P_1 and P_2 working in parallel. One of the rotary pumps, P_2 is connected to the ammonia system through a T-junction.

The ammonia source is a 120 -atmosphere pressure cylinder of anhydrous liquid ammonia. This cylinder is connected to a pressure reducing valve which is adjusted for about 30 lb/sq. inch output pressure. The various sections of the ammonia system are connected by $\frac{1}{2}$" diameter copper pipes, and a brass junction box (J in Fig. 5.5.5) which is made of a block of brass with seven connecting points in order to keep the number of soldered junctions to a minimum. The ammonia is frozen in one of the two liquid nitrogen traps (T_1 and T_2 in Fig. 5.5.5). Any water vapour and air impurities in the ammonia gas are removed by pumping over the frozen ammonia. It is then stored in a 4 litre cast iron reservoir at a pressure greater than atmospheric. The pressure in the reservoir is monitored with an NGN, TC.1 thermocouple gauge. The flow of ammonia from the reservoir to the nozzle is first adjusted by a rough control valve and then by a fine control needle valve. The control valve is connected to the maser vacuum chamber by a Nitex $\frac{1}{4}$" diameter thick walled flexible nylon tube. The pressure (0.1 to 5 torr) behind the nozzle is measured by an Edwards Pirani gauge (head M5C, 10^{-3} to 10 torr). The background pressure in the maser vacuum chamber is monitored by an Edwards 1GHF2 ionisation gauge head, and NGN T1U1 Thermion combined Thermocouple-Ionisation control unit. The backing pumps reduce the pressure of the whole system to about 0.05 torr in about one hour and the diffusion pump reduces the pressure to about 10^{-5}

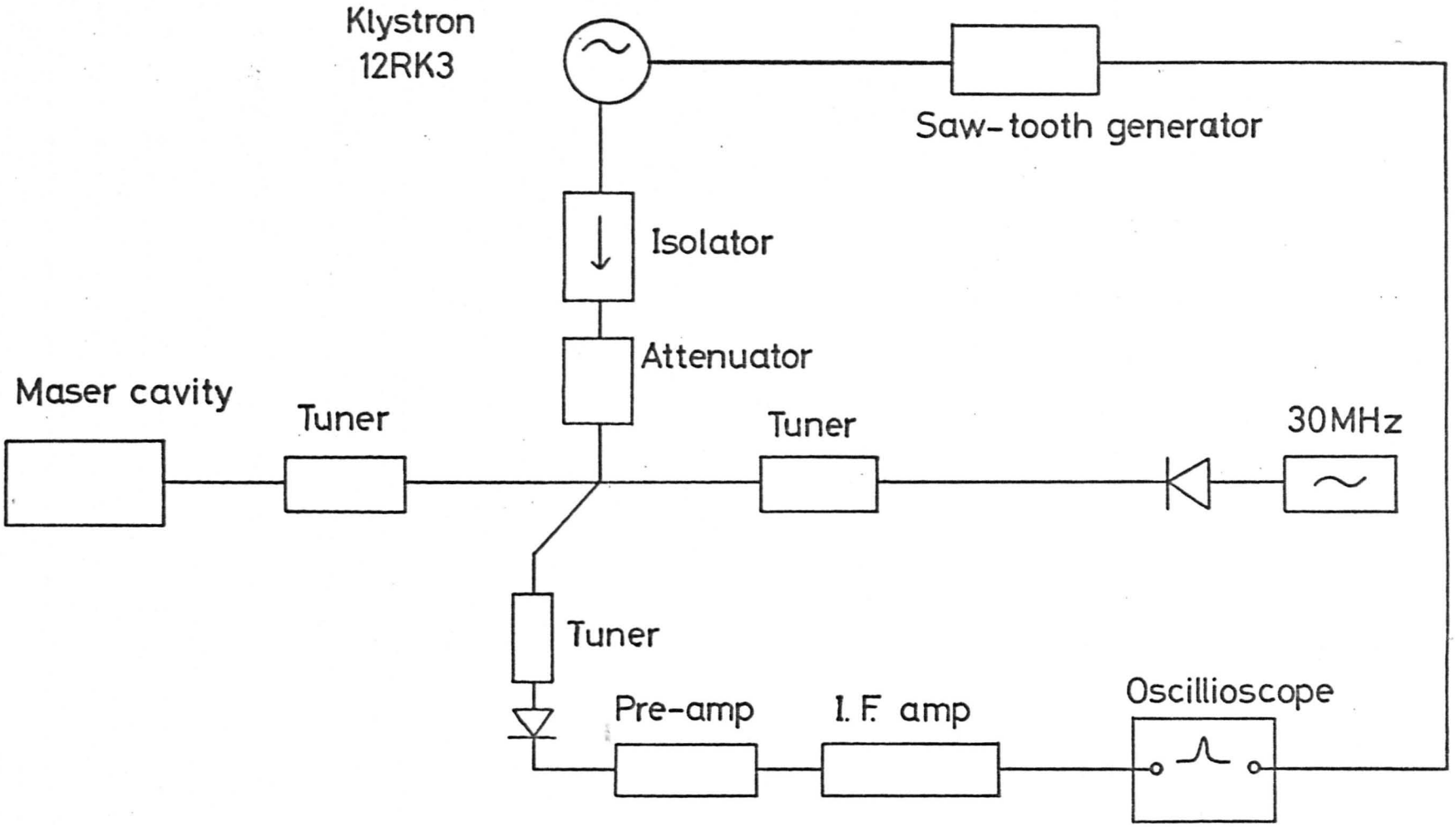

Fig. 5. 5. 10. Block diagram of maser system

torr in two hours. If the coiling coil is now filled with liquid nitrogen, the pressure falls to about 5×10^{-6} torr. The pressure characteristics of the system are given in Fig. 5.6.3.

5.5.c. Cavity Stabilization :

The cavity resonator is thermally expanded until it is tuned to the ammonia J = K = 3 inversion transition. The cavity is heated by a current flowing in a 10 ohm bifiliar coil of glass insulated "Eureka" wire around it. The coil is supplied from a 18 volt tapping of a transformer. The input potential is switched on and off by a relay system ('Airmec' type N299) operated by a copper resistance thermometer (8.9 ohm at 20°C) attached to the cavity. The cavity can be set and stabilised at any temperature between 20°C and 30°C to within 1/10° C. For a copper cavity, the resonant frequency will change by 0.4 MH_z per °C change in temperature and therefore the cavity should be stabilized within $\pm$ 20 KH_z. By Eq. 5.4d.9 therefore, the maser output frequency should only vary by $\pm$ 10 H_z, or 4 in 10^{10} in overall frequency. The unstabilised local oscillator Klystron is frequency stable however only to about one part in 10^4. Therefore, the noise in the system may arise due to Klystron frequency fluctuations.

5.5d. Microwave System :

The microwave and electronic detection system is shown schematically in Fig. 5.5.10. The source of microwave power is an unstabilised 'Elliott 12RK3' Klystron. The Klystron is air-cooled and its heater is supplied from a 6.3 volt external d.c. power supply unit,

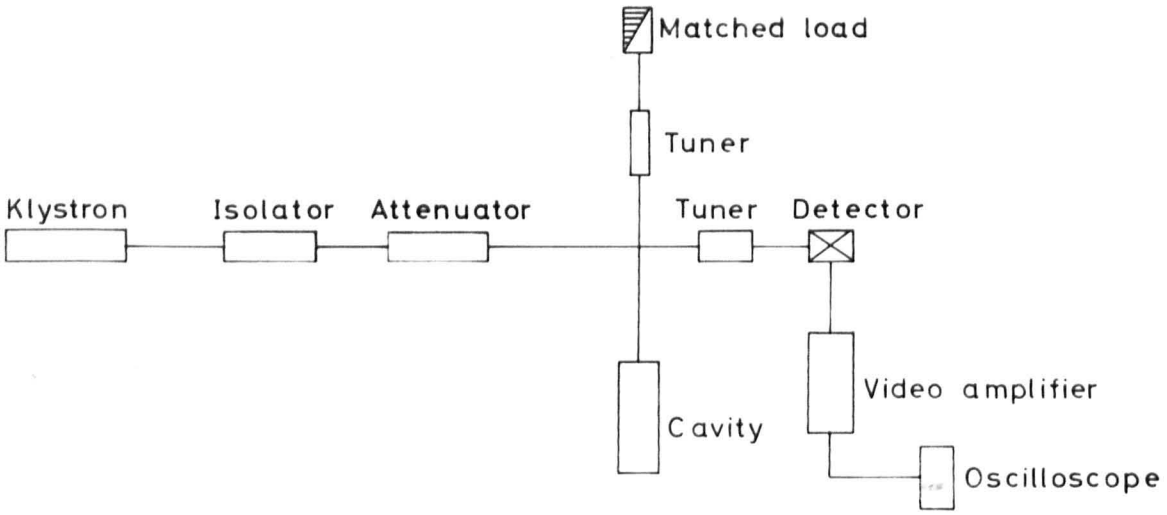

Fig. 5.5.11. Basic crystal video scheme.

the reflector sensitivity is 0.5 MHz per volt. The klystron is isolated from the rest of the system by a 'F.X.R.' K157A ferrite isolator, with a V.S.W.R. of 1.15 and better than 24 db isolation.

For detection, the power from the maser is mixed with the output of the klystron in a silicon diode, and the resulting signal amplified and displayed or recorded. The two signals are combined in a 'Mid-Century' Magic T which is balanced with slide screw tuners appropriately located. The system is operated in two different modes, namely, 'crystal video detection' and 'superheterodyne detection'. The microwave receiver in either mode is required to detect small variations in a relatively large signal power, rather than to detect small amounts of signal power. The power around the emission or absorption line can be cancelled out by r-f balancing and thus cause the spectrum line to appear as a small amount of unbalanced power.

The crystal video receiver[83,144,145] is much less sensitive than a superheterodyne receiver. For preliminary experiments however it is found that by employing the frequency sweep method with a crystal video receiver a simple and rapid microwave spectrometer can be made. In this mode of operation a saw-tooth waveform of up to 100 volts peak potential is applied to the reflector of the Klystron. This is sufficient to sweep the Klystron output frequency through a complete mode of nearly 50 MH_z, about a mean frequency of 23,870 MH_z. The crystal detector is mounted in a waveguide holder and is matched to the microwave line. The crystal is then directly connected to the video amplifier and the output is displayed on an oscilloscope (Fig. 5.5.11). The X-sweep of the oscilloscope is

synchronised with the original sawtooth and the mode of the Klystron is displayed with a small dip corresponding to the microwave cavity absorption. The microwave system can then be tuned up for maximum cavity absorption and the frequency measured with a cavity wavemeter. The response of the wavemeter can either be observed in absorption as a second dip on the Klystron mode or by a crystal detector connected to its reaction waveguide output and the signal displayed as a resonance on the second beam of the oscilloscope. When ammonia is introduced into the cavity, at a background pressure of 10^{-1} to 10^{-3} torr, it produces an absorption dip superimposed on the cavity absorption in antiphase. Under this condition the cavity temperature controller can be adjusted so that the cavity is exactly tuned to the molecular transition frequency.

5.5e. Superheterodyne Detection:

The crystal video detection scheme suffers at low powers because of the poor conversion gain of the crystal and at high powers because of excess crystal noise. The power output of the maser is only of the order of 10^{-11} watt, so for this to be detected a superheterodyne detector (SHD) [83, 146, 147] is used. An SHD scheme employs a crystal mixer driven by a CW microwave oscillator as the first detector, a vacuum tube IF amplifier at ordinary RF, and a second detector which yields a rectified signal. The scheme acts as a linear gain receiver in which the output power is proportional to the input power. The crystal output in the SHD system is usually at an intermediate frequency of 30 or 60 MH_z. It is desirable to amplify the signal at such a high frequency before detection in order to avoid the excessive low frequency noise from other sources such as flicker noise. The output noise of a crystal can be represented in

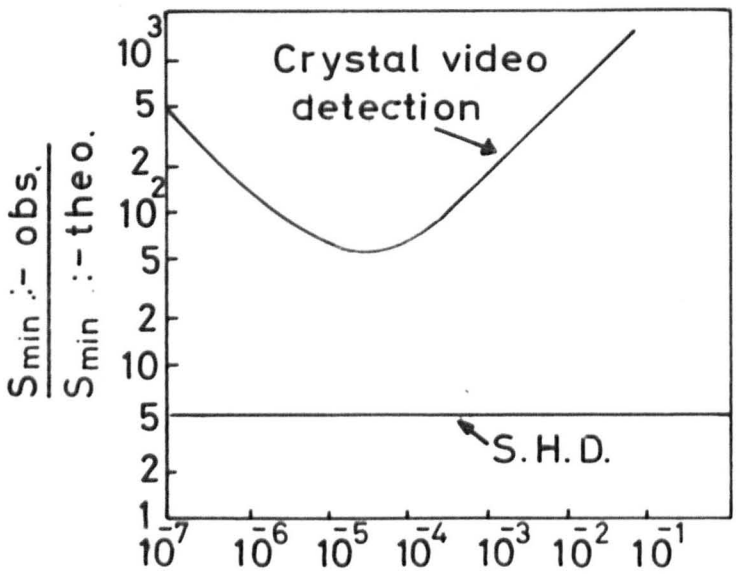

Fig. 5.5.12. The ratio of the minimum observable signal to the minimum theoretical value versus microwave power for different detection schemes (after Feher)

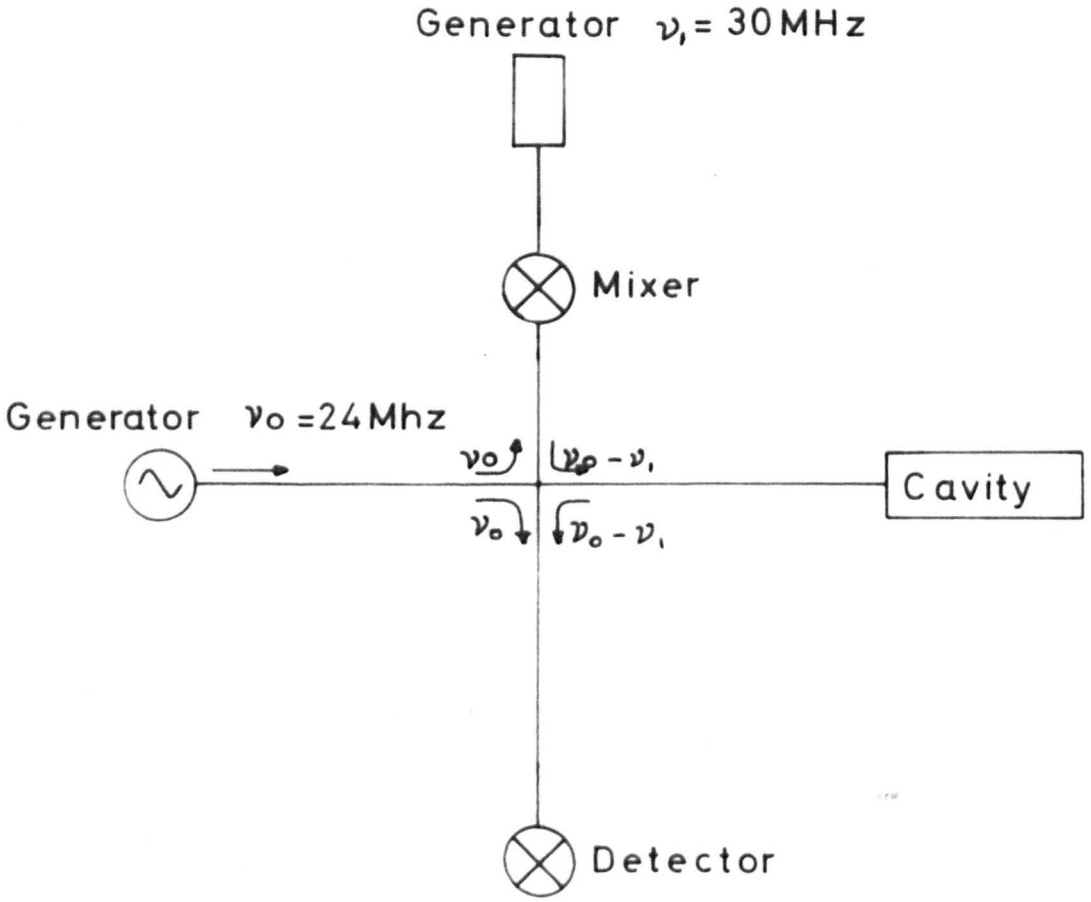

Fig. 5.5.13. Basic SHD scheme used in present experiments (after Bonanomi et al)

general by the relation

$P_N = (kT + CI^2/\nu)\Delta\nu$, [144, 148, 149] where I is the d.c. crystal current, ν the output frequency, C is a constant and is about 10^{-7} ohms[7] for a reasonably good K-band crystal. At room temperature $kT = 4 \times 10^{-21}$ watt/cycle/sec, which at 30 MH_z is of the same order as CI^2/ν for a crystal current of 1ma, and much less for smaller currents. It is thus seen that around frequencies of tens of megacycles or higher, the noise output of the crystal within the IF amplifier bandwidth is reduced practically to thermal noise. At such high frequencies the flicker noise components become negligible even at high powers where the conversion gain is good. The comparative sensitivities of crystal detection and SHD are shown in Fig. 5.5.12 adopted from Feher[147]. The SHD mode of operation in the present set up is obtained by inserting the IF amplifier and the second detector between the first detector and the audio amplifier in Fig. 5.5.11. Conventionally the IF frequency is obtained by beating the reflected signal from the cavity with a local oscillator (LO) which is removed from the signal by the I.F. frequency. Use of separate Klystrons for the source and local oscillator power needs some form of automatic frequency control[150] to keep the oscillators tuned. To avoid this complication, the same Klystron is used to provide the source and the local oscillator power. The scheme used here is due to Bonanomi and Herrmann,[151] and is represented in Fig. 5.5.13. (The principle of such a scheme was also mentioned earlier by Gordy.[83]). The elimination of the auxiliary LO Klystron removed one additional source of noise although this noise can

always be removed by the use of balanced mixers[150]. The carrier in the SHD is enormously larger than the useful absorption or emission signal. It persists at the output of the mixer and is amplified along with the signal. Thus, besides introducing its own noise the carrier may saturate the amplifier before the signal has reached a suitable level. The carrier can be reduced and overloading of the IF amplifier can be avoided by using a balanced bridge. The image frequency can also be rejected by using a preselector before the mixer. However, this is not considered important since the image frequency is displaced from the signal by twice the IF frequency, i.e. by 60 MH_z and the frequency dependence of the bridge circuit results in the unwanted side band being somewhat attenuated after careful adjustment.

In the case of stabilised SHD, the band width of the IF amplifier does not enter in the scheme[147]. In the present setup the Klystron is not stabilised and the frequency sweep method is used. In this situation the noise components within the bandwidth $\Delta\nu_{IF}$ of the amplifier can beat with each other and produce a noise output which would increase with bandwidth. It is shown by Rice[152] that if the carrier voltage V_c at the output of the IF is large enough the IF bandwidth $\Delta\nu_{IF}$ does not enter into the noise consideration. The criterion for this is that

$$V_c^2 > G^2\, 2kTZ\, \Delta\nu_{IF} \qquad (5.5e.1)$$

where G is the IF amplifier gain and Z the input impedance. This means that the noise which beats with the carrier should be greater than the

beat between two noise terms. Since the former is proportional to the carrier, its predominance can be easily ascertained by increasing the IF carrier and noting whether the noise output increases proportionally. If it does, the above criterion is fulfilled. It is desirable that $\Delta\nu_{IF}$ be reasonably large because any fluctuations in the centre frequency will cause an amplitude (and phase) change in the transmitted signal. Since it is difficult to construct an amplifier to be stable to better than $\pm$ 25 KH_z at 30 MH_z, to keep such fluctuations at a few per cent a bandwidth of at least 2 or 3 MH_z is desirable. With $\Delta\nu_{IF}$ = 3 MH_z, $Z = 10^3\ \Omega$, $V_c \sim 1V$, condition 5.5e.1 shows that G has to be less than approximately 10^5. If on the other hand G is very small the signal level at the audio amplifier input is so low that the flicker noise of the detector can still come in. A good practical figure for the IF gain is about 60 db. This can be easily obtained with a combination of pre-amplifier and main amplifier. The noise figure of the microwave receiver is given by

$$F_{db} = L_c + 10 \log (N_{IF} + N_r - 1) \qquad (5.5e.2)$$

where L_c is the conversion loss of the crystal (the first detector), N_{IF} is the noise factor of the IF amplifier, and N_r is the noise factor of the first detector. For most of the experiments the silicon 1N26A crystal has been used. The conversion loss L_c for 1N26 is typically $\simeq$ 7.5 db, and $N_r \simeq 2$. The IF amplifier has a noise factor of about 1.5. The noise figure of the receiver thus obtained is F = 11.5 db. For some low noise experiments a germanium D4089 crystal has also been used,

and for this the values are L_c = 6.5 db, N_r = 1.5, F = 9.5 db.

To reduce the overall noise figure, a pre-amplifier has been used in some experiments. The overall noise factor F_T in this case is given by

$$F_T = F_1 + \frac{F_2 - 1}{G_1} \qquad (5.5e.3)$$

where F_1 is the noise factor of the first stage (the pre-amplifier) and F_2 is the noise factor of the receiver i.e. the remainder of the amplifier, and G_1 is the gain of the first stage. A pre-amplifier designed by Smith[153] with a cascode first stage after a configuration suggested by Wallman et al[154] has been used. This has a noise figure of about 1.5 db and a gain of 35 db; that is $F_1 \simeq 1.7$ and $G_1 \simeq 4000$; the receiver has a noise figure F = 9.5 db, that is a noise factor F_2 = 9. From Eq. 5.5e.3, the overall noise factor is then F_T = 1.7 + (9-1)/4000 = 1.702 or a noise figure of ≃ 1.5db. Thus the amplification of the second stage does not influence the result. This pre-amplifier was later replaced by a battery operated, transistorised Decca IF 30/3P amplifier. The main IF amplifier has a midband frequency 30 MH_z, and a gain which can be varied from 40 to 80 db by varying the high tension from 130 to 250 volts. The smoothing capacitor in the output filter circuit of this amplifier is varied to suit particular experiments.

It is found that instabilities in the microwave bridge due to mechanical vibrations and thermal drifts can contribute considerable noise. For this reason the bridge is mounted on rubber pads, the rotary pumps are shock-mounted and connected to the rest of the assembly by

flexible rubber couplings. No special precautions are taken to control the room temperature.

5.5f. General Electronics :

The essential electronic components are shown in the block diagram in Fig. 5.5.10. For exciting the state separator a 'Brandenburg' S.0530 E.H.T. unit is used. This provides 0 - 30 KV potential difference with a stability better than 0.25% and a ripple of less than 0.1% at full output.

The power units used to supply the dc potentials for the various IF amplifiers are stabilised commercial supply units by 'Siemens-Ediswan' and 'A.P.T.' An 'A.E.I.' transistor power supply giving 3 amps at 0 - 30 volt. is used to supply some sub-circuits. A 'Leak' power amplifier and a 'Telequipment' two channel preamplifier type P.A.3 are used. For display, normally a double beam 'Telequipment' oscilloscope has been used.

5.6. Operation and Basic Characteristics :

The following procedure is followed to obtain maser action. The nozzle and the focuser are first assembled outside the vacuum chamber in the tripod made of glass rods and triangular brass discs to support them. They are then carefully aligned using a bulb below the nozzle which is transparent enough to be seen through. The tripod is then placed inside the maser chamber, the H.T. and the ammonia supply point are connected up. The top plate carrying the microwave cavity is then placed in position and the whole system is aligned again looking down the cavity, with a low voltage bulb below the nozzle. The top of the cavity is then connected

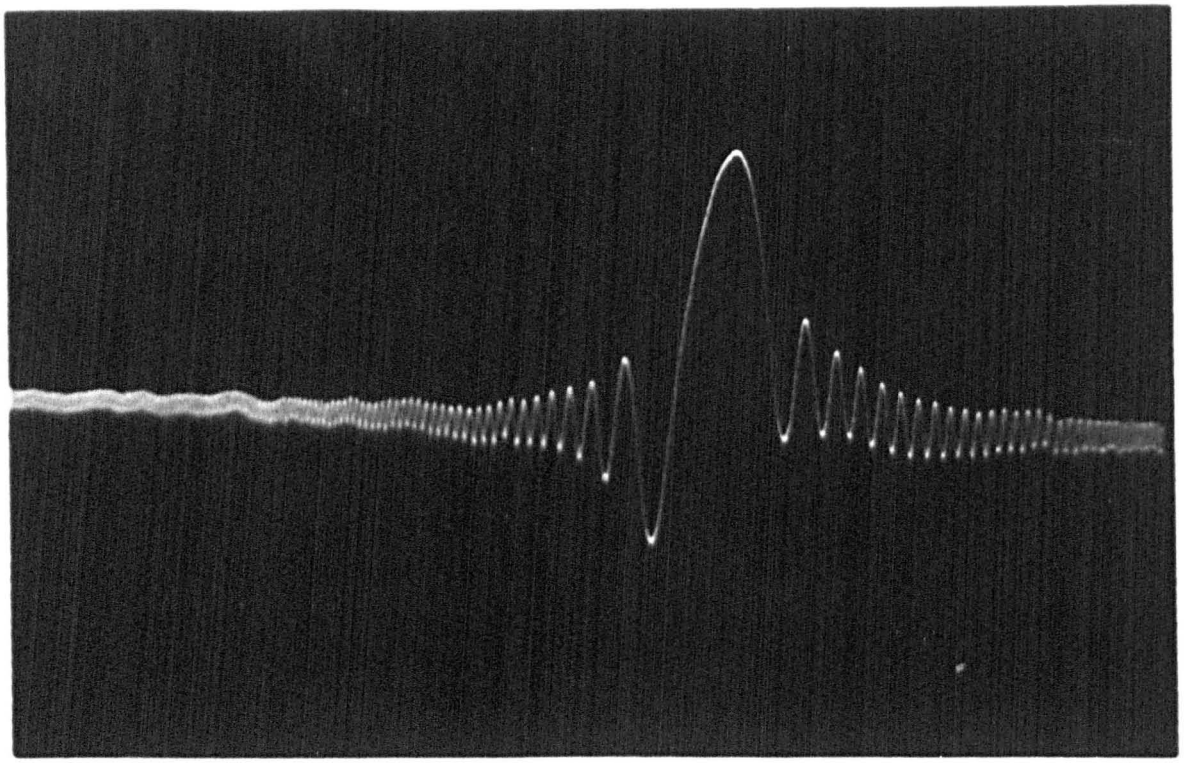

Fig. 5.6.1. Starting of maser oscillation. (99)

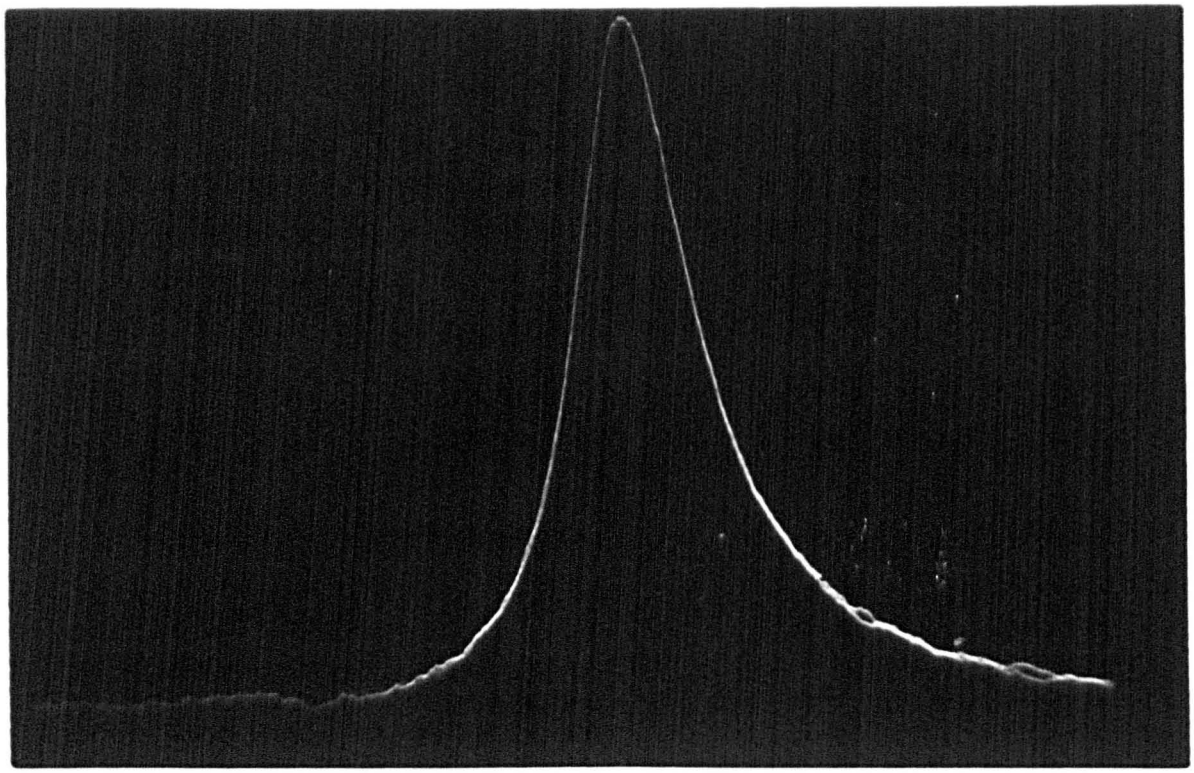

Fig. 5.6.2. Maser Oscillation Signal (99)

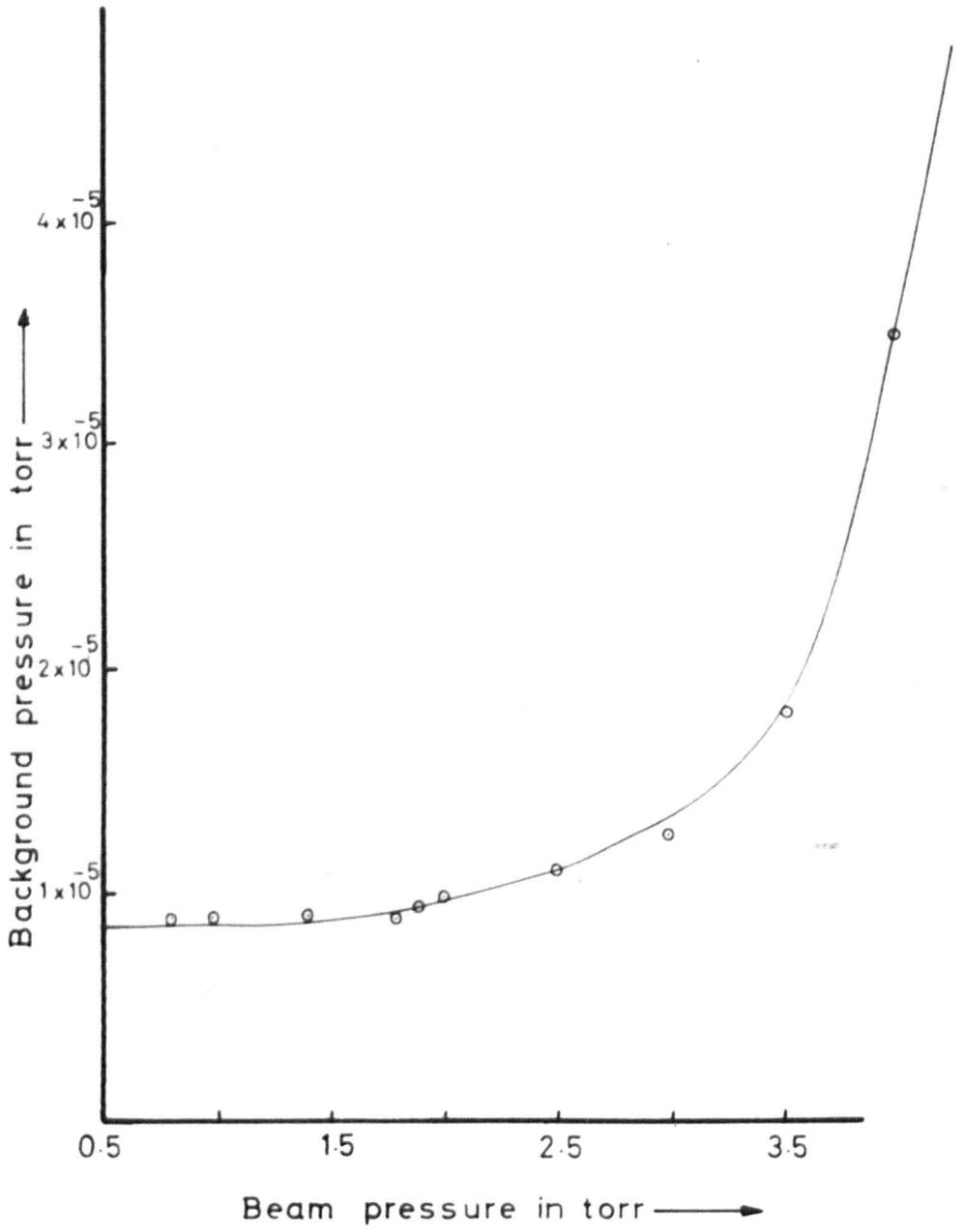

Fig. 5.6.3 Pressure characteristics of the maser chamber.

to the U-shaped cold trap, and thus sealed at the same time. The vacuum is then reduced to 10^{-5} torr as described in Section 5.5b. The ammonia reservoir is then filled with clean dry ammonia after purification as described in the same section. The microwave system is then tuned up on the cavity absorption curve. The cavity is then thermally tuned precisely on the ammonia absorption signal, with a beam pressure of about 1.5 torr behind the nozzle. The klystron is now offset by 30 MH_z and the system is switched from crystal video to superheterodyne detection. The EHT supply to the focuser is then switched on and increased to about 25 KV. Stimulated emission is obtained under these conditions. Beam pressure, microwave power level and the microwave bridge are adjusted to maximise the stimulated emission signal till the system begins to oscillate and the signal looks as in Fig. 5.6.1. At this stage the 30 MH_z signal generator is switched off, and the frequency sweeping of the klystron increased. The maser oscillation signal now beats with the klystron and gives an output signal at 30 MH_z. Fig. 5.6.2. shows the maser oscillation signal as displayed on the oscilloscope. Fig. 5.6.3. shows the pressure characterisitics of the vacuum chamber with liquid nitrogen cooling. The detection system here is used in the linear response region. The output amplitude of oscillation is therefore directly proportional to the field in the cavity and therefore to the oscillation parameter θ defined in Eq. 5.4a.11. The amplitude of oscillation can be varied by changing the E.H.T. on the focuser or the beam pressure. From Eq.5.4a.16 it can be easily shown that $dN/dV \propto V$ where N is the number of molecules entering the cavity and V is the focuser voltage. Thus the beam flux varies as

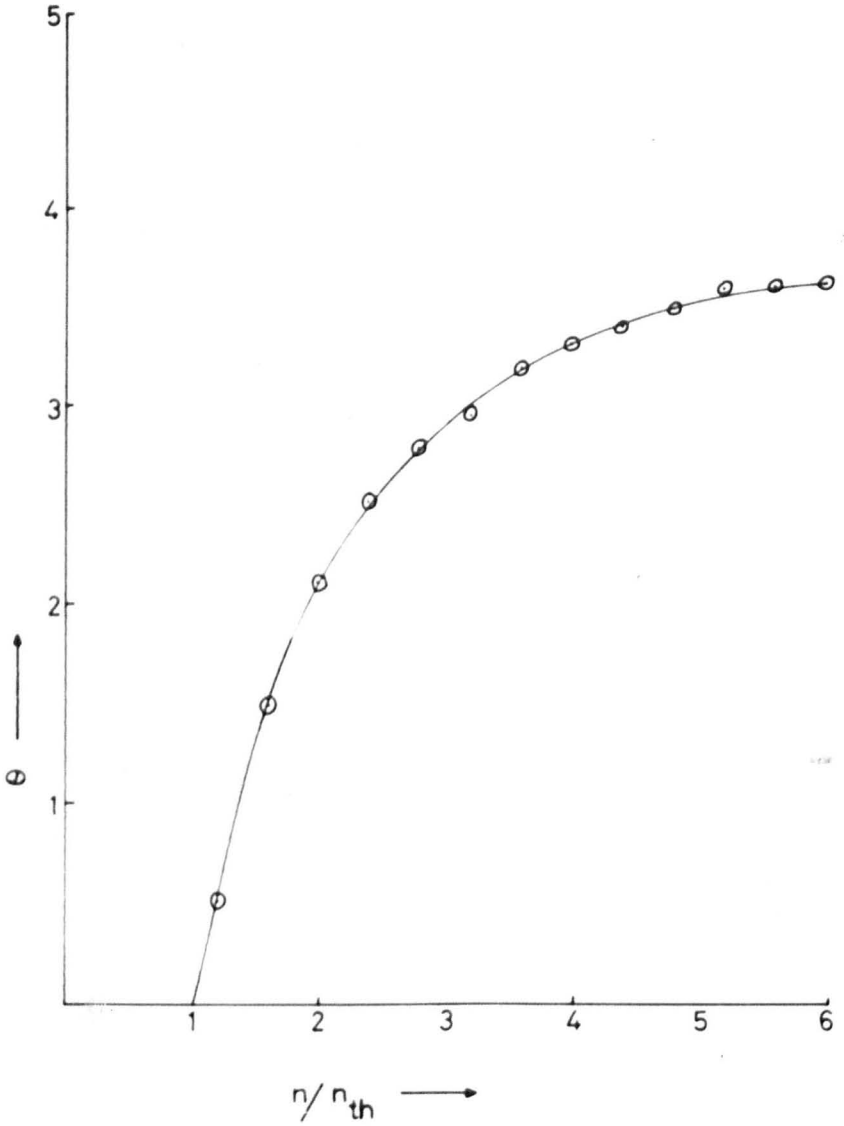

Fig. 5.6.4. Maser oscillation characteristic.

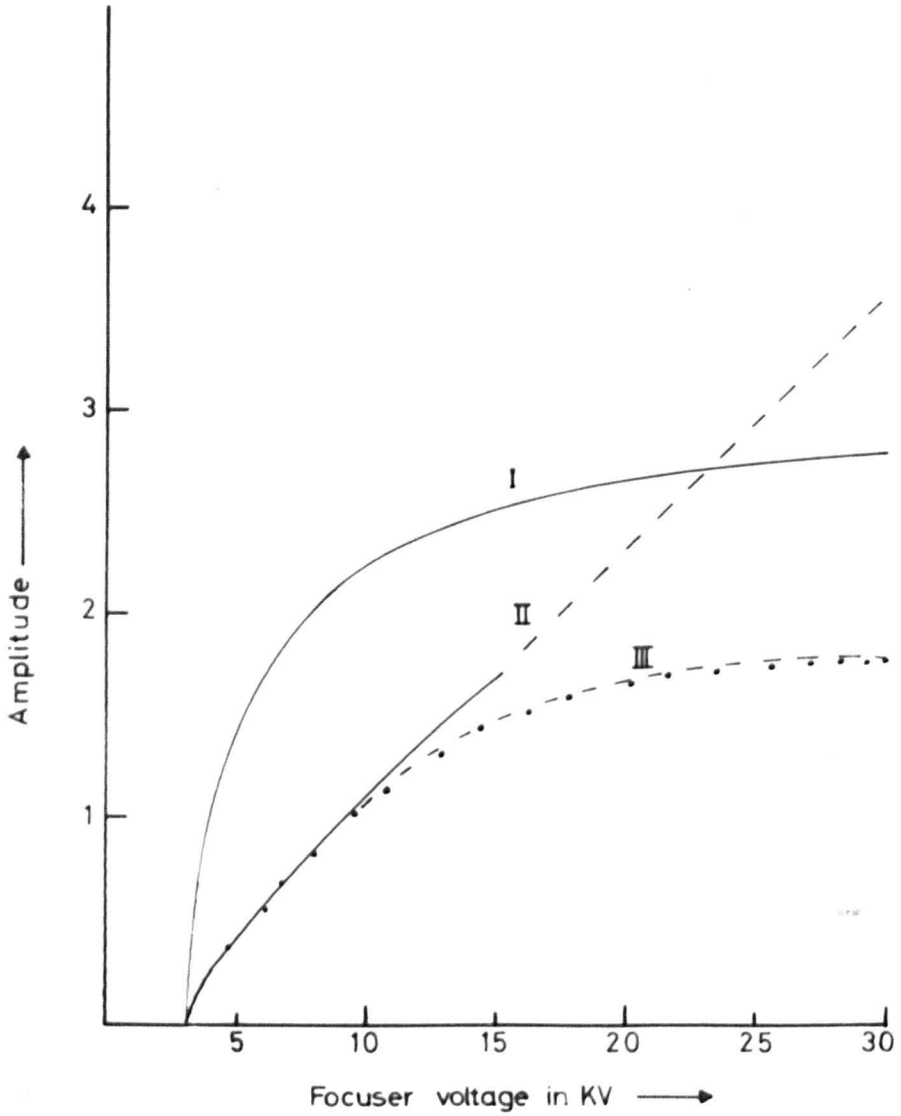

Fig. 5.6.5. Observed and theoretical maser oscillation characteristics for comparison. I - Univelocity theory of SWT. II - Velocity distribution theory of Shimoda. III - circles: observed values of Shimoda.

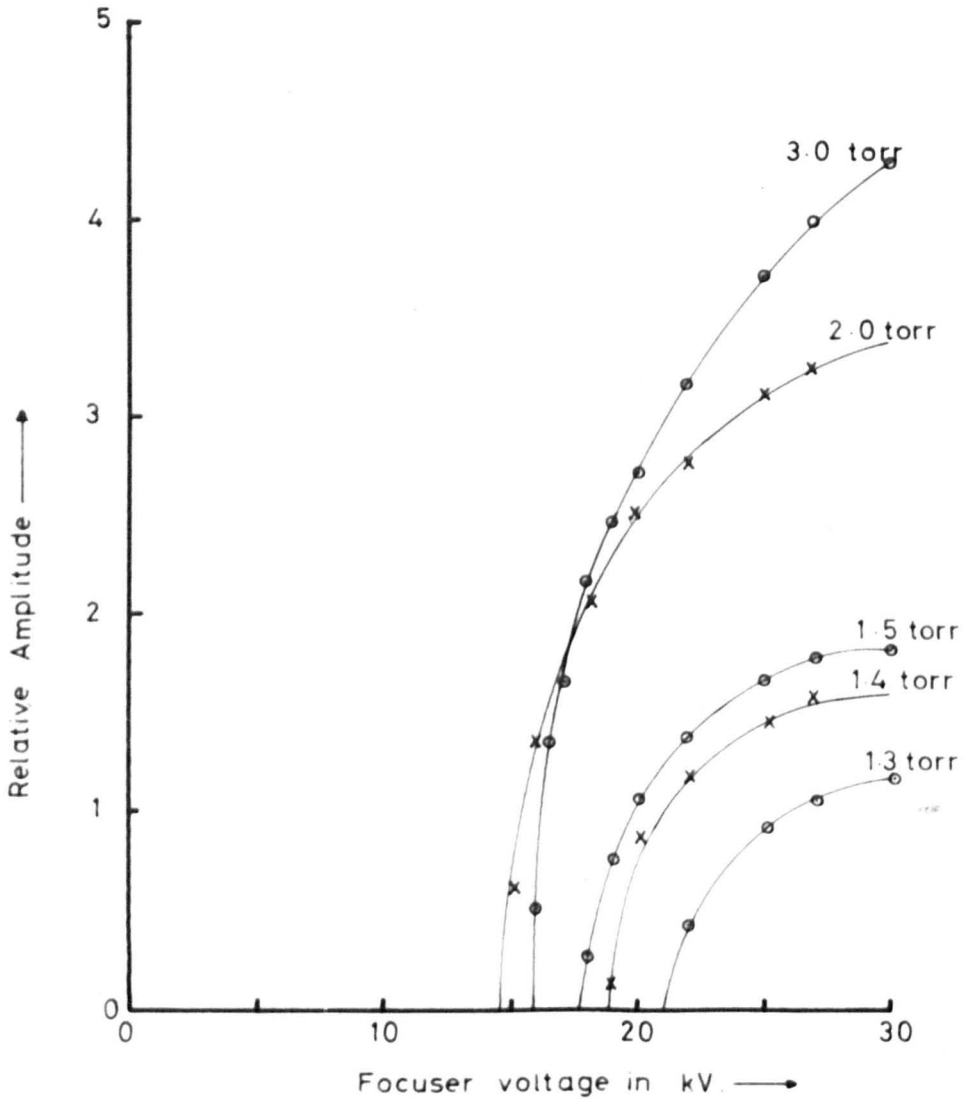

Fig. 5.6.6 Variation of maser oscillation amplitude with focuser potential at various nozzle pressures.

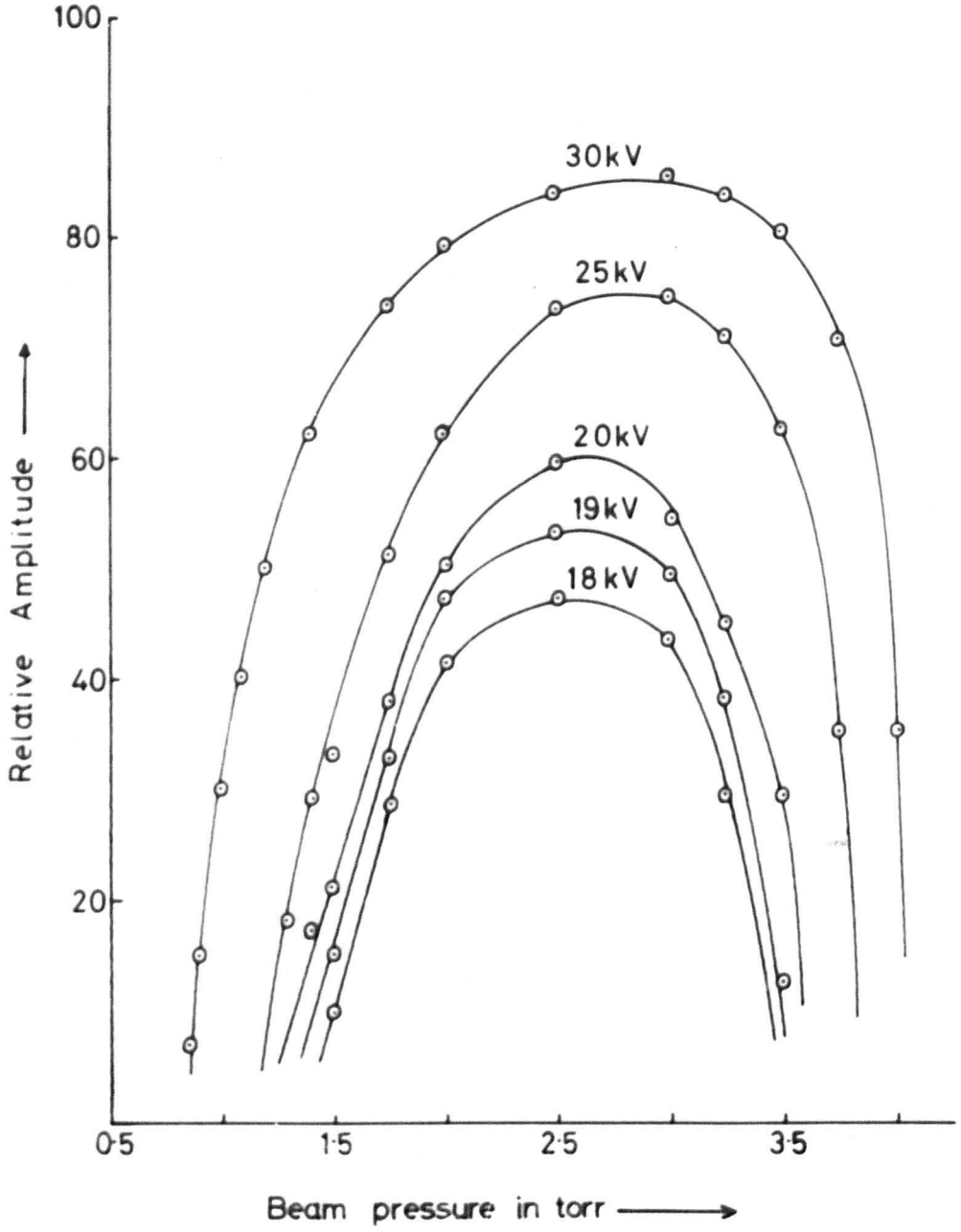

Fig 5.6.7 Maser oscillation amplitude at various beam pressures.

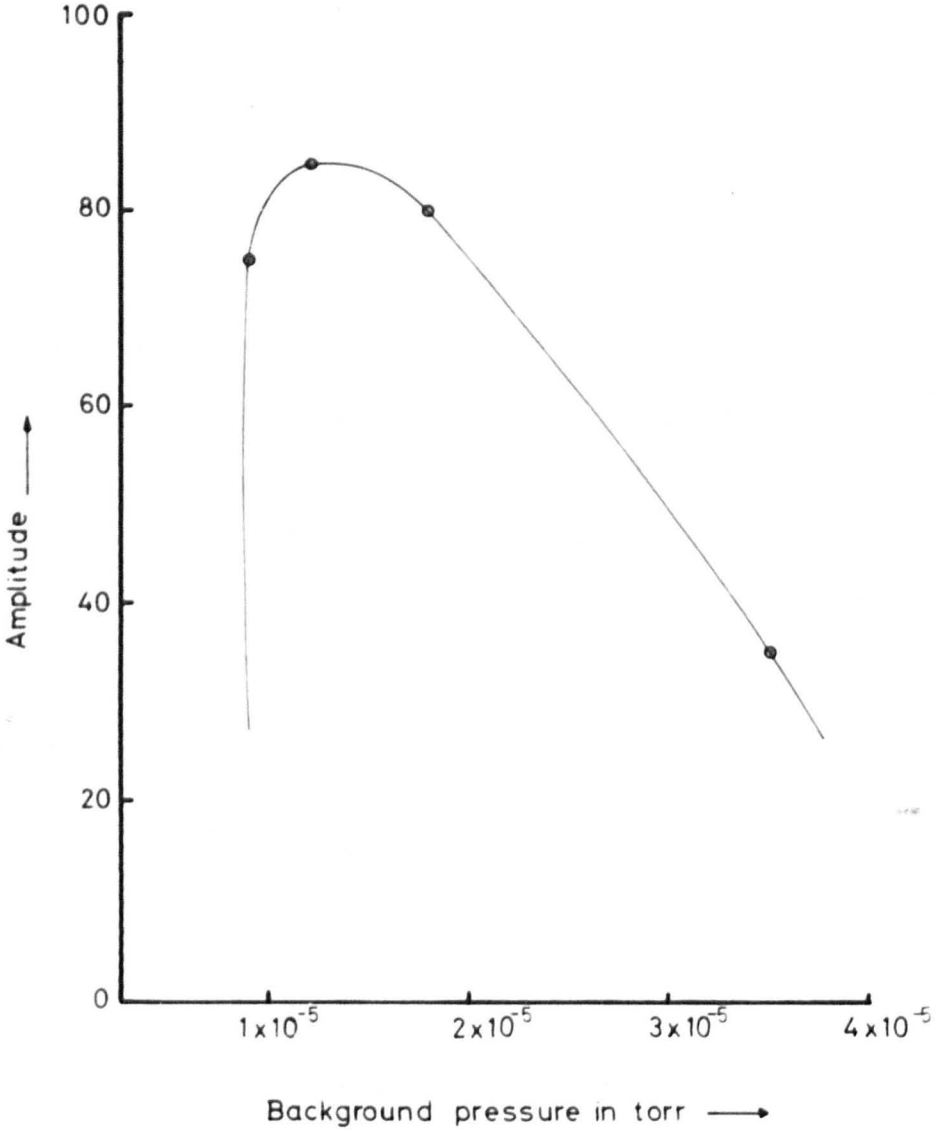

Fig 5.6.8 Amplitude vs background pressure at a focuser voltage of 30kV as nozzle pressure is changed.

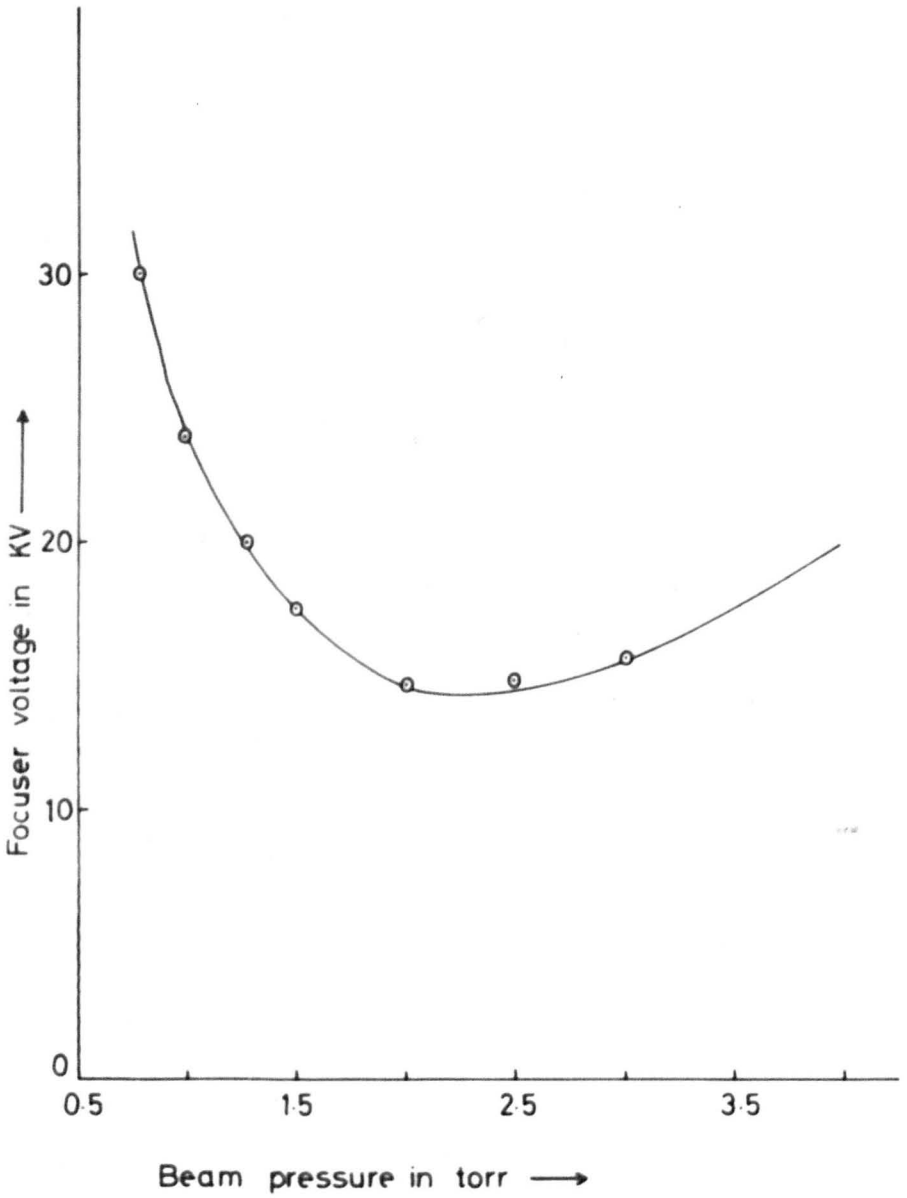

Fig 5. 6. 9. Threshold characteristics of maser oscillation

the focuser voltage and there the quantity n/n_{th} defined in Section 5.4a is directly proportional to the focuser voltage. Fig. 5.6.4. which is a plot of amplitude versus focuser voltage at a beam pressure of 1.5 torr, thus represents the θ - n/n_{th} characteristic. It can be seen that this curve is similar to the predicted form of the characteristic $n/n_{th} = \theta^2/\sin^2\theta$ of SWT[80] derived on the basis of a univelocity theory, but do not reach saturation in the predicted way. Shimoda[42] took account of the velocity distribution and predicted a characteristic which does not show saturation. Present results as well as Shimoda's[43] results however corroborate this theory only at low amplitudes as can be seen from a comparison with Fig. 5.6.5. Fig. 5.6.6. shows the variation of oscillation amplitude with focuser voltage at different beam pressures. It is evident that the peaks of the curves move towards higher pressures at higher focuser voltages. It would appear from this that the nozzle and focuser combination works more efficiently at higher potentials. Fig. 5.6.7. represents the variation of amplitude with beam pressure, and Fig. 5.6.8. gives the amplitude at corresponding backgrouns pressure. It can be seen that the optimum beam pressure for this set up is about 2.75 torr. Fig. 5.6.9. shows the variation of the oscillation threshold with focuser voltage and beam pressure. This shows that the system operates best with a beam pressure between 1.75 to 3 torr.

CHAPTER VI

ALTERNATE GRADIENT FOCUSING OF A MOLECULAR BEAM.

6.1. Introduction :

Alternate Gradient (AG) focusing has been an established method of space focusing and guiding charged particles in Nuclear Physics over the last fifteen years. The principle was discovered concurrently by Courant et al (1952) and Christofilos in their attempt to find a method which would overcome the limitations of the particle accelerators then existing[155-160]. For example, the "synchrotron" in its most elementary form, employs a magnetic field throughout an annular shaped region in order to guide and to focus the particles as they gain energy within the vacuum chamber of this accelerator. The strength of the magnetic field is made to rise during the acceleration by application of a radio frequency pulse so as to maintain a constant radius in its equilibrium-orbit for particles of increasing energy. These orbits are phase stable and results in a stable oscillation of the energy about its value appropriate to the frequency of the system[158]. The radial variation of the magnetic field normal to the median plane, at points in the neighbourhood of a circular equilibrium orbit of radius R is characterized by the "field index" n defined by the relation

$$n = -\frac{R}{B}\frac{dB}{dR} \qquad (6.1.1)$$

where B is the magnetic induction. The frequencies of small-amplitude

radial and axial oscillations about the equilibrium orbit are given by

$$Q_r = f_r/f_o = (1 - n)^{\frac{1}{2}}$$

$$Q_v = f_v/f_o = (n)^{\frac{1}{2}} \qquad (6.1.2)$$

respectively. Here f_o is the orbital frequency. The requirement for stability in both transverse planes is therefore that

$$0 < n < 1 \qquad (6.1.3)$$

that is, the free transverse oscillation frequency is a small fraction of the orbital frequency. It follows from the above equations that the maximum energy to which particles can be accelerated is limited by the condition given in Eq. 6.1.3. This limitation of the constant gradient type of focusing can be removed if the field index is caused to vary with azimuthal position in a suitable manner so as to alternate between large positive and negative values. This is the basis of the AG focusing of charged particles. In the AG system the particle passes alternately through strong focusing and defocusing lenses and is deflected alternately inward and outward. On the average, the particle is displaced further from its orbit in the focusing lenses than in the defocusing lenses. This is obviously so, since before reaching a focusing lens, the particle is thrown outward by the preceding defocusing lens. Since the field acting as the lens has a gradient, that is the field is proportional to the displacement and the focusing (or defocusing) force is proportional to the fields, therefore, the focusing (or defocusing) force is also proportional

to the displacement. Consequently, the overall effect of having the particle generally further displaced in focusing sections is to produce a net focusing force on the particles. The net restoring force on the particle, though not nearly so strong as the individual focusing or defocusing force, can still be made much stronger than can be attained in the constant gradient system. The optical and neutral particle analgues of the AG system are discussed in the following sections.

6.2. Optical Analogue :

The AG focusing has analogies in various other fields of science and engineering which are well understood. The most poignant analogy is in the field of lens optics. Any text book on elementary optics will show that if two thin lenses, one convex and one concave, with focal lengths f_1 and f_2 which are positive and negative respectively, are separated by a distance d, then the overall focal length F is given by

$$\frac{1}{F} = \frac{1}{f_1} + \frac{1}{f_2} - \frac{d}{f_1 f_2} \qquad (6.2.1)$$

If for simplicity the focal lengths are assumed to be such that $f_1 = -f_2 = f$, then $F = |f|^2/d$, which is positive and independent of the order of the lenses. The conclusion remains valid for any finite separation d if the two lenses are equal in magnitude of their focal lengths. Obviously the argument can be extended to an infinite sequence of lenses periodically positive and negative. It is evident that the trajectory will on the whole be at a greater distance from the optics axis in the regions occupied by positive lenses, and hence may experience

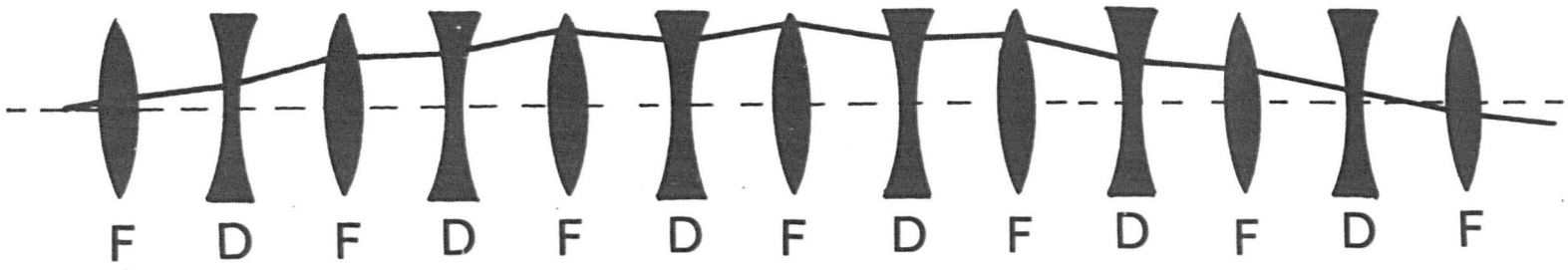

Fig. 6.2.1. OPTICAL ANALOGUE OF ALTERNATE-GRADIENT FOCUSING, SHOWING A RAY TRAVERSING A PERIODIC SEQUENCE OF FOCUSING (F) AND DEFOCUSING (D) LENSES. (104).

a net focusing effect under the action of the sequence of lenses. The sequence will be continuously converging if spacings between lenses are so arranged that an off-axis ray never crosses the optic axis. This restricts the spacings to the range $-2F < s < 2F$. Fig. 6.2.1. shows the optical analogue of alternate-gradient focusing showing a ray transversing a periodic sequence of converging and diverging lenses.

6.3 Neutral Particle Analogue :

The criteria for focusing neutral particles were established in Section 4.2 of Chapter IV. It was shown that if F is the applied force on the particles, then static focusing requires that $\nabla.F$ be negative. This condition is met in the schemes used for separation and focusing of ammonia molecules in an upper energy rotation-inversion quantum state. However, certain field configurations may generate a force field acting on a molecule such that $\nabla.F = 0$. In this, the force field is analogous to the force field in the AG focusing system for ions. The basic element of such a system is a magnetic or electric quadrupole. The transverse motion of the ion in such a system can be separated in two principal perpendicular planes. In one plane, e.g. the x-plane, the effect of the applied field is a linear restoring force that tends to deflect the ion towards the axis. In the y-plane the effect is reversed. Thus, $k_x = -\partial F_x/\partial_x$ is positive and $k_y = -\partial F_y/\partial_y$ is negative. But since $\nabla.F = 0$ for ions, $k_x + k_y = 0$. By alternating the planes of successive lens elements, it is therefore possible to produce a net convergent AG focusing system. An analogous field is generated for molecules by a two-wire configuration used by Rabi[161] et al for measuring the magnetic

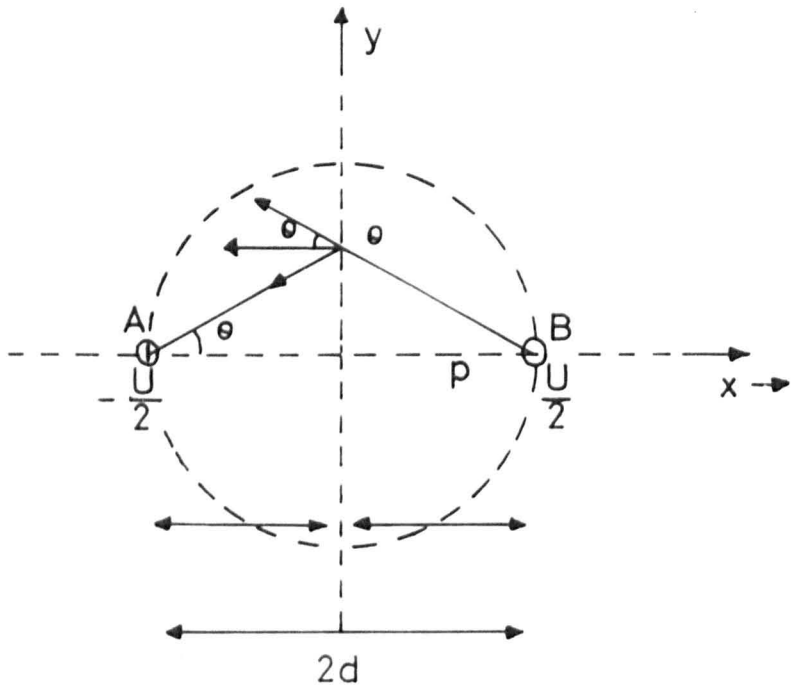

Fig. 6. 4. 1. Schematic diagram of a dipole.

moment of the proton. A two-charge configuration also generates a similar field at the midpoint between the two equal and opposite charges. Thus, the two-wire or two-charge fields can be looked upon as the neutral-beam analogues of the electric or magnetic quadrupole used for charged beams. The feasibility of AG focusing of molecular beams with the dipole two-wire field has been discussed theoretically by Auerbach, Bromberg and Wharton[162]. The theory of an AG system for molecular beams with a two charge dipolar field is developed below in the following section.

6.4. AG Focusing of a Molecular Beam with Dipolar Multiplets :

In this section the possibility of focusing a molecular beam using an array of electric dipoles arranged in an AG scheme is shown mathematically and conclusions are drawn with particular reference to a beam of ammonia molecules. A typical dipole with the coordinate system assumed is shown in Fig. 6.4.1. The z-axis is perpendicular to the plane of paper and coincides with the beam axis. The two electrodes are assumed to be at potentials - U/2 and + U/2 and constitute the dipole AB. It is assumed that the beam is confined to the region within the array where $|x| < d$, $|y| < d$. Assuming for the time being that the z-variation over the small element dz is negligible, the electric fields and their gradients at points shown on the xz plane and yz plane are calculated as followes :

$$(E_x)_P = \frac{U}{d} \left| \xi + \xi^3 + \xi^5 + ... \right|$$

$$\left(\frac{\delta E}{\delta x}\right)_P = \frac{U}{d^2} \left| 1 + 3\xi^2 + 5\xi^4 + ... \right|$$

$$(E_x)_Q = \frac{U}{d}\left|1 - \eta^2 + \eta^4 - \ldots\right|$$

$$\left(\frac{\delta E}{\delta y}\right)_Q = \frac{U}{d^2}\left|-2\eta + 4\eta^3 - 6\eta^5 + \ldots\right|$$

$$\left(E\frac{\delta E}{\delta x}\right)_P = \frac{U^2}{d^3}\left|\xi + 3\xi^3\right| \qquad (6.4.1a)$$

$$\left(E\frac{\delta E}{\delta y}\right)_Q = -\frac{2U^2}{d^3}\left|\eta - 3\eta^3\right| \qquad (6.4.1b)$$

where $\xi = x/d < |1|$ and $\eta = y/d < |1|$ are the reduced coordinates and the higher order terms are neglected. For ammonia molecules the Stark energy equations are

$$W = W_o \pm \left[\frac{\delta o}{2} + \frac{\mu^2 E^2}{\delta_o}\right] \qquad (6.4.2)$$

where $\delta_o = \frac{h\nu_o}{2}$, $A = \frac{\mu_o MK}{J(J+1)}$

In Eq. 6.4.2. the upper sign refers to the upper inversion state molecules and the lower sign refers to the lower inversion state molecules. This convention of signs will be followed throughout. From Eq. 6.4.2. the focusing force is given by

$$f_r = -\frac{\delta W}{\delta r} = \mp \frac{2\mu^2}{\delta_o} E_r \frac{\delta E}{\delta r} \qquad (6.4.3)$$

The motion of a molecule in the two principal planes is considered below.

Motion of upper state molecules :

The equation of motion of the upper state molecules in the xz plane is given by

$$m \frac{d^2x}{dt^2} = - \frac{2\mu^2}{\delta_o} E \frac{\delta E}{\delta x} \qquad (6.4.4)$$

where m is the mass of the molecule.

Since $\xi = x/d$, Eq. 6.4.4 becomes

$$\frac{d^2\xi}{dt^2} = - \frac{2\mu^2}{mdh\nu_o} \left| \frac{U^2}{d^3} \right| \left| \xi + 3\xi^3 \right| \qquad (6.4.5)$$

Defining the following parameters

$$\alpha = \frac{2\mu^2U^2}{h\nu_o md^4} = P \left| \frac{U^2}{d^4} \right| \qquad (6.4.6)$$

$$\beta = 3\alpha, \qquad P = 2\mu^2/h\nu_o m$$

the equation of motion becomes

$$\frac{d^2\xi}{dt^2} = - \alpha\xi - \beta\xi^3 \quad \text{(focusing plane)} \qquad (6.4.7)$$

For the Y - motion of the upper state molecules similarly

$$\frac{d^2\eta}{dt^2} = \gamma\eta - \delta\eta^3 \quad \text{(defocusing plane)} \qquad (6.4.8)$$

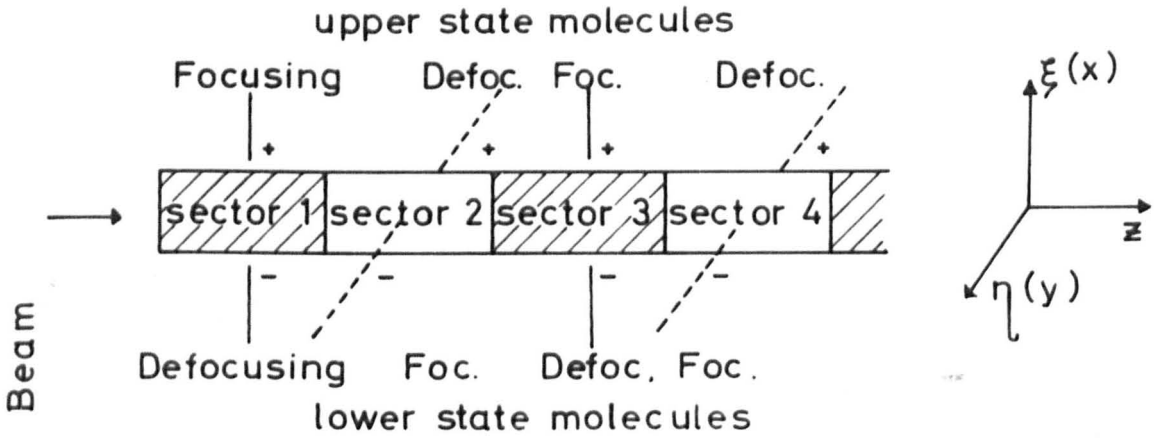

Fig 6·4·2 Schematic of dipolar array.

where $$\gamma = \frac{4\mu^2 U^2}{h\nu_o m d^4} = 2P\left|\frac{U^2}{d^4}\right| = 2\alpha \qquad (6.4.9)$$

$$\delta = 3\gamma = 6\alpha$$

In the array of dipoles, the axis of the first dipole will be taken as the x - axis and this coordinate system will be followed throughout this analysis. The system is represented diagrammatically by Fig. 6.4.2.

By analogy, the corresponding equations of motion for the lower state molecules can be written down as

$$\frac{d^2\xi}{dt^2} = \alpha\xi + \beta\xi^3 \quad \text{(defocusing plane)} \qquad (6.4.10)$$

$$\frac{d^2\eta}{dt^2} = -\gamma\eta + \delta\eta^3 \quad \text{(focusing plane)} \qquad (6.4.11)$$

The equations of motion as they appear above cannot be solved in a simple way to give a periodic and stable solution. The complicating factor here is the cubic term in the equations of motion. This term represents a small perturbation. To realize the extent of this perturbation, one of the equations is examined in detail here. For this purpose, Eq. 6.4.7. is rewritten as

$$\ddot{\xi} + \alpha\xi + \beta\xi^3 = 0 \qquad (6.4.12)$$

This equation can be solved in a straight forward manner by using elliptic integrals[163], with the conditions $\alpha, \beta > 0$ and $(\xi)_o = 0$ where $(\xi)_o$ is the ξ- velocity of the molecule at time $t = 0$. The solution thus obtained is

$$\xi = \xi_o \ \text{cnu} = \xi_o \ \text{cn}\left|\, t(\alpha + \beta\xi_o^2)^{\frac{1}{2}} \,\right| \qquad (6.4.13)$$

where $\xi_o = x_o/d$, and x_o is the initial displacement at t = 0. Here cnu is the cosine type of Jacobi's elliptic function[164]. The solution given above is both periodic and stable. Eq. 6.4.13 can be rewritten as

$$\xi = \xi_o \cos\phi = \xi_o \, \mathrm{cn}\, u \tag{6.4.14}$$

defining

$$u = t\,(\alpha + \beta\xi_o^2)^{\frac{1}{2}} = F(\lambda, \phi) \tag{6.4.15}$$

$$t = \frac{1}{(\alpha + \beta\xi_o^2)^{\frac{1}{2}}} F(\lambda, \phi) \tag{6.4.16}$$

$$\tau = \frac{4}{(\alpha + \beta\xi_o^2)^{\frac{1}{2}}} F(\lambda, \pi/2) \tag{6.4.17}$$

$$\lambda^2 = \frac{\beta\xi_o^2}{2(\alpha + \beta\xi_o^2)} \tag{6.4.18}$$

$$\theta = \sin^{-1}\lambda \tag{6.4.19}$$

$$F(\lambda, \phi) = \int_o^{\phi} \frac{d\psi}{(1-\lambda^2\sin^2\psi)^{\frac{1}{2}}} \tag{6.4.20}$$

Here $F(\lambda, \phi)$ is an incomplete elliptic integral of the first kind with modulus λ, and τ is the time period of the motion. Numerical values of the function $F(\lambda, \phi)$ or $F(\theta, \phi)$ can be obtained from standard tables.[164] Since $\alpha, \beta > 0$, therefore $|\lambda| < 1$ for real ξ_o, and the solution is always periodic and stable. It follows that if a molecule enters the

region where it is acted upon by the force $f(\xi) = m \frac{d^2\xi}{dt^2}$ at the intitial position $\xi = \pm \xi_o$, it will execute a periodic motion about the centre $\xi = 0$. The periodic nature follows from the relation $\xi = \xi_o \cos \phi$. The period of the motion is given by τ (Eq. 6.4.17) which, it will be noticed, decreases with increase in α, β, ξ_o individually or collectively.

However, under the same initial conditions, all the equations of motion, namely Eq. 6.4.7-8 and Eq. 6.4.10-11 cannot be solved to give stable and periodic motion. In what follows, it will be shown that the cubic term in the equations of motion represents a small perturbation which can be neglected and the equations solved in a simple way to reveal the general nature of the process to the order of our approximation.

For illustration the case of J = K = 3 state of ammonia is considered here. Inserting the numerical values of the various constants, $(\mu^2/h\nu_o m) = 2.113 \times 10^2$ and the average of $\langle M^2 \rangle = 7$, from Eq. 6.4.6.

$$\alpha = 4.23 \times 10^2 \, (U^2/d^4) \qquad (6.4.21)$$

where U is in cgs units and d is in cm. With an excitation potential U = 30 KV and 2d = 2 mm, $\alpha = 4.23 \times 10^{10}$ in cgs units at the mid-point of the dipole. To take account of the shape of the field, over a small region along the z - axis the average value of $\bar{\alpha}$ is taken to be $\bar{\alpha} = a^2\alpha$ where a is an averaging factor of the field and is taken to be 1/2 for calculation. Thus $\bar{\alpha} = 1.06 \times 10^{10}$. The average value of β is given by $\bar{\beta} = 3\,\bar{\alpha}$. For the present purpose, this approximation is justified. It is assumed now that over any focusing or defocusing sector the effective values of α, β. are given by $\bar{\alpha}$, $\bar{\beta}$. For paraxial molecules,

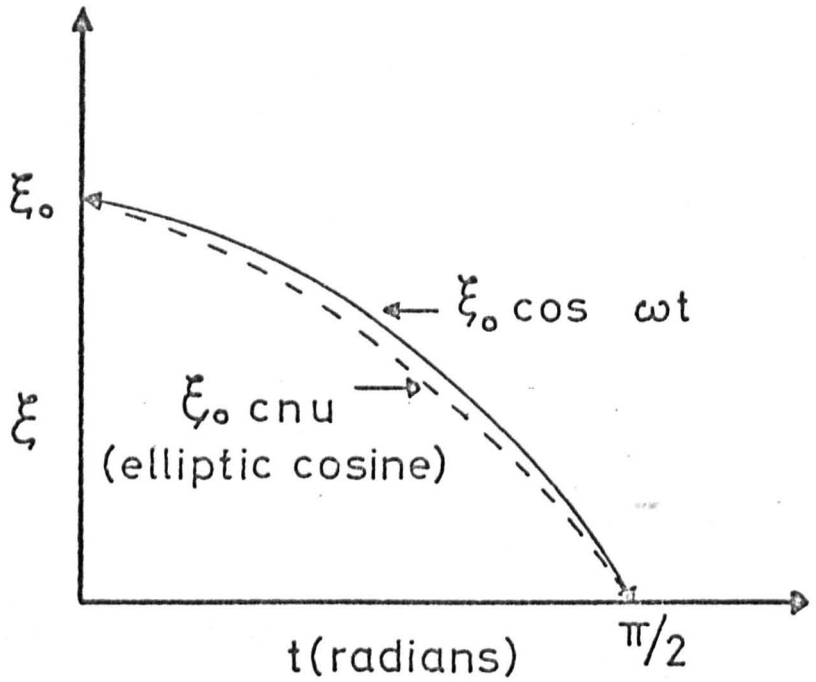

Fig 6.4.3

Effect of a small perturbation on simple harmonic motion (see text)

assuming $|\xi_o| = 0.1$, that is $|x| = 0.01$ cm, from Eq. 6.4.18

$$\lambda = 0.1207, \quad \theta = \sin^{-1}\lambda \simeq 7^{\circ}$$

and from standard tables $F(7^{\circ}, \frac{\pi}{2}) \simeq 1.5767$.

Using Eq. 6.4.17, the period and frequency of motion are then obtained as

$$\tau = 6.04 \times 10^{-5} \text{ sec.}, \quad \omega_o = 1.04 \times 10^{5} \text{ sec}^{-1}$$

If the equation of motion is written as $\ddot{\xi} + \alpha\xi = 0$, the frequency given by $\omega = (\alpha)^{\frac{1}{2}} = 1.03 \times 10^{5}$ sec^{-1} which is not very different from the value of ω_o calculated above. To calculate ωt for any chosen value of ϕ, value of ω_o as obtained above and $F(7^{\circ}, \phi)$ obtained from tables for various values of ϕ chosen are used with Eq. 6.4.16. The results of such calculations are shown in Fig. 6.4.3. By plotting $\xi = 0.1 \cos\phi$ against t, the first quarter period of the Jacobian Elliptic function $\text{cn } u = \cos\phi$ i.e. the elliptic cosine is obtained as shown in Fig. 6.4.3. For comparison the ordinary or circular cosine of equal period and amplitude ($\xi = 0.1 \cos\omega t$) is plotted alongside. It is clear that the motion is simple harmonic to the order of approximation used not withstanding the factor $\beta\xi^3$, and the solution curve $\xi = \xi_o \cos\phi$ can be analysed into a Fourier series. A reasonable first approximation is therefore of the form

$$\xi = A \cos\omega t + B \cos 3\omega t \qquad (6.4.22)$$

i.e. the factor $\beta\xi^3$ gives rise to a third harmonic component. However the amplitude of this harmonic can be shown to be only a small fraction of the fundamental. To the order of approximation used here, $\beta\xi^3$ and similar terms will therefore be neglected in any further analysis.

Assuming what has been found above to be sufficient justification for neglecting the cubic term in all the equations of motion, the equations of motion can be written in the form

$$\text{Upper state} : \ddot{\xi} + \alpha\xi = 0 \quad (6.4.23) \qquad \ddot{\eta} - \gamma\eta = 0 \quad (6.4.24)$$

$$\text{Lower state} : \ddot{\xi} - \alpha\xi = 0 \quad (6.4.25) \qquad \ddot{\eta} + \gamma\eta = 0 \quad (6.4.26)$$

The above equations refer to the sectors in which the x - axis is also the dipole axis. The method adopted in the following for calculating molecular trajectories is analogous to the method given by Teng[165] for alternate gradient electrostatic focusing of charged particles in linear accelerators.

(a) Solutions for upper state molecules in the ξ-plane of sector 1 are given by solving Eq. 6.4.23, that is by

$$\xi = \xi_o \cos \omega t + \dot{\xi}_o \omega^{-1} \sin \omega t$$

$$\dot{\xi} = -\xi_o \omega \sin \omega t + \dot{\xi}_o \cos \omega t \qquad (6.4.27)$$

where $\omega = \alpha^{\frac{1}{2}}$. At $z = z_1$, $t = t_1$, the position and velocity are given by

$$\xi' = \xi_o \cos k_1 z_1 + \frac{\dot{\xi}_o}{k_1 v} \sin k_1 z_1$$

$$\dot{\xi}' = -\xi_o k_1 v \sin k_1 z_1 + \dot{\xi}_o \cos k_1 z_1 \qquad (6.4.28)$$

where v is the velocity of the molecules through the array and therefore

$$vt_1 = z_1, \quad \omega t_1 = \omega z_1/v = k_1 z_1, \quad \alpha^{\frac{1}{2}} = \omega = k_1 v \qquad (6.4.29)$$

Eq. 6.4.28 can now be rewritten as

$$\xi' = \xi_o \cos k_1 z_1 + \left(\frac{\dot{\xi}_o}{v}\right) \frac{1}{k_1} \sin k_1 z_1 \qquad (6.4.30)$$

$$\left(\frac{\dot{\xi}}{v}\right)' = -\xi_o k_1 \sin k_1 z_1 + \left(\frac{\dot{\xi}_o}{v}\right) \cos k_1 z_1$$

(b) In sector 2, the equation of motion in the ξ - plane becomes

$$\ddot{\xi} - \gamma\xi = 0 \tag{6.4.31}$$

with solutions of the form

$$\xi = C \cosh \nu t + D \sinh \nu t \tag{6.4.32}$$

where $\nu = \gamma^{\frac{1}{2}}$ and $\gamma = 2\alpha$. In above notations at time $t = t_2$

$$\begin{aligned} \xi'' &= \xi_o' \cosh k_2 z_2 + \left(\frac{\dot{\xi}_o'}{v}\right) \frac{1}{k_2} \sinh k_2 z_2 \\ \left(\frac{\dot{\xi}_o''}{v}\right) &= \xi_o' k_2 \sinh k_2 z_2 + \left(\frac{\dot{\xi}_o'}{v}\right) \cosh k_2 z_2 \end{aligned} \tag{6.4.33}$$

where $k_2 = \nu/v$. Eq. 6.4.30 represents focusing of upper state molecules in the ξ-plane in sector 1 and Eq. 6.4.33 represents defocusing in the same plane in sector 2 as defined. The corresponding equations for the lower state molecules are :

(c) Sector 1 : defocusing of lower state molecules

$$\ddot{\xi}_1 - \alpha\xi = 0$$

$$\begin{aligned} \xi' &= \xi_o \cosh k_1 z_1 + \left(\frac{\dot{\xi}_o}{v}\right) \frac{1}{k_1} \sinh k_1 z_1 \\ \left(\frac{\dot{\xi}'}{v}\right) &= \xi_o k_1 \sinh k_1 z_1 + \left(\frac{\dot{\xi}_o}{v}\right) \cosh k_1 z_1 \end{aligned} \tag{6.4.34}$$

(d) Sector 2 : focusing of lower state molecules

$$\ddot{\xi} + \gamma\xi = 0$$

$$\xi' = \xi_o' \cos k_2 z_2 + \left(\frac{\dot{\xi}_o'}{v}\right) \frac{1}{k_2} \sin k_2 z_2$$

$$\left(\frac{\dot{\xi}'}{v}\right) = - \xi_o' k_2 \sin k_2 z_2 + \left(\frac{\dot{\xi}_o'}{v}\right) \cos k_2 z_2 \qquad (6.4.35)$$

In order to understand the behaviour of a beam of molecules as it moves through an array of lenses alternatingly focusing and defocusing, let us break up the system into a sequence of triplet lenses consisting of the second half of one dipolar lens, the whole of the next lens and the first half of the following one. It will be assumed, for the sake of generality, that the lenses are alternately of length z_1 and z_2. For simplicity, the field gradients will be assumed to be the same, alternating in sign for molecules in a given quantum state.

The lower state molecules are considered first, In the η - plane, they are focused in the first sector, defocused in the second and then focused again in the third sector (Fig. 6.4.4). It follows from the form of equations 6.4.34-35 that the position and transverse velocity at the exit of an η - focusing element, η and $\dot{\eta}$, are given in terms of the position η_o and velocity $\dot{\eta}_o$ at the entrance by the matrix equation

$$\begin{vmatrix} \eta \\ \dot{\eta}/v \end{vmatrix} = \begin{vmatrix} \cos k_2 z & (1/k_2) \sin k_2 z \\ - k_2 \sin k_2 z & \cos k_2 z \end{vmatrix} \begin{vmatrix} \eta_o \\ \dot{\eta}_o/v \end{vmatrix} \qquad (6.4.36)$$

where z is the length of the element. For an η - defocusing element the equation would be

$$\begin{vmatrix} \eta \\ \dot{\eta}/v \end{vmatrix} = \begin{vmatrix} \cosh k_1 z & (1/k_1) \sinh k_1 z \\ k_1 \sinh k_1 z & \cosh k_1 z \end{vmatrix} \begin{vmatrix} \eta_o \\ \dot{\eta}_o/v \end{vmatrix} \qquad (6.4.37)$$

The transformation matrix which gives the final position and velocity of a molecule after it has transversed through a basic triplet is obtained simply by multiplying the three matrices representing the three lens elements. For lower state molecules in the η - plane, when the first element is focusing (Fig. 6.4.4.), the transformation matix is

$$|T_1| = \begin{vmatrix} \cos k_2 z_2/2 & \frac{1}{k_2} \sin \frac{k_2 z_2}{2} \\ -k_2 \sin k_2 z_2/2 & \cos \frac{k_2 z_2}{2} \end{vmatrix} \begin{vmatrix} \cosh k_1 z_1 & \frac{1}{k_1} \sinh k_1 z_1 \\ k_1 \sinh k_1 z_1 & \cosh k_1 z_1 \end{vmatrix}$$

$$\begin{vmatrix} \cos \frac{k_2 z_2}{2} & \frac{1}{k_2} \sin \frac{k_2 z_2}{2} \\ -k_2 \sin \frac{k_2 z_2}{2} & \cos \frac{k_2 z_2}{2} \end{vmatrix}$$

$$= \begin{vmatrix} M_1 & N_1 \\ G_1 & H_1 \end{vmatrix} \qquad (6.4.38)$$

where the final matrix elements M_1 etc. are

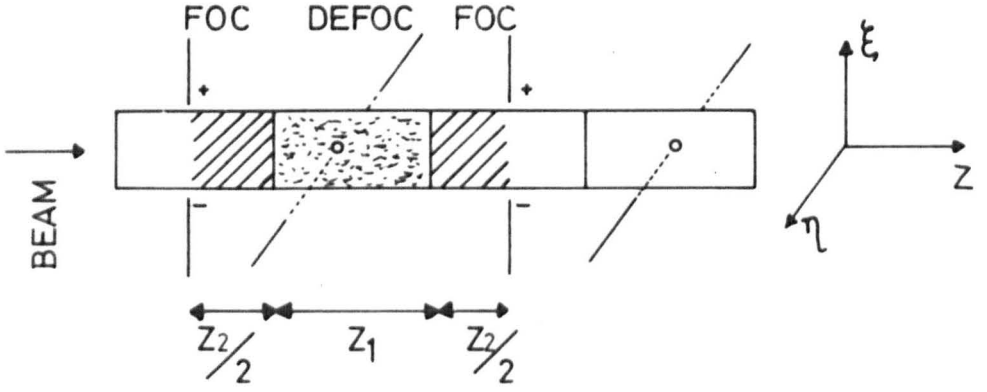

Fig 6.4.4 Lower state molecules in η-plane.

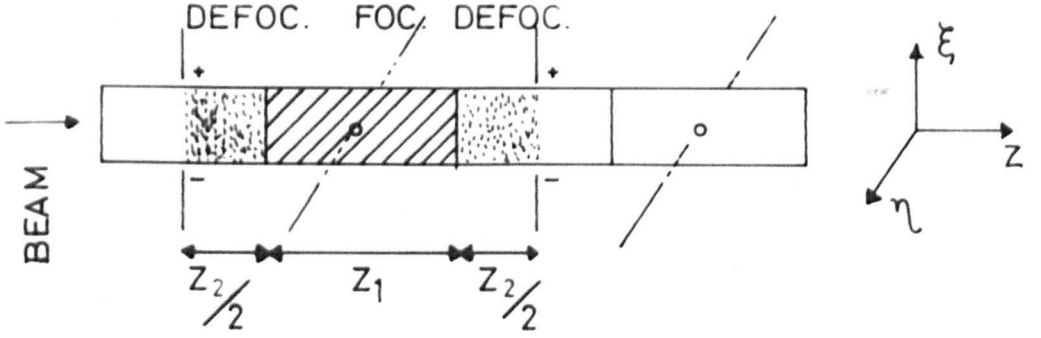

Fig 6.4.5 Upper state molecules in η-plane

$$M_1 = \cosh k_1 z_1 \cos k_2 z_2 + K \sinh k_1 z_1 \sin k_2 z_2$$

$$G_1 = - K_2 \cosh k_1 z_1 \sin k_2 z_2 + (k_1 + K k_2 \cos k_2 z_2) \sinh k_1 z_1$$

$$N_1 = \frac{1}{k_2} \cosh k_1 z_1 \sin k_2 z_2 + \left(\frac{k_1}{k_2} - \frac{k_2}{k_1} \cos k_2 z_2\right) \sinh k_1 z_1$$

$$H_1 = \cosh k_1 z_1 \cos k_2 z_2 + K \sinh k_1 z_1 \sin k_2 z_2$$

$$K = \tfrac{1}{2} \left(\frac{k_1}{k_2} - \frac{k_2}{k_1}\right) \qquad (6.4.39)$$

η and $\dot{\eta}$ are now obtained from

$$\begin{vmatrix} \eta \\ \dot{\eta}/v \end{vmatrix} = \begin{vmatrix} M_1 & N_1 \\ G_1 & H_1 \end{vmatrix} \begin{vmatrix} \eta_o \\ \dot{\eta}_o/v \end{vmatrix} \qquad (6.4.40)$$

or, $$\eta = \eta_o M_1 + (\dot{\eta}_o/v) N_1$$

$$\dot{\eta}/v = \eta_o G_1 + (\dot{\eta}_o/v) H_1 \qquad (6.4.41)$$

If it is assumed that the initial transverse velocity is zero, i.e. $\dot{\eta}_o = 0$, then $\eta = \eta_o M_1$. After traversing two triplets $\eta = \eta_o M_1^2$, after three triplets $\eta = \eta_o M_1^3$ etc.

The upper state molecules in η - plane in the same triplet as considered above suffers defocusing in the first element (Fig. 6.4.5). The corresponding transformation matrix T_2 can be calculated as before and the matrix element M is given by

$$M_2 = \cosh k_2 z_2 \cos k_1 z_1 - K \sinh k_2 z_2 \sin k_1 z_1 \qquad (6.4.42)$$

For the ξ - plane in the same triplet the M - elements for the lower and upper states are

$$M_3 = \cosh k_1 z_2 \cos k_2 z_1 + K \sinh k_1 z_2 \sin k_2 z_1 \qquad (6.4.43)$$

$$M_4 = \cosh k_2 z_1 \cos k_1 z_2 - K \sinh k_2 z_1 \sin k_1 z_2 \qquad (6.4.44)$$

respectively. If the elements are of identical length, then $z_1 = z_2 = z$, and therefore

$$M_1 \equiv M_3 = \cosh k_1 z \cos k_2 z + K \sinh k_1 z \sin k_2 z \qquad (6.4.45)$$

$$M_2 \equiv M_4 = \cosh k_2 z \cos k_1 z - K \sinh k_2 z \sin k_1 z \qquad (6.4.46)$$

M_1 and M_2 are the focusing matrix elements for lower state and upper state molecules respectively. They will be called the focusing factors.

It will be noted from Eqs. 6.4.45,46, that when all the lens elements are of the same length, irrespective of whether we start in a defocusing or a focusing plane we arrive at identical conditions for any particular species of molecules. The conditions for continuous focusing through the whole array are

$$\begin{aligned} -1 < M_1 < +1 \quad & \text{for lower state molecules} \\ -1 < M_2 < +1 \quad & \text{for upper state molecules} \end{aligned} \qquad (6.4.47)$$

When $|M_1| < 1$ and $|M_2| > 1$, the lower state molecules will be focused in preference to upper state ones. The reverse will happen when $|M_1| > 1$, $|M_2| < 1$. For focusing the whole beam the condition is

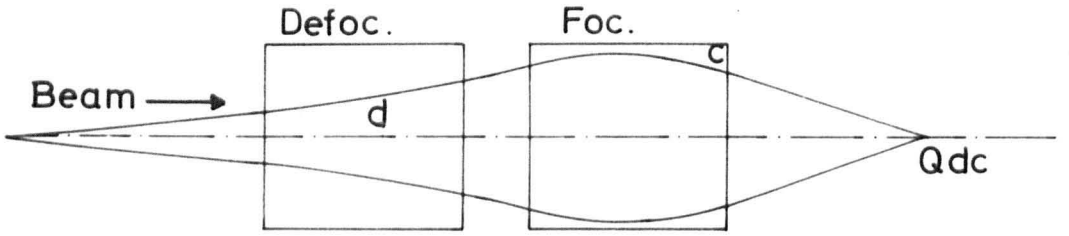

Fig 6.4.6 Beam envelope in the defocusing-focusing plane of a simple doublet scheme.

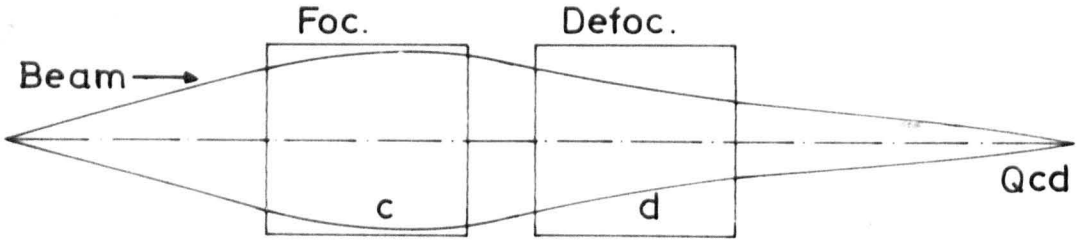

Fig 6.4.7 Beam envelope in the focusing-defocusing plane.

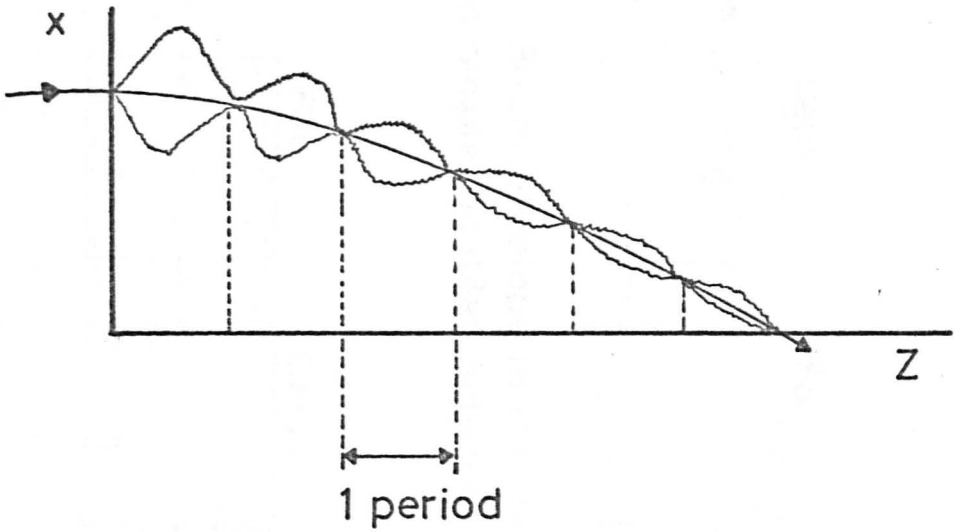

Fig 6.4.8 General nature of the trajectories through a succession of AG elements. The full curve-mean trajectory. Broken curves actual trajectories in the two transverse planes.

$M_1 = M_2 = M$ and $|M| < 1$. It is evident that by adjusting the various parameters a system can be designed which will preferentially focus any particular species of molecules while the others are completely defocused or only weakly focused.

It will also be noticed that by making $0 < M_i < 1$, a highly axial beam of the i species of molecules can be obtained. From the stability diagram for lower state molecules of NH_3 (Fig. 6.7.1) this region is seen to be $0 < k_1 z < 0.9$. At negative values of $k_1 z$ the molecules will oscillate about the z axis. A general indication of the beam envelope in the case of a simple combination of two AG elements only is given in Figs. 6.4.6,7, while Fig. 6.4.8 illustrates the general nature of the molecular trajectory in an AG multiplet.

6.5 Adiabatic Conditions :

A molecule moving in the inhomogeneous field of the dc operated AG system discussed above (or an ac variation of it) is acted on by a time varying field in the reference system of the particle. This variation must be sufficiently slow in order that the molecule does not make any non-adiabatic transition during the flight through the focuser and that the molecular state energy itself slowly varies according to the Stark field. According to the adiabatic theorem in quantum mechanics, for a system in which the Hamiltonian H(t) varies with time the wave function $\psi(t) = \Sigma_i\, a_i(t)\, \psi_i(t)$, where $\psi_i(t)$ is an eigenfunction of H(t), has the property that the expansion coefficients $a_i(t)$ do not change appreciably with time, provided that H(t) changes sufficiently slowly. The criterion for adiabaticity is[166]

$$\frac{\hbar\,(\partial H/\partial t)_{ij}}{(E_i - E_j)^2} \ll 1 \qquad (6.5.1)$$

which in the present case becomes

$$\frac{\Delta H}{\tau \hbar \omega^2} \ll 1 \qquad (6.5.2)$$

where ΔH is the change in the Hamiltonian of the interaction of the molecule with the field; τ is the transit time of the molecule in the part of the field considered. In order to satisfy the above criterion therefore care must be taken so that the field in the path of the beam does not fall catastrophically to zero. In the two charge model considered here the condition can be easily met. In a two wire field model or an ac model extra care may have to be taken to provide a residual field so that the field seen by the molecule never quite falls to zero.

6.6. Velocity Effects :

As in the case of multipole focusers (Chapter IV, Section 4.8) the maximum radial velocity V_r of the molecules trapped in the potential well of the focuser is given by

$$\frac{1}{2} m V_r < \Delta W \equiv \frac{1}{2} m V_c^2 \qquad (6.6.1)$$

where ΔW is the maximum Stark energy, and V_c is the critical radial velocity. It can be shown that $V_c \propto U$ where U is the excitation potential, and from Eq. 6.4.41 for example assuming the initial radial velocity is zero, $V_r \propto V_z$ where V_z is the axial velocity of the molecule.

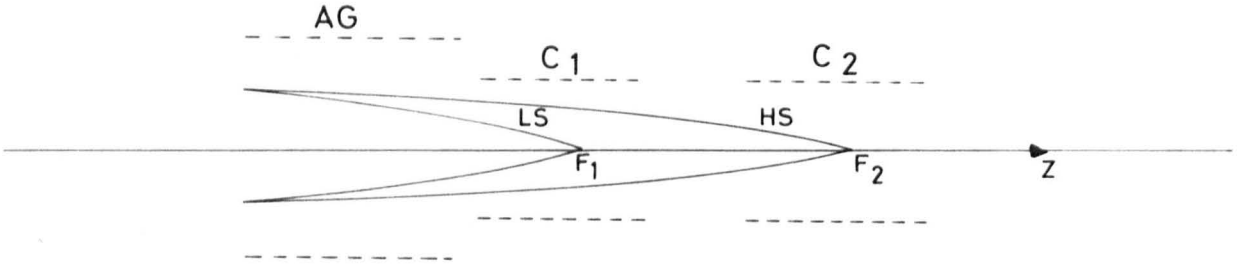

Fig 6·6·1 Expected Beam Envelope in the AG in the AG system.

The conclusion arrived at therefore for the molecules focused

$$V_z < AU \qquad (6.6.2)$$

where the constant A is a function of the various molecular and design parameters. This shows that as the excitation potential U rises, increasingly higher velocity molecules will be accepted. As will be shown in the following section (Eq. 6.7.3)

$$k_1 z = R\,(U/V_z) \qquad (6.6.3)$$

where R is a constant for the particular design parameters of the type considered and $K_1 z$ is defined by Eq. 6.4.29. Referring to Fig. 6.7.1. therefore, the conclusions derived are that (i) at constant potential U, in the lower velocity region conditions for higher state separation is better satisfied, (ii) in any particular velocity range, conditions for higher state separation improves with increased potential; the reverse conclusions will hold for the lower state molecules. In the simple system envisaged, separation with respect to velocity, that is to say, selection of molecules in a monokinetic state - is not expected to be large and therefore, while one species of molecules (e.g. ammonia molecules in the lower inversion state) is strongly focused, some molecules of the other species (in this example the higher state molecules) will also be focused, that is to say that defocusing of the latter type will not be complete. In effect the general nature of the beam envelope expected is as shown in Fig. 6.6.1. The expected variation of the focusing characteristic of the AG system with variation of the distance between the AG and the

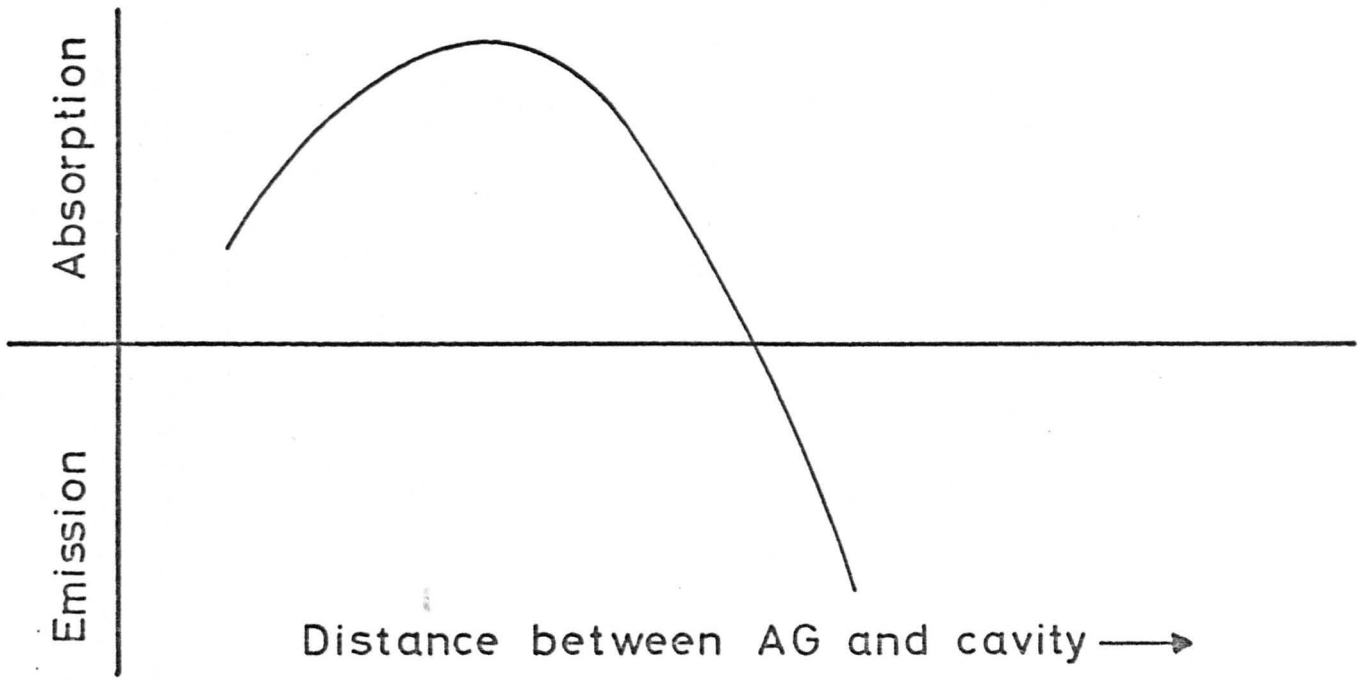

Fig 6.6.2 Diagrammatic representation of the expected effect of the variation of the separation of the AG and the resonant cavity.

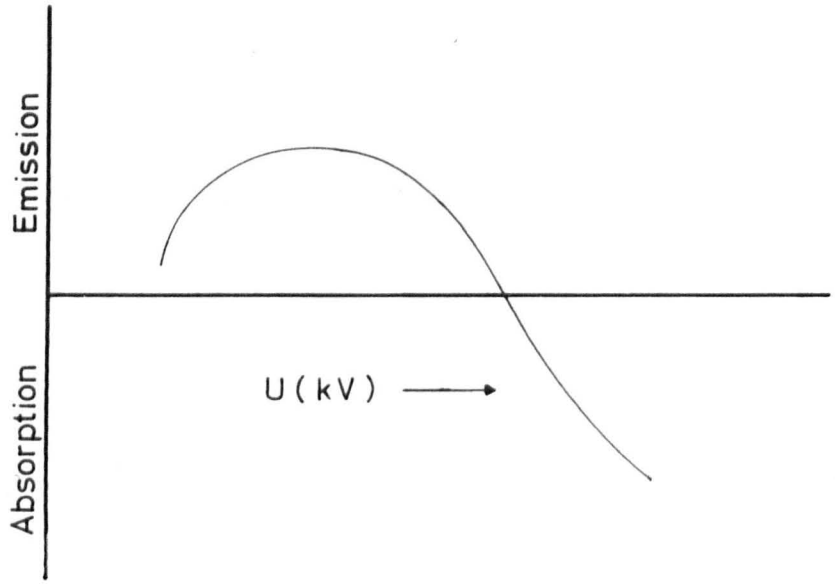

Fig 6·6·3 Diagrammatic representation of the excitation potential when cavity is in position C in fig 6·6·1

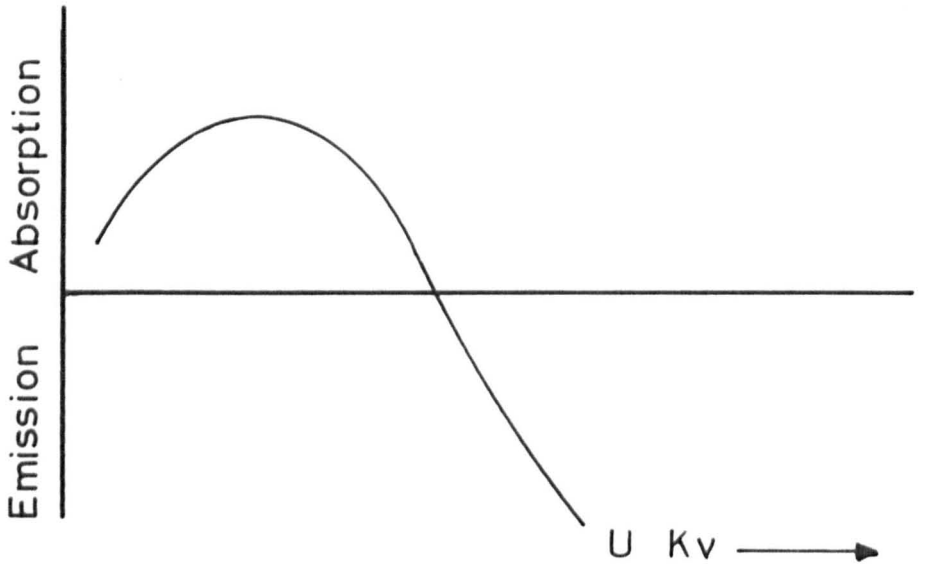

Fig 6·6·4 Expected effect of excitation voltage when cavity is in position C_1 in fig 6.6.1

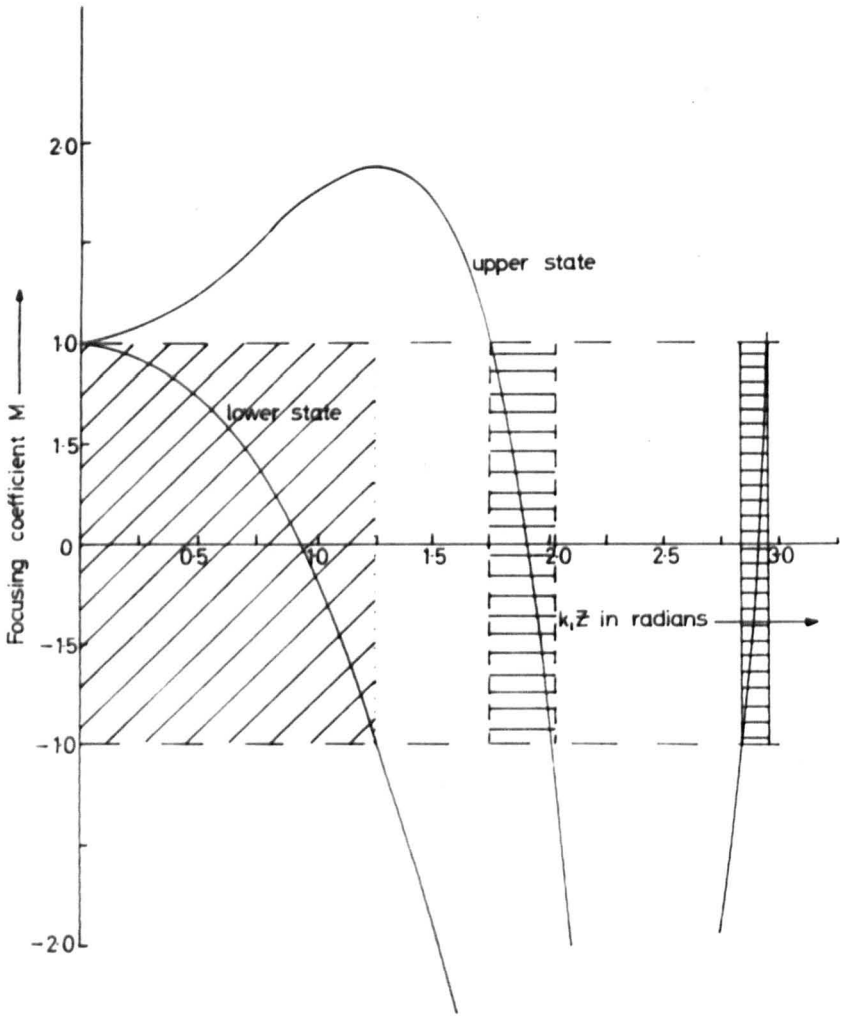

Fig. 6.7.1. Stability diagram of the ammonia J=K=3 inversion states. (121)

detecting cavity is illustrated diagrammatically in Fig. 6.6.2. Expected variation of the focusing characteristic of the AG system with change of excitation potential U, when the cavity is in position C_2 in Fig. 6.6.1. is similarly illustrated in Fig. 6.6.3. Fig. 6.6.4. shows diagrammatically the expected behaviour of the system when operated in the C_1 mode as defined in Fig. 6.6.1.

6.7 Design Considerations :

From definitions given in the preceding section (Eq. 6.4.29) $k_1/k_2 = (\alpha/v)^{\frac{1}{2}}$ which is a constant and is independent of any of the molecular parameters. K as defined in Eq. 6.4.39 is then given by $K = -0.353$. M_1 and M_2 can now be calculated from Eqs. 6.4.45, 46. The result is shown in Fig. 6.7.1. For the ammonia J = K = 3 inversion transition, α as defined by Eq. 6.4.6. is given by

$$\alpha = 4.23 \times 10^2 \, (U^2/d^4) \qquad (6.7.1)$$

where all units are in cgs. Here, 2d is the separation of the two point charges constituting the ideal dipole element. Writing U in kilovolts,

$$\alpha = 4.7 \times 10^3 \, (U^2/d^4) \qquad (6.7.2)$$

The average value of α is assumed to be $\bar{\alpha} = \alpha/4$ over the length z of one element which is the same as the distance between the successive dipoles in alternate planes. Since $k_1 = (\bar{\alpha})^{\frac{1}{2}}/v$ (Eq. 6.4.29) where v is the molecular velocity, the design parameters are given by the following relation within the order of approximation,

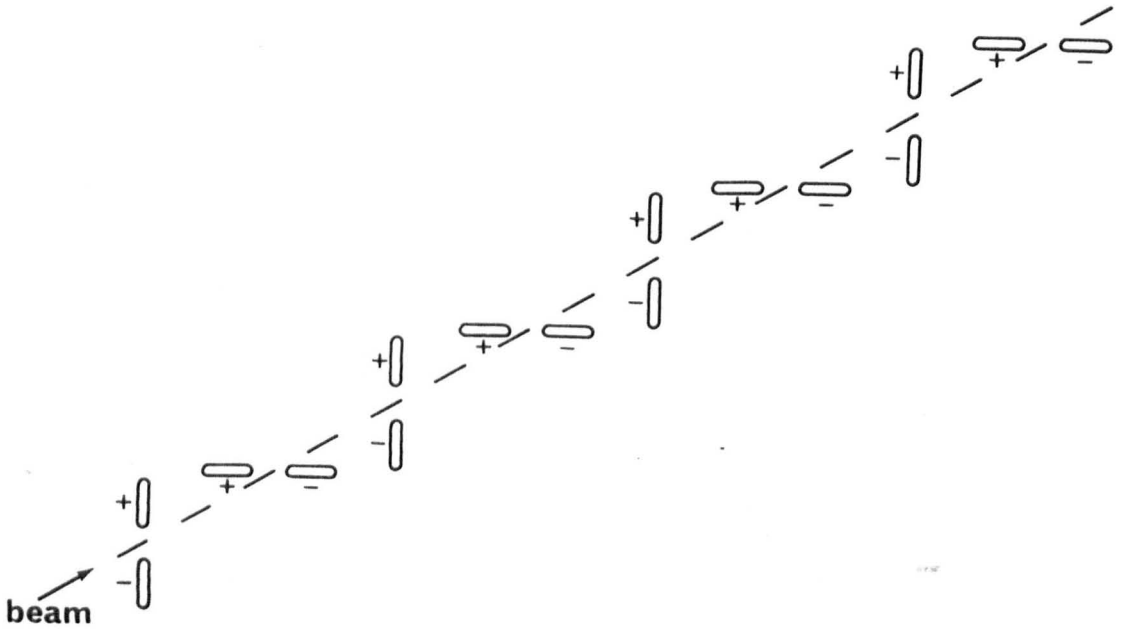

Fig.6.7.2 A Dipolar Array for Alternate Gradient Focusing of a Molecular Beam. (122)

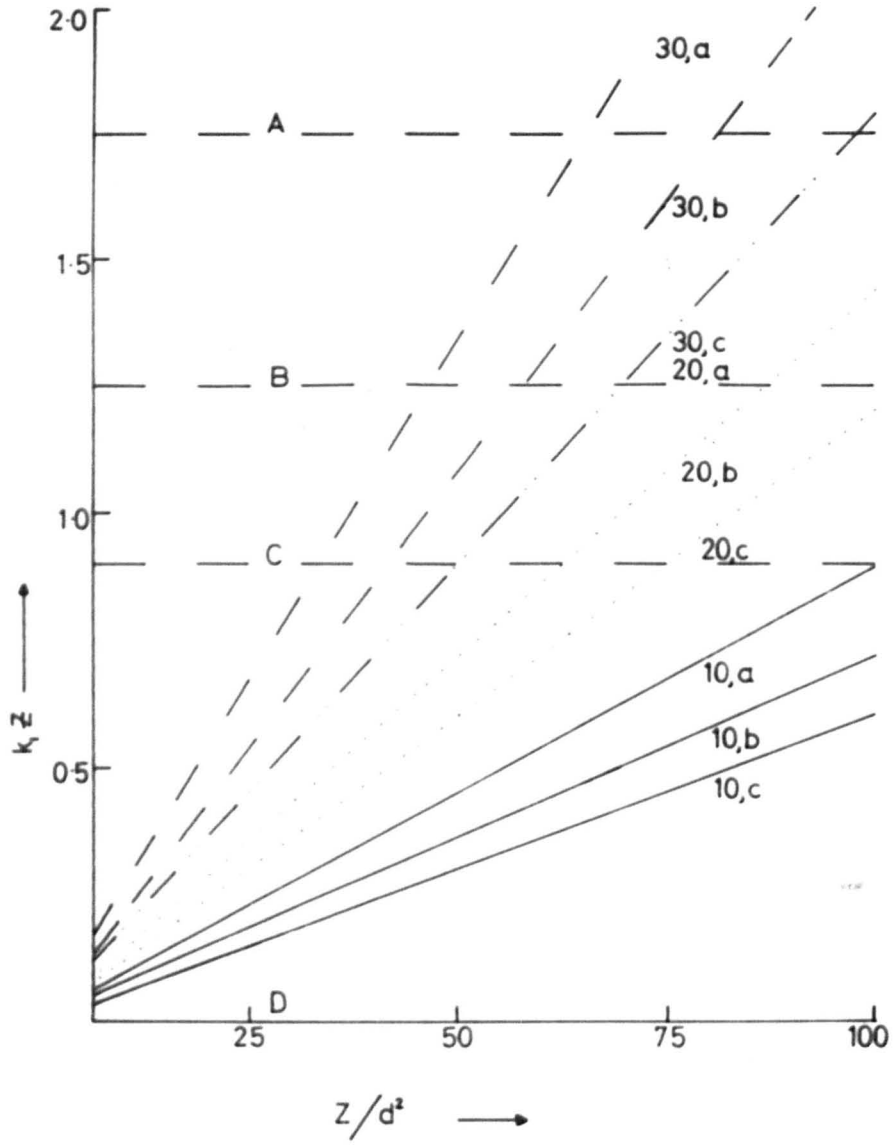

Fig. 6.7.3. Variation of k, Z with the ratio Z/d^2.
The numerical figures on the curves refer to the A G potential in kV; molecular velocities are given by the letters as $a = 4\times10^4$, $b = 5\times10^4$, $c = 6\times10^4$ cm sec.
A, B and C are defined in the text.

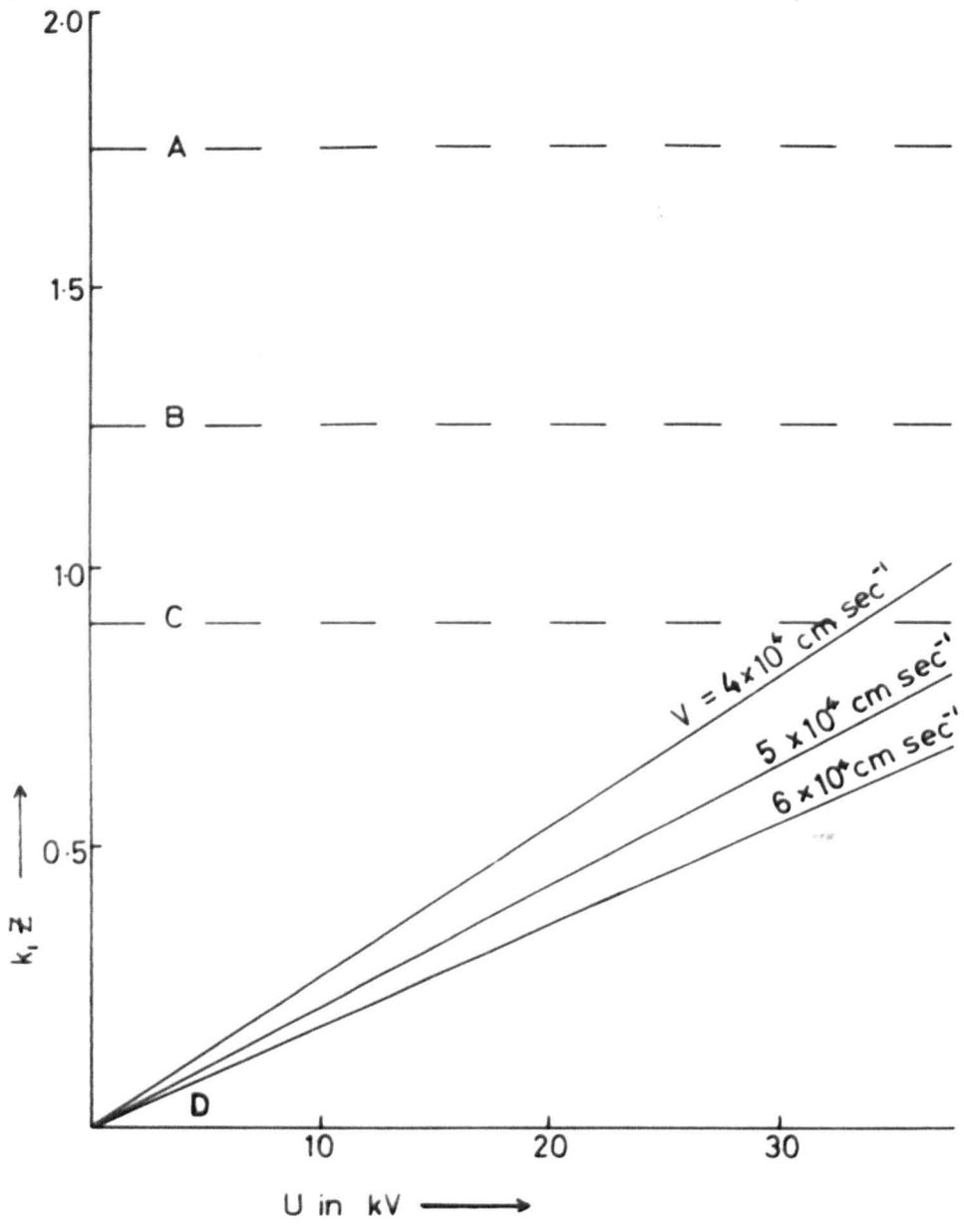

Fig 6.7.4a. Voltage sensitivity characteristics for $Z/d^2 = 30$

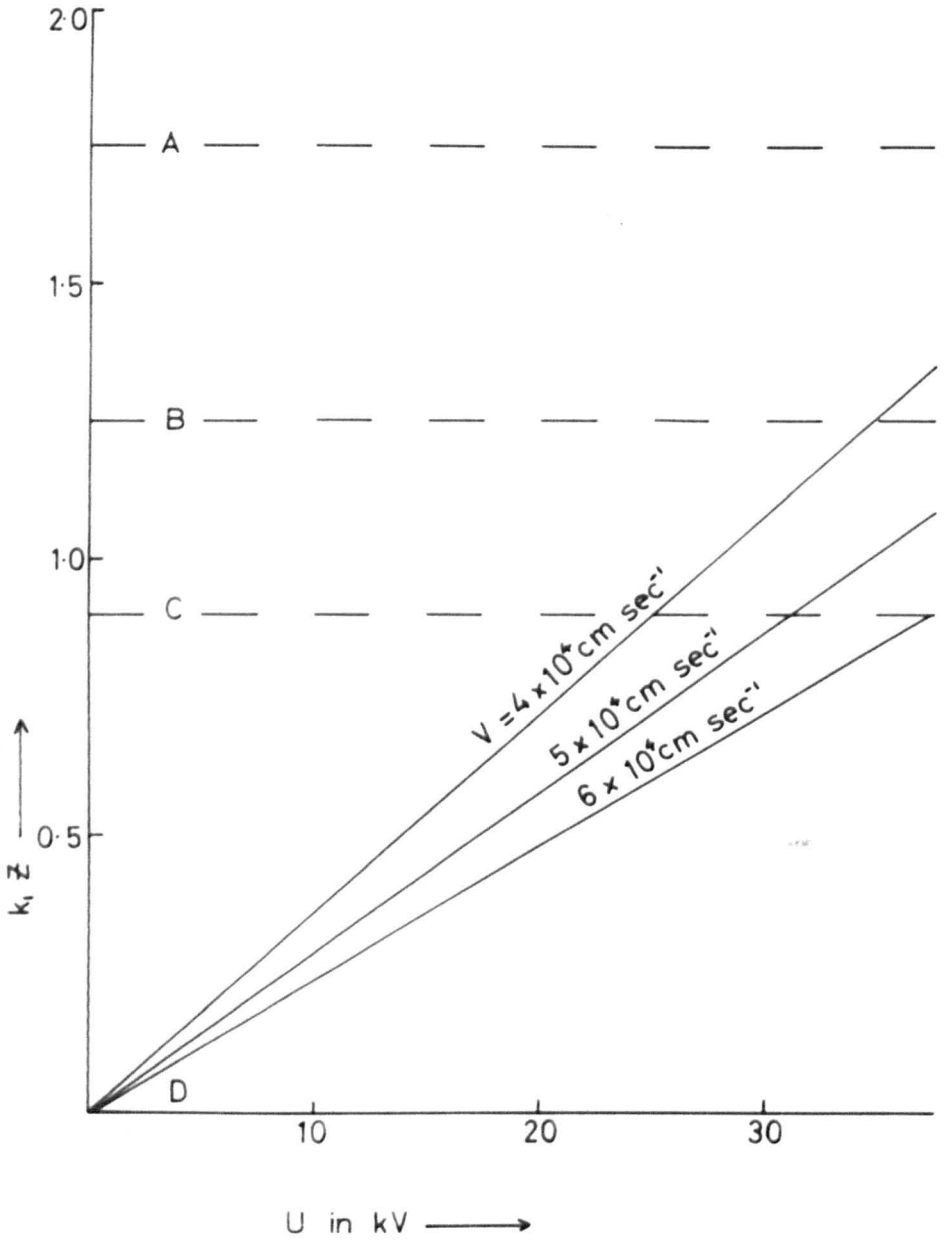

Fig 6·7·4b Voltage sensitivity characteristics for $Ƶ / d^2 = 40$

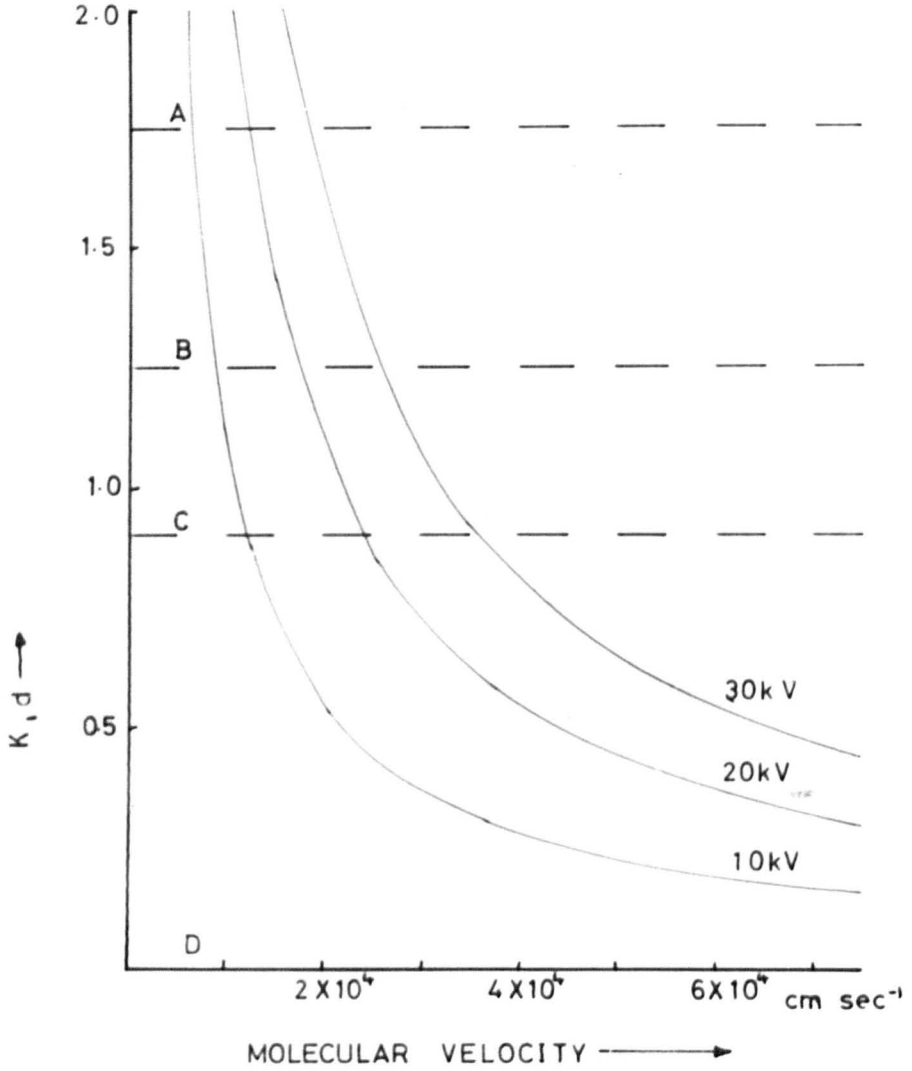

Fig 6·7·5 a Velocity sensitivity characteristics at various excitation potentials for $Z / d^2 = 30$

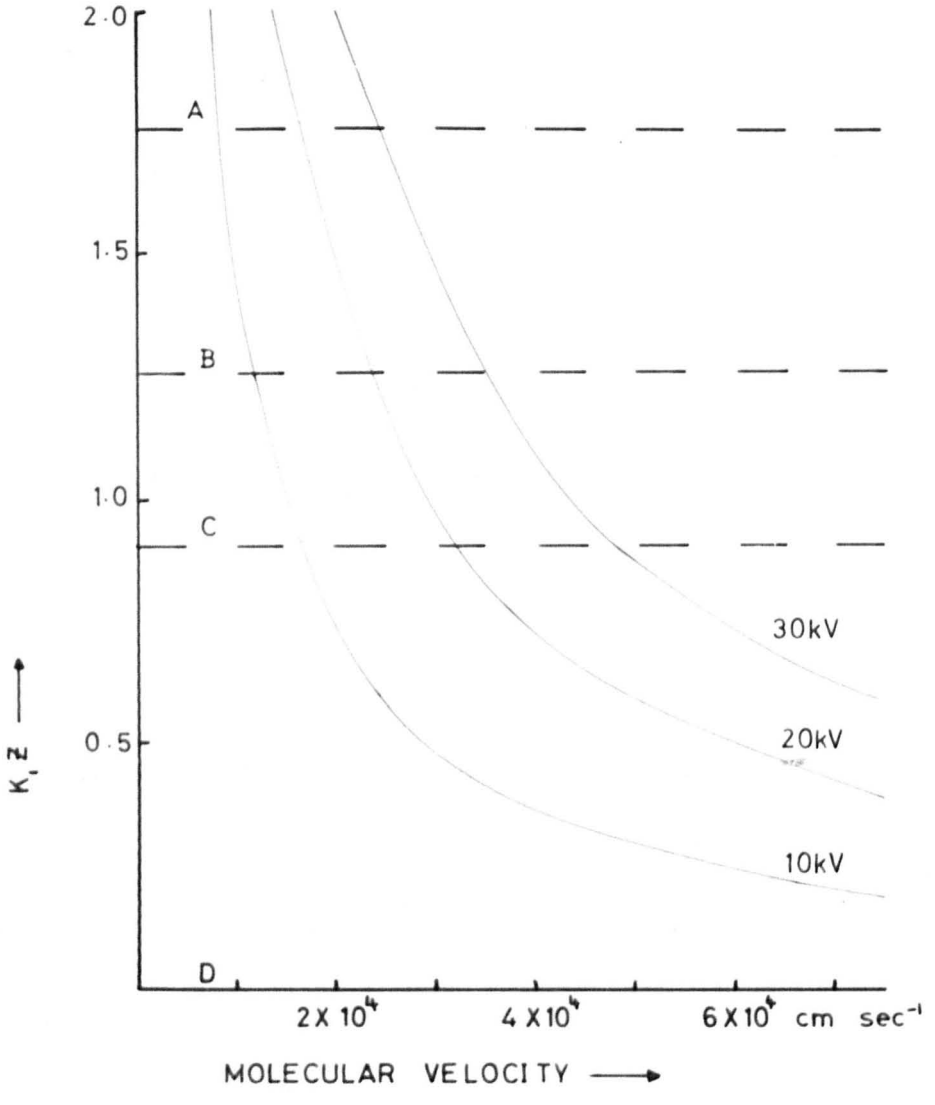

Fig 6·7·5 b Velocity sensitivity characteristics at various excitation potentials for $Z/d^2 = 40$

$$k_1 z = 36 \left(\frac{U}{v}\right) \left(\frac{z}{d^2}\right) \qquad (6.7.3)$$

A simple scheme based on the above considerations is shown in Fig. 6.7.2. For designing a system for any particular species of molecules, the appropriate value of $k_1 z$ can be chosen from a graph as in Fig. 6.7.1, and the ratio (z/d^2) calculated. In the simple system envisaged d and z must be so adjusted that interference between neighbouring dipolar fields can be neglected. For a system with large resolution in respect of velocity and quantum state sophisticated arrangements will be necessary. To meet the conditions of adiabaticity, extra electrodes or drift spaces as they are called in nuclear parlance, may be necessary; in an RF operated version a residual dc field may have to be provided.

Some design characteristics of the AG system are given in Figs. 6.7.3, 6.7.4a, 6.7.4b, 6.7.5a, 6.7.5b, illustrating the behaviour of the system with respect to molecular velocity and excitation potential. Illustrations are given for two models : one for $z/d^2 = 30$ and the other for $z/d^2 = 40$. In Figs. 6.7.3 - 5 dashed lines are drawn parallel to the abscissa at $k_1 z = 1.75$ (A), 1.25(B), 0.90 (C). In the region of $k_1 z > 1.75$ (above the line A), conditions for upper state focusing are satisfied. In the region $k_1 z < 1.25$ (below the line B) conditions for lower state focusing are satisfied. As mentioned in Section 6.6, from these diagrams an overlapping effect due to velocity distribution can be expected. The condition for state focusing of the lower inversion state of ammonia is best satisfied when the value of $k_1 z$ is around the line C, as would be expected from the stability diagram Fig. 6.7.1.

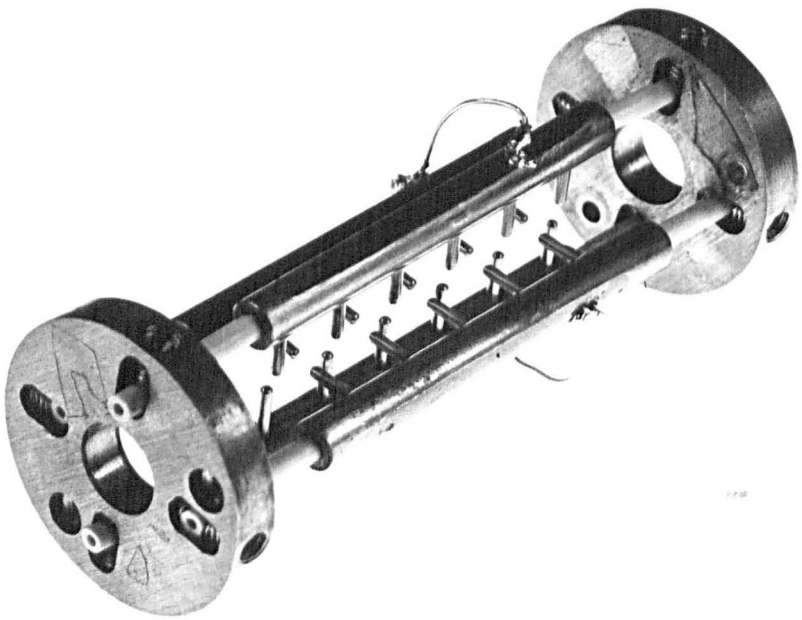

Fig. 6.8.1a. A View of the AG Focuser Used. (123)

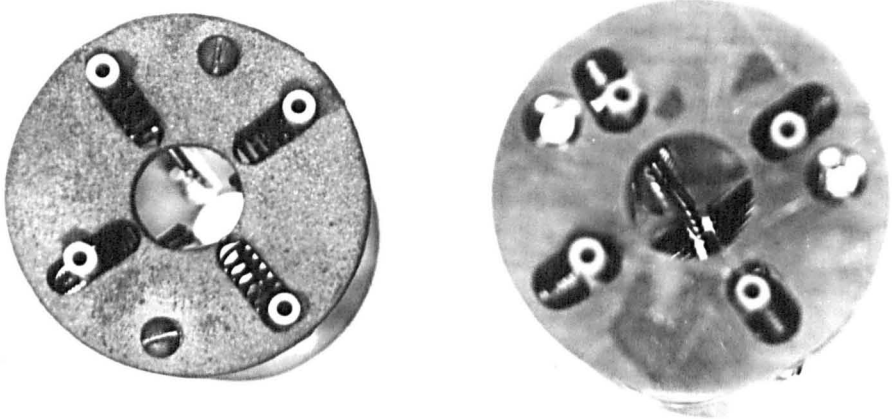

Fig.6.8.I.b. A View of the End Plates of the AG Focuser.(I23)

Fig. 6.8.2 Series Arrangement of
Octapole and AG System.

6.8 Experimental :

The AG focuser is made of short electrodes made of 0.16 cm diameter brass rods mounted on 0.6 cm diameter brass rods. The end of each electrode is made hemispherical and polished with abrasives. Four such rods with appropriately located electrodes and ceramic spacers at the end of the supporting rods are assembled together with two end-plates to form the AG array. The end plates have grooves made in them fitted with springs and adjusting screws to hold the electrode systems in their correct positions. This arrangement gives flexibility to the system, since the transverse dipole separation 2d can be easily adjusted by working on the springs. Also z_1 and z_2 can be varied if desired. In the present investigation z_1 and z_2 are kept identical. The system has also the advantage of tilting the electrode systems and use it as a parabolic AG array (C.F. Non-uniform maser focusers, Section 4.5.) The significance of this arrangement will be discussed in Chapter VIII. A view of the AG focuser and the end plates is given in Fig. 6.8.1. Several models have been made and tested, with different values of z_1 and d. Typical values are $d = 0.12$ cm, $z_1 = 0.5$ cm, total focusing length = 5 cm, and $z_1/d^2 \simeq 35$. This particular model has 5 dipoles in one plane and 6 on the other transverse plane. The two high voltage electrode systems are connected to a common terminal while the other two are connected to a common earth point. The complete focuser is mounted to a tripod made of glass rods with triangular brass discs to support the focuser. In some experiments the AG focuser is mounted in series with an octapole maser focuser. This is shown in Fig. 6.8.2.

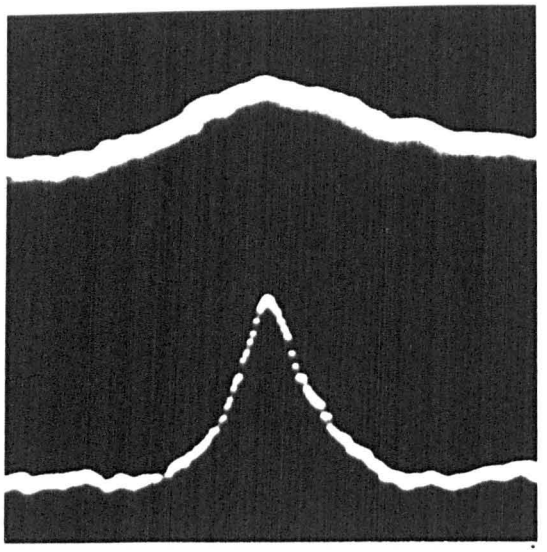

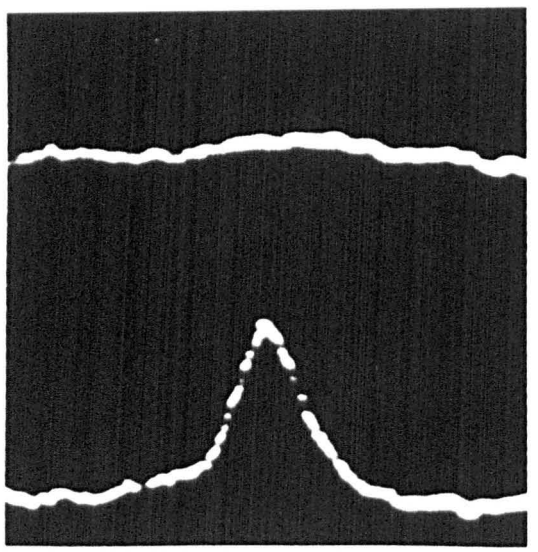

ENHANCEMENT OF MOLECULAR BEAM ABSORPTION BY ALTERNATE-GRADIENT FOCUSING

Fig.6.9.1 (124)

A superheterodyne beam maser experimental set up is used to operate the AG system. Details of this system are already given in Chapter V and will not be discussed further here. A digital memory oscilloscope (DMO) (Northern Scientific-Inc., NS-5/3) has been used in some experiments to improve signal to noise ratio. This improves the signal to noise by a factor of about five. The upper limit of the detection sensitivity is determined by the frequency instability of the unstabilized klystron. A chart recorder has been used in conjunction with the DMO. In some experiments diaphragms have been used at various positions to confine the AG action to the region near the axis in order to rule out the possibility of spurious effects. In dc operation as in the present investigation, possibility of non-adiabatic transitions is very small in the structure described, since the fields do not really drop to zero catastrophically along the axis. In addition, the conducting rods on which the dipole electrodes are mounted provide a steady component of electrostatic field along the axis which provides the necessary residual field for non-adiabaticity, although this is achieved at the expense of accurate quantitative analysis.

6.9. Operation and basic characteristics :

The maser set up is operated as described in Chapter V, except that the maser focuser is replaced by the AG focuser and also sometimes both the maser focuser and the AG focuser are used in series. Fig. 1 in Appendix shows the first evidence ever obtained of AG action (Kakati, Laine, 1967). The mode of operation is C_1 as defined in Fig. 6.6.1. Fig. 6.9.1. shows some results of the actual enhancement of an ammonia

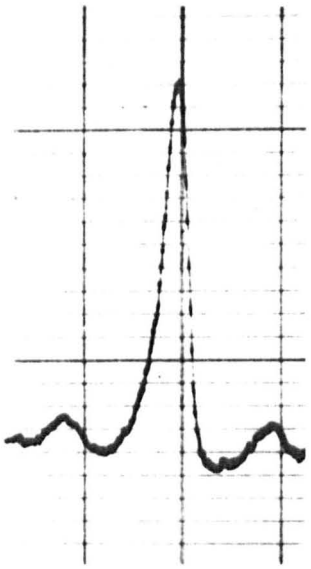

Fig 6·9·2 The J = K = 3 inversion line of ammonia flanked on either side by the magnetic satellites as obtained by AG operation in C_1 mode.

absorption signal when 30 Kv is applied to the AG focuser. In the upper picture, for a gas pressure of 1.5 torr behind the molecular beam effuser, an absorption largely due to a high background pressure of ammonia is observed which shows appreciable Doppler broadening. When the molecular beam is focused by the AG device, the absorption signal increases and shows spectral narrowing as a result of improved directivity (focusing) into the cavity.

The lower diagram in Fig. 6.9.1. which gives the results for 1.0 torr behind the effuser, shows the very considerable enhancement of molecular beam absorption that can be obtained. The linewidth is now given by the time of flight of the molecules through the cavity which in this case would yield a linewidth ~ 8 KH_z. The results presented are obtained with a DMO to enhance the signal to noise ratio. A similar signal to noise ratio has later been achieved without averaging with a DMO.

As would appear from the theory given in Section 6.4, state separation very near the axis is poor and in fact along the axis there would not be any state separation. To eliminate these unfocused molecules a circular beam stop of ~ 1.5 mm diameter is placed after the AG focuser (between AG and cavity). The absorption after AG focusing now increased several fold, enabling direct oscilloscope presentation without averaging to be made with a signal-to-noise ratio of ~ 10. Signal averaging in this case gave a signal to noise ratio of ~ 50, and the enhancement of the absorption is also of the same order of magnitude. The result is shown in Fig. 6.9.2. In obtaining this trace the resonance is slightly

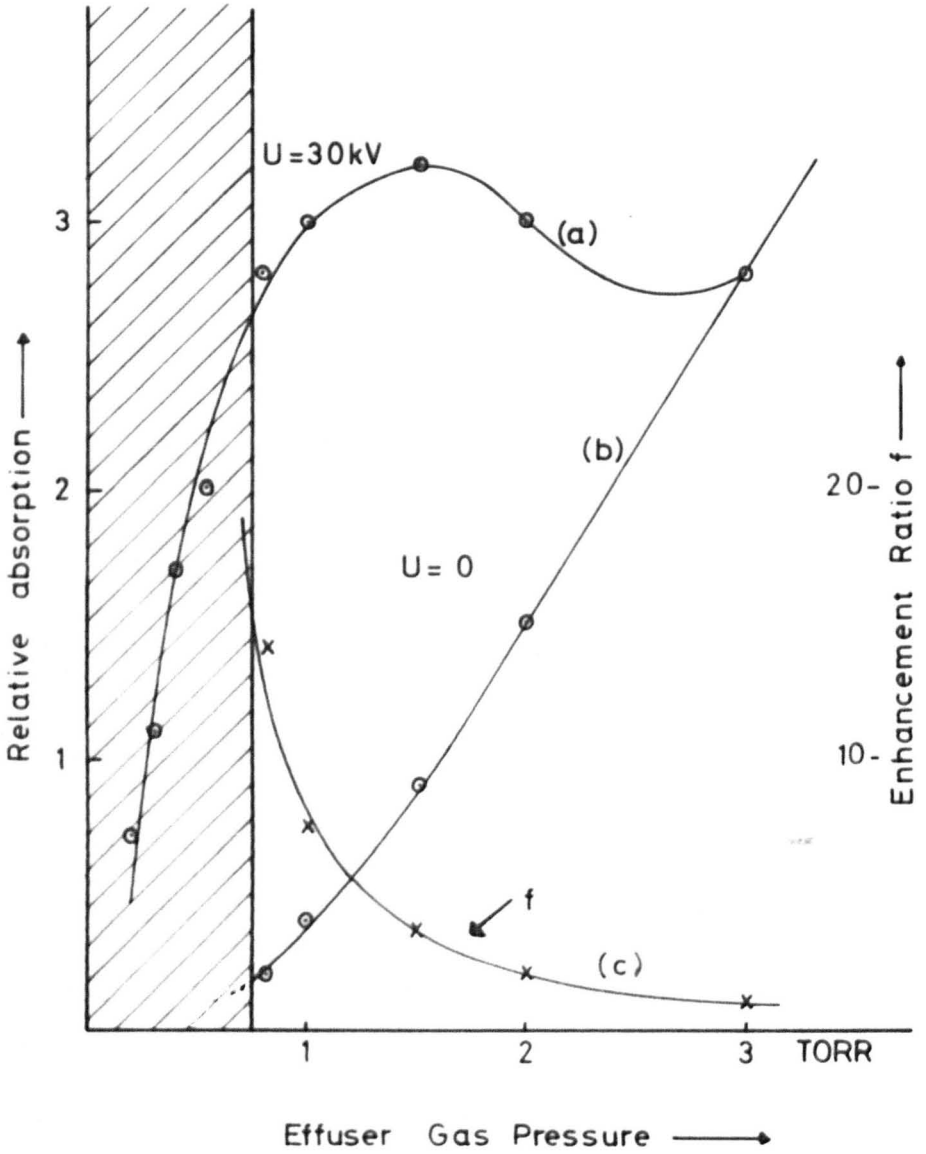

Fig 6.9.3 a Relative Enhancement of Absorption with AG Focusing.

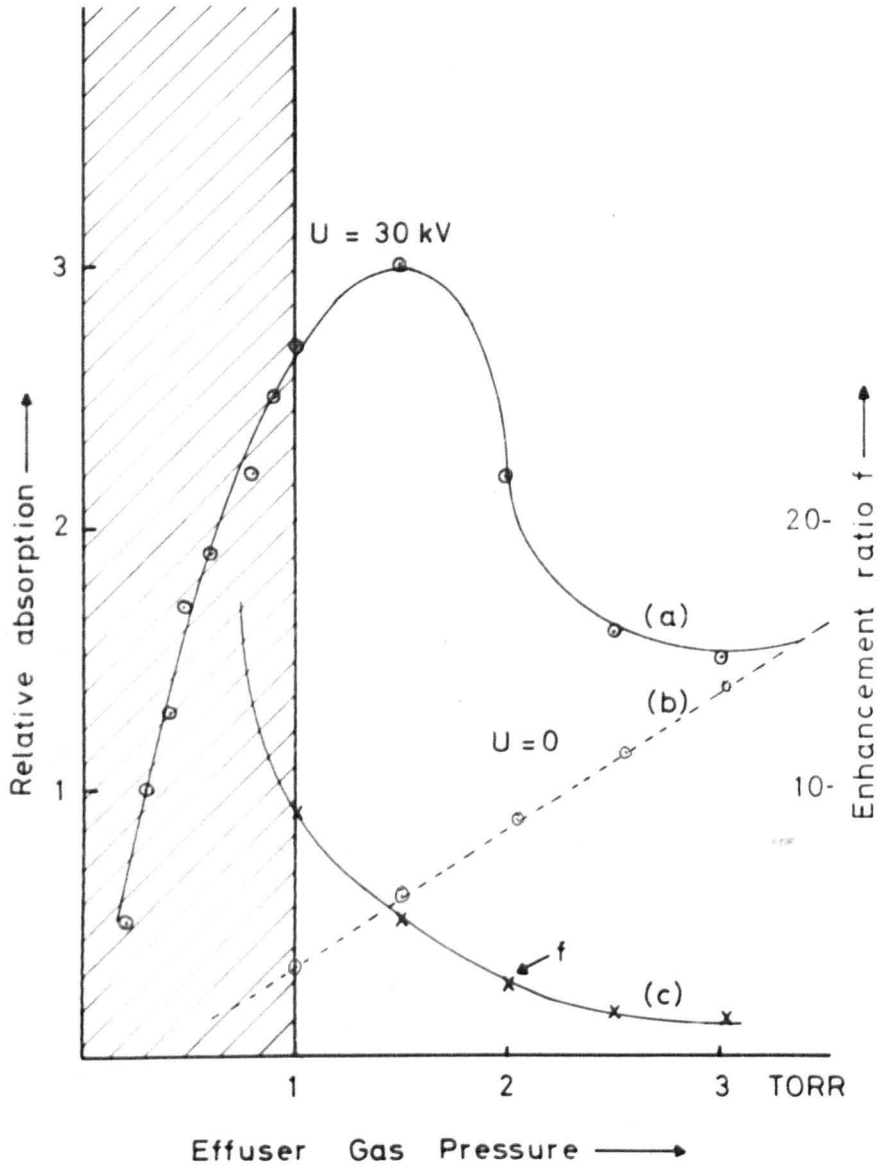

Fig 6.9.3 b Relative Enhancement of Absorption with AG focusing.

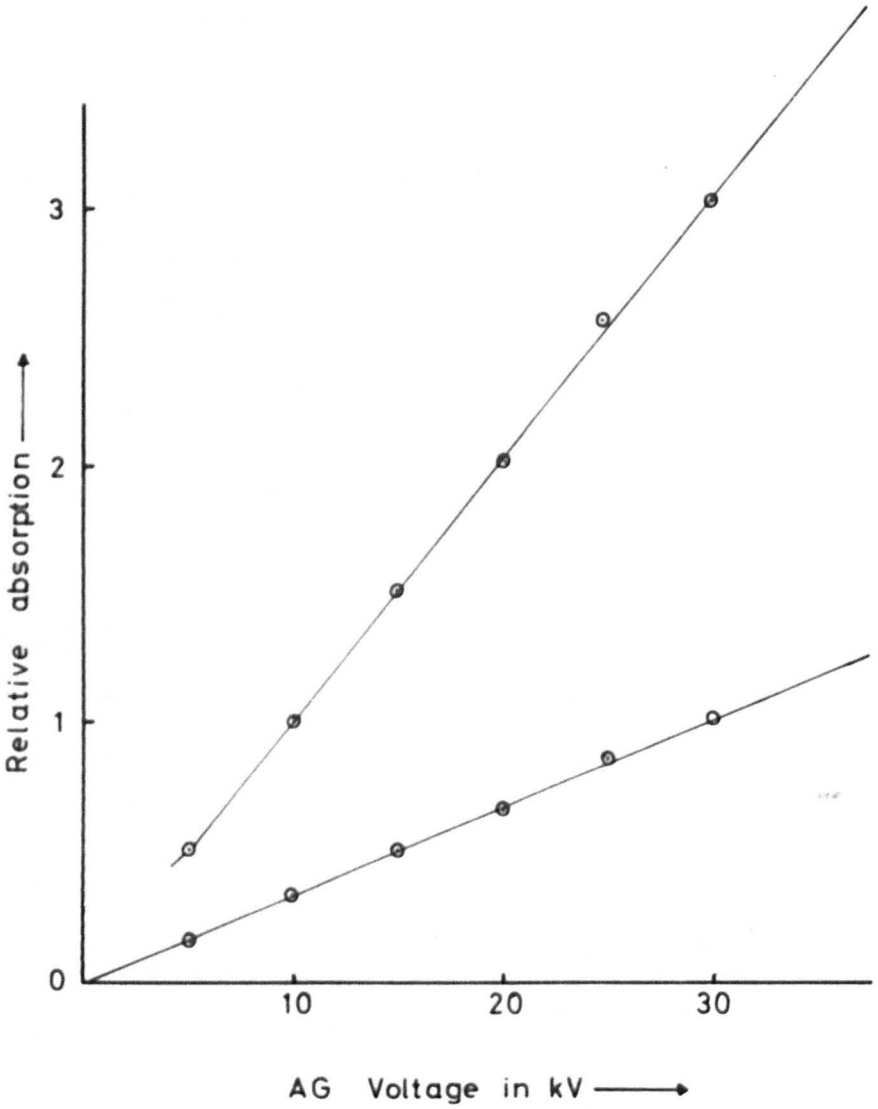

Fig 6.9.4 Linear operation of AG in C_1 mode.

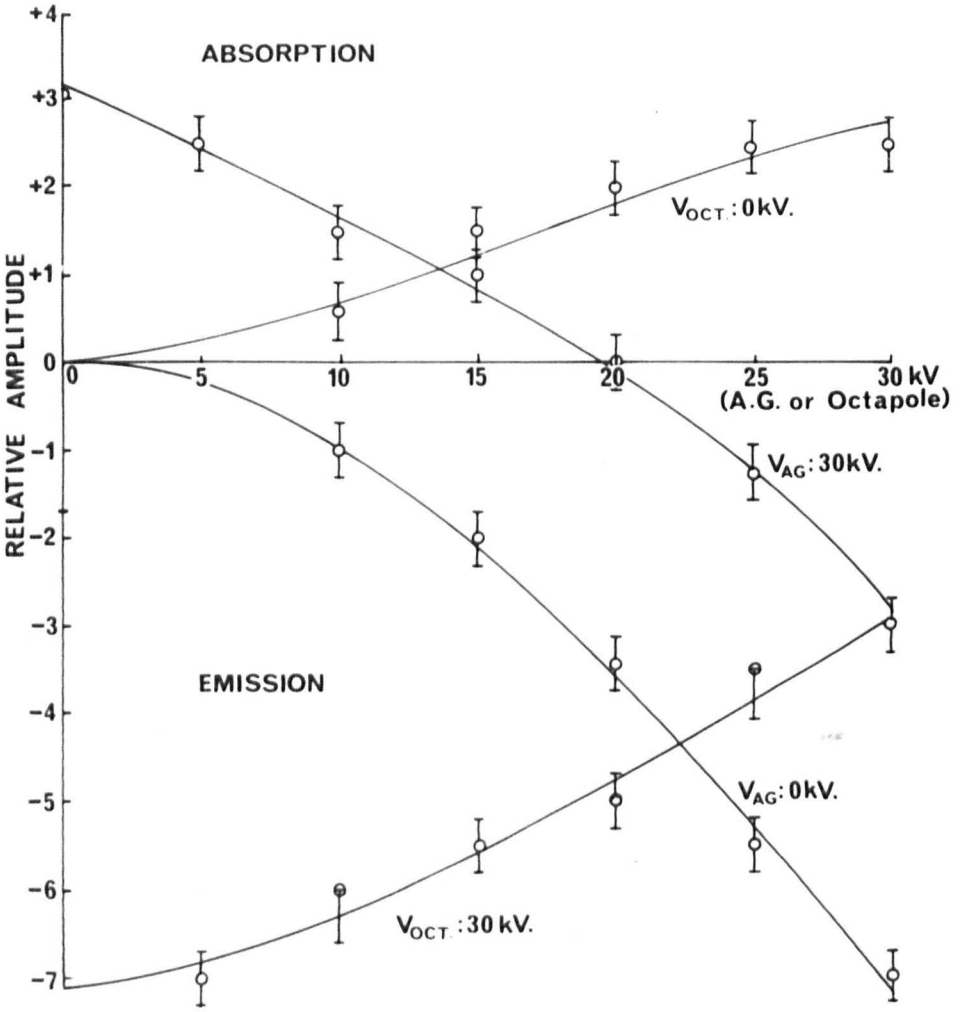

MOLECULAR BEAM FOCUSING WITH OCTAPOLE UPPER STATE AND ALTERNATE-GRADIENT SYSTEMS IN SERIES.

Fig.6.9.5 (126)

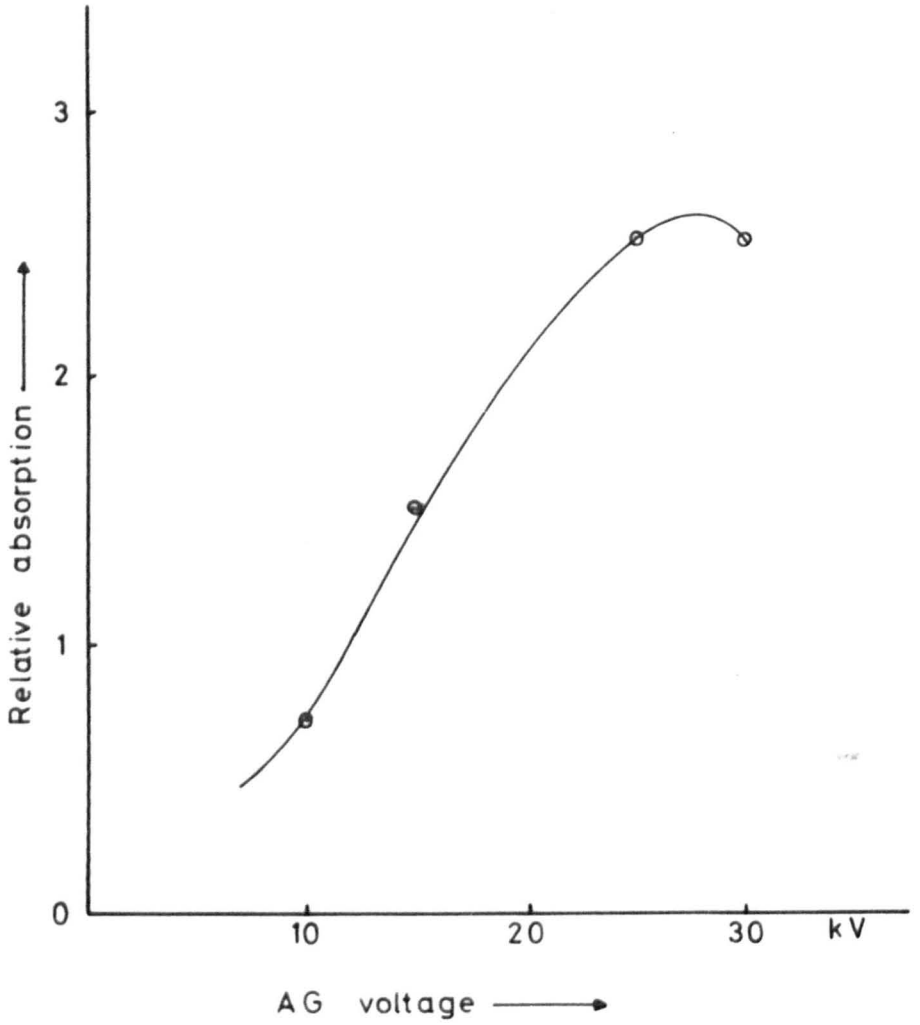

Fig 6.9.6a Voltage sensitivity of AG

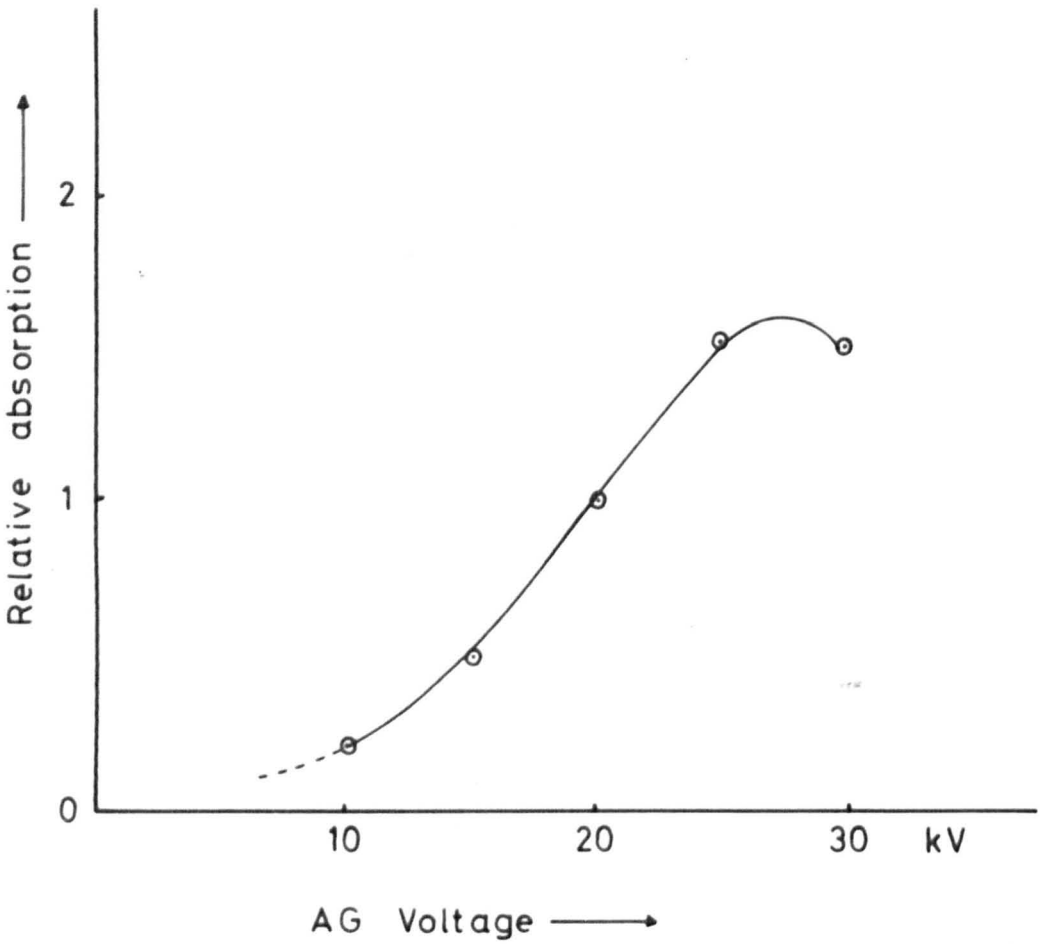

Fig 6.9.6b Voltage sensitivity of AG

saturated in order that the magnetic satellites could be seen more clearly above the background noise.

Fig. 6.9.3a, b, show for two different models (i.e. different values of z/d^2) the relative absorption with and without AG focussing as the effuser gas pressure increases. It will be noted that at low beam flux enhancement of an order of magnitude are obtained. At higher values of beam flux, the background pressure rises and the thermalisation of the molecular beam occurs and the focusing of the beam is spoilt. At very high beam flux the background pressure is too high for a molecular beam to be formed and the absorption at the full Doppler line width is due to background gas in the absorption cavity and so no enhancement occurs. The curves for the enhancement f is also shown in Fig. 6.9.3.a,b. The shaded regions show that the AG operates linearly over a certain pressure range, when the conditions for any one mode of operation (C_1 or C_2 in Fig. 6.6.1) are satisfied. This is illustrated in Fig. 6.9.4. The pressure behind the effuser is here 0.8 torr and background pressure is 5.6×10^{-6} torr. To confirm AG operation in the C_1 mode (i.e. when the AG predominantly focuses the lower state molecules) an experiment is done with an AG and an octapole focuser in series. The result is illustrated in Fig. 6.9.5. It is seen that the AG is predominantly focusing lower state molecules and defocusing upper state molecules as expected from the theory.

Figs. 6.9.6.a,b, show that when the AG is operated in the linear region of beam flux in mode C_1, the absorption increases to a maximum around U = 30 KV and then begins to decrease, i.e. the mode

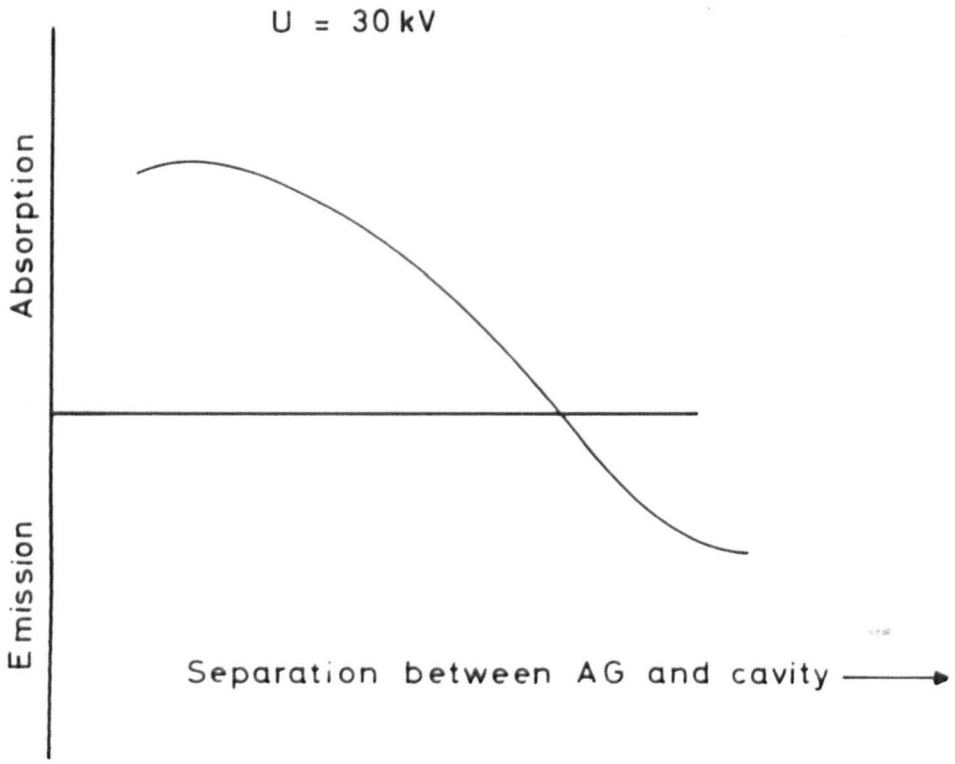

Fig 6.9.7 Diagrammatic representation of results observed with various separation between cavity and AG.

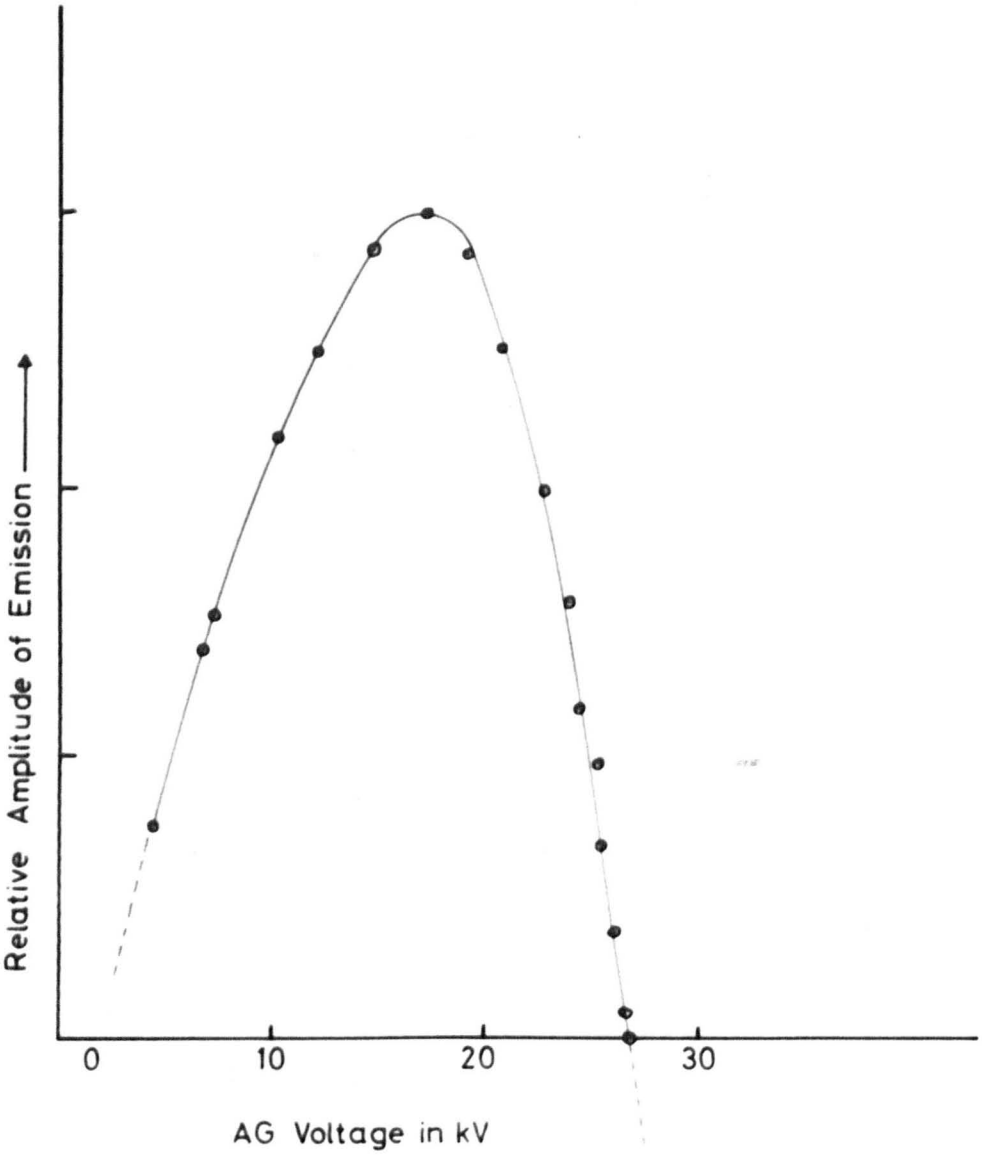

Fig 6.9.8 AG Operation in the C_2 mode.

of operation changes to C_2 mode. The transition is smooth because of the velocity distribution of the molecules. This confirms the expectation from the theory. The complete turn over of the effect could not be actually demonstrated as the excitation voltage above 30 KV was not available.

Experiments were performed by placing the AG at different distances from the cavity. The nature of the results is shown in Fig. 6.9.7. The transition towards mode C_2 operation is obvious. Results of the C_2 mode of operation is shown in Fig. 6.9.8. The system is now basically emissive within the limits of excitation potential. It will also be noticed that the system is now more voltage sensitive than when operated in the linear region of the C_1 mode.

Within the limits of various approximations made these results are found to be in excellent agreement with theory.

CHAPTER VII.

COHERENCE PHENOMENA AND RELAXATION PROCESSES IN A MOLECULAR SYSTEM.

7.1. Introduction :

The observation of "molecular ringing" in a single cavity ammonia beam maser was reported by Laine in 1966.[168] This was a significant advance in so far as it was another step which helped to form a coherent pattern of the various transient phenomena in a molecular system reported by various authors.[122-128, 169-170]

It was commented in Chapter I, Section 1.2, that in radio-frequency physics, the wavelength of the emitted radiation may be much larger than the distance between the neighbouring radiating objects, and that this leads to the fact that the molecules of a radiating gas cannot be considered as emitting spontaneous radiation independently of each other. Dicke [171] pointed out that generally speaking, if the assembly of radiating particles occupies a volume whose linear dimensions are small in comparison to the wavelength, then even if the particles do not interact directly with each other, the emission does not occur independently. As a matter of fact there is a strong indirect interaction through the radiation field of the individual particles, and consequently the entire assembly of particles is in a state of spontaneous coherent emission, or in a "superradiative state" as it is called by Dicke. Dicke's theory will be discussed briefly in a later section.

7.2. The NMR Analogue :

Analogous transient effects in nuclear magnetic resonance phenomena however have been a well-understood subject for a long time. Bloembergen et al [172] first reported the"wiggles" which always occur after the magnetic field has passed through resonance in a time short compared to the relaxation time. A theoretical analysis of the wiggles was given by Jacobshon and Wangness[173]. Further work was done to utilise these transient phenomena by Bloch[174], Hahn[175], Meiboom and Gill[176] to measure nuclear relaxation times. Studies of transient nutations of the nuclear magnetic moment under the action of radio frequency pulses have been reported by Torrey[177, 178]. The effect of a rapidly varying magnetic field on an oriented atom possessing nuclear spin has been discussed by Rabi[179,180]. The various transient effects in molecular systems reported in references 122-128, 169-170 are analogous to the closely associated phenomena of wiggles[172, 173] and spin-echo[175] in NMR.

7.3. The Optical Analogue :

The analogous effect in the optical region has been recently observed by Kurnit et al (1964)[181], Abella et al (1966)[182], McCall and Hahn (1967)[183] Patel and Slusher (1967)[184]. These phenomena called "photon-echoes" in analogy to "spin-echoes" in NMR parlance were first observed for two ruby laser pulses incident on an absorbing ruby sample.[181, 182]. The echoes result from the coherent excitation of the electric dipoles of a two level absorbing medium as in the case of spin-echoes in NMR.

7.4a. Theoretical Approach :

From the accumulated experimental results mentioned in the foregoing sections, it is evident that a general approach can be made extending over any assembly of two-level systems. In practice an ideal system consisting of only two energy levels is difficult to realise. However it is possible - as in the case of the ammonia microwave inversion transition - that the interaction of the field may have a clearly defined resonance character in which case the effect of the other levels can be neglected, at least in so far as the physicist wants an insight of the general nature of the processes involved. The bulk of the experimental data obtained so far is still the object of considerable attention as already mentioned. Normally a model system is assumed to reflect the behaviour of the actual system. The pertient experimental data collected by various authors over the years are by no means complete enough to make any of the theories or models to be accepted as the final and the only one. However, a mutual refinement of theory and experimental techniques is continually taking place as will appear from this and the following chapter.

7.4b. A Direct Approach

In view of the experiments first reported by Laine[168] in 1966, a direct approach to treat the transient effects in a molecular system seems to be to examine the behaviour of the polarization of a molecular beam under the action of an alternating field with variable phase and amplitude. On the basis of some calculations made by Liubimov and Khokhlov (1958)[186] an attempt is made here to present a simplified approach

to this problem. For a two level system with energies W_1 and W_2 ($W_2 > W_1$), the state of the molecular beam in the resonanator can be described by the density matrix[102]

$$\begin{vmatrix} \rho_{11}(z,t) & \rho_{12}(z,t) \\ \rho_{21}(z,t) & \rho_{22}(z,t) \end{vmatrix} \tag{7.4b.1}$$

The matrix elements ρ_{11} and ρ_{22} determine at point z and time t the density of molecules in states 1 and 2 moving with velocity v. The elements ρ_{12} and ρ_{21} determine the polarization vector P of the beam due to transitions between states 1 and 2 under the action of the field. The polarization of the beam can then be expressed as

$$P(z,t) = \mu \left| e^{i\omega_o t} \rho_{12} + e^{-i\omega_o t} \rho_{21} \right| \tag{7.4b.2}$$

where ω_o is the frequency of the molecular transition and μ is the dipole moment of the molecule. The quantity

$$D(z,t) = \rho_{22}(z,t) - \rho_{11}(z,t) \tag{7.4b.3}$$

characterizes the population distribution in the two states. It is assumed for simplicity that $D = 1$ and $\rho_{12} = \rho_{21} = 0$ at $z = 0$.

The external field is assumed to be of the form

$$E(t) = E_o(t) \cos \left[\omega_o t + \phi(t) \right] \tag{7.4b.4}$$

where the amplitude $E_o(t)$ and phase $\phi(t)$ are slowly varying functions of time as compared to the period $T = 2\pi/\omega_o$. Under these conditions,

the polarization of the beam can be written as a linear combination of a real and a reactive part[186]

$$P = P_1 + P_2 \qquad (7.4b.5)$$

Neglecting terms which vary rapidly in time (at a frequency $2\omega_o$) in the right hand side of Eq. 7.4b.5 P_1 and P_2 can be expressed in terms of the various parameters already mentioned, and a differential equation for D can be obtained, which can in principle be solved if certain limitations are imposed on the phase and amplitude of the field. In the case in which the frequency of the external field E is equal to the frequency of the molecular transition but the field amplitude E_o varies arbitrarily, it can be shown that the reactive part P_2 of the polarization vanishes and the real part P_1 can be expressed as

$$P_1 = -\mu \sin \theta \qquad (7.4b.6)$$

where θ is a function of the molecular parameters and the field amplitude averaged over an interval z/v which is of the order of the molecular time of flight through the cavity. The corresponding expression for the polarization of the beam is finally obtained as

$$P(z,t) = -\mu \sin \omega_o t \sin \delta t \qquad (7.4b.7)$$

where $\delta = \mu E/h$. It would appear from Eq. 7.4b.7 that after passage of the exciting signal (E) through molecular resonance, a beat pattern can be expected.

When the external field acting on the molecules varies rapidly

either in frequency or amplitude as compared with the time of flight of the molecules through the cavity, the differential equations for the polarization can still be solved approximately and within the order of approximation the beam polarization can be written as

$$P = P_s + P_f \qquad (7.4b.8)$$

where P_s and P_f are the slowly and rapidly varying parts of the polarization respectively.

In conclusion, it would seem that this approach deserves further attention and refinement.

7.4c. The Mixed Energy State Model :

Historically the transient effect in the microwave region (the so-called "molecular ringing") in a molecular beam maser type system was experimentally observed in two-cavity systems [122-128] as contrasted with the one cavity system of Laine[168]. In the cascaded two-cavity (or multi-cavity) system a beam of state selected molecules passes through the cavities in succession. The maser self-oscillation mode is produced in the first cavity, and a highly monochromatic oscillation is produced in the second cavity. The frequency of oscillation in the second cavity follows the frequency of oscillation in the first cavity. To explain the phenomena under this type of experimental conditions Basov et al [127,128] advanced a model in which the molecules are considered to be in a mixed energy state. The mechanism of maser oscillation is visualised as follows : (i) an electromagnetic field E (r,t) polarizes the molecules of the medium creating electric dipole moments P_i (r,t), (ii) these moments add up to produce a macroscopic polarization density P(r,t),

(iii) this polarization acts further as the source of a reaction field $E(r,t)$ according to Maxwell's equations. The complete maser oscillation process can thus be schematically represented as

$$E(r,t) \xrightarrow{\text{quantum mechanics}} \langle P_i \rangle \xrightarrow{\text{Statistical summation}} P(r,t) \xrightarrow{\text{Maxwell's equations}} E(r,t)$$

The polarization vector P of the molecular beam is defined in terms of the average dipole moment vector μ per unit volume of the medium as follows,

$$P = N \, Sp \, (\rho \, \mu) \qquad (7.4c.1)$$

where N is the number of molecules per unit volume, μ is the molecular dipole moment operator. Here ρ is the density matrix operator satisfying the Schrödinger equation

$$i\hbar \, \delta\rho/\delta t = |H,\rho| \qquad (7.4c.2)$$

The interaction Hamiltonian operator H is given by

$$H = Ho - \mu E \qquad (7.4c.3)$$

The density matrix has only the four elements shown in Eq. 7.4b.1. in the preceding section. In the present case the states being non-degenerate, the diagonal matrix elements of the dipole moment vanish. Further, in the case of the maser the quantity $\mu_{12} E/h$ is small compared to the characteristic time τ of the problem, where τ is the transit time of the

molecules through the cavity. Under these circumstances (7.4c.1) can be solved in conjunction with Maxwell's equations and eventually the polarization of the beam in an electromagnetic field is obtained as

$$P = 2 \text{ Re } N\left|\mu_{12}\,\rho^{o}_{21} + i\,\frac{\mu_{12}}{h}\,(\rho^{o}_{22} - \rho^{o}_{11})\int_{t_o}^{t} E(t)\,e^{-i\,\omega_{21}t}\,dt\right|\, e^{i\omega_{21}t}$$

$$\text{or} \quad P = A\,\rho^{o}_{21} + B(E)\,(\rho^{o}_{22} - \rho^{o}_{11}) \qquad (7.4c.4)$$

where $\rho^{o}_{21} = \rho^{o*}_{12} = \rho_{21}\,e^{-i\omega_{12}t_o}$ and ρ_{21} is taken at the moment $t = t_o$. It is seen from Eq. 7.4c.4 that the second term is proportional to the external field and varies synchronously with it. The phase of this term is specified completely by the external field E (t), since the value $D_o = \rho^{o}_{22} - \rho^{o}_{11}$ is real. However the first term containing ρ^{o}_{21} which is complex, is independent of the external field but its phase is dependent on the pre-history of the molecular assembly. When the molecules enter a cavity from a molecular beam source where the molecules are in thermodynamic equilibrium, then $\rho^{(o)}_{12} = 0$ since ρ is diagonal in thermodynamic equilibrium. Therefore it follows from Eq. 7.4c.4 that in the first cavity the polarization depends only on the number of active molecules given by $N(\rho_{22} - \rho_{11})$. However, when the molecules enter the second cavity the non-diagonal elements of the density matrix do not vanish i.e. $\rho^{o}_{12} \neq 0$ or in another word the molecules entering the second cavity are in a mixed energy state. The polarization now has a term which does not vanish when the external field vanishes. This term provides the driving field for the forced oscillation in the second cavity.

This model described the oscillation phenomena in cascaded multicavity maser experiments adequately enough. This is only to be expected because, in a state selected beam of molecules the population difference between the two levels is so large that there results an oscillating net macroscopic polarization (as assumed in this section). The system therefore need not be regarded as a single quantum mechanical system as in the Dicke model in the following section, and a classical approach is adequate.

7.4d. The Correlation Model of Dicke :

None of the two models discussed above is however adequate for a general description of all the transient phenomena mentioned in Sections 7.1-3. Dicke's[171] model put forward in 1954 still remains the only one which provides an elegant foundation for further refinement of theoretical models to suit different experimental conditions which include the very recent developments like photon-echo,[181,182] self-induced transparency by pulsed coherent light[183] etc. Dicke's theory is briefly outlined in the following.

The basic premises of the theory are that the gas of the radiating molecules act as a single quantum mechanical system, in that the molecules are interacting through a common radiation field and therefore an independent molecule picture is wrong in principle. The problem is therefore that of evaluating the interaction between the radiation field and a system of N identical particles which have two energy levels, and are contained within a limited volume e.g. the resonator used in maser type systems described in this investigation. Such an ensemble of identical two-level quantum objects forms a resonant medium in which under

certain conditions either the emission or the absorption processes can take place in a special manner. If the time evolution of these processes is examined under the conditions that (i) there are no quanta at the commencement of the process and, (ii) the molecular distribution in the two levels is fixed, it will be found that the molecules will radiate idependently of each other to begin with as would be expected from the perturbation theory. Soon however, the system acts as a collective one, and the process of collective stimulated emission takes over; that is to say that after some characteristic time of the medium, the molecules cease to radiate independently. This characteristic time after which the collective process starts is several orders of magnitude shorter than the lifetime of the isolated molecule.

Dicke's model consists of a system of molecules in two non-degenerate levels E_+ and E_- ($E_+ > E_-$), placed in a cavity whose dimensions are smaller than the wavelength λ. The radiation of the molecule is considered in the dipole approximation. It is assumed that the wave functions of the molecules do not overlap. The Hamiltonian of the n-molecule gas in absence of the radiation field can be written as

$$H = H_o + E\sum_{j=1}^{n} R_{j3} \qquad (7.4d.1)$$

with $$R_k = \sum_{j=1}^{n} R_{jk}, \quad k = 1,2,3. \qquad (7.4d.2)$$

Here $E = h\omega_o = E_+ - E_-$

H_o = the energy of translational motion of the molecules and the energy of intermolecular interaction.

ER_{j3} = the internal energy of the jth molecule and has the eigenvalues $\pm \frac{1}{2} E$.

H_o operates on the coordinates of the centre of mass of the molecules. The vector R_j with the three components R_{j1}, R_{j2}, R_{j3} are analogous to the Pauli spin operators in the energy space and satisfy the same kind of commutation relations.

The operators H_o and the R_{j3}s commute with each other and therefore state functions can be chosen which will simultaneously be eigenfunctions of H_o, R_{13}, R_{23}, R_{n3} and are of the form

$$\psi_{gm} = U_g (r_1 \ldots r_n) \; |+ - - \ldots + - - +| \qquad (7.4d.3)$$

where $r_1 \ldots r_n$ are essentially coordinates of the centres of mass of the n molecules whereas the symbols + and - represent the internal energies of the different molecules. If there are n_+ molecules in the + state and n_- molecules in the - state, then the Dicke quantum number "m" is defined by

$$m = \tfrac{1}{2} (n_+ - n_-)$$

$$n = n_+ + n_- = \text{total number of molecules} \qquad (7.4d.4)$$

Defining now (i) Eg as the energy of translational motion and interaction of the molecules, (ii) $E_m = mE$ as the internal energy of the molecules and (iii) E_{gm} as the total energy of the gas system, in Dicke's formalism as outlined here, the following equations can be written

$$E_{gm} = E_g + E_m \tag{7.4d.5}$$

$$R^2 = R_1^2 + R_2^2 + R_3^2 \tag{7.4d.6}$$

$$H = H_o + E R_3 \tag{7.4d.7}$$

$$R_3 \psi_{gm} = m \psi_{gm} \tag{7.4d.8}$$

The operators R_1, R_2, R_3 are analogous to the components of angular momentum in their commutation properties. It follows therefore that the interaction energy operator obeys the selection rule $\Delta m = \pm 1$, i.e. it has non-vanishing matrix elements only between the states given by Eq. 7.4d.3 and other states which differ in m by unity. Any chosen stationary state must comply with this condition. Since H and R^2 commute, it is therefore possible to choose eigenstates of R^2 as stationary states. These new states will be linear combinations of the states 7.4d.3. i.e.

$$\psi_{gmr} = \sum \psi_{gm} \tag{7.4d.9}$$

$$H\psi_{gmr} = (E_g + mE)\, \psi_{gmr} \tag{7.4d.10}$$

$$R^2\psi_{gmr} = r(r+1)\psi_{gmr} \tag{7.4d.11}$$

Dicke calls the eigenvalue "r" of the operator R^2 as the "<u>cooperation number</u>" of the gas. The quantum number r is integral or half-integral and positive such that

$$|m| \leq r \leq \tfrac{1}{2} n \tag{7.4d.12}$$

and

$$m_{max.} = r_{max.} = \tfrac{1}{2}n \tag{7.4d.13}$$

The state satisfying 7.4d.3 is non-degenerate in the internal coordinates. All the states with $r = \frac{1}{2}n$ but different values of m are also non-degenerate.

On the basis of the above model, the intensity of spontaneous radiation from a molecular system in the state (r,m) is found to be

$$I = I_o (r + m)(r - m + 1) \qquad 7.4d.14)$$

where I_o is the intensity of spontaneous emission from an isolated molecule. The following cases may be considered for a system of n molecules,

(i) $r = (1/2)n$, $m = 0$: Here $I \simeq \frac{1}{4} n^2 I_o$ (7.4d.15)

(ii) $r = m = o$: No radiation at all. (7.4d.16)

That is, there are states of the gas which radiate spontaneously with an intensity which is proportional to the square of the number of molecules. On the other hand there are also states with zero radiation. In all cases however the quantum number r ("cooperation number") does not change during the radiative transitions, since the operator R^2 is a constant of motion.

In thermal equilibrium $n_+ = n_- \exp(-E/kT)$ and the average value $\bar{m}$ over the Boltzmann distribution is given by

$$\bar{m} \simeq -\frac{1}{4} \frac{nE}{kT} \qquad (7.4d.17)$$

Also in this case $\bar{r} = |\bar{m}|$ (7.4d.18)

As contrasted with the implications of Eq. 7.4d.14, the intensity of total emission or absorption in the presence of an external

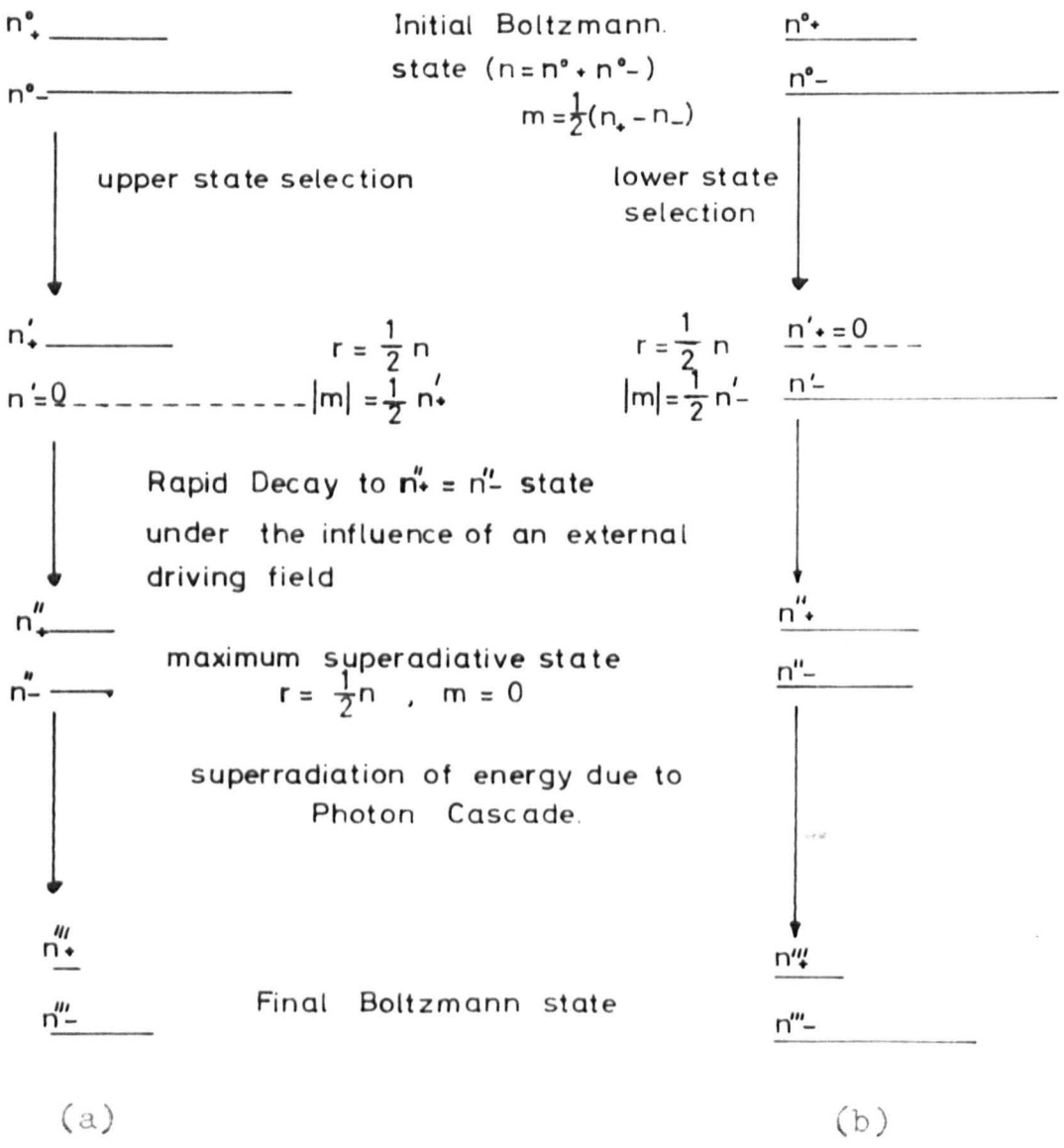

Fig 7·4d·1 Schematic representation of Superradiative Processes in state selected beams (a) upper state selected beam (b) lower state selected beam.

field always remains proportional to the number of active molecules which is $(n_- - n_+) = -2m$ from Eq. 7.4d.4. In spontaneous emission m can only be reduced by unity, whereas an external field brings in (i) induced emission with a reduction in m i.e. $m \rightarrow m - 1$, (ii) as well as induced absorption with an increase in m i.e. $m \rightarrow m + 1$; the intensity of total emission or absorption in this case is proportional to 2 m which is consistent with the foregoing comments.

It follows from the preceding paragraphs that the gas will have a maximum radiating state (a state of <u>maximum "superradiance"</u>) at $m = r = (1/2)n$, where $n = n_+ + n_-$ = total number of molecules involved. After some characteristic time the state becomes $r = (1/2)n$, $m = 0$ i.e. r remains the same but now $n_+ = n_-' = (1/2)n$. The two energy levels are now equally populated but are correlated to each other by the maximum value of the correlation number r (= (1/2)n), and the gas emits spontaneous coherent radiation at the maximum level for the system.

To bring the gas to this maximum supperradiative condition needs state selection of the molecules at the commencement of the process. This can be done in two ways :

(i) by upper state selection of the molecules using for example an octapole focuser in a maser as described in Chapter V. (or even using an AG focuser in the appropriate mode)

(ii) by lower state selection of the molecules using an AG focuser as described in Chapter Vl. The two processes are schematically represented in Fig. 7.4d.1.

The Dicke model has both the elegance and the generality that

may be demanded by the Physicist. The above analysis tacitly assumed that there are many radiators in the volume λ^3 where λ is the wavelength radiated. This is valid for the experiments in the microwave region (λ = 1.25 cm) done in the present series of investigations as also the spin-echo experiments of Hahn and the two-cavity maser experiments reported by various authors. All these experiments are in the radio- or micro-wave region. The photon echo experiments mentioned in Section 7.3 are, however, in the optical region. Here the linear dimensions of the radiating object are larger than the emitted wavelength. This apparent difficulty can however be circumvented by slight modification of the above analysis and has indeed been discussed by Oraevskii[187].

Dicke's theory has been further extended and developed to suit special cases in recent years[187-203]. A geometrical representation of the model is given by Feynman et al[203]. In its essence the Feynman et al model shows that the behaviour of an assembly of two level electric dipoles (e.g. NH_3 molecules) can be analysed in a way analogous to the rotating co-ordinate procedures of Rabi[204] et al as applied to transitions between two magnetic levels of a spin 1/2 particle.

7.5. Experimental :

The single cavity beam maser set up described in detail in Chapter V has been used. The exciting signal frequency obtained from the Klystron is scanned rapidly. Assuming a mean molecular velocity of 5×10^4 cm/sec, a linear frequency scanning rate > 30 MHz/sec allows passage of the driving signal through the molecular resonance in a time shorter than the mean transit time (~ 200 μ sec) of the molecules through

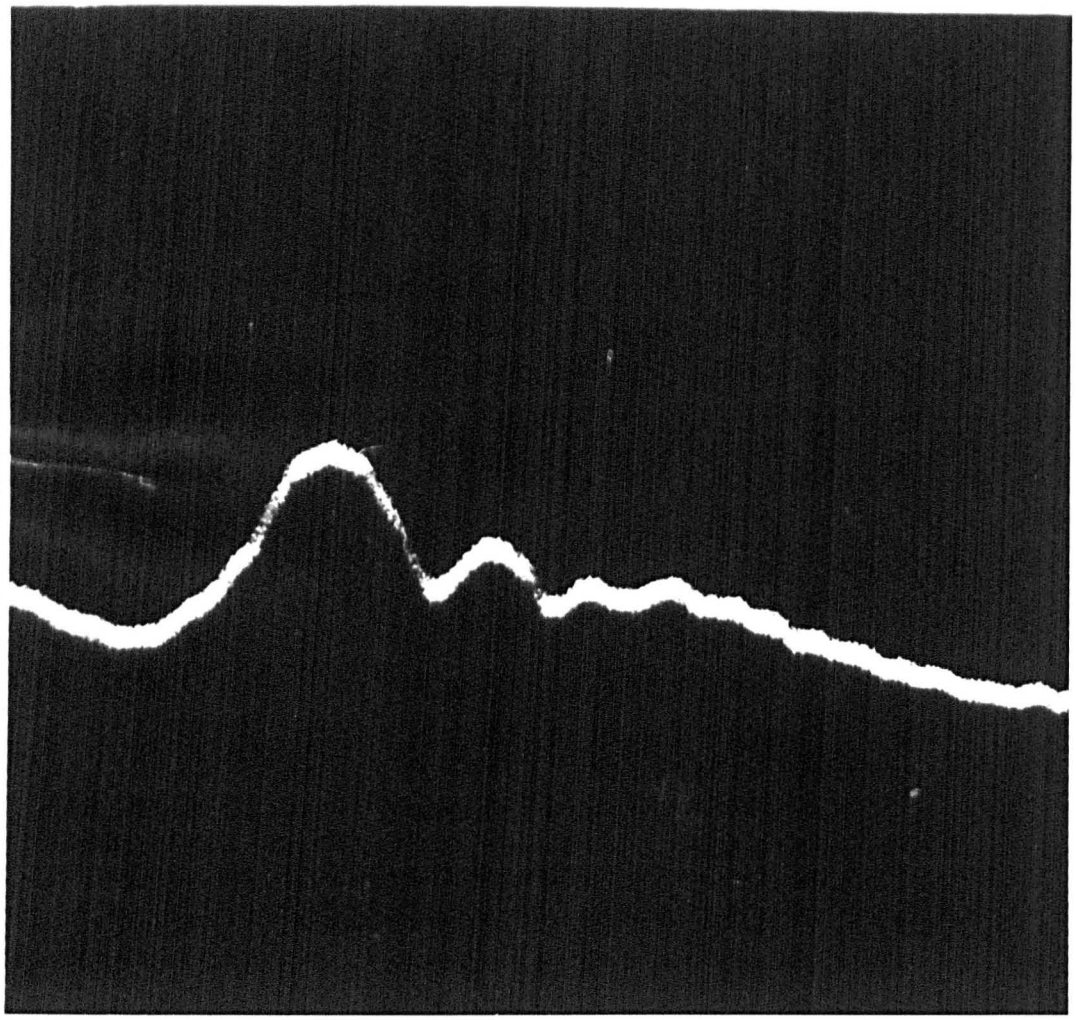

Fig. 7.6.1 First Experimental Evidence of a Superradiative transition in an Absorptive Molecular Beam.

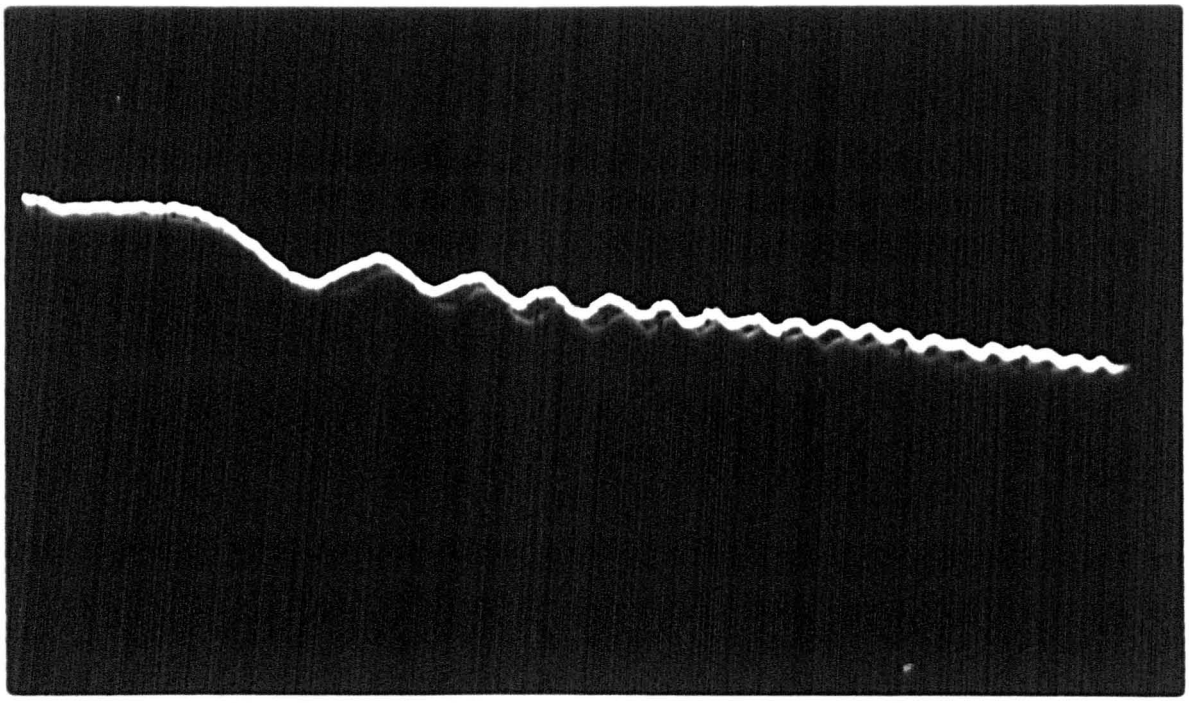

Fig. 7.6.2 Superradiative Transition in an Emissive Beam

the resonator. Thus immediately after the "rapid" passage, the molecules will be in a superradiative state (described in the preceding sections), which diminishes as the molecules finally pass out of the cavity or collide with the cavity walls. The decaying ringing signal beats with the applied signal (which itself varies in phase during the process) and produces alternate maxima and minima. To display these high frequency beats a wide band Hewlett Packard oscilloscope (Model 175 A) in conjunction with a high pass filter was used.

7.6. Results and Comments :

(a) State selected beam of lower state molecules of NH_3 J = K = 3 inversion state using AG focusing :

Fig. 7.6.1. shows the result of this experiment. The sensitivity of the AG system used at this stage was not particularly good. However, the evidence of the supperradiative transition is quite clear. The first of the maxima is due to ammonia absorption under AG operation. Frequency scanning rate of the exciting signal used is of the order 30 MHz/sec ; background pressure = 2.7×10^{-5} torr and pressure behind the nozzle = 2.5 torr. This is the first experimental evidence of a supperradiative transition in an absorptive molecular beam (reported by Laine and Kakati[205]).

(b) State selected beam of upper state molecules of NH_3 J = K = 3 inversion state using an Octapole focuser :

Figure 7.6.2. shows a typical trace obtained from this experiment. The octapole focuser used is superior in terms of efficiency for a net focusing of upper state molecules than the AG focuser used to obtain

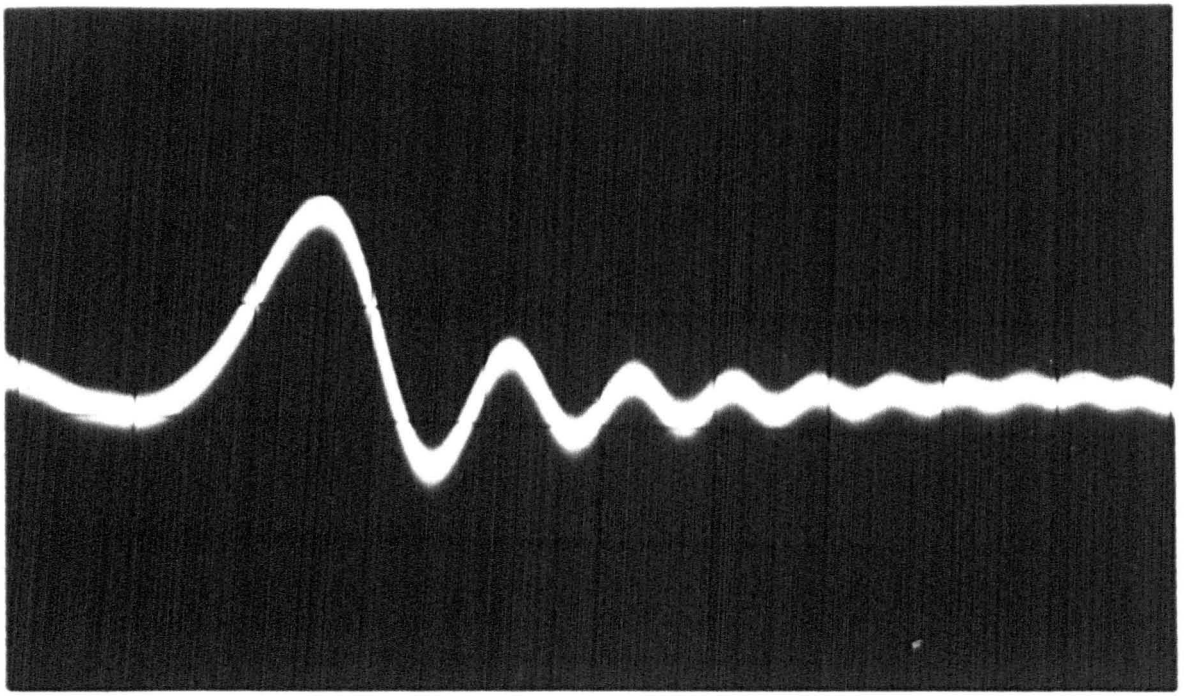

Fig. 7.6.3 Molecular Ringing in Bulk Gas due to the NH_3, J = K = 3, $\Delta F = \Delta F_1 = 0$ transition

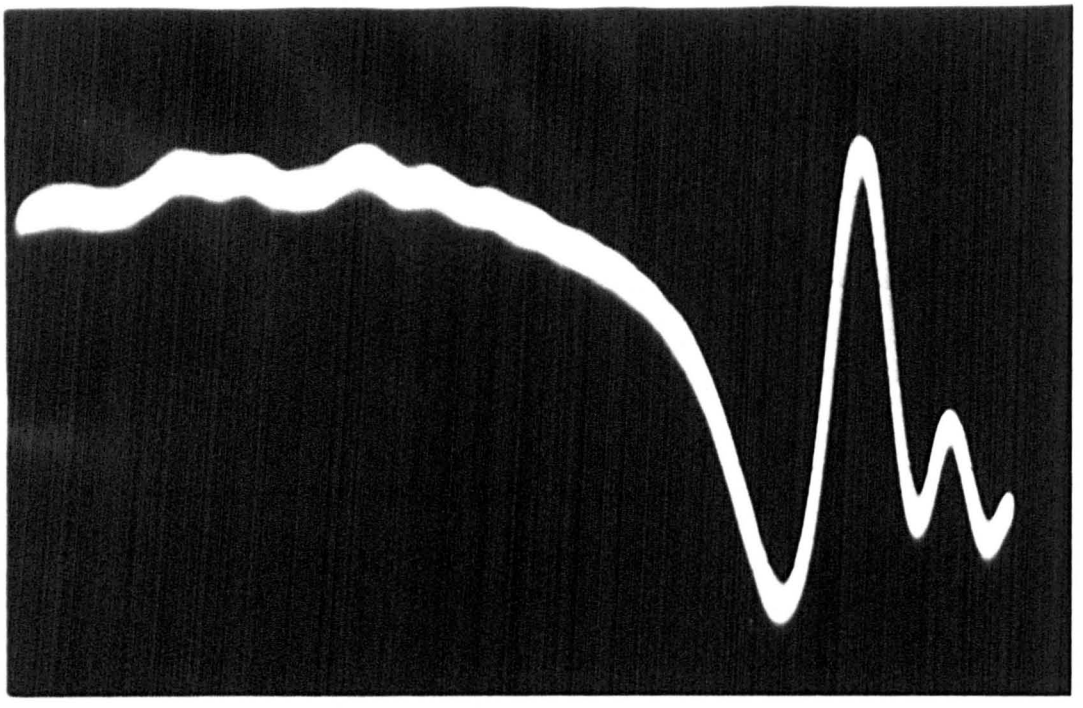

(a)

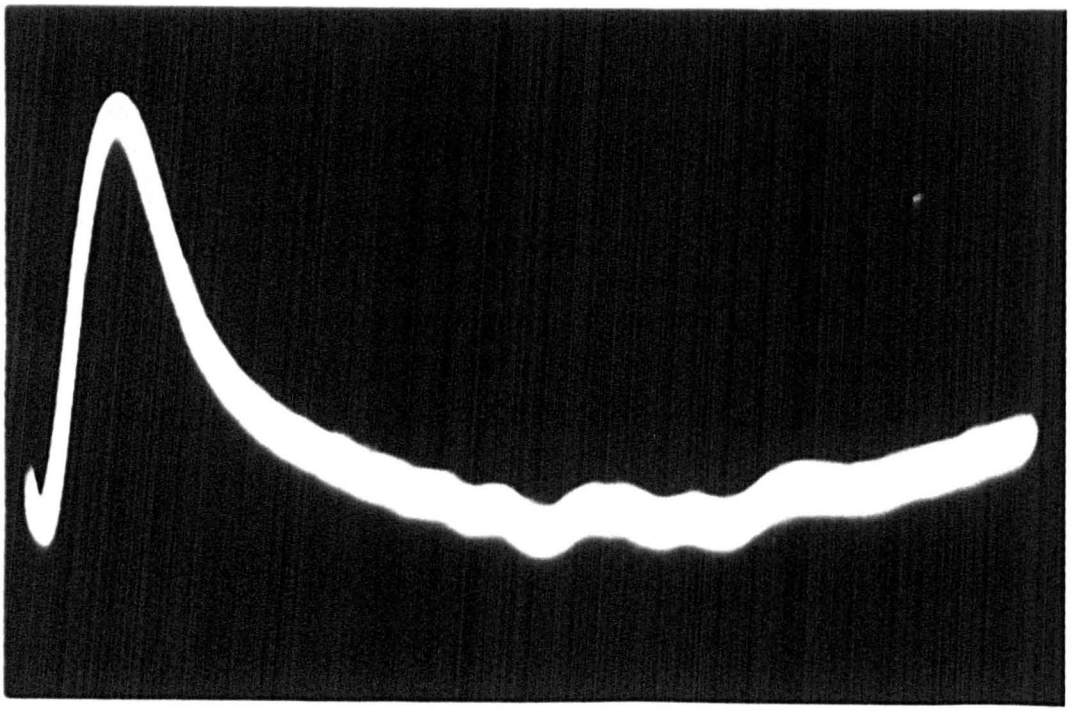

(b)

Fig. 7.6.4a, b. Molecular Ringing of the Quadrupolar Satellites of the main line of the Ammonia J = K = 3 Transitions

the trace 7.6.1. in view of its state selection properties. This means that the cooperation number r has higher value in this experiment. This explains why the effect is much more pronounced here than in the preceding case.

(c) Superradiative transition in bulk gas :

In this experiment no state separator has been used. Consequently liquid nitrogen cooling is also not necessary. The applied exciting signal frequency was scanned at 35 MHz with 10 - 20 KHz saw-tooth obtained from a Telequipment Oscilloscope, that is to say, that the frequency scanning rate is of the order of 10^{12} Hz/sec. Fig. 7.6.3. shows a typical trace of the molecular ringing of the $J = K = 3$, $F = F_1 = 0$ transition of ammonia. Fig. 7.6.4a-b show the ringing of the quadrupole satellites on either side of the main line. The resonant cavity was tuned thermally to the frequency of the satellites in order to enhance their intensity.

There is an apparent difference between the experimental approach made in this experiment and that of Dicke and Romer[170] based on Dicke's theory[171]. These earlier experiments were basically designed to investigate what happens when an electromagnetic field applied to a molecular assembly is suddenly switched off. The present experiment would seem to correspond more closely to the direct model described in Section 7.4b. than the Dicke model. The difference in approach is, however, only apparent. In the present experiment although the molecular resonance is frequency swept rather than pulsed, in fact two things are happening :

(i) the molecules are subjected to an external field which decays in amplitude. This in effect corresponds to Dicke and Romer's pulse,

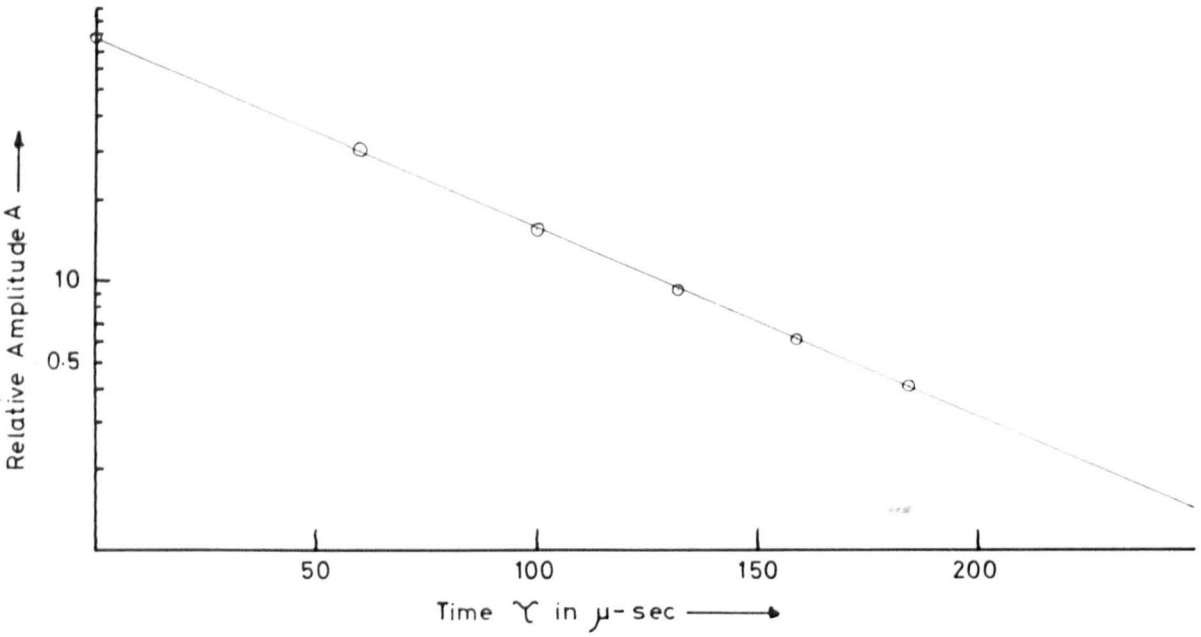

Fig 7·6·5 A typical plot of $\log_a$ versus Δt

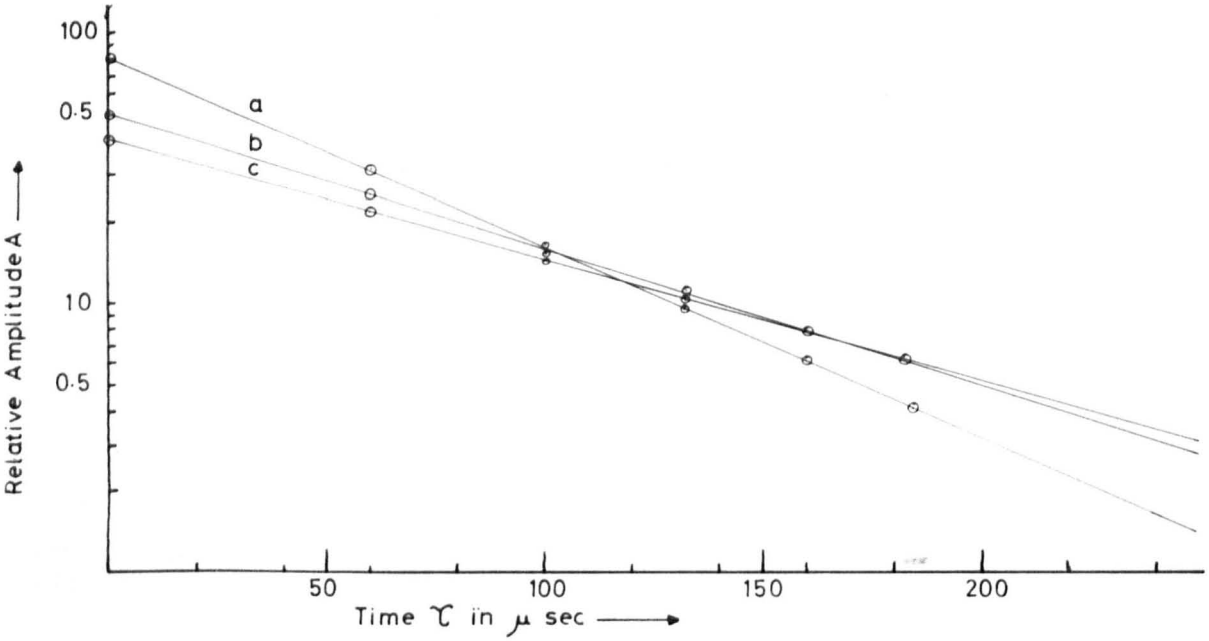

Fig 7·6·6 Relaxation time measurements at various pressures.
Pressure behind nozzle in torr a = 2·0 b = 1·3 c = 1·2

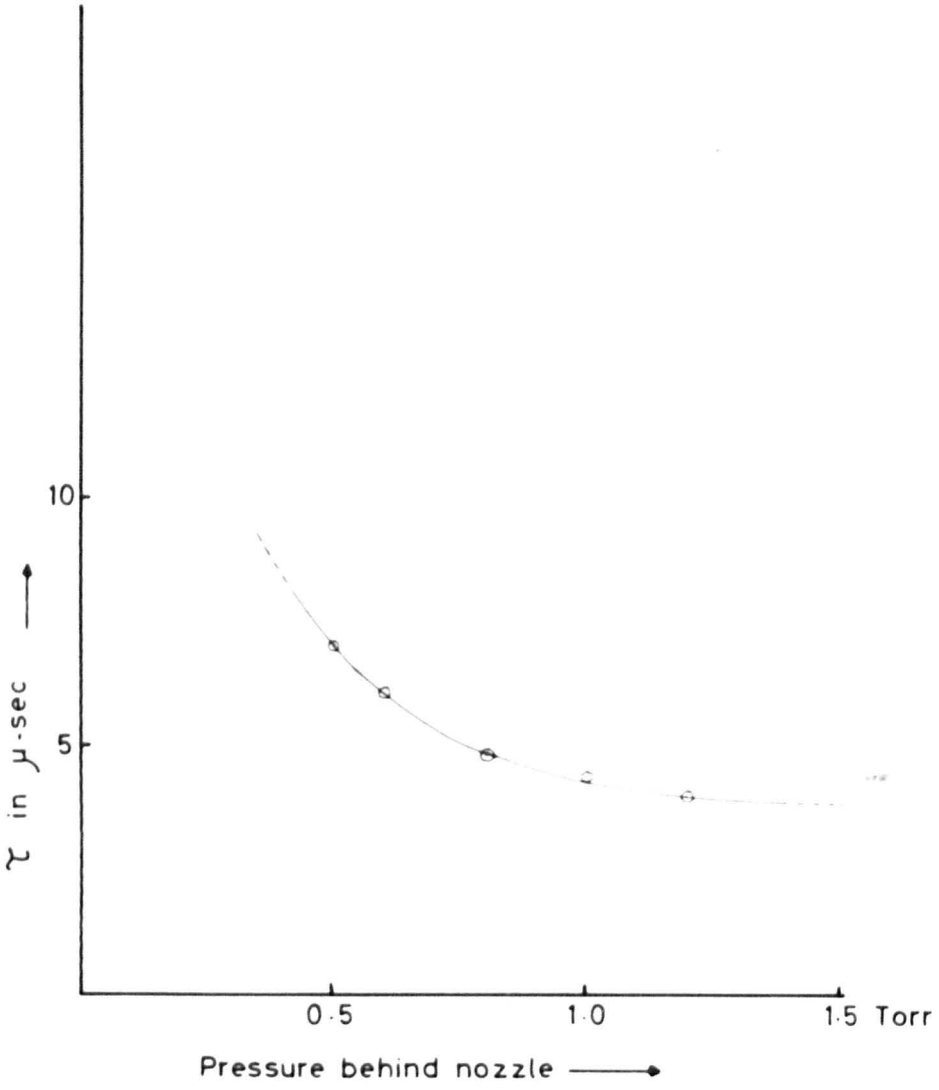

Fig 7·6·7 Variation of relaxation time τ in bulk with pressure. (145)

particularly so if the sweeping is at very high frequency, i.e. very rapid passage ;

(ii) at the same time the frequency of the external field is changing and this gives beats (wiggles) with the molecular emission which of course remains at the constant transition frequency ω_o, and this helps to display the effect on an oscilloscope. The present approach makes the experimental techniques far simpler than those of Dicke and Romer.[170]

The present series of experiments establishes the generality of the phenomena of supperradiance for a two level quantum mechanical system.

(d) Measurement of Relaxation Times:

If the detection of the beat pattern in the above type of experiment is not limited by the pass-band of electronic detection system, an exponential decay of the wiggles is to be expected. Following Arditi and Carver[206] a semilogarithmic plot of the ratio of initial amplitudes of the exponential decay Ao/A against time is made, and from this the relaxation time of the system is evaluated from the slope of the straight line through the experimental points. The definition of the relaxation processes involved is given by Laine, Kakati[207] and others.

Fig. 7.6.5. shows a typical plot of log A versus time where A is the relative amplitude. The relaxation time in the bulk gas from this measurement is $\tau \sim 4$ μ sec. Fig. 7.6.6. shows such measurements at various pressures. Fig. 7.6.7. shows variation of τ with beam pressure.

It is clear from Fig. 7.6.5, 6 that the decay is exponential, and the measurements are not limited by the pass-band of the detection

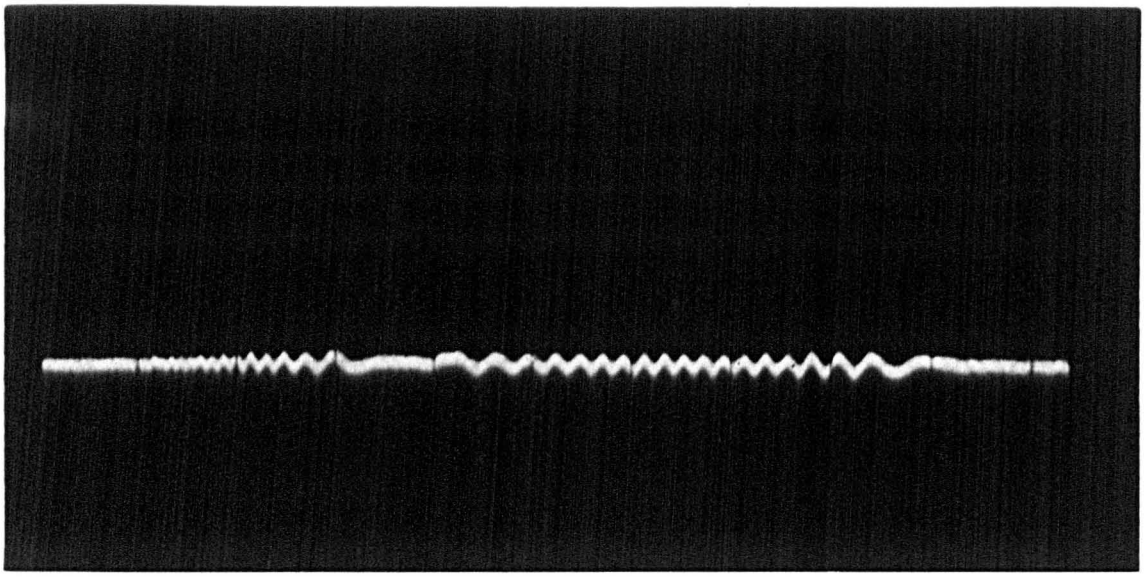

Fig. 7.6.8 Pre-ringing in Molecular Resonance (146)

system.

(e) Pre-Ringing of Molecular Resonance :

To rule out the possibility of any such limitations mentioned above, however, measurements can be made on the pre-ringing of the molecular resonance and compared with the ringing signals following the resonance (Andrew[208]). An oscilloscope presentation of pre-ringing with sinusoidal modulation of the exciting signal is shown in Fig. 7.6.8. From these results it can be seen that molecular beam experiments can be carried out with pre-ringing enabling more precise measurements of relaxation time.

(f) Line width Measurements :

From the data obtained from the experiments discussed in this chapter, using the relation $\Delta\nu = 1/\pi\tau$, the line width obtained is found to be of the order of 63 KHz for bulk gas at a pressure of $\sim 10^{-5}$ torr. This is somewhat smaller than the full Doppler width. This is not surprising since in the present set up the molecules effusing into the cavity through the nozzle retain some degree of directivity at this pressure even in the absence of focusing. In the case of a state selected beam the line width is found to be of the order of 10 KHz. The discrepancy between this result and the results obtained by Laine[168] may be attributed to the difference in geometrical and other conditions. The measurements made in the present series of experiments are strongly dependent on geometry. In addition there may be some influence of radiation damping [170] as well. These aspects are being investigated in detail by Smart[209].

CHAPTER VIII

Further Comments on Transient Phenomena, Dielectric Relaxation, Chemical Kinetics and AG-System.

8.1. Introduction :

It seems fair to comment at the present stage of development in various fields of physical science that at least apparently to date there has been a significant lack of a unified understanding of the three fields - (i) Microwave Spectroscopy, (ii) Dynamics of Chemical Reactions and (iii) Dielectric Relaxation processes in the condensed phase of matter.

The progress in the three areas in recent years has been fast and it seems that a coherent pattern of all the accumulated data and theories is imminent. The requirements of the fast developing area of space physics would demand such a unified picture in particular. A good example of the process of interrelating data of different areas of work and theoretical models has emerged out of the present investigation as shown in Chapter VII, e.g. the link shown between the Dicke model, Liubimov et al's calculations, Laine's single cavity ringing experiment and the present series of AG experiments with neutral ammonia molecules.

It is difficult to state categorically whether progress in all the fields has been going on at the same pace. One notable example is the development of a neutral particle focuser and accelerator.

Magnetic deflection of neutral particles (silver atoms) was

demonstrated by Stern and Gerlach as far back as in 1922. Some methods of accelerating charged particles were available around 1930. In the decade which followed many important experiments were done with some form or other of magnetic or electrostatic focusing. It is surprising that after Kazachok's[53] paper on electrodynamic slowing down of molecules in 1965, the possibility of accelerating molecules, as for example ammonia molecules in the upper inversion state as a test case and its implications has not hitherto been considered. Presumably this has arisen because of the fact that maser physicists have always been obsessed with the idea of developing an increasingly better frequency standard and obtaining slow molecules for this purpose (without much success either). However, the AG-experiments of the present investigation has shown that a neutral particle focuser can indeed be operated and with necessary modifications can be made to accelerate or decelerate molecules. Amongst various new possibilities opened up by this system one important exploitation of the features of an AG system may be the possibility of releasing the chemical kineticist from the restrictions involved in averaging molecular parameters over a Boltzmann distribution and providing a method as nearly precise and sophisticated as those that have been available to the nuclear physicists since the mid 1930's. These points will be further discussed in a later section.

Instead of giving a comprehensive list of references a bibliography with a number of key papers is given[210-228].

In the following section a nuclear analogue is described in order to draw a comparison of the state of art in molecular physics and

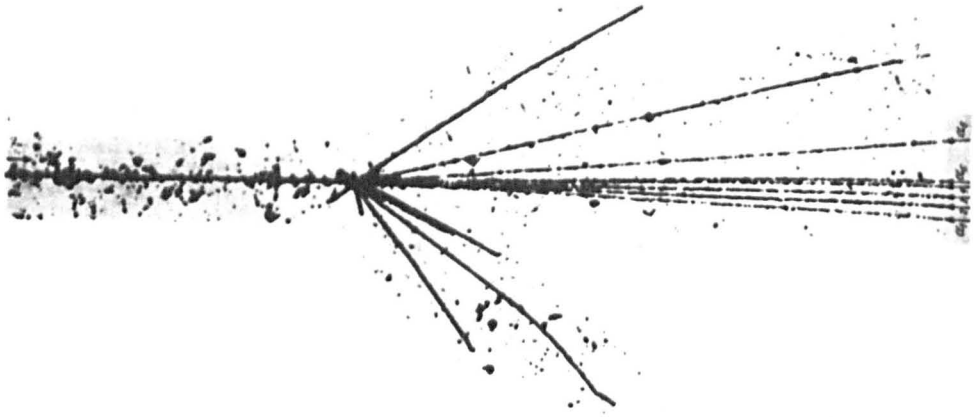

Fig 8·2·1 A Nuclear Event in Emulsion (Kakati and Deka, by courtesy of D.A.E Unit, Gauhati, India) (149)

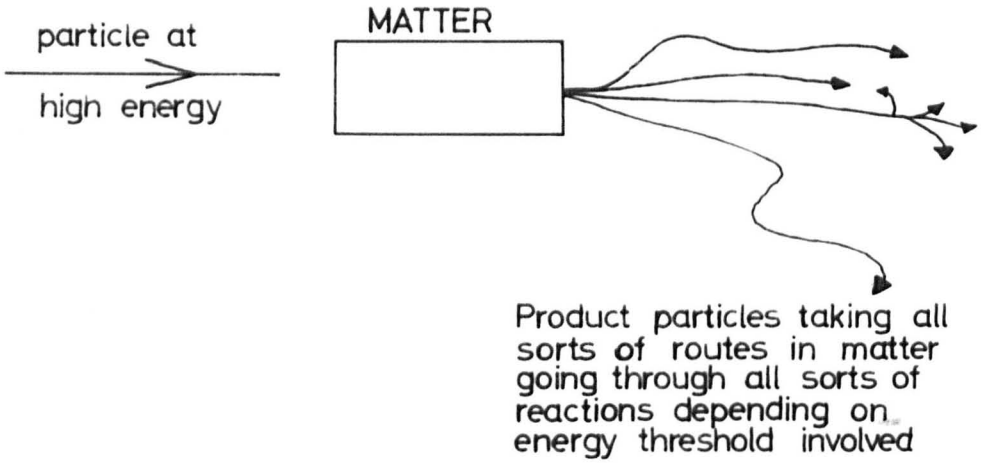

Fig. 8.2.2. Schematic of a high energy nuclear interaction in matter.

chemistry and highlight the possibilities that may be hopefully expected in the area of the dynamics of chemical interactions in view of the current trend in aerothermochemistry particularly.

8.2. State of the Art in Nuclear Physics :

A brief mention will be made here of the photographic emulsion techniques as developed by Powell (1947). This method is apparently very simple and at the same time is unique in the way it gives detailed and extremely precise information about nuclear interactions event by event. Fig. 8.2.1. shows a typical nuclear event: a Mg (z = 12) or an Aℓ (z = 13) nucleus of the heavy primary cosmic rays undergoes nuclear fragmentation as a result of collision with an emulsion nucleus. This has been identified from the delta-ray measurement. The primary nucleus breaks into six alpha particles, then the emulsion nucleus evaporates giving rise to a star. By measuring the grain density, range, scattering, delta rays, angular distributions and by applying theories and empirical calibrations every detail of each individual isolated nuclear event can be evaluated. Consequently identification of the interacting and product particles and a complete picture of the dynamics of the interactions involved results. A schematic representation of such processes and their implications are shown in Fig. 8.2.2.

8.3. State of the Art and Some Current Problems in Chemistry :

As compared to the example cited in the preceding section, in chemical kinetics a reaction typically represented by an equation for example

$$AB + XYZ = AY + BXZ$$

could give information only in terms of the initial reactants, final products and rate coefficients in a particular environment defined by pressure, temperature and concentration, but nothing could be known about the fundamental dynamics of the reaction. An ideal situation would be a method by which a chemical reaction can be studied as isolated collisions between molecules in known energy states and velocities - as in the nuclear analogue discussed in the preceding section. The best that can be expected to be done is to study the reactions in gas phase and ensure that the fundamental parameters of the products (identity, velocity, energy state) can be measured before a secondary interaction. A great advance in this direction has recently been made by introducing molecular beam techniques in this area. A molecular beam can be used as the projectile and a gas in a vacuum chamber as the target molecules or two crossed beams can be used. In conjunction with surface ionization detectors (which, however, are sensitive only to alkali metals and alkali halides) such experiments can give information about the life time of the collision and the energy released by the reaction. Besides detection techniques, further limitations are imposed by the low beam intensity and low energy of the reactants. For example at thermal energies in a binary reaction already mentioned only one kind of reaction can occur which is in a sense predestined by energy thresholds. This limitation has been somewhat alleviated recently with the introduction of the shock tube and supersonic nozzle. Addition of some form of mechanical velocity selector has been of some help to get rid of the rigid restrictions imposed by the Boltzmann distribution.

Most ordinary chemical reactions at higher thermal energies obtained by simple heating occur at less than 1 eV, (e.g. NH_3 molecule at room temperature has a kinetic energy ~ 0.02 eV). At this level, as already mentioned, only one reaction can occur which is in a sense predestined. The problem here is how to separate which reaction is occurring at what energy; methods advanced so far have been (i) removal of slow molecules by a foreign material, (ii) or in the reverse way, to eliminate the high energy molecules by using a buffer gas as a moderator. None of these methods can however provide molecules in a controlled narrow band of velocity and internal energy.

As outlined above there are two approaches to chemical processes:

(a) the traditional macroscopic approach at a statistical level,

(b) the microscopic approach at molecular level which is of recent origin.

At the microscopic level binary or higher order collisions between single atoms or molecules may be studied through scattering of the reactant species in atomic and molecular beams. The quantity of interest in this approach is the reactive cross-section. A synthesis of the micro- and macro-approaches would need :-

(i) knowledge of the interaction forces between the reactant species as a function of inter-molecular distances, geometry, internal quantum state, etc.

(ii) knowledge of the reactive cross-section for the interaction of the reactant species as a function of molecular parameters (quantum states of reactants, products, relative velocities, scattering angles, etc.)

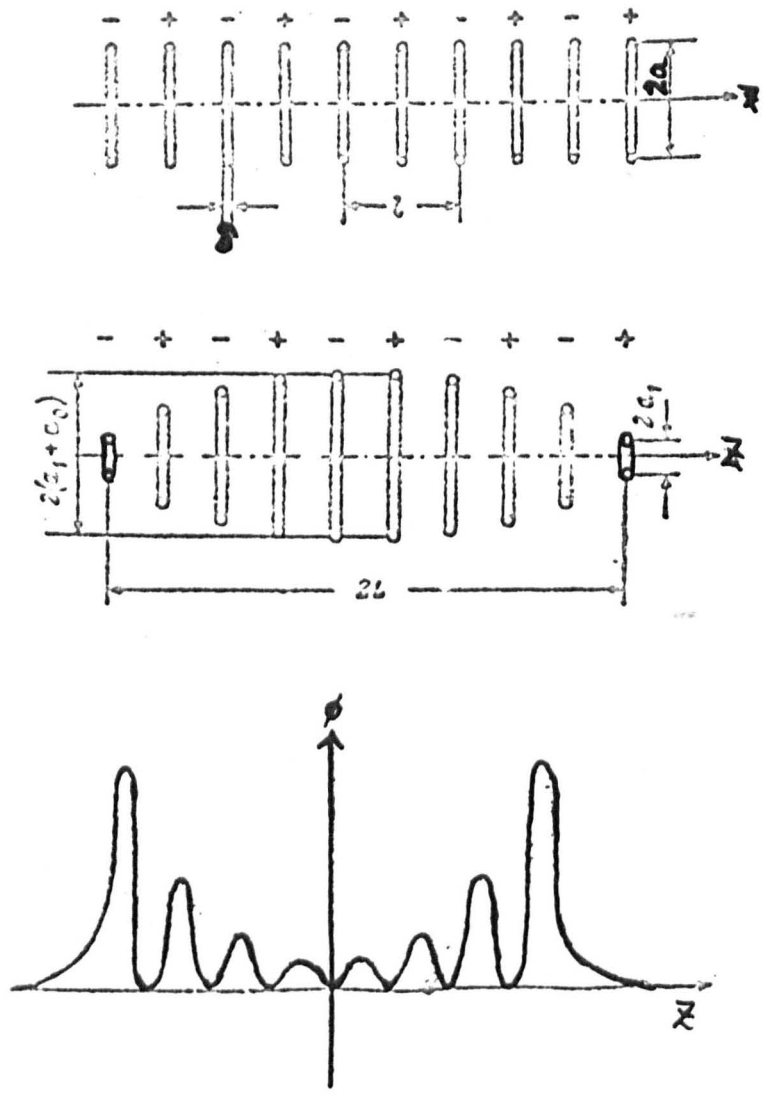

Fig.8.5.1 . Kazachok Scheme for Electrodynamic Slowing Down of Molecules

(iii) construction of the macroscopic rate co-efficient from the microscopic scattering cross-section through appropriate averaging. These aspects are discussed and their relevance to various problems in current space science are dealt with in detail in Reference 224.

8.4. State of the Art in Dielectric Relaxation Processes and Molecular Behaviour :

A similar situation to the one discussed in the preceding section exists in this area. The topic is broadly covered by Illinger in Reference 220. Here again the ideal approach would be to study the material in gas phase and then relate the data to the condensed phase through the Clausius-Mosotti equation and Onsager formula, with possible refinement of the theoretical models. The introduction of beam maser techniques has been a great advance in this area. It is suggested that superradiative measurements (possibly with AG systems) should yield more intrinsic dielectric parameters than available at present.

8.5. AG System :

The AG system described in this thesis may perhaps one day give some clues to some of the problems discussed in the preceding sections of this chapter. It has been shown in the present series of experiments that such an AG system is sensitive to velocity and quantum state of the molecules. With some modification the system can be made to accelerate or decelerate the molecules. To illustrate the process Kazachok's[53] scheme is shown in Figure 8.5.1. This scheme was proposed only to decelerate ammonia molecules in the upper inversion state.

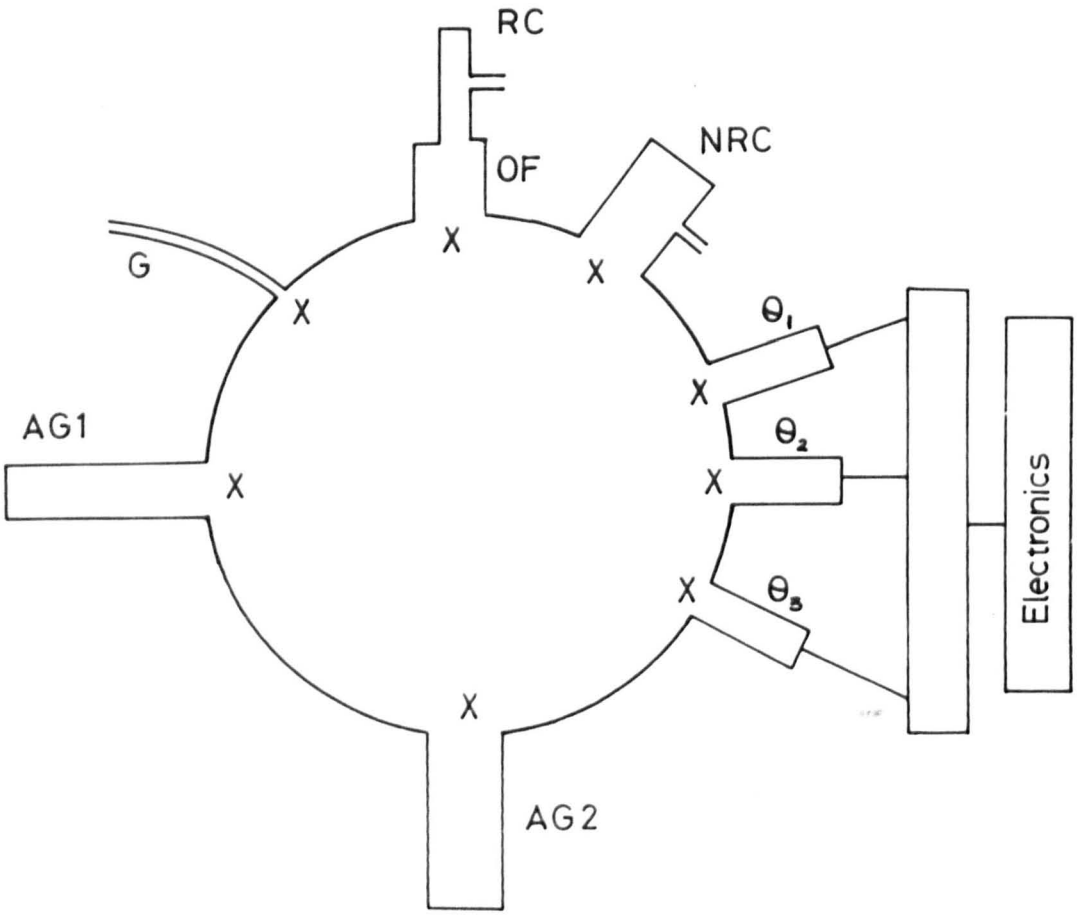

Fig. 8.6.1. A Conceptual Experimental Arrangement.

Normally, the kinetic energy gained and lost in entering and leaving a potential hill compensate each other. The problem therefore is merely to destroy this compensation along the path of the molecule. This can obviously be achieved by RF pulsing. By using only half of the system and shaping the pulse either acceleration or deceleration of either inversion state can be obtained by dc operation. In the AG system described in this thesis there is provision for changing the parameter $k_1 z$ by tilting the electrodes in the desired direction. A further flexibility will be given by changing the electrode spacing z to match the focusing condition with continuous change of the molecular velocity. The change in velocity can be detected by measuring the line width of the molecular resonance.

With a beam of accelerated molecules a host of new experiments may be possible, and the state of art in molecular dynamics may perhaps be developed to something as precise and detailed as the nuclear analogue described in Section 8.2.

8.6. A Conceptual Experiment:

(a) An Experimental Arrangement :

A possible experiment is schematically represented in Fig. 8.6.1. The circle represents a vacuum chamber. The two AG systems AG1 and AG2 can provide two molecular beams at right angles at pre-determined velocity and quantum state. The products can be analysed as regards yield, angular distribution, identification etc. by the array of quadrupole mass spectrometers Q_1, Q_2, Q_3 etc. Maser spectroscopic measurements can be done in the resonant cavity RC. This cavity can be mounted as described in Chapter V. so that it can be easily replaced

to suit different resonant frequencies. Superradiative measurements in bulk gas can be made in the non resonant cavity NRC.

Gas can be introduced at desired pressures by the additional channel G, and one AG operated to use a beam as projectiles and the gas in the chamber as target molecules, or crossed beam experiments can be done with the two AG systems.

(b) Possibility of Obtaining Non-Boltzmann Distribution without Electric or Magnetic Focusing :

An interesting experiment that may be possible to do with the arrangement described here is to study the processes involved in an expanding flow of a molecular system and investigate the possibility of obtaining maser action (or inverse process) by this means. When a molecular flow expands into a high vacuum, the temperature and density will fall continuously. The energy exchanges which continuously take place in a molecular system in order to maintain the normal Boltzmann distribution will be reduced by the above process. Presence of a buffer gas will further enhance the rate of diminishing such energy exchanges. As a result the energy exchange rates will not be able to follow adiabatically the Boltzmann restrictions of molecular dynamics. Consequently a non-Boltzmann distribution will be created which will make possible

(i) maser action without the complications of conventional electric or magnetic state-separation, or

(ii) enhanced absorption experiments as described in this thesis.

8.7. Further Application of the AG System :

Some further applications of AG system are mentioned by Wharton of Chicago[226] in a private communication to the present investigator. It is understood that an AG accelerator with 700 elements is under construction.

END.

REFERENCES

1. Troup, G., "Masers and Lasers", 1963, Methuen, London, 2nd Ed.

2. Singer, J.R., "Masers", 1960, Wiley, London.

3. Vuylsteke, A.A., "Elements of Maser Theory", 1960, D. Van Nostrand, New York.

4. Heavens, O.S., "Optical Masers, 1964, Methuen, London.

5. Wittke, J.P., Proc. I.R.E., 45 (1957) pp. 291.

6. Weber, J., Rev. Mod. Phys., 31 (1959) pp. 681.

7. Townes, C.H. and Schawlow, A.L., "Microwave Spectroscopy", 1955, McGraw Hill, London.

8. Ingram, D.J.E., "Spectroscopy at Radio and Microwave Frequencies", Butterworths, London, 1955.

9. Siegman, A.E. "Microwave Solid State Masers", 1964, McGraw Hill, New York.

10. Louiselle, W.H., "Radiation and Noise in Quantum Electronics", 1964, McGraw Hill, New York.

10a. Barnes, F.S., "Quantum Electronics", C.H. Townes, (Ed.), New York 1960, Colombia University Press.

11. Herzberg, G., "Infrared and Raman Spectra of Polyatomic Molecules", D. Van Nostrand, New York, 1947.

12. Seel, F., "Atomic Structure and Chemical Bonding", Methuen, London, 1963.

13. Sugden, T.M., Kenney, C.N., "Microwave Spectroscopy of Gases", D. Van Nostrand, London, 1965.

14. McWeeney, R., "Symmetry", Pergamon, 1963.

15. Dennison, Hardy, Phys. Rev. 39 (1932) pp. 938.

16. Dennison, Uhlenbeck, Phys. Rev. 41 (1932) pp. 313.

17. Wright, Randall, Phys. Rev. 44 (1933) pp. 391.

18. Cleeton, Williams, Phys. Rev. 45 (1934) pp. 234.

19. Good, W.E., Phys. Rev. 70 (1946) pp.213.

20. Sheng, H., Barker, E.F., Dennison, D.M., Phys. Rev. 60 (1941) pp. 786.

21. Newton, R.R., Thomas, H.H., J. Chem. Phys. 16 (1948), pp. 1941.

22. Swalen, J.D., Ibers, J.A., J. Chem. Phys. 36 (1962), pp.310

23. Bagdanskis, N.I., Bulanin, M.O., Soviet Physics Opt. and Spec. 19 (1965) 128.

24. Costain, C.C., Phys. Rev. 82 (1951),pp. 108

25. Gunther-Mohr, C.R., White, R.L., Schawlow, A.L., Goof, W.E., Coles, D.K., Phys. Rev. 94, (1954) pp. 1184.

26. Gunther-Mohr, G.R., Townes, C.H., Van Vleck, J.H., Phys. Rev., 94 (1954) pp. 1191.

27. Gordon, J.P., Phys. Rev. 99 (1955) pp. 1253.

28. Kukolich, S.G., Phys. Rev. 138 (1965) pp. A1322.

29. Kukolich, S.G., Phys. Rev. 156 (1967) pp. 83.

30. Shimoda, K., Wang, T.C., Rev. Sci. Inst., 26 (1955) pp. 1148

31. Janch, J.M., Phys. Rev. 72 (1947) pp. 715.

32. Coles, D.K., Good, W.E., Bragg, J.K., Sharbaugh, A.H., Phys. Rev. 82 (1851) pp. 877.

33a. Higa, W.H., External Publication No. 381, "Maser Engineering", 1957, Jek Propulsion Laboratory, U.S.A.

33b. Hughes, H.K., Phys. Rev. 72 (1947) pp. 614.

34. Friedberg, H., Paul, W., Naturwiss, 38 (1951) pp. 159.

35. Bennewitz, J.G., Paul, W., Z. Physik, 139 (1954) pp. 489

36. Ramsey, N.F., "Molecular Beams", Oxford University Press, London, (1959).

37. Gordon, J.P., Zeiger, H.J., Townes, C.H., Phys. Rev., 95 (1954) pp. 282.

38. Gordon, J.P., Zeiger, H.J., Townes, C.H., Phys. Rev., 99 (1955), pp. 1264.

39. Basov, N.G., Prokhorov, A.M., Doklady, S.P., 101 (1955) pp.47.

40. Basov, N.G., Prokhorov, A.M., Trans. Faraday Soc., No.19 (1955) pp. 96.

41. Basov, N.G., Prokhorov, A.M., S.P.JETP 3 (1956) pp. 426.

42. Shimoda, K., J. Phys. Soc., Japan, 12 (1957) pp. 1006.

43. Shimoda, K., J. Phys. Soc., Japan, 13 (1958) pp. 939.

44. Shimoda, K., Proc. Int. School of Physics, E. Fermi, XVII, "Topics on Radio Frequency Spectroscopy", Academic Press (1962).

45. Vonbun, F.O., J. App. Phys., 29 (1958) pp. 632.

46. Hirono, M., J. Radio Res. Lab., 6 (1959) pp. 515.

47. Shimizu, T., Shimoda, K., J. Phys. Soc. of Japan, 16 (1961) pp. 777.

48. Becker, G., Zeit. angew. Phys. 15 (1963) pp.13.

49. Becker, G., Proc. 3rd Int. Quantum Electronics Conference, Paris, 1963, pp. 393.

50. Basov, N.G., Zuev, V.S., S.P. Instruments and Experimental Techniques 1 (1961) pp. 122.

51. Basov, N.G., Zuev, V.S., Svidzinskii, K.K., Soviet Maser Research ... pp. 149.

52. Krupnov, A.F., Izv. Vuz. MVO SSSR (Radiofizika) 2 (1959) pp. 658 (English Translation).

53. Kazachok, V.S., SP Technical Physics, 10 (1965), pp. 882.

54. Mednikov, O.I., Parygin, V.H., Radio Eng. and Electronic Physics, 8 (1963) pp. 685.

55. Krupnov, A.F., Skvorkov, V.A., Radio Eng. and Electronic Physics, 10 (1965) pp. 320.

56. Helmer, J.C., Jacobus, F.B., Sturrock, P.A., J.App. Phys., 31 (1960) pp. 458.

57. Helmer, J.C., Microwave Journal, 7 (1964) pp. 60.

58. Becker, F., 1963 Paris Conference, Ed. by Grivet, P., Bloembergen, N., Columbia University Press, New York, pp. 393.

59. Shimoda, K., Ibid, pp. 349.

60. Smart, G.D.S., University of Keele, U.K., private communication.

61. Helmer, J.C., Jacobus, F.B., Sturrock, P.A., Quantum Electronics, Ed. by C.H. Townes, (1960), Colombia Univ. Press, New York. pp. 78.

62. Peter, M., Strandberg, M.W.P., J. Chem. Phys., 26 (1957) pp. 1657.

63. Peter, M., Venkates, H.G.R., Strandberg, M.W.P., J. App. Phys., 31 (1960) 693.

64. Bloch, F., Phys. Rev. 70 (1946) pp. 460.

65. Purcell, E.M., Pound, R.V., Phys. Rev. 81 (1951) pp. 279.

66. Weber, J., Trans. I.R.E. P.G.E.D. 3 (1953) pp.1.

67. Strandberg, M.W.P., Dreicer, H., Phys. Rev. 94 (1954) pp. 1393.

68. Johnson, H.R., Strandberg, M.W.P., Phys. Prev. 85 (1952) pp.503.

69. Shimoda, K., Takahasi, H., Townes, C.H., J. Phys. Soc. Japan, 12 (1957) pp. 686.

70. Serber, R., Townes, C.H., Quantum Electronics, Ed. C.H. Townes, Columbia University Press, New York 1960, pp. 233.

71. Siegman, A.E., Proc. I.R.E. 49 (1961) pp.633.

72. Heffner, H., Solid State Electronics 4 (1962) pp.3.

73. Ditchfield, C.R., Solid State Electronics 3 (1962) pp. 171.

74. Smith, F.G., Solid State Electronics, 4 (1962) pp. 3.

75. Mockler, R.C., "Advances in Electronics and Electron Physics", Vol. 15. No.1. L. Marton, Ed., New York, Academic Press, 1961, pp. 1.

76. Giordmine, J.A., Wang, T.C., J. App. Phys. 31 (1960) pp. 463.

77. Ghose, R.N., "Microwave Circuit Theory and Analysis", (1963) McGraw Hill Book Co., New York.

78. Montgomery, C.G., Radiation Laboratory Series, Vol. 11, (1947), McGraw Hill Book Co., New York.

79. Moreno, T., Microwave Transmission Design Data, (1958), Dover Publications, New York.

80. Shimoda, K., Wang, T.C., Townes, C.H., Phys. Rev. 102, (1956) pp. 1308.

81 Townes, C.H., Geschwind, S., J. App. Phys., 19 (1948) pp. 795.

82. Hershberger, W.D., J. Appl. Phys., 19 (1948) pp. 411.

83. Gordy, W., Rev. Mod. Phys., 20 (1948) pp. 668.

84. Beers, Y., Rev. Sci. Inst., 32 (1961) pp. 23.

85. Townes, C.H., Phys. Rev. Letters, 5 (1960) pp. 428.

86. Muller, M.W. Phys. Rev. 106 (1957) pp. 8.

87. Strandberg, M.W.P., Phys. Rev. 10c (1957) pp. 617.

88. Weber, J., Phys. Rev. 108 (1957) pp. 537.

89. Gordon, J.P., White, L.D., Proc. I.R.E. 46 (1958) pp. 1588.

90. Stitch, M.L., J. App. Phys. 29 (1958) pp. 782.

91. Helmer, J.C., Phys. Rev. 107 (1957) pp. 902.

92. Gordon, J.P., White, L.D., Phys. Rev. 107 (1957) pp. 1728.

93. Alsop, L.E., Giordmaine, J.A., Townes, C.H., Wang, T.C., Phys. Rev. 107 (1957) pp. 1450.

94. Townes, C.H., Proc. Int. Scholl of Physics, E. Fermi, XVll, "Topics on Radiofrequency Spectroscopy", Academic Press, 1962.

95. Gordon, J.P., Walker, L.R., Louisell , W.H., Phys. Rev. 130, (1963) pp. 806.

96. Oraevskii, A.N., "Soviet Maser Research", Ed. D.V. Skobeltsyn, (translation of P.N. Lebedev Physics Institute Proceedings, Vol. 21), Consultants Bureau, New York, (1964) pp.1.

97. Strakhovskii, G.M., Cheremiskin, I.V., Ibid, pp. 56.

98. Basov, N.G., Strakhovskii, G.M., Cheremiskin, I.V., Radiotekhnika i Elektronika, 3 (1956) pp. 1298.

100. Mukhamedgaliya, A.F., Khokhlov, R.V., Izv. VUZ. Radiofizika 4 (1961) pp. 259 (English Translation).

101. Helmer, J.C., J. App. Phys. 28 (1957) pp. 212.

102. Klimontovich, I.L., Shotlov., R.V., JETP 5 (1957) pp. 937.

103. Fain, V.M., S.P. JETP, 6 (1958) pp. 726.

104. Grasink, A.Z., Oraevskii, A.N., Proc. Int. School of Physics, E. Fermi Course 31, Ed. by Townes and Miles.

105. Bonanomi, J., De Prins J., Herrmann, J., Kartaschoff, P., Rossel, J., Proc. 6th Ampere Coloquium, St. Malo, (1957).

106. Gundlach, F.W., "Solid State Electronics," 4 (1962) pp. 189.

107. Mukhamedagaliya, A.F., Strakhovskiy, G.M., Radio Eng. and Electronic Physics, II (1966) pp. 818.

108. Shimoda, K., I.R.E. Trans. Inst. I-II (1962) pp. 195.

109. Barnes, F.S., Proc. I.R.E. 47 (1959) pp. 2085.

110. Barnes, J.A., Allan, D.W., Wainwright, A.E., I.R.E. Trans. Inst. I-II (1962) pp. 26.

111. Gordon, J.P., I.R.E. Trans. Inst. PGI-4 (1955) pp. 155.

112. Linbimov, G.P., Khokhlov, R.V., S.P. JETP, 6 (1958) pp. 1074.

113. Tsaregradskii, V.B., Soviet Radio Physics, 8 (1965) pp. 361.

114. Tsaregradskii, V.B., Ibid, 8 (1965) pp. 488.

115. Tsaregradskii, V.B., Ibid, 8 (1965) pp. 654.

116. Chikin, A.I., S.P. JETP, 15 (1962) pp. 451.

117. Thaddeus, P., Krisher, L.C., Rev. Sci. Instr. 32 (1961) pp. 1083.

118. Vonbun, F.O., Rev. Sci. Instr., 29 (1958) pp. 792.

119. Basov, N.G., Oraevskii, A.N., Strakhovskii, G.M., Tatarenkov, V.M., S.P. JETP, 18 (1964) pp. 1211.

120. Strakhovskii, G.M., Tatarenkov, V.M., Shumyatskii, P.S., Radio Eng. and Electronic Physics, 2 (1966) pp. 438.

121. Bonanomi, J., Hermann, J., De Prins, J., Kartachoff, P., Rev. Sci. Instr. 28 (1957) pp. 879.

122. Sher, N., Proc. I.R.E. (1958) Nat'l Conv. Record, Part I, pp. 27.

123. Reder, F.H., Bickart, C.J., Rev. Sci. Instr., 31 (1960) pp. 1164.

124. Higa, W.H., Rev. Sci. Instr., 28 (1957) pp. 726.

125. Wells, W.H., J. Appl. Phys. 29 (1958) pp. 714.

126. Strakhovskii, G.M., Tatarenkov, V.M., S.P. JETP, 15 (1962) pp. 625.

127. Basov, N.G., Oraevskii, A.N., S.P. JEPT, 15 (1962) pp. 1062.

128. Basov, N.G., Oraevskii, A.N., Strakhovskii, G.M., Tatarenkov, V.M., Quantum Electronics III, New York, Columbia Univ. Press, 1964, pp. 377.

129. Laine, D.C., Srivastava, R.C., Radio Electro. Engr. 26 (1963) pp. 173.

130. Laine, D.C., Smith A.L.S., Physics Letters, 20 (1966) pp. 374.

131. Laine, D.C., Smith, A.L.S., I.E.E.E. J. Quantum Electronics, QE-2, (1966) pp. 399.

132. Kukolich, S.G., Proc. I.E.E.E., 52, (1964) pp. 211.

133. Basov, N.G., Oraevskii, A.N., Strakhovskii, G.M., Uspenskii, A.V., S.P. JETP (1966) pp. 305.

134. De Prins, J., I.R.E. Trans. Instr. I_II (1962) pp. 200.

135. Saburi, Y., Kobayashi, M., Yasuda, Y., Harada, K., I.R.E. Trans. Instr. I-II (1962) pp. 204.

136. Mukhamedgalieva, A.F., Strakhovskii, G.M., Soviet Radio Physics, 8, (1965) pp. 590.

137. Veselago, V.G., Oraevskii, A.N., Strakhovskii, G.M., Tatarenkov, V.M., JETP Letters 2 (1965) pp. 49.

138. Mc Coubrey, A.O., Proc. I.E.E.E. 54 (1966) pp. 116.

139. Basov, N.G., Oraevskii, A.N., S.P. JETP 10 (1960) pp. 761.

140 Townes, C.H., J. Appl. Phys. 28 (1957) pp. 920.

141. Marchenko, Y.I., Rubanik, V.P., Soviet Radio Physics, 8 (1965) pp. 481.

142. Suchkin, G.L., Radio Eng. and Electronic Physics, II (1966) pp. 212.

143. Helmer, J.C., J. Appl. Phys. 30 (1959) pp. 118.

144. Torrey, H.C., Whitmer, C.A., Crystal Rectifiers, Rad. Lab. Series 15, McGraw Hill, New York, 1948.

145. Wheeler, G.J., Introduction to Microwaves, Prentice Hall, Englewood Cliffs, N.J. 1964.

146. Robinson, F.N.H., Noise in Electrical Circuits, Oxford, 1962.

147, Feher, G., Bell. Syst. Tech. J., (1957) 449.

148. Miller, P.H., Noise Spectrum of Crystal Rectifiers, Proc. I.R.E. 35, (1947) pp. 252.

149. Nicoll G.R., Noise in Silicon Microwave Diodes, Proc. I.E.E. 101 (1954) pp. 317.

150. Pound, R.V., Microwave Mixers, Rad. Lab. Series, McGraw Hill, New York, 1947.

151. Bonanomi, J., Herrmann, J., Helv. Phys. Acta, 29 (1956) pp. 225.

152. Rice, S.O., Bell Syst. Tech. J. 23, (1945) pp. 282, Ibid 24 (1945) pp. 46½

153. Smith, A.L.S., Doctoral Thesis, Keele University, 1966.

154. Wallman, H., Mcnee, A.B., Gadsen, C.P., Proc. I.R.E., 36 (1948) pp. 700.

155. Courant, E.D., Livingston, M.S., Snyder, H.S., Phys. Rev. 88 (1952) pp 1190.

156. Livingwood, J.J., Principles of Cyclic Particle Accelerators, D. Van Nostrand, Princeton , (1961)

157. Livingston, M.S. Blewett, J.P., Particle Accelerators, McGraw Hill, New York, (1962).

158. McMillan, E., Phys. Rev. 80 (1950) pp. 493.

159. Boussard, D., Focusing of Charged Particles, Edited by Septicer, A., Vol. II., Academic Press, 1967, New York. pp. 327.

160. Laslett, L.J. Ibid, pp. 355.

161. Rabi, I.I., Kellogg, J.M.B., Zacharias, J.R., Phys. Rev. 46 (1934) pp. 157.

162. Auerbach, D., Bromberg, E.E.A., Wharton, L., J. Chem. Phys. 45 (1966) pp. 2160.

163. Any standard book on differential equations.

164. Korn and Korn, Mathematical Handbook for Scientists and Engineers.

165. Teng, L.C., Rev. Sci. Instr. 25 (1954) pp. 264.

166. Schiff, L.I. "Quantum Mechanics", McGraw Hill,(1955).

Bohm, D., "Quantum Theory" (GIFML), 1961.

167. Kakati, D., Laine, D.C., Physics Letters, 24 (1967) pp. 676.

168. Laine, D.C., Physics Letters, 23, 9 (1966) pp. 557.

169. Goldenberg, H.M., Kleppner, D., Ramsey, N.F., Phys. Rev. Letters, 5 (1960) pp. 361.

170 Dicke, R.H., Romer, R.H., Rev. Sci. Instr. 26 (1955) pp. 915.

171. Dicke, R.H., Phys. Rev., 93 (1954) pp. 99.

172. Bloembergen, Purcell, Pound, Phys. Rev. 73 (1947 pp.

173 Jacobsohn B.A., Wangness, R.K., Phys. Rev. 73 (1948) pp. 942.

174. Bloch, F., Phys. Rev. 70 (1946) pp. 460.

175. Hahn, E.L. Phys. Rev. 80 (1950) pp. 580.

176. Meiboom, S., Gill, D., Rev. Sci. Instr., 29 (1958) pp. 688.

177. Torrey, H.C., Phys. Rev. 59 (1941) pp. 293.

178. Torrey, H.C., Phys. Rev. 76 (1949) pp. 1059.

179. Rabi, I., Phys. Rev. 49 (1936) 324.

180 Rabi, I., Phys. Rev. 51 (1937) pp. 652.

181 Kurnit, N.A., Abella, I.D., Hartman, S.R., Phys. Rev. Letters 13 (1964) pp. 567.

182. Abella, I.D., Kurnit, N.A., Hartman, S.R., Phys. Rev. 141 (1966) pp. 391.

183. McCall, S.L. Hahn, E.L., Phys. Rev. Letters 18 (1967) pp. 908.

184. Patel, C.K.N., Slusher, R.E., Phys. Rev. Letters 19 (1967) pp. 1019.

185. Patel, C.K.N., Slusher, R.E., Phys. Rev. Letters, 20 (1968) pp. 1087.

186. Liubimov, G.P., Khokhlov, R.V., S.P. JETP, 6 (1958) pp. 1074.

187. Oraevskii, A.N., S.P. Uspekhi, 10 (1967) pp. 45-51.

188. Bloom, S., J. App. Phys. 27 (1956) pp. 785.

189. Gordon, J.P., Walker L.R., Louisell, W.H., Phys. Rev., 130 (1963) pp. 806.

190. Alekseev, A.I., Vdovin, Yu. A., Galitskii, V.M., S.P. JETP 19 (1964) pp. 220.

200. Chel'tsov, V.F., S.P. JETP, 20 (1965) pp. 376.

201. Chel'tsov, V.F., S.P. JETP, 21 (1965) pp. 761.

202. Tavis, M., Cummings, F.W., Phys. Rev., 170 (1968) pp. 379.

203. Feynman, R.P., Vernon, F.L., Hellwarth, R.W., J. App. Phys. 28 (1957) pp. 49.

204. Rabi I.I. Ramsey N.F. Schwinger, J., Rev. Mod. Phys. 26 (1954) pp. 167.

205. Laine, D.C., Kakati, D., to be published in Proc. Phys. Soc. (Journals of Physics B : Atomic and Molecular)

206. Arditi, M., Carver, T.R., Phys. Rev. 136 (1964) pp. A643.

207. Laine, D.C., Kakati, D. and others, "Observation of Steady State Transient Wiggles Phenomena in Bulk Gas", To be published.

208. Andrew, E.R., Nuclear Magnetic Resonance, Cambridge University Press, 1958.

209. Smart, G.D.S. University of Keele, U.K., private communication.

210. Buckingham, A. D., Pople, J.A., Trans. Faraday Soc. 51 (1955) pp. 1179.

211. Birnbaum, G., Maryott, A.A., J. Chem. Phys. 41 (1964) pp. 154.

212. Maryott, A.A., Kryder, S.J., J. Chem. Physics 31 (1959) pp. 617.

213. Maryott, A.A., Birnbaum, G. J. Chem. Phys. 36 (1962) pp. 2026, 2062.

214. Gebbie, H.A. Stone, N.W.B., Proc. Phys. Soc. 82 (1963) pp. 543.

215. Maryott, A.A., Kryder, S.J., J. Chem. Phys., 41 (1964) pp. 1580.

216. Davidson, D.W., Auty, R.P., Cole, R.H., Rev. Sci. Instr. 22 (1951) pp. 678.

217. Roberts, S., Von Hippel, A., J. App. Phys., 17 (1946) pp. 610.

218. Powell, C.F., Fowler, P.H., Perkins, D.H., "The Study of Elementary Particles by the Photographic Method", Pergamon Press, London, 1959.

219. Ross, J., "Molecular Beams" (Advances in Chemical Physics, Vol. X.), Interscience Publishers (John Wiley), New York,(1966).

220. "Progress in Dielectrics" Vol. 4. (1962)

221. Bottcher, C.J.F., "Theory of Electric Polarisation", Elsevier, Amsterdom, 1952.

222. Cottrell, T.L., Ream, N., "Transition Probability in Molecular Encounters", Trans. Faraday Soc., 51 (1955) pp. 159.

223. Discussion of Faraday Society, No. 44 (1966).

224. "Recent Advances in Aerothermochemistry" Vol. I and II, AGARD, North Atlantic Treaty Organization, 1967.

225. Rutherford, S.L., "The Mass Filter Characteristics of a Quadrupole Analyzer", 1965 AVS Presentation VR-37, Varian Associates.

226. Wharton, L., University of Chicago, U.S.A., Private communication.

QUOTATION

a. Tonnelat, M.A., "Einstein's Unified Field Theory" (English Translation), Gordon and Breach, 1966.

b. Schawlow, A.L., Stanford University, U.S.A. Private Communication.

LIST OF DIAGRAMS

			facing page
I.	I.I.I.	SCHEMATIC OF A BEAM MASER.	3
2.	2.3.I.	SCHEMATIC OF A ONE PHOTON ABSORPTION PROCESS	I5
3.	2.3.2.	SCHEMATIC OF A ONE PHOTON EMISSION BY AN ATOM IN EXCITED STATE.....	I5
4.	3.I.Ia.	GEOETRICAL STRUCTURE OF THE AMMONIA MOLECULE	2I
5.	3.I.Ib.	DIAGRAM OF A SYMMETRIC TOP PQ_3 VIEWD ALONG THE FIGURE AXIS.....	2I
6.	3.2.I.	TWO EQUIVALENT GEOMETRIC ARRANGEMENTS OF THE AMMONIA MOLECULE.....	24
7.	3.3.I.	VIBRATIONAL MODES OF THE AMMONIA MOLECULE	25
8.	3.3.2a,b.	DIAGRAMMATIC REPRESENTATION OF ENERGY LEVELS AND POTENTIAL ENERGY FUNCTION (UPPER) ·· AND LOWEST TWO WAVE FUNCTIONS (LOWER) ····· FOR (a) A SIMPLE HARMONIC OSCILLATOR,.....AND (b) AN OSCILLATOR WITH A HINDERING POTENTIAL	26
9.	3.5.I.	RELATIVE INTENSITIES AT ROOM TEMPERATURE OF VARIOUS ROTATIONAL COMPONENTS OF THE AMMONIA INVERSION SPECTRUM.....	3I
IO.	3.6.I.	MOLECULAR COUPLING SCHEME OF $N^{I4}H_3$	34
II.	3.6.2.	HYPERFINE STRUCTURE OF THE J=K=3 LINE OF AMMONIA	35
I2.	3.6.3.	QUADRUPOLE TRANSITIONS OF AMMONIA	35
I3.	3.6.4.	STRUCTURE OF THE F_I COMPONENTS OF AMMONIA..	35

I4.	3.7.I.	ENERGY LEVELS OF THE ~~XKE~~ AMMONIA MOLECULE IN AN ELECTRIC FIELD.....	37
I5.	3.7.2.	DETAILS OF THE ABOVE	37
I6.	4.3.I.	SCHEMATIC OF THE FIELD OF AN ELECTRIC QUADRUPOLE	45
I7.	4.3.2.	CROSS SECTION OF A QUADRUPOLE FOCUSER AND UPPER STATE POTENTIAL WELL	46
I8.	4.3.3.	COMPARISON OF FOCUSING CHARACTERISTICS OF MULTI-POLE FOCUSERS WITH DIFFENT NUMBER OF ELECTRODES	46
I9.	4.3.4.	CRITICAL RADIAL VELOCITY OF AMMONIA IN AN OCTAPOLE FOCUSER.....	47
20.	4.4.I.	RING TYPE FOCUSER	48
2I.	4.4.2.	LENS EQUIVALENT OF A RING TYPE FOCUSER.....	49
22.	4.7.I.	HIGH FIELD STARK EFFECT IN LINEAR RIGID ROTORS...	52
23.	5.3.I.	CHARACTERISTIC DEPENDENCE OF BEAM SHAPE ON THE HALF-WIDTH.....	6I
24.	5.3.2.	SCHEMATIC OF A CIRCULAR CYLINDRICAL CAVITY	62
25.	5.4.I.	TIME VARIATION OF THE PROBABILITIES OF A MOLECULE BEING IN THE UPPER AND THE LOWER ENERGY STATES	67
26.	5.4.2.	TRANSITION PROBABILITIES BETWEEN ENERGY STATES AS A FUNCTION OF TIME FOR MOLECULES INITIALLY IN ONE OF TWO MICROWAVE COUPLED STATES WHEN SUBJECTED TO MICROWAVE RADIATION AT OR NEAR THE RESONANCE FREQ.	67
27.	5.4.3.	TRANSITION PROBABILITIY FOR THE AMMONIA MOLECULE AS A FUNCTION OF FREQUENCY.....	68

28. 5.4.4. THEORETICAL SATURATION CHARACTERISTICS OF A MASER 72

29. 5.5.I. GENERAL VIEW OF THE MASER SYSTEM 85

30. 5.5.2. GENERAL VIEW OF THE MASER ASSEMBLY AND DETECTION SYSTEM..... 85

31. 5.5.3. OCTAPOLE FOCUSER USED 86

32. 5.5.4. RING FOCUSER USED 86

33. 5.5.5. MASER VACUUM SYSTEM AND AMMONIA SOURCE 87

34. 5.5.6. MASER VACUUM CHAMBER 87

35. 5.5.7. AMMONIA VAPOUR-PRESSURE v.s. TEMPERATURE 88

36. 5.5.8. INTERIOR OF THE MASER CHAMBER SHOWING THE LIQUID NITROGEN COOLING COIL. 88

37. 5.5.9. CAVITY CONNECTION AT THE TOP PLATE... 89

38. 5.5.IO. BLOCK DIAGRAM OF THE MASER SYSTEM.... 9I

39. 5.5.II. BASIC CRYSTEL VIDEO SYSTEM... 92

40. 5.5.I2. RATIO OF THE MINIMUM OBSERVABLE SIGNAL TO THE MINIMUM v.s. MICROWAVE POWER... FOR DIFFERENT DETECTION SCHEMES..... 94

41. 5.5.I3. BASIC SHD SCHEME USED 94

42. 5.6.I. STARTING OF MASER OSCILLATION..... 99

43. 5.6.2. MASER OSCILLATION SIGNAL.... 99

44. 5.6.3. PRESSURE CHARACTERISTICS OF THE MASER. I00

45. 5.6.4. MASER OSCILLATION CHARACTERISTIC I00

46. 5.6.5. OBSERVED AND THEORETICAL MASER OSCILLATION CHARACTEROSTICS FOR COMPARISON..... I00

47.	5.6.6.	VARIATION OF OSCILLATION AMPLITUDE WITH FOCUSER POTENTIAL.....	100
48.	5.6.7.	MASER OSCILLATION AMPLITUDE AT VARIOUS BEAM PRESSURES.....	100
49.	5.6.8.	AMPLITUDE vs BACKGROUND PRESSURE....	100
50.	5.6.9.	THRESHOLD CHARACTERISTIC OF MASER OSCILLATION.....	100
51.	6.2.1.	OPTICAL ANALOGUE OF AG FOCUSING.....	104
52.	6.4.1.	SCHEMATIC DIAGRAM OF A DIPOLE.....	105
53.	6.4.2.	SCEMATIC OF A DIPOLAR ARRAY.....	108
54.	6.4.3.	EFFECT OF A SMALL PERTURBATION ON SIMPLE HARMONIC MOTION.....	111
55.	6.4.4.	LOWER STATE MOLECULES IN n-PLANE....	
56.	6.4.5.	UPPER STATE MOLECULES IN n-PLANE....	116
57.	6.4.6.	BEAM ENVELOPE IN THE DEFOCUSING-FOCUSING PLANE OF A SIMPLE DOUBLET SCHEME.....	118
58.	6.4.7.	BEAM ENVELOPE IN THE FOCUSING-DEFOCUSING PLANE OF A SIMPLE DOUBLET SCHEME.....	118
59.	6.4.8.	GENERAL NATURE OF THE TRAJECTORIES THROUGH A SUCCESSION OF AG ELEMENTS.	118
60.	6.6.1.	EXPECTED BEAM ENVELOPE AND DEFINITION OF TWO MODES OF OPERATION.....	120
61.	6.6.2.	EXPECTED EFFECT OF THE VARIATION OF THE SEPARATION OF THE AG AND THE	

62. 6.6.3. EXPECTED EFFECT OF THE EXCITATION POTENTIAL WHEN THE CAVITY IS IN POSITION C_2 IN FIG. 6.6.1..... 121
63. 6.6.4. EXPECTED EFFECT OF THE EXCITATION POTENTIAL WHEN THE CAVITY IS IN POSITION C_1 IN FIG. 6.6.1..... 121
64. 6.7.1. STABILITY DIAGRAM OF THE AMMONIA J=K=3 INVERSION STATES..... 121
65. 6.7.2. A DIPOLAR ARRAY FOR AG FOCUSING..... 122
66. 6.7.3. VARIATION OF $k_1 z$ WITH THE RATIO z/d^2 122
67. 6.7.4a. VOLTAGE SENSITIVITY CHARACTERISTIC FOR $z/d^2 = 30$..... 122
68. 6.7.4b. VOLTAGE SENSITIVITY CHARACTERISTIC FOR $z/d^2 = 40$..... 122
69. 6.7.5a. VELOCITY SENSITIVITY CHARACTERISTICS AT VARIOUS EXCITATION POTENTIALS FOR $z/d^2 = 30$..... 122
70. 6.7.5b. VELOCITY SENSITIVITY CHARACTERISTICS AT VARIOUS EXCITATION POTENTIALS FOR $z/d^2 = 40$..... 122
71. 6.8.1a. A VIEW OF THE AG FOCUSER USED..... 123
72. 6.8.1b. A VIEW OF THE END PLATES OF THE AG FOCUSER..... 123
73. 6.8.2. VIEW OF THE AG FOCUSER MOUNTED IN SERIES WITH THE OCTAPOLE MASER FOCUSER..... 123

74. 6.9.1. ENHANCED ABSORPTION OF AMMONIA BY C_1 MODE OPERATION OF AG FOCUSER..... 124

75. 6.9.2. THE J=K=3 INVERSION LINE OF AMMONIA FLANKED ON EITHER SIDE BY THE MAGNETIC SATELLITES AS OBTAINED BY AG OPERATION IN C_1 MODE..... 125

76. 6.9.3a. RELATIVE ENHANCEMENT OF ABSORPTION WITH AG FOCUSING..... 126

77. 6.9.3b. SAME AS ABOVE FOR A DIFFERENT VALUE OF z/d^2..... 126

78. 6.9.4. LINEAR OPERATION OF AG IN C_1 MODE... 126

79. 6.9.5. RESULTS OF A SERIES ARRANGEMENT OF OCTAPOLE AND AG SYSTEM..... 126

80. 6.9.6a. VOLTAGE SENSITIVITY OF AG (EXPERIMENTAL RESULTS)..... 126

81. 6.9.6b. SAME AS ABOVE FOR A DIFFERENT VALUE OF z/d^2..... 126

82. 6.9.7. DIAGRAMMATIC REPRESENTATION OF RESULTS OBSERVED WITH VARIOUS SEPARATION BETWEEN CAVITY AND AG.... 127

83. 6.9.8. AG OPERATION IN C_2 MODE..... 127

84. 7.4d.1. SCHEMATIC REPRESENTATION OF SUPERRADIATIVE PROCESSES IN STATE SELECTED BEAMS

(a) UPPER STATE SELECTED BEAM

(b) LOWER STATE SELECTED BEAM..... 141

85. 7.6.1. FIRST EXPERIMENTAL EVIDENCE OF A SUPERRADIATIVE TRANSITION IN AN ABSORPTIVE MOLECULAR BEAM..... 143

86. 7.6.2. SUPERRADIATIVE TRANSITION IN AN EMISSIVE BEAM..... 143

87. 7.6.3. MOLECULAR RINGING IN BULK GAS DUE TO THE NH_3, J=K=3, F= F_1=0 TRANSITION. 144

88. 7.6.4a-b. MOLECULAR RINGING OF THE QUADRUPOLAR SATELLITES OF THE MAIN LINE OF THE AMMONIA J=K=3 TRANSITIONS 144

89. 7.6.5. A TYPICAL PLOT OF LOG A VERSUS t... 145

90. 7.6.6. RELAXATION TIME MEASUREMENTS AT VARIOUS PRESSURE..... 145

91. 7.6.7. VARIATION OF RELAXATION TIME WITH PRESSURE IN BULK GAS..... 145

92. 7.6.8. PRE-RINGING IN MOLECULAR RESONANCE.. 146

93. 8.2.1. A NUCLEAR EVENT IN EMULSION..... 149

94. 8.2.2. SCHEMATIC OF A HIGH ENERGY NUCLEAR INTERACTION IN MATTER..... 149

95. 8.5.1. KAZACHOK SCHEME FOE ELECTRODYNAMIC SLOWING DOWN OF MOLECULES..... 152

96. 8.6.1. A CONCEPTUAL EXPERIMENTAL ARRANGEMENT..... 153